STUDY ON

CONTRIBUTION OF SURFACE DIFFUSION ON

MASS TRANSFER OF ACTINIDES AND

FISSION PRODUCTS IN GRANITE

TETSUJI YAMAGUCHI

2001

Study on Contribution of Surface Diffusion on Mass Transfer of Actinides and Fission Products in Granite

by

Tetsuji Yamaguchi

JAERI
Tokai, Ibaraki 319-1195, Japan

January 2001

Abstract

When long-lived radionuclides are transported with groundwater through fractures in rock mass surrounding a high-level radioactive waste repository, diffusion into pores in the rock matrix and ensuing sorption onto mineral surfaces reduce the concentration of the nuclides transported through the geosphere. Owing to this mechanism, frequently fractured rock mass in Japan may have considerable retardation capacity against the transport of radionuclides. To take the matrix diffusion into account in evaluating the migration of radionuclides in deep geologic formations for the safety assessment of the repository, it is essential to understand the mechanisms of the diffusion of radionuclides into the rock matrix and to quantify the diffusivity.

The pore structure was characterized by water-saturation porosimetry, mercury intrusion porosimetry and SEM observation for Inada granite that is well known domestic biotitic granite from the Inada mine in the Ibaraki prefecture, eastern Japan. The distribution of the pore diameter of the granite was approximately logarithmic normal; the pore structure is uniform. The porosity was (0.49 ± 0.07) % with the modal diameter of 160 nm. The fact that the pore is much larger in size than the diffusing ions allows the application of the Fick's diffusion law to interpret the mass transfer of the aqueous species in the granite.

The effective diffusivity (D_e) in the Inada granite was measured for Ba^{2+}, Sr^{2+}, Mg^{2+}, Co^{2+}, Ni^{2+}, UO_2^{2+}, HTO, Cs^+ and I^-. A positive correlation was observed between the D_e value in the granite and diffusivity in bulk solution (D_v) for most of the ions. However, an unexpectedly high D_e value was obtained for strontium accompanied with high distribution ratio. Based on this result, a model which takes into account contribution of both the surface and the pore diffusion was proposed for the sorbed species.

A through-diffusion experiment was performed for $^{85}Sr^{2+}$ to examine the effect of sorption on minerals on the diffusivity. The granite and the groundwater were obtained from 240-m level of Underground Research Laboratory (URL) of Atomic Energy of Canada Limited (AECL) in Manitoba, Canada. A fair amount of strontium was removed from the solution and was adsorbed on the granite, which corresponded to the sorption distribution ratio, R_d, of $0.091 - 0.180$ m^3 kg^{-1}. Nevertheless, R_d value assessed from the apparent diffusivity and the effective diffusivity was 0.0041 m^3 kg^{-1}. The contribution of the surface diffusion can explain this discrepancy; the retardation of the apparent diffusive transport is smaller than that predicted from the sorption R_d value because part of the adsorbed strontium is mobile in adsorbed state.

The effective diffusivity and distribution ratio of $^{133}Ba^{2+}$ in Inada granite have been determined by the through-diffusion method. Experiments were performed in triplicate for

0.1, 1, 10 and 10^2 mol m^{-3} BaCl$_2$ solution. The D_e value obtained for the BaCl$_2$ concentration of 10 mol m^{-3} agreed to the estimated value based on the pore diffusion model. The lower BaCl$_2$ concentration yielded the higher D_e value and higher R_d value than those for 10 mol m^{-3}. The variation in D_e was neither due to the speciation of barium in the solution nor variation in physical properties of the pore structure in the rock. Contribution of diffusion in adsorbed state should be responsible for the variation in D_e. The result is strongly indicative of the diffusion in adsorbed state.

The effective diffusivity of ^{125}I$^-$ was determined in Inada granite and in compacted bentonite by the through-diffusion method. The effective diffusivity of I$^-$ in compacted bentonite is smaller than the value estimated based on the pore diffusion model. This is because accessible pore space in the compacted bentonite is limited for anionic species due to electrostatic repulsion between the species and negatively charged surface of the pores. This was not the case for the diffusion of I$^-$ in the granite, where the size of the pore space is much larger than the range of the electrostatic repulsion so that the accessible pore space in the granite for anionic species is virtually the same as that for neutral and cationic species.

Effective diffusivities for uranium and plutonium, in Inada granite, of $(1.42\pm0.29)\times10^{-13}$ m^2 s^{-1}, and $(5.1\pm2.3)\times10^{-14}$ m^2 s^{-1}, respectively, have been obtained in a 10^2 mol m^{-3} NaHCO$_3$ solution at pH 9.3 where uranium is present predominantly as UO$_2$(CO$_3$)$_3^{4-}$. The effective diffusivity of UO$_2$(CO$_3$)$_3^{4-}$ in the granite was found to be four times larger than that of the uncomplexed UO$_2^{2+}$ obtained in 10^2 mol m^{-3} KCl at pH 4. The effective diffusivity of UO$_2$(CO$_3$)$_3^{4-}$ in the granite and the estimated bulk diffusivity of this species, $(6.6\pm0.4)\times10^{-10}$ m^2 s^{-1}, are consistent with an empirical correlation between D_e and D_v obtained in this study. The diffusivity of neptunium and plutonium in the granite was also studied by the through-diffusion method under reducing conditions in atmosphere-controlled chambers in which oxygen concentration was lower than a few ppm. A 10^3 mol m^{-3} NaHCO$_3$ solution was used in the neptunium experiment where neptunium is present as Np(CO$_3$)$_4^{4-}$ and Np(CO$_3$)$_5^{6-}$. A D_e value of $(4.0\pm1.5)\times10^{-13}$ m^2 s^{-1} and a rock capacity factor $(\varepsilon+\rho R_d)$ value of 0.15 ± 0.22 were obtained. A 10^2 mol m^{-3} NaHCO$_3$ solution was used in the plutonium experiment where plutonium is present predominantly as Pu(CO$_3$)$_2$(OH)$_2^{2-}$. A D_e value of $(2.0\pm1.4)\times10^{-13}$ m^2 s^{-1} and a $(\varepsilon+\rho R_d)$ value of 1.5 ± 0.7 were obtained. The effective diffusivities for Np and Pu were also considered to be consistent with the pore diffusion model. Another diffusion experiment for plutonium through granite from URL was performed using the groundwater obtained from the same location. Most of the Pu initially contained in the source reservoir was adsorbed on the granite and diffusion through 5×10^{-3}-m thick granite was not observed in the experimental period of 945 days. Enhancement of the diffusivity by surface diffusion was not observed even in the case that Pu was significantly adsorbed on granite. The contribution of the surface diffusion

is insignificant for actinide carbonate complexes which are adsorbed on the mineral surfaces through chemical reactions or surface complexation.

In order to predict the diffusing species of Pu, equilibrium constant for Pu(IV) carbonate complex species was determined and compiled in a database. Solubility of Pu(IV) was measured over a total carbonate concentration range of 10^{-4} to 10^{-1} mol kg^{-1}. The measured solubility was proportional to the square of the bicarbonate concentration at the pH range of 9.4 - 10.1. The equilibrium constant of

$$PuO_2 \cdot xH_2O + 2HCO_3^- = Pu(CO_3)_2(OH)_2^{2-} + xH_2O \qquad K=10^{-2.7\pm0.5}$$
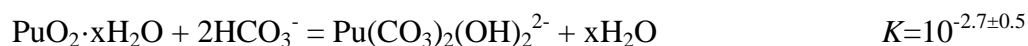
was obtained at ionic strength of 0.1 mol kg^{-1}. At pH 12 and 13 where carbonate ion is dominant, the equilibrium constant of

$$PuO_2 \cdot xH_2O + 2CO_3^{2-} = Pu(CO_3)_2(OH)_4^{4-} + (x-2)H_2O \qquad K=10^{-4.98\pm0.31}$$
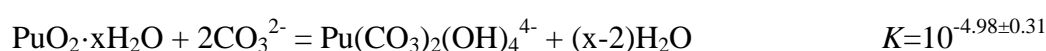
was obtained. Literatures were reviewed to compile equilibrium constant of formation of aqueous species and compounds for Np and Pu for the speciation of these elements.

Aqueous species including actinide complex species can diffuse into micro-pores in intact granites. The diffusivity can be higher than the value expected from the pore-diffusion model due to the contribution of the surface diffusion. Both the pore and the surface diffusion should be considered to predict diffusive behavior of radionuclides in geosphere and in engineered barrier system.

Contents

1. General introduction

1.1. Background

   After emplacement of high-level radioactive waste in a deep underground repository, long-lived radionuclides may be leached from the wastes and may subsequently be transported through the surrounding rock mass. One may not expect retardation capacity against radionuclide transport to the rock mass in Japan, where water-bearing fractures are frequently observed due to diastrophism. If the pores or micro fissures in the rock matrix are accessible to the radionuclides transported with groundwater through the fractures in the rock surrounding the repository, diffusion into the pores or micro fissures in the rock matrix and ensuing sorption onto mineral surfaces reduce the concentration of the nuclides transported through the geosphere (Neretnieks, 1980). Owing to this mechanism, frequently fractured rock mass in Japan may have considerable retardation capacity against the transport of radionuclides. To take the matrix diffusion into account in evaluating the migration of radionuclides in deep geologic formations for the safety assessment of the repository, it is essential to understand the mechanisms of the diffusion of radionuclides into the rock matrix and to quantify the diffusivity. Granite was used in this study because it occurs widely in Japan and is being considered as a potential host rock for the deep underground disposal of the high-level radioactive waste.

1.2. Previous studies

Neretnieks (1980) applied pore-diffusion model to the diffusion of ions in rock matrix that had been proposed for the diffusion in macro-porous media by Brakel & Heertjes (1974).

$$D_a = D_v \delta \tau^{-2}/(1 + \rho R_d/\varepsilon) = D_p/(1 + \rho R_d/\varepsilon) = D_e/(\varepsilon + \rho R_d) \qquad (1\text{-}1)$$

where D_v : diffusivity in bulk solution ($m^2\ s^{-1}$),

   δ : constrictivity of the pores (-)

   τ : tortuosity of the pores (-)

   ρ : bulk density of the rock ($kg\ m^{-3}$),

   R_d: distribution ratio ($m^3\ kg^{-1}$),

   ε : porosity of the rock (-),

   D_p : pore diffusivity ($m^2\ s^{-1}$).

D_a is an apparent diffusivity defined as

$$J = -D_a \partial C/\partial x \tag{1-2}$$

where J : diffusive flux (mol m^{-2} s^{-1} or Bq m^{-2} s^{-1})

           C : amount of a diffusing species in unit volume of porous material (mol m^{-3} or Bq m^{-3})

           x: length coordinate in diffusion direction (m)

D_e is an effective diffusivity or intrinsic diffusivity defined as

$$J = -D_e \partial c/\partial x \tag{1-3}$$

where c : concentration of diffusing species in pore water (mol m^{-3} or Bq m^{-3}).

In the pore-diffusion model, D_e is modeled as

$$D_e = D_v \varepsilon \delta \tau^{-2} \tag{1-4}$$

Many researchers investigated the apparent diffusivity or the effective diffusivity and discussed the applicability of Eq. (1-1) to the diffusion of sorbed species in rocks. Skagius & Neretnieks (1982) determined the effective diffusivity of cesium and strontium from the rate of sorption into pieces of granite, which were more than ten times higher than expected from the results of non-sorbed species and the electrical resistivity measurements. They interpreted the results as an effect of surface diffusion. Their determination of the effective diffusivity, however, was not very accurate due to incomplete attainment of the sorption equilibrium. Bradbury & Stephen (1986) performed the through-diffusion experiments for ^{85}Sr, ^{137}Cs and ^{95m}Tc in sandstone and found that the effective diffusivity of Sr was higher than that of iodide by 4-5 times. They suggested that a different diffusion mechanism or process may be occurring. Smith (1989) performed the through-diffusion experiments for ^{85}Sr, ^{137}Cs and ^{125}I in sandstone and found that the effective diffusivity of ^{85}Sr is higher than those of ^{137}Cs and ^{125}I by a factor of more than 6. Bradbury et al. (1986) performed the through-diffusion experiments for ^{85}Sr, ^{137}Cs and ^{95m}Tc in sandstone anhydrite and upper magnesian limestone and found that the diffusive transport was orders of magnitude higher than predicted from the pore-diffusion model. They mentioned that the results may be explained by a second diffusion mechanism, namely surface diffusion. Skagius & Neretnieks (1988) performed both the in-diffusion experiment and the through-diffusion experiment for cesium and strontium in biotite gneiss and found the diffusive transport was higher than expected from the pore diffusion model. They concluded that both the pore diffusion and the surface diffusion had to be included to interpret the experimental data. Tsukamoto & Ohe (1991) performed intraparticle diffusion experiments into crushed granite for cesium and strontium and determined the apparent diffusivity. They interpret the results taking both the surface and the

pore diffusion processes. Their determination of the apparent diffusivity, however, was not accurate because they used the crushed granite. Berry & Bond (1992) determined the effective diffusivity of HTO, iodide, cesium, strontium and americium in sandstone by the through-diffusion method and calculated the contribution of the surface diffusion to the effective diffusivity as 73 % for strontium and 62 % for americium. They concluded that evidence has been obtained for the apparent existence of the process of surface diffusion in the migration of strontium and americium, but not cesium, through the sandstone. Brace et al. (1965) and Ohlsson & Neretnieks (1998) suggested the existence of surface diffusion from electrical conductivity measurements. The evidence of the surface diffusion obtained from the electrical conductivity measurements is, however, quite indirect.

Several researchers observed higher diffusivity for strontium and cesium in rocks than expected from pore diffusion model using geometric parameters of the pores obtained for iodine. This comparison is insignificant because diffusivity of iodine in rocks may be reduced by electrostatic repulsion between iodide anion and negatively charged surface of the pores. Some researchers attributed the higher diffusivity for strontium and cesium in rocks to the contribution of the surface diffusion. The evidence of the surface diffusion, however, has not been provided. Systematic and careful data acquisition is necessary to prove the diffusivity in rock is higher than expected from the pore-diffusion model and to explain the reason.

Since the surface diffusion is driven by the gradient of the adsorbed species on the surface of the pores, it may enhance mass transfer of the actinides that is adsorbed on the mineral surfaces in rocks. Information on the contribution of the surface diffusion on the diffusivity of actinide in rocks is, however, scarce. Many attempts to determine the diffusivity of actinides in rocks were not successful (Torstenfelt et al., 1982; Muuronen et al., 1986; Sato et al., 1986; Berry et al., 1987; Triay et al., 1993; Puukko et al., 1993) because of low solubility and high sorption onto minerals. Several researchers determined apparent diffusivity of actinides in rocks (Ittner et al., 1988; Suksi et al., 1989; McKeegan et al., 1989 and Brink et al., 1991a and 1991b; Idemitsu et al., 1991, 1992 and 1993). The contribution of the surface diffusion can not be discussed based on these apparent diffusivity because estimation of the apparent diffusivity based on the pore-diffusion model requires distribution ratio of the actinides for intact rocks, which is not available. It is necessary to determine the effective diffusivity of the actinides in rocks from the through-diffusion experiment and to compare it with the value estimate from Eq. (1-4). Meier et al. (1988) and Berry et al. (1994) determined effective diffusivity of actinides in rocks by through-diffusion method. The contribution of the surface diffusion, however, cannot be discussed based on their data because extent of the contribution of the pore-diffusion on effective diffusivity is not known. Kumata et al. (1990) determined effective diffusivity of neptunium in granite by through-diffusion method. The contribution of the surface diffusion cannot be discussed based on their data because neptunium was in

pentavalent state and little adsorbed on the granite under the employed condition. Berry & Bond (1992) determined the effective diffusivity of HTO, iodide, cesium, strontium and americium in sandstone by the through-diffusion method and calculated the contribution of the surface diffusion to the effective diffusivity as 62 % for americium. This is the only experimental result that suggests the apparent existence of the surface diffusion in the diffusion of actinide in rocks. Their estimation of the contribution of the pore-diffusion based on the diffusivity of Am^{3+} in water, however, contains large error due to uncertainty in speciation of americium in aqueous solution. In order to investigate the contribution of the surface diffusion on the diffusion of actinides in rocks, the effective diffusivity should be determined by the through-diffusion experiment in a well-characterized rock under the conditions that the chemical speciation of the actinide is known.

1.3. Objective of this study

The objectives of this study are

- to characterize pore structure of a Japanese granite and to quantify the contribution of the pore-diffusion on effective diffusivity of sorbed species in the granite and to clearly present that the effective diffusivity of the sorbed species is higher than expected from the pore-diffusion model.

- to prove that the higher diffusivity of sorbed species in granite occurs under geological conditions by performing diffusion experiments under anoxic conditions using granite and groundwater obtained from deep underground.

- to provide a direct evidence of surface diffusion, which is an increase of diffusive flux with increasing distribution ratio for a cation in the Japanese granite.

- to determine the effective diffusivity for some actinide carbonate complexes and to clarify the contribution of the surface diffusion on the diffusion of actinides in rocks

- to compile a thermodynamic database for Np and Pu that is necessary for predicting their dominant diffusing species in granite pore water by literature review and experiments to obtain important lacking data for Pu(IV) carbonate complexes.

To achieve these objectives, the most satisfactory method of measuring diffusion of sorbed species in granite is through-diffusion experiments, in which steady-state diffusive flux is determined (Lever, 1986).

2. Microporous structures

2.1. Introduction

It is well-known that the Fick's diffusion law can be applied to the diffusion in porous materials.

$$J = -D_a \partial C/\partial x \qquad (2\text{-}1)$$

where J : diffusive flux (mol m^{-2} s^{-1} or Bq m^{-2} s^{-1})

D_a : apparent diffusivity (m^2 s^{-1})

C : amount of a diffusing species in unit volume of porous material (mol m^{-3} or Bq m^{-3})

x : length coordinate in diffusion direction (m)

When this theory is applied to the diffusion of ions in a rock, the pore size is assumed to be significantly larger than the diffusing ions. This assumption should be verified.

In order to understand the diffusivity of ions in rocks quantitatively and to discuss the contribution of the surface diffusion, porosity of the rock is one of essential parameters determining the effective diffusivity of ions in rock as shown in Eq. (1-4). It is, however, difficult to determine the porosity precisely for low-porosity rocks. Nishiyama et al. (1990) analyzed the pores for several kinds of rocks by water saturation method and mercury intrusion porosimetry. The total porosity of Inada granite determined by two methods differed by a factor of 2. The porosity of the rock must be determined as highly precisely as possible considering the critical role of the porosity in estimating the effective diffusivity of ions in the rock.

Agterberg et al. (1984) presented that the pore size distribution of a kind of granite was bi-modal. In such a case, theoretical understanding of the diffusivity in rocks is complicated (Wakao & Smith, 1962; Skagius & Neretnieks, 1986; Lever, 1986; Nishiyama et al., 1990). Knowledge on micro-porous structure in a rock is necessary before applying theories to the diffusion of ions in the rock.

The objectives of this chapter are to characterize pore structure of a granite and to examine the assumptions in applying the Fick's diffusion law to the diffusion of ions in the rock.

2.2. Experimental

The porosity, ε, was determined by water saturation for a granite from Inada, Ibaraki, eastern Japan and a granite obtained from an exploratory borehole, JE-2, that was drilled into the

rockmass surrounding the vertical fracture JZ 2 in the underground research Laboratory (URL) of AECL, in Manitoba, Canada. Although the technique has been commonly used to characterize pores in rocks, special cares are taken to analyze low-porosity rock precisely. The water saturation method uses water-saturated weight, submerged weight and dry weight of the rock samples to calculate the porosity. The errors accompanied in the measurements of the water-saturated weight often bring about significant errors in determination of the porosity. Analysis of drying curves of water-saturated weight enabled precise measurements of porosity. The method developed by Melnyk and Skeet (1986) was applied to a 5×10^{-3}-m thick, 4×10^{-2}-m diameter Inada granite disk and to a 5×10^{-3}-m thick 6.1×10^{-2}-m diameter URL granite disk. A granite disk was saturated with water under vacuum and then wiped with a piece of wet paper. The granite disk was suspended by a wire from a balance and enclosed by a plexiglass box to reduce air currents. A drying curve was obtained by correcting sample weights by a personal computer every minute for about 30 minutes until the sample was visually dry. The sample was then re-saturated with deionized water and another drying curve was obtained. Three drying curves were obtained for each sample. After plotting a drying curve, the water-saturated but surface-dry weight, W_s, was obtained from the point of intersection of the initial and final straight-line portions as described by Melnyk and Skeet (1986). The W_s values obtained from the 3 drying curves were averaged.

The sample was saturated with deionized water again, placed on a hanger suspended under the balance and immersed in a vessel containing deionized water. A small jack under the vessel was used to bring the water level to a reference mark on the hanger. The weight was corrected for the weight of the hanger immersed to the same reference mark to obtain the submerged sample weight, W_u. The determination was repeated 3 times and the results were averaged.

After the sample was dried at 105 °C for 20 days in an oven, the sample was equilibrated with laboratory air for about 1 hour, and then weighed. This sequence was repeated 3 times and the results were averaged to give the dry weight, W_d. The porosity of the sample was obtained from

$$\varepsilon = V_p \,/\, V_r = (W_s \text{ - } W_d) \,/\, (W_s - W_u) \qquad\qquad (2\text{-}2)$$

where V_p : volume of the pore space in the granite sample (m^3),

   V_r : bulk volume of the granite sample (m^3).

The uncertainties were propagated from the weight measurements to the porosity. The measurement were performed for 4 Inada granite samples, D1, D2, D3 and D4, and 7 URL granite samples, F1, F4, F7, F10, F11, G1 and G2. For several samples, the saturated weight was obtained by weighing the water-saturated sample immediately after wiping the surfaces with a damp cloth for comparison.

After the porosity measurement by water saturation, an Inada granite sample, D2, was cut into 5 segments whose dimensions were around 5×10^{-3} m x 1×10^{-2} m x 2.5×10^{-2} m by a diamond saw (ISOMET Low Speed Saw, BUEHLER). Sharp points on the edges of the pieces were removed by a piece of carborundum paper. The mercury intrusion porosimetry was applied to these segments to determine the pore size distribution. In the mercury intrusion porosimetry, a major part of the error in the porosity determination is due to rough surfaces of the sample. The rock sample was cut into rectangular parallelepipeds by diamond low-speed saw, instead of crushing, to reduce the surface roughness. The detection limit of the mercury intrusion is also a cause for the error for low-porosity samples. Five samples whose total volume was 6×10^{-6} m^3 were simultaneously put in the measurement cell of the porosimeter to increase the amount of intruding mercury. A mercury porosimeter, Pore sizer 9310 (micromeritics), was used. The pressure range was $(0.1 - 207) \times 10^6$ N m^{-2}, which corresponded to the pore-diameter range of 10,000 - 6 nm. The minimum detectable amount of mercury intruded in the sample was 1.08×10^{-10} m^3. Another Inada granite sample, D4, and a URL granite sample, G1, were cut into small pieces with the same dimension and used for porosity determination by mercury intrusion. Inada granite core was crushed and 10 segments whose total weight was about 5 g were picked up and analyzed for comparison. As described in detail by Katsube & Hume (1987), the pressure required to force mercury into the pores is correlated with the pore-diameter by the following equation assuming that the pores are cylindrical:

$$D = -4\gamma\cos\theta / p \qquad\qquad (2\text{-}3)$$

where D : diameter of the pores (m),

γ : surface tension of mercury (0.48 N m^{-1}),

θ : contact angle (139°, Good & Mikhail, 1981),

p : pressure (N m^{-2}).

The pore structure of Inada granite was observed by SEM (S-650, Hitachi, Super Scan 330 FEG, Shimadzu) after depositing carbon on the surfaces. A 4.0×10^{-2}-m diameter, 5×10^{-3}-m thickness Inada granite sample was cut into 4 fan-shaped segments with a diamond low-speed saw. One of the segments was polished up to No. 6000 on a glass plate and up to 1/4 μm diamond paste on a nylon buff. Care was taken to keep the surface flat and to prevent the sample from cracking. The surface was cleaned and observed by optical microscope in each step of polishing to obtain good polished surfaces for contacting parts of minerals and for cleavable mica and feldspar.

2.3. Results and discussion

The saturated weight, W_s, of the disk was determined based on the following weight changes due to drying as a function of time as shown in Fig. 2-1. Three W_s values obtained from the triplicate measurements were almost identical and averaged to obtain the W_s value tabulated in Table 2-1. The saturated weights obtained by weighing the water-saturated sample immediately after wiping the surfaces with a damp cloth were shown in parenthesis in Table 2-1. These measurements overestimated the W_s value by 10-15 mg, which lead to an overestimation of the porosity by 0.002. Submerged weights of the samples were determined as an average of triplicate measurements as shown in Table 2-1. Figure 2-2 shows the weight change of a sample while dying at 105 °C. The weight change becomes negligibly small after 19 days, which indicates complete dryness. Figure 2-3 shows the weight change of a dried sample equilibrated with laboratory humidity. The weight change becomes negligibly small after 1 hour, which indicates that the outer surface of the sample was equilibrated with the laboratory humidity. The W_d value was determined as an average of triplicate measurements and shown in Table 2-1. The porosity of each sample was determined from W_s, W_u and W_d by Eq. (2-2) and shown in Table 2-1. The porosity of Inada granite sample was determined to be (0.49±0.07) % as an average of the results for 4 samples. The porosity of URL granite sample was determined to be (0.40±0.10) % as an average of the results for 7 samples.

The results of the mercury intrusion porosimetry for the cut Inada granite samples and for the crushed ones were compared in Fig. 2-4. No difference was observed between 2 samples in the partial porosity obtained in the pore diameter range smaller than 400 nm. The differences observed in the pore diameter range larger than 400 nm is due to the differences in the roughness of the sample surfaces. Mercury intruded into cavities on the sample surfaces was counted. The results of the mercury intrusion porosimetry were shown in Table 2-2 and in Fig. 2-5 with literature data for Lac du Bonnet granite (Agterberg et al., 1984). The pore-size distribution of the granite was nearly logarithmic normal with the modal diameter of 160 nm for Inada granite and 340 nm for URL granite. The bi-modal distribution that had been typically observed for Lac du Bonnet granite was not seen in the present measurements. Total porosity determined by mercury intrusion agrees with the value that had been determined by water saturation. The specific surface areas were determined to be 70 m^2 kg^{-1} for Inada granite and 20 m^2 kg^{-1} for URL granite.

Figure 2-6 shows the optical microscope images of the polished surface. In SEM image for the polished surface, pores of a few tens – a few hundreds nm wide were observed. A typical image was shown in Fig. 2-7. In this figure, pores of 100 nm wide were observed between quartz and other minerals. In plagioclase, pores of several tens nm in width were observed as shown in Fig. 2-7.

2.4. Conclusion

The water saturation method and the mercury intrusion porosimetry were applied to the characterization of micropores in granite. Although these techniques have been commonly used to characterize pores in rocks, special cares should be taken for precise measurement of the porosity and the pore size of low-porosity rocks. In the water saturation method, analysis of drying curves of water-saturated weight enabled precise measurements of porosity. In the mercury intrusion porosimetry, a major part of the error due to rough surfaces of the sample can be reduced by cutting the samples into rectangular parallelepipeds, instead of crushing. The volume of the rock sample put into the measurement cell of the mercury porosimeter should be optimized. The porosity of Inada granite was determined to be (0.49 ± 0.07) % with the modal diameter of 160 nm. The micropores of a few tens to a few hundred nanometers in width were observed by SEM. The URL granite had the porosity of (0.40 ± 0.10) % and the modal diameter of 340 nm. When the Fick's diffusion law is applied to the diffusion of ions in rocks, the pore size is assumed to be significantly larger than the diffusing ions. The assumption was confirmed for Inada granite and for URL granite. Since the pore size was found to be uniform, the contribution of the pore-diffusion to the effective diffusivity of ions in the granite can be estimated precisely based on the porosity of the granite obtained in this chapter.

Table 2-1 Saturated weight, submerged weight and dry weight for the Inada granite and for URL granite samples, and their porosity.

Sample No.	Saturated weight, W_s (10^{-3} kg)	Submerged weight, W_u (10^{-3} kg)	Dry weight W_d (10^{-3} kg)	Pore volume[a] V_p (10^{-6} m^3)	Rock volume[b] V_r (10^{-6} m^3)	Porosity[c] ε (%)
Inada						
D1	16.811±0.002 (16.826)[d]	10.428±0.002	16.778±0.001	0.033±0.002	6.383±0.002	0.52±0.03
D2	16.822±0.001 (16.834)[d]	10.446±0.002	16.789±0.001	0.033±0.002	6.376±0.002	0.51±0.03
D3	15.915±0.002 (15.925)[d]	9.882±0.001	15.887±0.001	0.028±0.002	6.033±0.002	0.46±0.04
D4	16.437±0.003 (16.451)[d]	10.222±0.001	16.407±0.001	0.030±0.003	6.215±0.003	0.48±0.05 av. 0.49±0.07
URL						
F1	33.561±0.001	20.866±0.003	33.522±0.001	0.039±0.001	12.696±0.003	0.31±0.01
F4	32.858±0.001	20.426±0.003	32.802±0.001	0.056±0.001	12.431±0.003	0.45±0.01
F7	35.920±0.001	22.319±0.006	35.861±0.001	0.059±0.001	13.600±0.006	0.43±0.01
F10	35.423±0.001	22.020±0.002	35.365±0.001	0.059±0.001	13.403±0.003	0.44±0.01
F11	35.204±0.003	21.874±0.003	35.148±0.001	0.056±0.003	13.330±0.004	0.42±0.02
G1	61.134±0.002	37.932±0.007	61.044±0.001	0.090±0.002	23.202±0.007	0.39±0.01
G2	32.920±0.001 (32.981)[d]	20.452±0.004	32.877±0.001	0.043±0.001	12.468±0.004	0.34±0.01 av. 0.40±0.10

a: $V_p = (W_s - W_d)/\rho$, ρ : density of water (1.00x10^3 kg m^{-3})
b: $V_r = (W_s - W_u)/\rho$
c: $\varepsilon = V_p/V_r$
d: W_s values in parentheses were obtained by weighing the water-saturated granite sample immediately after wiping the surface water with damp cloths.

10

Table 2-2 Pore size distribution for Inada granite and URL granite obtained by mercury intrusion and lieterature data for Lac du Bonnet granite.

Pore diameter (10^{-9} m)	Partial porosity (%)				
	Inada granite		URL granite		Lac du Bonnet granite *
	A	B	C	D	E
6.3 - 10.0	0	0	0	0	0
10.0 - 15.8	0	0	0	0	0
15.8 - 25.1	0	0.001	0	0	0
25.1 - 39.8	0.020	0.019	0	0	0.029
39.8 - 63.1	0.045	0.051	0.004	0.004	0.043
63.1 - 100	0.080	0.070	0.015	0.017	0.063
100 - 158	0.102	0.095	0.033	0.033	0.063
158 - 251	0.106	0.102	0.050	0.048	0.037
251 - 398	0.087	0.072	0.068	0.066	0.029
398 - 631	0.046	0.034	0.059	0.068	0.027
631 - 1000	0.017	0.018	0.043	0.061	0.037
1000 - 1585	0	0.008	0.032	0.049	0.024
1585 - 2512	0	0.004	0.021	0.030	0.055
2512 - 3981	0	0.003	0.017	0.019	0.047
3981 - 6310	0	0	0.014	0.014	0.037
6310 - 10000	0	0	0.010	0.012	0
10000 - 15850	-	-	-	-	0.003
15850 - 25120	-	-	-	-	0.003
Total porosity	0.503	0.477	0.366	0.421	0.496

* average of ten samples (Agterberg et al., 1984)
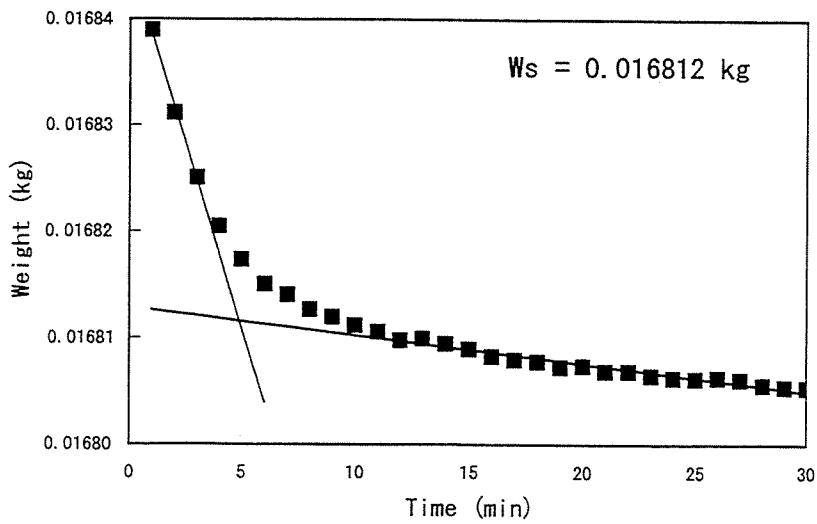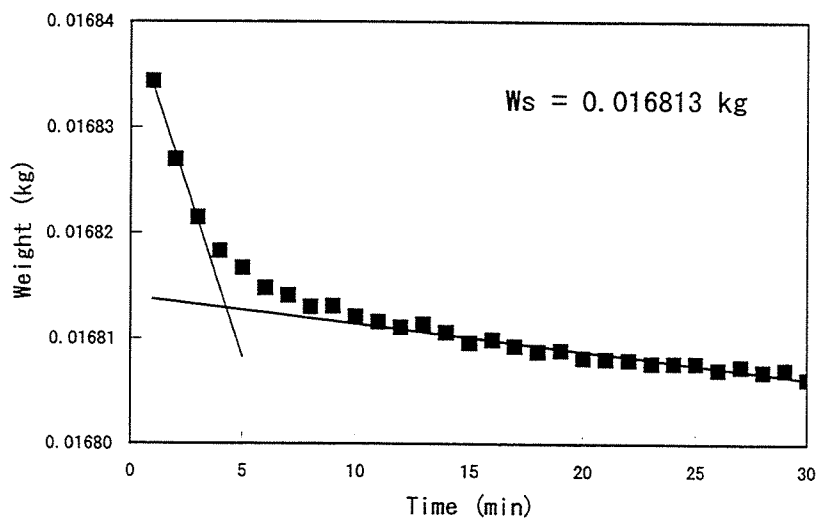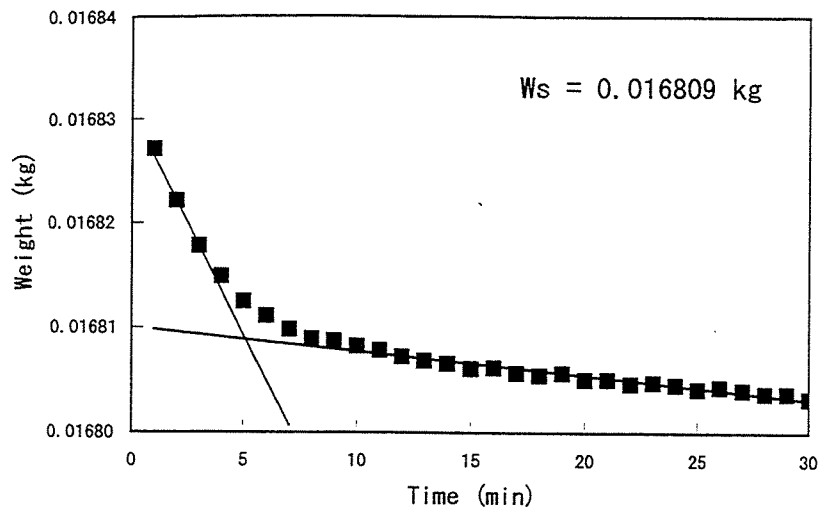
Fig. 2-1 Drying curve of granite disk in saturated weight determination.
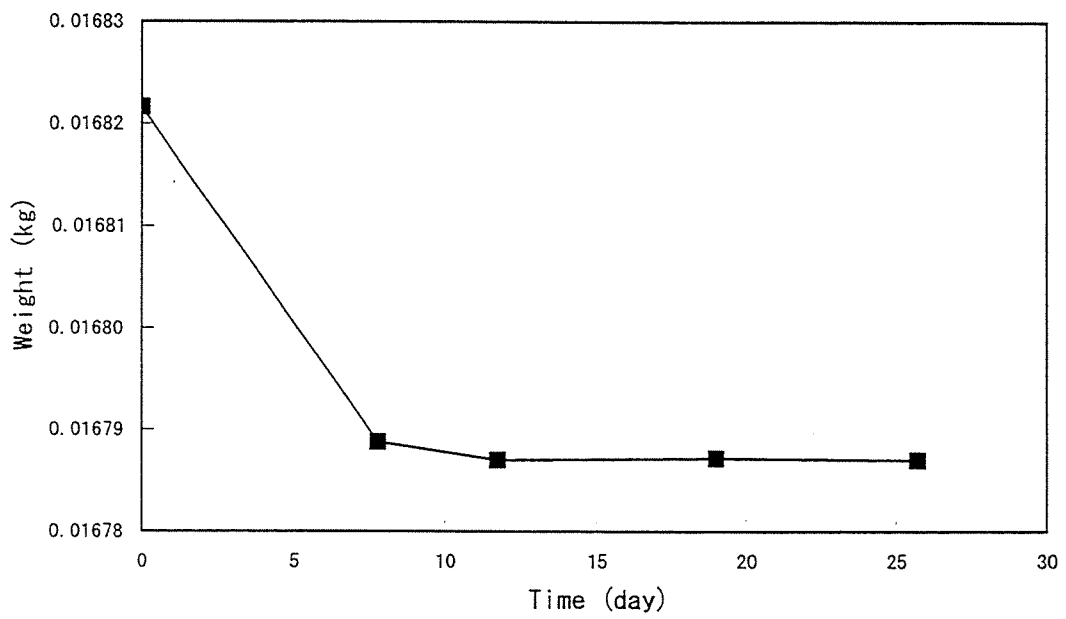
Fig. 2-2   Drying curve of granite disk in dry weight determination.
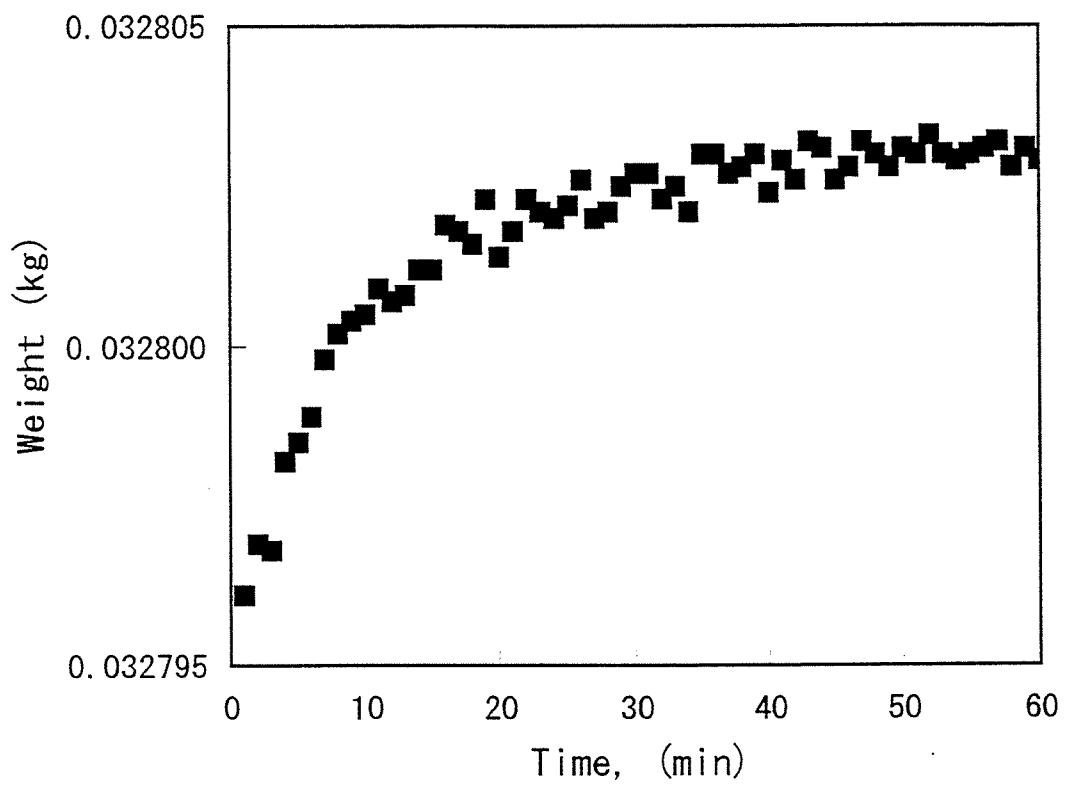
Fig. 2-3 Weight gain curve of a granite disk equilibrated with laboratory air.
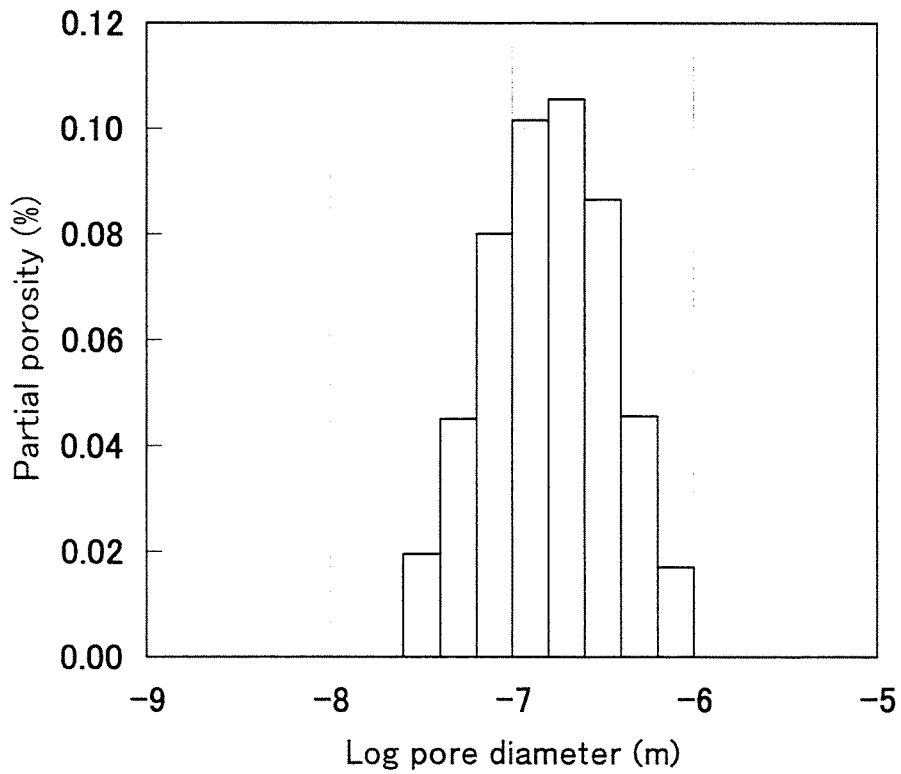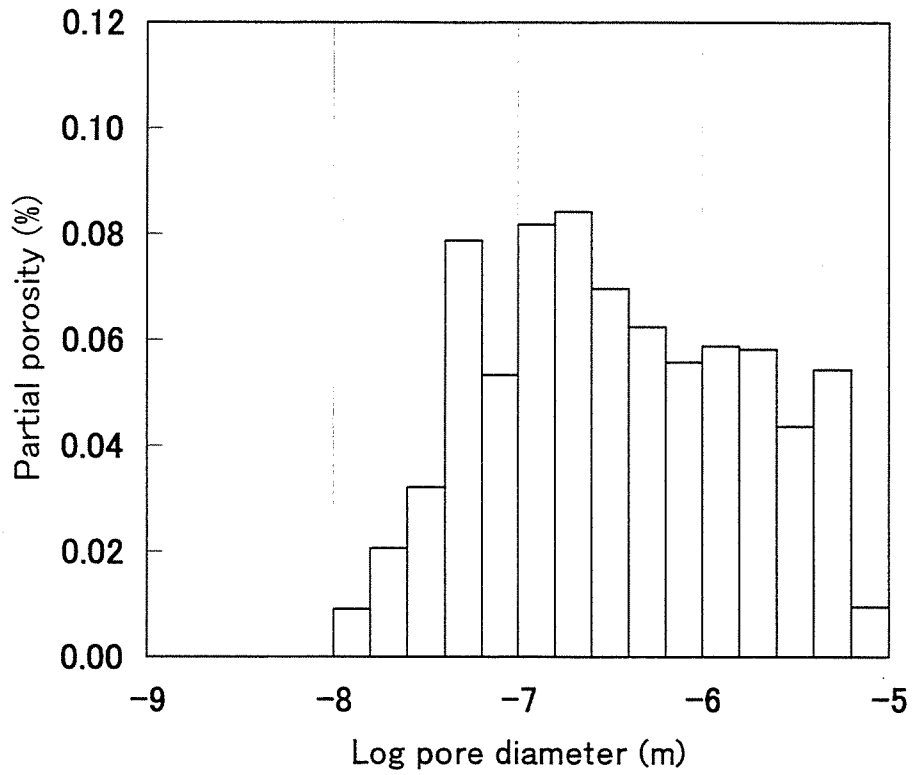
Fig. 2-4   Pore size distribution obtained for crushed granite segments (upper) and for granite
samples cut smoothly with a diamond low-speed saw (lower).
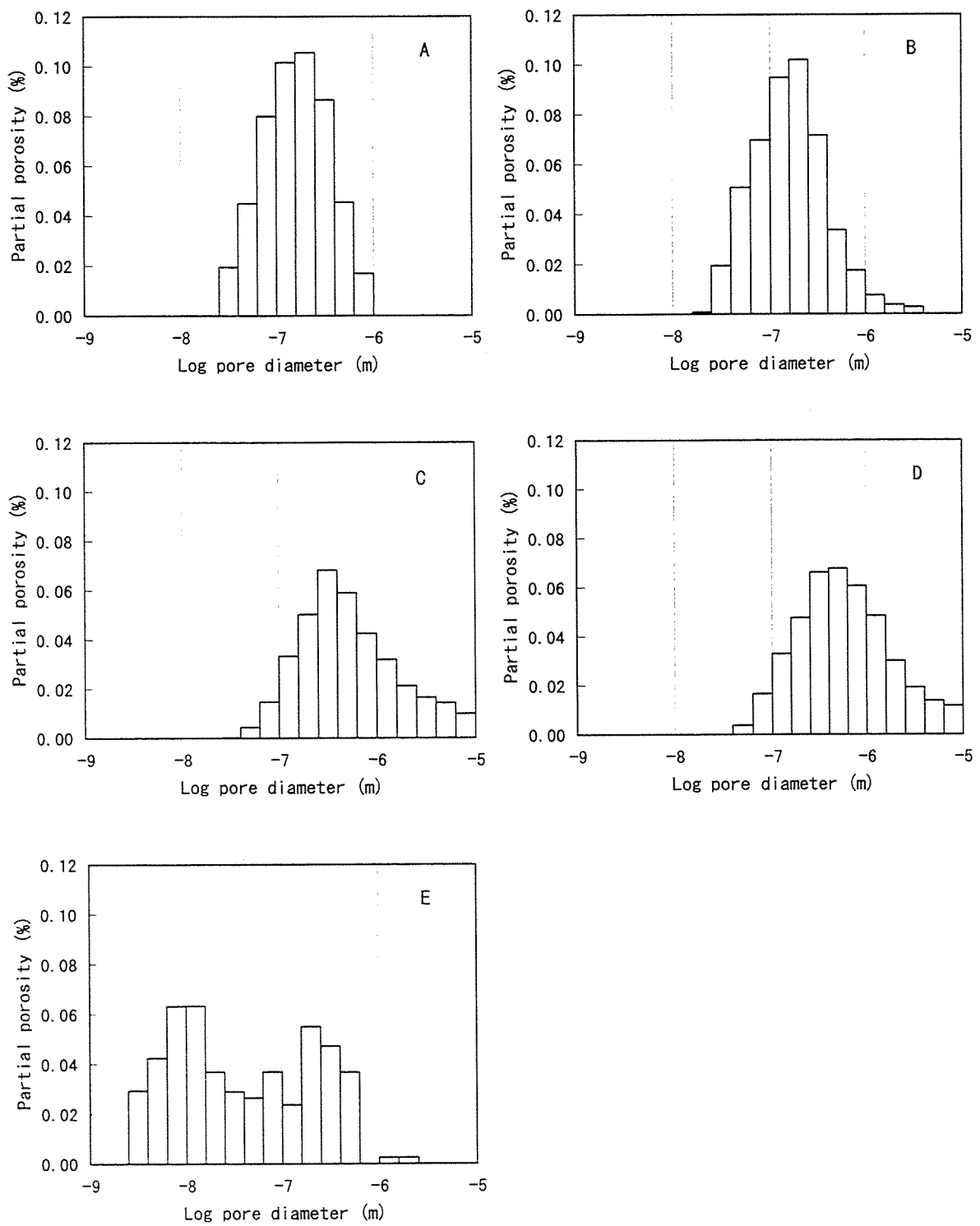
Fig. 2-5 Pore size distribution for Inada granite (A, B), URL granite (C, D) and Lac du Bonnet granite (E: Agterberg et al., 1984).

16
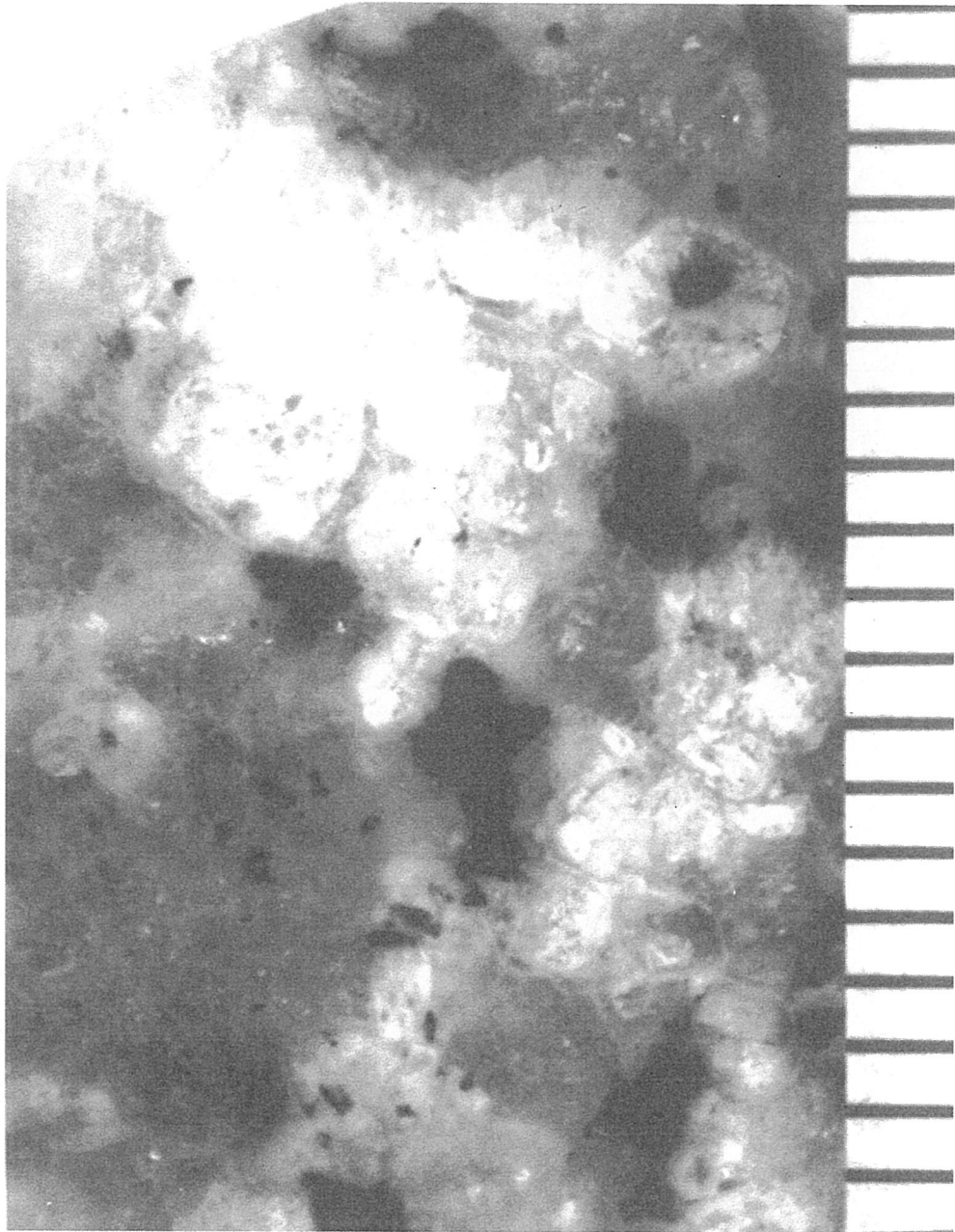
Fig. 2-6 Optical image of Inada granite. The interval of the minimum scale is 0.5 mm.
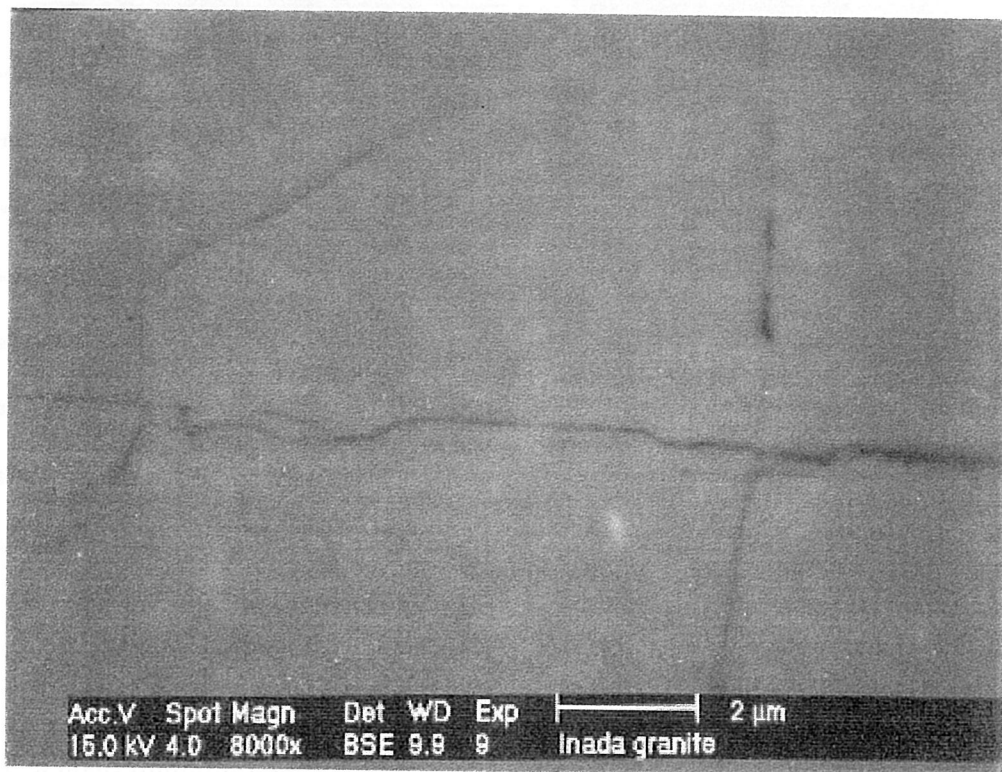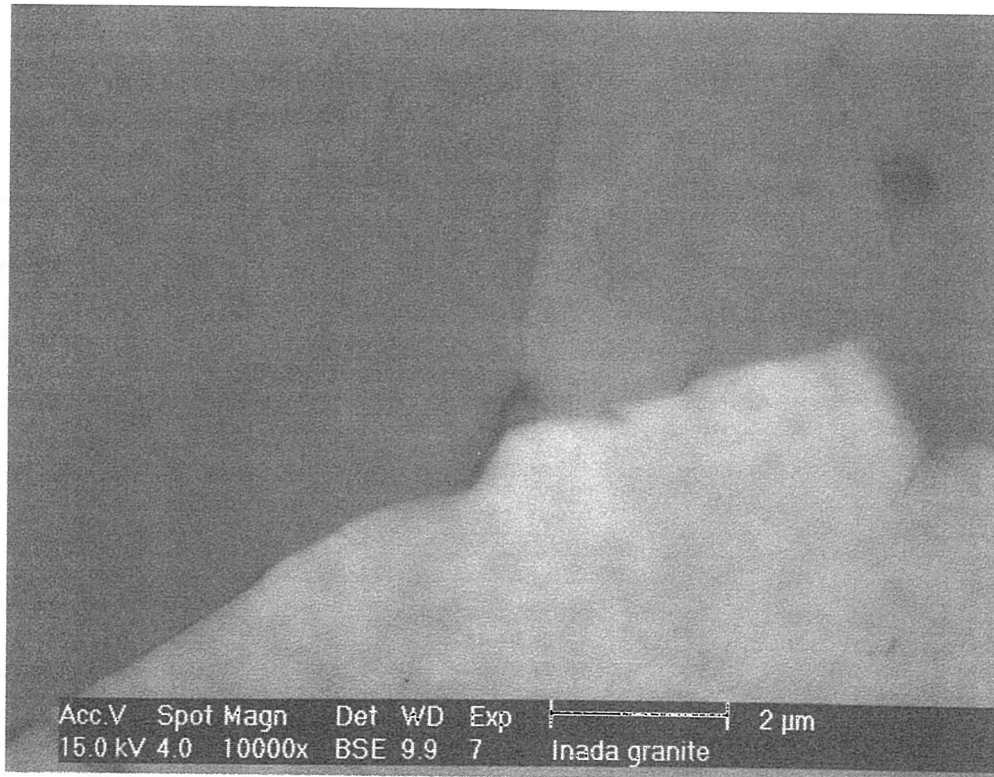
Fig. 2-7   SEM images of Inada granite

3. Relationship between D_e and D_v

3.1. Introduction

Radionuclide migration analysis has to deal with concentration of radionuclides in pore water, c (mol m^{-3} or Bq m^{-3}), while Eq. (2-1) dealing with amount of a diffusing species in unit volume of porous material, C. Correlation between C and c is given as:

$$C = \varepsilon c + \rho R_d c \qquad (3-1)$$

where ε : porosity of the rock (-),

ρ : bulk density of the rock (kg m^{-3}),

R_d : distribution ratio (m^3 kg^{-1}).

Combining Eq. (3-1) with Eq. (2-1), diffusion equation for the concentration of radionuclides in pore water is obtained.

$$J = -D_a(\varepsilon + \rho R_d)\, \partial c/\partial x \qquad (3-2)$$

The terms $\varepsilon + \rho R_d$ and $D_a(\varepsilon + \rho R_d)$ are often called rock capacity factor and effective diffusivity, D_e (or intrinsic diffusivity, D_i), respectively.

$$J = -D_e \partial c/\partial x \qquad (3-3)$$

The effective diffusivity of an aqueous species through the interconnected pore space in a rock matrix is often assumed to be proportional to its diffusivity in bulk solution (D_v) and to the geometric parameters of the rock: ε (porosity), δ (constrictivity) and τ^{-2} (τ: tortuosity) (Neretnieks, 1980; Skagius and Neretnieks, 1982; 1986; 1988; Nishiyama et al., 1990; Kumata et al., 1990; Tsukamoto and Ohe, 1991; Idemitsu et al., 1992).

$$D_e = D_v \varepsilon \delta \tau^{-2} \qquad (3-4)$$

This relationship has been proposed for diffusion in macro-porous media by Brakel and Heertjes (1974), and has been applied to the diffusion in rock matrix by Neretnieks (1980). Although it is convenient to use this relationship to describe diffusion in rock, it is very difficult to verify the relationship because of micro-inhomogeneity of intact rock. Nishiyama et al. (1990) measured the effective diffusivity of Γ in various rocks and investigated the proportional relationship between D_e and ε. They found that D_e was roughly proportional to ε. They also suggested that the term $\delta\tau^{-2}$ was approximately expressed as $3 \times 10^{-3}\varepsilon^{0.3}$. Equation (3-4) states the proportional relationship between D_e and D_v, but this has not been verified. The objective of this chapter is to examine the relationship between D_e and D_v.

3.2. Experimental

Preparation

The rock used in this study was Inada granite, whose chemical and mineral compositions are shown in Table 3-1 (Idemitsu et al., 1992; Yamaguchi et al., 1993). A granite core having a diameter of 4.0×10^{-2} m was cut to 5×10^{-3} m thickness with a diamond saw. Granite disks without visible cracks were used in the experiments.

The method described by Garrel et al. (1949) was modified in this study. The acrylic diffusion cell used in this study is shown in Fig. 3-1. A granite disk was fitted tightly into the central part of the cell and any gap between the rock disk and the acrylic were filled with a silicone gasket. The central support member containing the granite disk was sandwiched between the two reservoirs, each with a capacity of 1.16×10^{-4} m^3. The assembled diffusion cell was soaked in the solution to be used in the diffusion experiments under vacuum to evacuate all air from the interconnected pores in the granite. The diffusion cell was then kept under atmospheric pressure for 30 days to pre-condition the granite disk with the solution at the same pH. Solutions were prepared from reagent grade chemicals (Wako Pure Chemical Industries, Ltd., Tokyo) and deionized water (Milli-Q Labo System, Millipore).

Series 1

The 1st series of experiments was performed to measure effective diffusivity of Ba^{2+}, Sr^{2+}, Mg^{2+}, Co^{2+} and Ni^{2+} in the granite. The source solution was prepared by dissolving $Ba(NO_3)_2$, $Sr(NO_3)_2$, $MgCl_2$, $CoCl_2$, $NiCl_2$ and KCl powders in deionized water to get the concentration of 10^2 mol m^{-3} for each metal ion. The pH of the solution was adjusted to 4.0 with dilute KOH to prevent hydrolysis, carbonate complexation and precipitation of the metal ions. The diffusion experiment was started by placing the source solution in one reservoir (source reservoir) and 10^2 mol m^{-3} KCl solution in the other (measurement reservoir). The experiment was sextupled using granite disks: B3, B6, B9, B10, B19 and B21 at 25°C in a water bath. Two milliliters aliquot of the solution was taken from the measurement reservoir at 10 days intervals. The concentrations of the tracers in the solutions were determined by inductively coupled plasma (ICP) emission spectrometry.

Series 2

In the 2nd series of experiments, the effective diffusivities of Sr^{2+} in the granite were measured. The source solution was prepared by dissolving $Sr(NO_3)_2$ powders in deionized water to get the concentration of 10^2 mol m^{-3} for Sr^{2+}. The pH of the solution was 5.5. The diffusion experiment was started by placing the source solution in the source reservoir and deionized water in the measurement reservoir. The experiment was triplicated at room

temperature. Sampling and the concentration measurement were performed as the same manner as those in the 1st series of experiments.

Series 3

In the 3rd series of experiments, the effective diffusivities of UO_2^{2+} in the granite was measured. Uranium-233 was chemically purified by anion exchange and prepared as a 8.9×10^{-1} mol m^{-3} solution in 10^3 mol m^{-3} HCl. The source solutions for the diffusion experiments were prepared by adding a 3×10^{-6} m^3 volume of the stock solution to 3.45×10^{-4} m^3 volume of 10^2 mol^{-3} KCl in a polypropylene bottle. The pH was adjusted to 4.0 with dilute KOH. The concentration of uranium in the source solution was 7.7 mol m^{-3}. The diffusion experiments were started by placing the source solution in the source reservoir and an equal volume of the 10^2 mol m^{-3} KCl solution at pH 4.0 in the measurement reservoir. Experiments were performed in triplicate using granite disks: B11, B14 and B16 at room temperature (20 - 25 °C). At 10 days intervals, a 5×10^{-8} m^3 aliquot was taken from the measurement reservoir and diluted to prevent the salt from interfering with α-spectrometry of the samples. A 5×10^{-8} m^3 aliquot of the diluted sample solution was evaporated on a stainless steel planchet and its activity determined by α-spectrometry.

Series 4

In the 4th series of experiments, the effective diffusivity of water in the granite was measured using tritiated water as a tracer. Concentration of ^{3}H in the water stock solution was 8.34×10^{11} Bq m^{-3}. After the granite disk was soaked in deionized water under vacuum for a couple of days to evacuate all air from the interconnected pores, the diffusion experiment was started by adding 1.25×10^{-7} m^3 of tritiated water stock solution into the source reservoir. The concentration of ^{3}H in the solution in the source reservoir was planned to be 8.62×10^8 Bq m^{-3}. To make sure the concentration of ^{3}H in the source solution, 1×10^{-7} m^3 aliquot was withdrawn and its activity determined by liquid scintillation counter, TRI-CARB 2550 TR/AB, Packard. The pH of the solution was 5.5. The experiment was triplicated using granite disks: D4, D7 and D9 at (25.0 ± 0.5)°C in a water bath. At 7 days intervals, 1×10^{-6} m^3 aliquot was taken from the measurement reservoir and mixed with a 3×10^{-6} m^3 volume of liquid scintillation cocktail to determine its radioactivity by the liquid scintillation counter. The 1×10^{-6} m^3 aliquot removed from the measurement reservoir was replaced by an equal volume of the deionized water to maintain the water levels in the two reservoirs.

Series 5

In the 5th series of experiments, the effective diffusivity of Cs$^+$ and I$^-$ in the granite was measured using ^{134}Cs and ^{125}I as tracers. Stock solution of ^{134}Cs was prepared as a 1.62×10^{13} Bq m^{-3} solution in 10 mol m^{-3} HCl. Stock solution of ^{125}I was prepared as a 3.24×10^{13} Bq m^{-3} solution in NaI/Na$_2$S$_2$O$_3$ solution in which the concentrations of I$^-$ and S$_2$O$_3^{2-}$ were 3.3×10^{-1}

and 3.2×10^{-1} mol m^{-3}, respectively. After completing the 4th series of experiments, the solution in the diffusion cell D9 was replaced by a 10^2 mol m^{-3} KI solution. After pre-conditioning the granite disk with the 10^2 mol m^{-3} KI for 30 days, the solution in both reservoirs was replaced by fresh 10^2 mol m^{-3} KI solution, and a 1×10^{-8} m^3 portion of the ^{125}I stock solution and the same volume of the ^{134}Cs stock solution were added to the source reservoir to start the diffusion experiment. The pH of the 10^2 mol m^{-3} KI solution was 6.0. The experiment was performed at 25°C in a water bath. At 7 days intervals, 1×10^{-6} m^3 aliquot was taken from the measurement reservoir and its γ–radioactivity determined by pure Ge detector.

Sampling and analysis

The aliquot removed from the measurement reservoir was replaced by an equal volume of blank solution to maintain the balance of the water levels between the two reservoirs. This balancing avoids occurrence of pressure difference that leads to advective transport from the source to measurement reservoir. The concentration of tracers in the source reservoir was also determined periodically. At the termination of each experiment, the inner wall of the measurement reservoir was rinsed with 10^4 mol m^{-3} HCl to determine the amount of the tracers adsorbed on the cell walls. The amount of the adsorbed tracer was found to be less than 3 % of the final inventory in the measurement reservoir and can be ignored. The statistical error of the determination of the tracer concentration was 3 - 14 % in radioactivity measurement and 5 % in ICP-AES.

3.3. Data analysis

The rate of change of concentration of an ion in pore water due to diffusion in one-dimensional system is derived from Eq. (3-3) as:

$$(\varepsilon + \rho R_d)\partial c/\partial t = D_e \partial^2 c/\partial x^2 \tag{3-5}$$

The initial and boundary conditions are

$$c(x, 0) = 0 \quad \text{at } 0 < x \leqq L \tag{3-6}$$

$$c(0, t) = c_1 \tag{3-7}$$

$$c(L, t) = c_2 << c_1, \tag{3-8}$$

where L : thickness of the rock sample (m),

c_1 : concentration of a species in the source reservoir (mol m^{-3} or Bq m^{-3}),

c_2 : concentration of a species in the measurement reservoir (mol m^{-3} or Bq m^{-3}).

The solution of Eq. (3-5) had been given by Crank (1975). The concentration of a species in

the measurement reservoir after a long period is approximated as:

$$c_2(t)/c_1 = AV_2^{-1}(D_e L^{-1}t - (\varepsilon+\rho R_d)L/6)$$
(3-9)

where   A : cross section of the sample (m^2),

V_2 : volume of the measurement reservoir (m^3).

D_e and $(\varepsilon+\rho R_d)$ were determined from the slope and the intercept on the concentration axis of the extrapolated linear region of a diffusion curve.

3.4. Results

Figures 3-2a – 3-2e show the time dependence of the concentrations of Ba, Sr, Mg, Co and Ni in the measurement reservoirs from the 1st series of experiments. The concentrations increase linearly with time after 10 days. The effective diffusivity and the rock capacity factor were determined by the least squares fitting and are presented in Table 3-2 together with literature data.

Figure 3-3 shows the time dependence of the concentration of Sr in the measurement reservoirs from the 2nd series of experiments. Larger differences in concentration are observed between multiple diffusion run than those observed in the 1st series of experiments, which may be due to absence of coexisting cations. The portion of the diffusion curve where the concentration of Sr increased linearly with time was found for each diffusion run and fitted to the Eq. (3-9) by least squares to determine the effective diffusivity and the rock capacity factor as shown in Table 3-2.

Figure 3-4 shows the time dependence of the uranium concentration in the measurement reservoir from the 3rd series of experiments. The uranium concentrations increased linearly with time after 50 days. The effective diffusivity and the rock capacity factor were determined by the least squares fitting and are presented in Table 3-2 together with literature data. In aerated solutions, the dominant oxidation state of uranium is hexavalent. Speciation of uranium was calculated using the stability constants of the hydrolysis species expected to be present around pH 4 that are shown in Table 3-3. Complexation of UO_2^{2+} at pH 4 by chloride and by carbonate is negligible (Grenthe et al., 1992). The calculation shows that the uranium concentration in solution is limited by precipitation of $UO_2(OH)_2 \cdot H_2O$ above pH 6. In the present study, the uranium concentration in the source reservoir remained virtually constant as shown in Fig. 3-4, which suggests no significant removal of uranium by precipitation and/or sorption on reservoir walls. More than 93 % (96±3 %) of the uranium was calculated to be present as UO_2^{2+} throughout the experiment although the pH of the solution had increased to 4.1 by the end of the experiment. The average D_e value obtained in this experiment was

$(3.6\pm1.6)\times10^{-14}$ m^2 s^{-1} for the triplicate experiments. This value is close to that for uranine, but one order of magnitude lower than those obtained for Sr^{2+} and NpO$_2^+$, and two orders of magnitude lower than that obtained for I$^-$. The effective diffusivity differs significantly between UO$_2^{2+}$ and NpO$_2^+$, although they have similar ionic structures.

Figure 3-5 shows the time dependence of the concentration of ^{3}H in the measurement reservoirs from the 4th series of experiments. The concentrations increase linearly with time. The effective diffusivity and the rock capacity factor were determined by the least squares fitting and are presented in Table 3-2.

Figure 3-6 shows the time dependence of the concentrations of ^{134}Cs and ^{125}I in the measurement reservoir from the 5th series of experiments. The concentrations increase linearly with time. The effective diffusivity and the rock capacity factor were determined by the least squares fitting and are presented in Table 3-2.

3.5. Discussion

In order to check the validity of the constant proportionality between D_e and D_v assumed in Eq. (3-4), D_v's for the diffusing species under the experimental conditions were estimated by taking into account mode of diffusion (Li and Gregory, 1974) (salt diffusion or tracer diffusion), concentration of the diffusing species and ionic strength of the solution and temperature. The diffusion of metal ions in the 1st series of experiments is considered to be not tracer-diffusion but salt-diffusion. The diffusivities of BaCl$_2$, SrCl$_2$, MgCl$_2$, CoCl$_2$ and NiCl$_2$ at infinite dilution were given as 1.38×10^{-9}, 1.33×10^{-9}, 1.25×10^{-9}, 1.25×10^{-9}, and 1.25×10^{-9} m^2 s^{-1}, respectively by Li and Gregory (1974). The diffusivity of the metal ions in bulk of the working solution is reduced by 17 % from the value at infinite dilution due to concentration of the metal ion itself (Robinson & Stokes 1955). The uncertainty on D_v due to ionic strength of the working solution are estimated to be 3% based on the difference between the CaCl$_2$ diffusivity in a 5×10^2 mol m^{-3} solution and that in a 10^2 mol m^{-3} solution (Robinson & Stokes 1955). The D_v of Ba^{2+}, Sr^{2+}, Mg^{2+}, Co^{2+} and Ni^{2+} under the condition was estimated to be $(1.15\pm0.03)\times10^{-9}$, $(1.11\pm0.03)\times10^{-9}$, $(1.04\pm0.03)\times10^{-9}$, $(1.03\pm0.03)\times10^{-9}$ and $(1.04\pm0.03)\times10^{-9}$ m^2 s^{-1}, respectively. The diffusion of Sr^{2+} in the 2nd series of experiments is considered to be not tracer-diffusion but salt-diffusion. The diffusivity of Sr(NO$_3$)$_2$ in infinite dilution is 1.30×10^{-9} m^2 s^{-1} (Li and Gregory, 1974). The concentration of Sr(NO$_3$)$_2$ in the experiments was 10^2 mol m^{-3}, which would reduce the diffusivity by 17% on the basis of the data for CaCl$_2$ (Robinson & Stokes 1955). The temperature was room temperature (20 − 25) °C, which gives an uncertainty of 13% for D_v (Mills, 1961). The D_v of Sr^{2+} under the condition was estimated to be $(1.08\pm0.14)\times10^{-9}$ m^2 s^{-1}. The diffusivity of UO$_2^{2+}$ at infinite

dilution (Li and Gregory, 1974) can be used as the diffusivity in bulk solution in the 3rd series of experiments because the concentration of uranium was much lower than that of KCl, which assured tracer diffusion. The ionic strength of the solution was 10^2 mol m^{-3}, which gives an uncertainty of 3% fot D_v (Mills, 1961). The temperature was room temperature (20 – 25) °C, which gives an uncertainty of 13% for D_v (Mills, 1961). The D_v of UO_2^{2+} was estimated to be $(4.3\pm0.6)\times10^{-10}$ m^2 s^{-1} as shown in Table 3-2. The diffusivity of H_2O at infinite dilution (Li and Gregory, 1974) can be used as the diffusivity of HTO in bulk solution in the 4th series of experiments because the mode of this diffusion was self diffusion. The D_v of HTO was estimated to be 2.14×10^{-9} m^2 s^{-1} as shown in Table 3-2. The diffusion of cesium and iodine in granite in the 5th series of experiments were also considered to be tracer diffusion. The diffusivity of Cs^+ and I^- in 10^2 mol m^{-3} KI solution is 1.98×10^{-9} m^2 s^{-1} and 1.99×10^{-9} m^2 s^{-1}, respectively (Mills 1961).

Experimentally obtained D_e's for strontium, cobalt, uranium, tritiated water and iodine are plotted versus D_v in Fig. 3-7. Except for the data for Sr^{2+} obtained in the 2nd series of experiments, the data points lie on a curve. A positive correlation is observed between D_e values in the granite and diffusivity in bulk of the solution for most of the ions. The D_e/D_v ratios were, however, not constant but 3.6×10^{-4}, 2.9×10^{-4}, 2.4×10^{-4}, 2.3×10^{-4} and 8.4×10^{-5} for HTO, I^-, Sr^{2+} (1st series), Co^{2+} and UO_2^{2+}, respectively.

The D_e value for Sr^{2+} obtained in the 2nd series of experiments was higher than the value expected from Eq. (3-4) by 40 times. The D_e value for Sr^{2+} was higher than that obtained for I^- whose diffusivity in bulk solution is lower than that for Sr^{2+}. Similar high diffusivity of Sr^{2+} had been observed previously for a sandstone by Bradbury et al. (1986) and for a gneiss by Skagius & Neretnieks (1988). The value of $(\varepsilon + \rho R_d)$ obtained for Sr in the 2nd series of experiments was much higher than that obtained in the 1st series of experiments. In deionized water where the 2nd series of experiments were performed, adsorption site on the surface of the pores in the granite sample was available for strontium ion, while in the 10^2 mol m^{-3} KCl solution where the 1st series of experiments was performed, potassium ion occupied sorption sites on the surface of the pores in the granite sample and prevent strontium ion from being adsorbed. Effect of the presence of potassium ion on the adsorption of strontium had been reported by several researchers (Andersson et al., 1983; Ohe, 1984; Yamaguchi et al., 1991; Mahoney & Langmuir, 1991) and had been discussed based on the assumption that the cations are adsorbed onto rock through cation exchange reactions. In the 2nd series of experiments, the distribution ratio of strontium as well as effective diffusivity is higher than that in the 1st series of experiments. In the 1st series of experiments, cations diffuse through the granite and are hardly adsorbed on the surfaces of the pores. In the 2nd series of experiments, strontium is adsorbed on the surfaces of the pores and diffuse through the granite at higher effective

diffusivity than that in the 1st series of experiment. The results were well explained by supposing that the adsorbed Sr ions are mobile in adsorbed state.

In the case that surface diffusion and pore diffusion contribute to the diffusion of sorbed species, Eq. (3-5) can be expressed as follows (Skagius & Neretnieks, 1988)

$$\varepsilon \partial c/\partial t + \rho \partial q/\partial t = D_p \varepsilon \partial^2 c/\partial x^2 + D_s \rho \partial^2 q/\partial x^2 \tag{3-10}$$

where q : amount of ion adsorbed onto rock (mol kg^{-1}),

   D_p : pore diffusivity (m^2 s^{-1}),

   D_s : surface diffusivity (m^2 s^{-1}).

Since local chemical equilibrium may be reached at every point inside the sample, the relation between c and q is given by an equilibrium equation. Langmuir & Freundrich sorption isotherms are well known. Skagius & Neretnieks (1988) reported the analysis of diffusion experiments using these isotherms but enough agreement with the experimental data was not obtained. In the case of Sr, linear sorption isotherm may be applicable (Skagius et al., 1982; Bradbury & Stephen, 1986)

$$q = R_d c. \tag{3-11}$$

Using Eq. (3-11), Eq. (3-10) is simplified as

$$(\varepsilon + \rho R_d)\partial c/\partial t = (D_p \varepsilon + D_s \rho R_d)\partial^2 c/\partial x^2 \tag{3-12}$$

Equation (3-12) is converted into Eq. (3-5) if a different definition of D_e is made as

$$D_e = D_p \varepsilon + D_s \rho R_d \tag{3-13}$$

The diffusion equation including surface diffusion is, thus, solved in the above mentioned way. Eq. (3-13) states that D_e depends on ρR_d in the case that the surface diffusion is predominant. Figure 3-8 shows effective diffusivities of Sr in several rocks as a function of ρR_d. The effective diffusivity clearly depends on ρR_d. This might be due to the contribution of the second term of Eq. (3-13) or surface diffusion. Using the least squares method, the pore and the surface diffusivity are determined as

$$D_p \varepsilon = 10^{-12.68\pm0.15} \text{ m}^2 \text{ s}^{-1} = (2.1\pm0.7) \times 10^{-13} \text{ m}^2 \text{ s}^{-1}, \tag{3-14}$$

$$D_s = 10^{-11.50\pm0.09} \text{ m}^2 \text{ s}^{-1} = (3.5\pm0.7) \times 10^{-12} \text{ m}^2 \text{ s}^{-1}. \tag{3-15}$$

The present surface diffusivity is consistent with the former value determined by an intraparticle diffusion experiment (Tsukamoto & Ohe, 1991).

Equation (3-13) states that D_e depends on porosity, ε, in the case that ρR_d is low. Lang et al. (1986) measured the effective diffusivities of Sr through Kimmeridge and Coraloolith rock samples by the through-diffusion method in high saline ground water whose ionic strength

was 3.66. Sorptivities calculated based on their data are 0.047 and 0.18 for Kimmeridge and Coraloolith, respectively, which are fairly low because of the high ionic strength. These D_e values are expected to be explained mainly by pore diffusion. The effective diffusivities are related to porosity as shown in Fig. 3-9. The dependence on porosity is similar to that of iodide although the number of data points are limited. In the case of low distribution ratio, Sr diffuse mainly through the pores as if non-sorbed species. The effective diffusivity of Sr when distribution ratio is low can be expressed as

$$D_e = 2.1 \times 10^{-10} \varepsilon^{1.3}. \tag{3-16}$$

The effective diffusivities of iodide in rocks were expressed as $D_e = 6.4 \times 10^{-10} \varepsilon^{1.3}$ (Nishiyama et al., 1990), which is 3 times larger than that of Sr. This difference in D_e is reasonable because the diffusivity of I^- in bulk solution is larger than that of Sr^{2+} by 2.5 times (Li & Gregory, 1974). The effective diffusivities of Sr in rocks are successfully expressed as

$$D_e = 2.1 \times 10^{-10} \varepsilon^{1.3} + 3.5 \times 10^{-12} \rho R_d. \tag{3-17}$$

3.6. Conclusion

The effective diffusivities in Inada granite were measured for several species. A positive correlation was observed between D_e values in the granite and diffusivity in bulk solution for most of the ions. However, an unexpectedly high D_e value was obtained for strontium of high distribution ratio. A model that takes into account contribution of both the surface and the pore diffusion was proposed for sorbed species. Since experiments to determine the effective diffusivity in porous material are very time consuming, it is often suggested to estimate D_e values from a single D_e and the knowledge of D_v based on the proportionality between D_e and D_v. The results of this work indicate that this approach may introduce large errors.

27

Table 3-1 Composition of Inada granite

Chemical analysis[a] (weight %)	
SiO_2	76.49
Al_2O_3	12.06
K_2O	3.02
CaO	1.98
Na_2O	3.00
TiO_2	0.19
MnO_2	0.03
Fe_2O_3	0.57
FeO	1.16
MgO	0.20
$H_2O(+)$	0.30
$H_2O(-)$	0.40
Activation analysis[b] (ppm)	
Ba	1330 ± 350
V	64 ± 9
Co	$\leqq 2.3$
Th	$\leqq 22$
U	$\leqq 3.0$
Ni	$\leqq 4100$
Sr	$\leqq 157$
Minerals[c] (weight %)	
Quartz	49
Albite	24
Feldspars	23
Biotite	5

(a) Uematsu (1988)

(b) Yamaguchi et al. (1993)

(c) Idemitsu et al. (1992)

Table 3-2　Effective diffusivity (D_e) and rock capacity factor ($\varepsilon+\rho R_d$) of species in Inada granite.

Species	D_e (m^2 s^{-1})	$\varepsilon+\rho R_d$	Solution	Temp.	Reference	D_v (m^2 s^{-1})
Ba^{2+}	2.1×10^{-13}	-0.004	10^2 mol m^{-3} KCl pH = 4	25°C	This work	$(1.15\pm0.03)\times10^{-9}$
	3.5×10^{-13}	$+0.031$				
	3.0×10^{-13}	$+0.045$				
	2.5×10^{-13}	$+0.050$				
	2.9×10^{-13}	$+0.048$				
	1.9×10^{-13}	$+0.034$				
	avg. $(2.7\pm0.6)\times10^{-13}$	avg. 0.034 ± 0.018				
Sr^{2+}	2.1×10^{-13}	$+0.002$				$(1.11\pm0.03)\times10^{-9}$
	3.6×10^{-13}	$+0.014$				
	3.1×10^{-13}	$+0.019$				
	2.6×10^{-13}	$+0.022$				
	2.6×10^{-13}	$+0.003$				
	2.0×10^{-13}	$+0.019$				
	avg. $(2.7\pm0.6)\times10^{-13}$	avg. 0.013 ± 0.008				
Mg^{2+}	1.9×10^{-13}	-0.023				$(1.04\pm0.03)\times10^{-9}$
	3.3×10^{-13}	$+0.011$				
	2.9×10^{-13}	-0.005				
	2.3×10^{-13}	-0.005				
	2.4×10^{-13}	-0.017				
	1.9×10^{-13}	-0.045				
	avg. $(2.5\pm0.5)\times10^{-13}$	avg. -0.014 ± 0.018				
Co^{2+}	2.1×10^{-13}	-0.009				$(1.03\pm0.03)\times10^{-9}$
	3.4×10^{-13}	$+0.030$				
	2.6×10^{-13}	$+0.013$				
	2.2×10^{-13}	$+0.020$				
	2.5×10^{-13}	$+0.018$				
	1.6×10^{-13}	$+0.013$				
	avg. $(2.4\pm0.6)\times10^{-13}$	avg. 0.014 ± 0.012				

Table 3-2   (concluded)

Species	D_e (m² s⁻¹)	$\varepsilon+\rho R_d$	Solution	Temp.	Reference	D_v (m² s⁻¹)
Ni²⁺	2.0×10^{-13} 3.4×10^{-13} 2.9×10^{-13} 2.4×10^{-13} 2.5×10^{-13} 1.9×10^{-13} avg. $(2.5\pm0.5)\times10^{-13}$	-0.010 $+0.023$ $+0.014$ $+0.013$ -0.003 $+0.010$ avg. 0.008 ± 0.011	10^2 mol m⁻³ KCl pH = 4	25°C	This work	$(1.04\pm0.03)\times10^{-9}$
Sr²⁺	3.2×10^{-12} 9.5×10^{-12} 1.7×10^{-11} avg. $(1.0\pm0.6)\times10^{-11}$	2.4 1.5 1.7 avg. (1.87 ± 0.39)	10^2 mol m⁻³ Sr(NO₃)₂ → DDW	Room	This work	$(1.08\pm0.14)\times10^{-9}$
UO₂²⁺	avg. $(3.6\pm1.6)\times10^{-14}$	0.011 ± 0.010	10^2 mol m⁻³ KCl pH = 4	Room	This work	$(4.3\pm0.6)\times10^{-10}$
HTO	$(8.97\pm0.07)\times10^{-13}$ $(7.78\pm0.06)\times10^{-13}$ $(6.41\pm0.07)\times10^{-13}$ avg. $(7.7\pm1.4)\times10^{-13}$	$+0.11\pm0.05$ -0.19 ± 0.15 $+0.10\pm0.14$ avg. (0.01 ± 0.20)	DDW	25°C	This work	2.14×10^{-9}
I⁻	$(5.80\pm0.05)\times10^{-13}$	$+0.36\pm0.15$	10^2 mol m⁻³ KI	25°C	This work	1.99×10^{-9}
Cs⁺	$(5.04\pm0.18)\times10^{-13}$	$+1.98\pm0.22$				1.98×10^{-9}
uranine	avg. $(4.4\pm0.9)\times10^{-14}$	0.03 ± 0.04	1% uranine solution	Room	Kumata et al. 1990	$(4.5\pm0.6)\times10^{-10}$
NpO₂⁺	avg. $(2.5\pm0.4)\times10^{-13}$	0.010 ± 0.006	groundwater pH = 7.2~7.5 $I = 0.077$	Room	Kumata et al. 1990	

Table 3-3 Equilibrium constants for U(VI) hydrolysis reaction: $mUO_2^{2+} + nH_2O$ $= (UO_2)_m(OH)_n^{2m-n} + nH^+$. Equilibrium constants at 25℃ and $I = 0$ are taken from Grenthe et al. (1992) unless otherwise noted, and corrected for ionic strength to 0.1 by using the method recommended in the literature.

Species	$\log K_{sp}$	$\log \beta$
$UO_2(OH)_2 \cdot H_2O(cr)$	-5.2 ± 0.4	
$UO_2(OH)^+$		-5.4 ± 0.3
$UO_2(OH)_2^0$		-12.43 ± 0.09 [*]
$UO_2(OH)_3^-$		-19.2 ± 0.4
$UO_2(OH)_4^{2-}$		-33 ± 2
$(UO_2)_2(OH)^{3+}$		-2.5 ± 1.0
$(UO_2)_2(OH)_2^{2+}$		-5.84 ± 0.04
$(UO_2)_3(OH)_4^{2+}$		-12.3 ± 0.3
$(UO_2)_3(OH)_5^+$		-16.21 ± 0.12
$(UO_2)_3(OH)_7^-$		-31 ± 2
$(UO_2)_4(OH)_7^+$		-22.8 ± 1.0

(*) taken from Choppin and Mathur (1991)
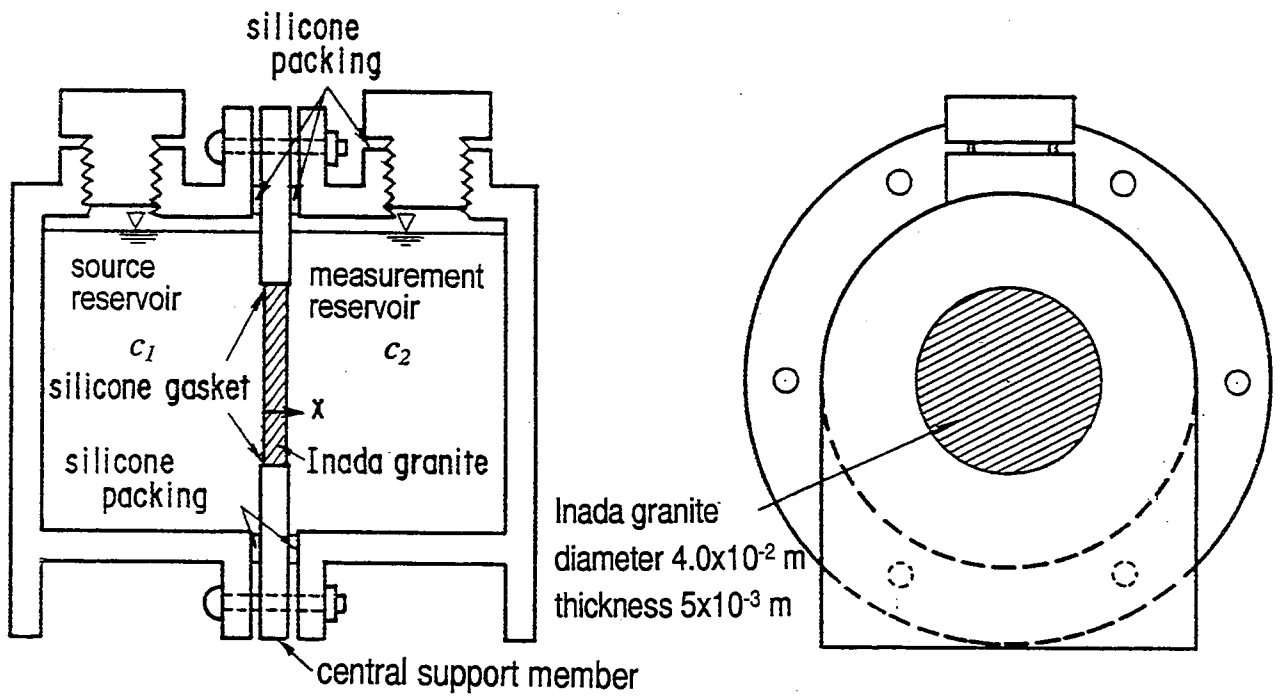
Fig. 3-1   Diffusion cell used in experiment.
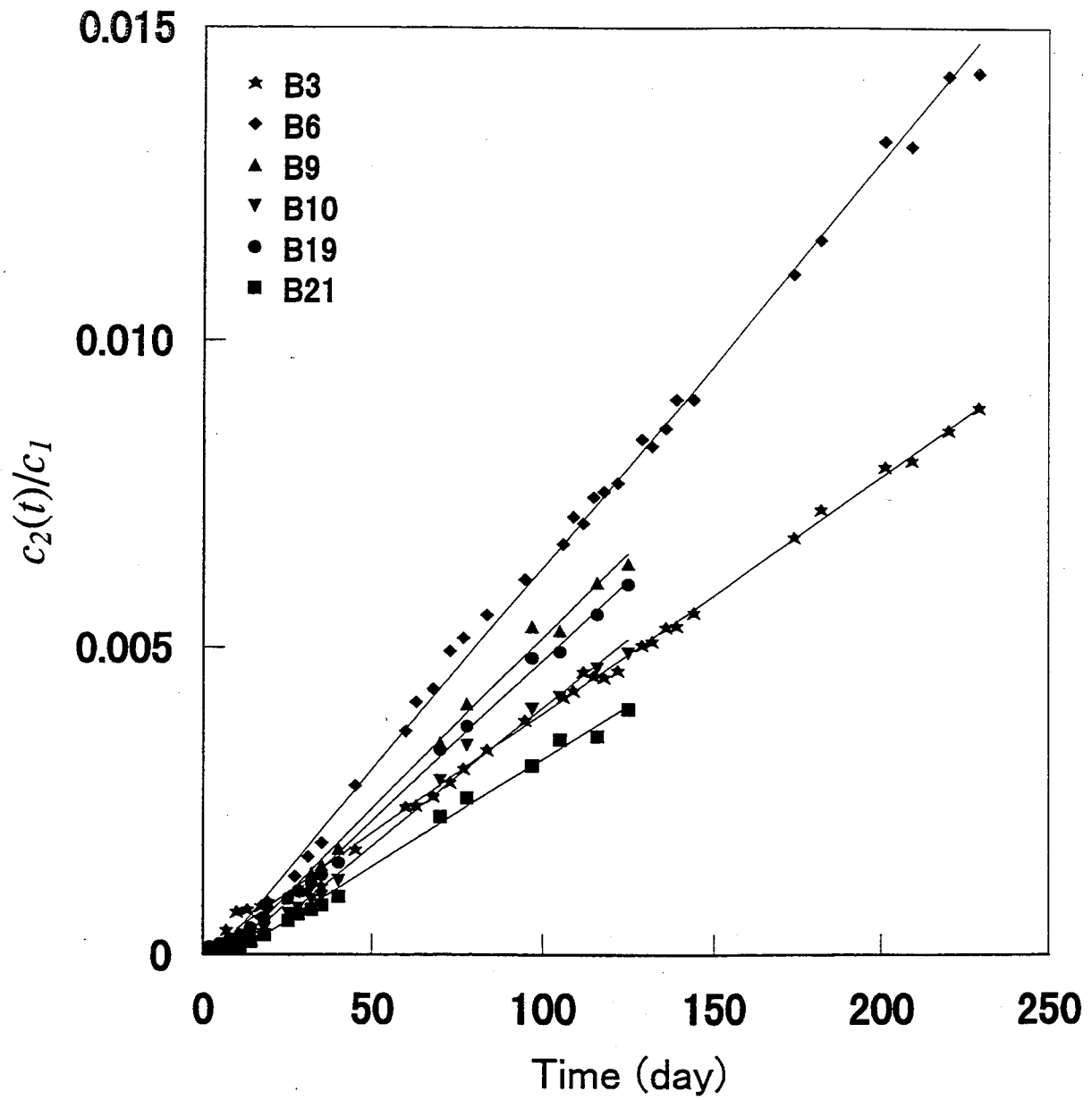
Fig. 3-2a Diffusion curves of barium through 5×10^{-3}-m thick Inada granite disks, B3, B6, B9, B10, B19 and B21 in the 1st series of experiments.
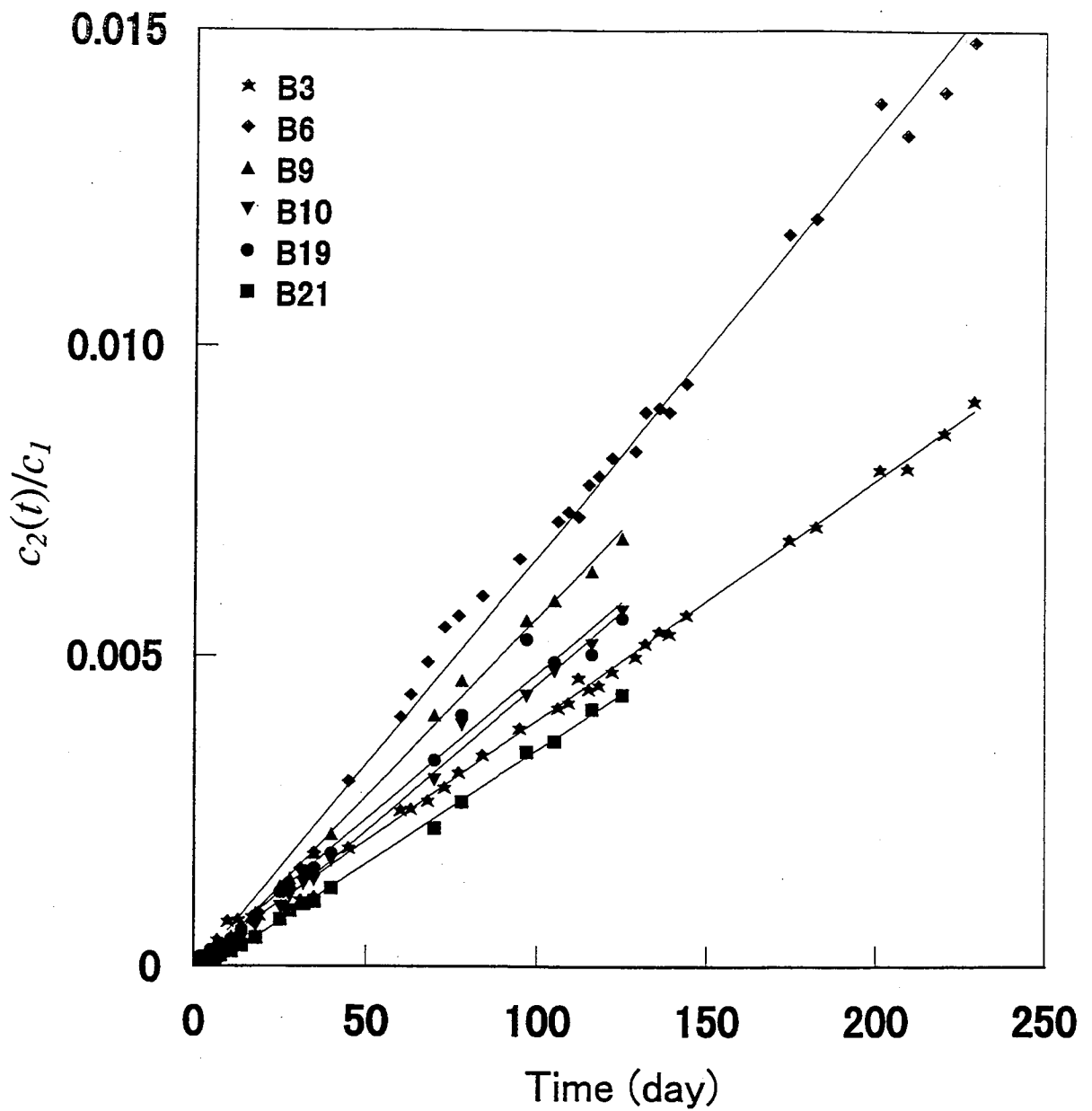
Fig. 3-2b Diffusion curves of strontium through 5×10^{-3}-m thick Inada granite disks, B3, B6, B9, B10, B19 and B21 in the 1st series of experiments.
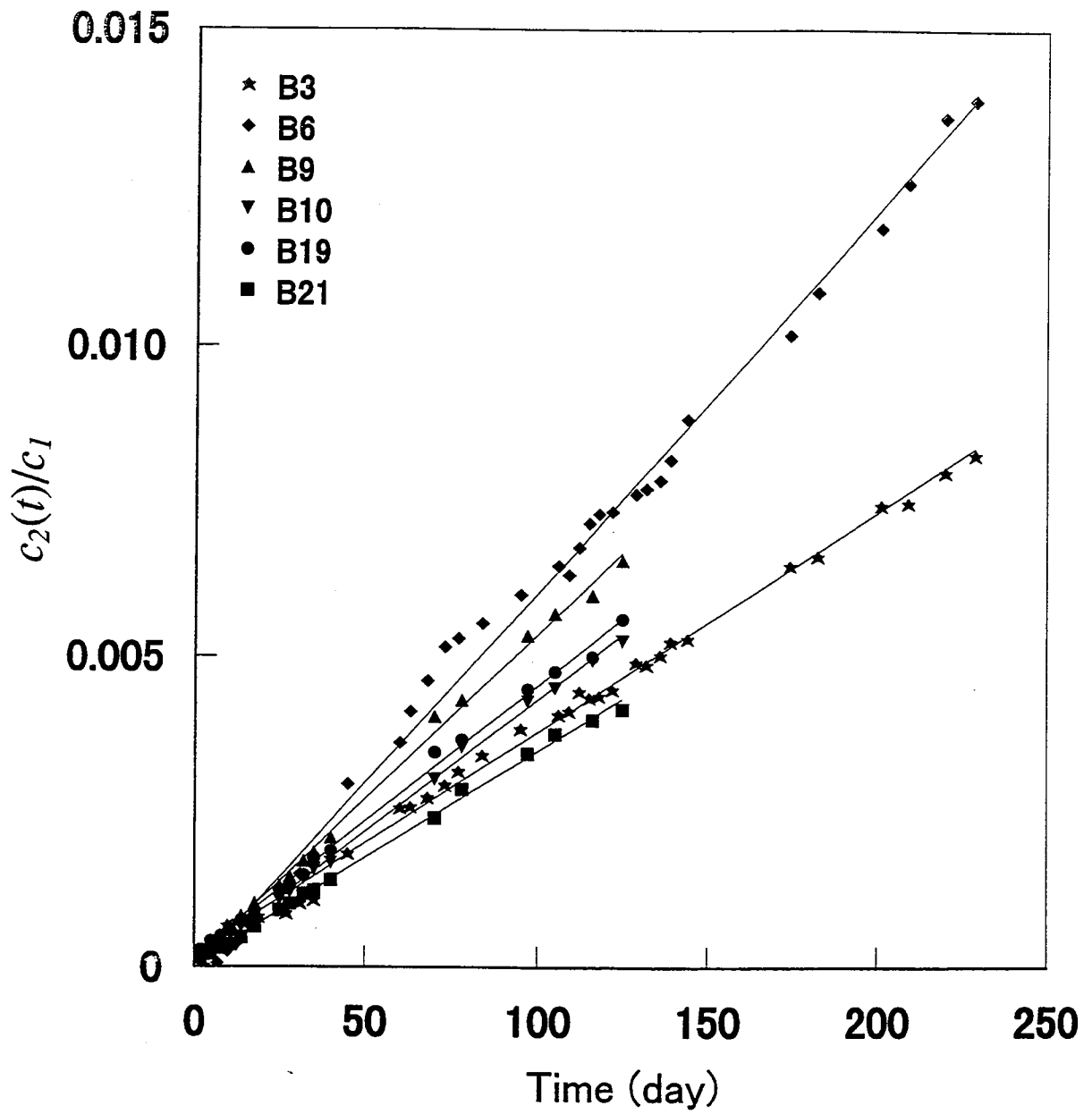
Fig. 3-2c Diffusion curves of magnesium through 5×10^{-3}-m thick Inada granite disks, B3, B6, B9, B10, B19 and B21 in the 1st series of experiments.
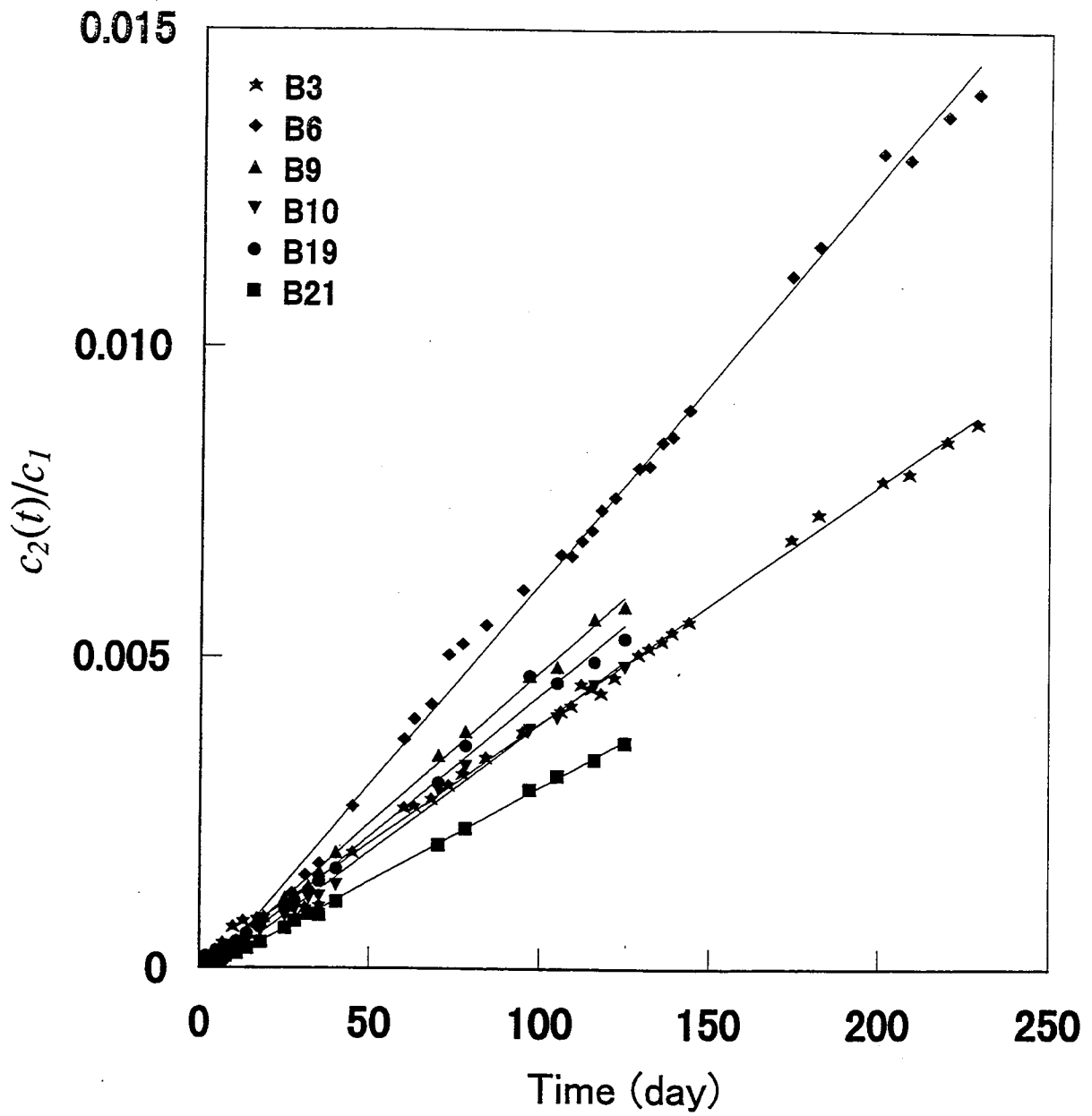
Fig. 3-2d Diffusion curves of cobalt through 5×10^{-3}-m thick Inada granite disks, B3, B6, B9, B10, B19 and B21 in the 1st series of experiments.
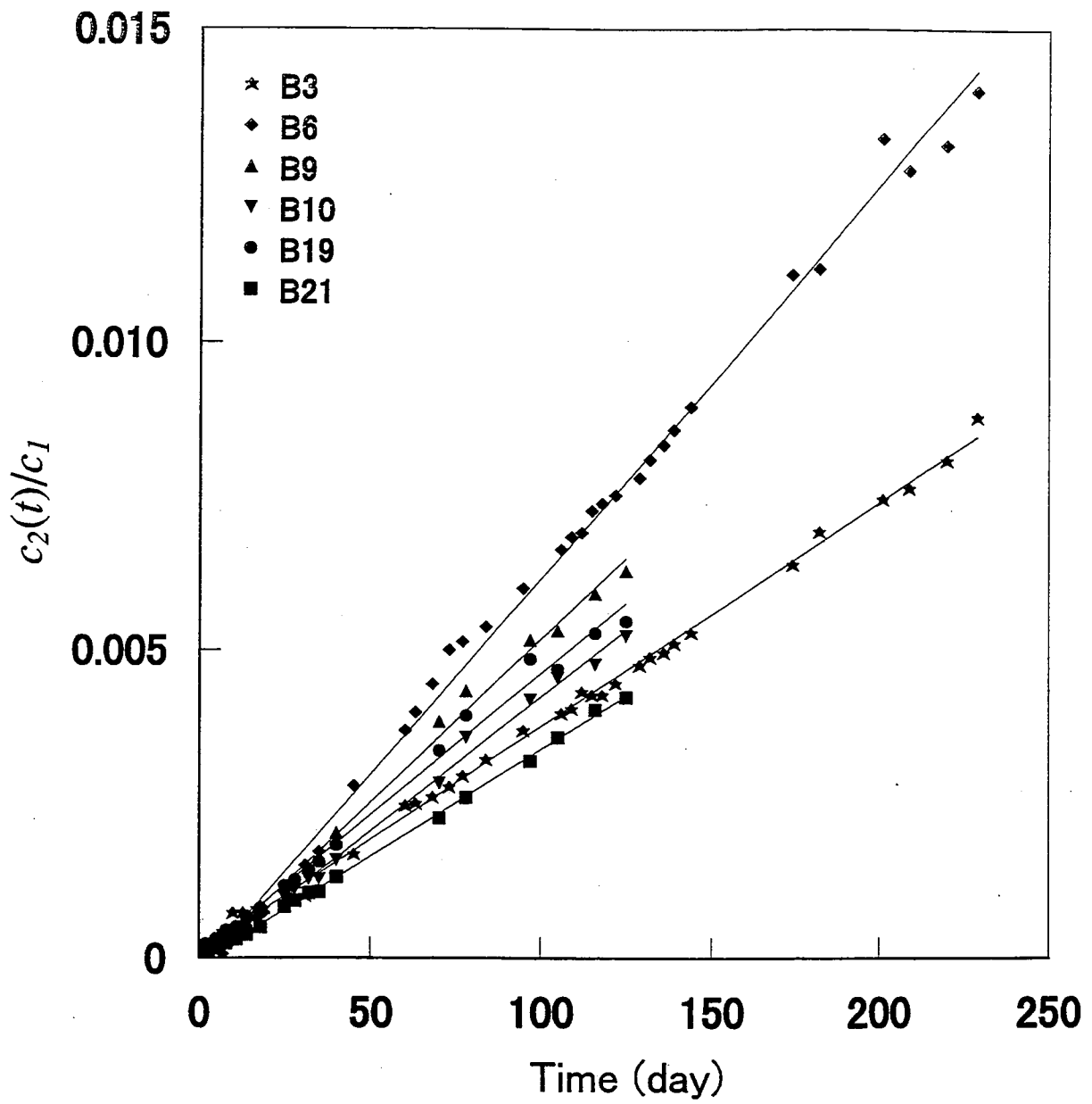
Fig. 3-2e Diffusion curves of nickel through 5×10^{-3}-m thick Inada granite disks, B3, B6, B9, B10, B19 and B21 in the 1st series of experiments.
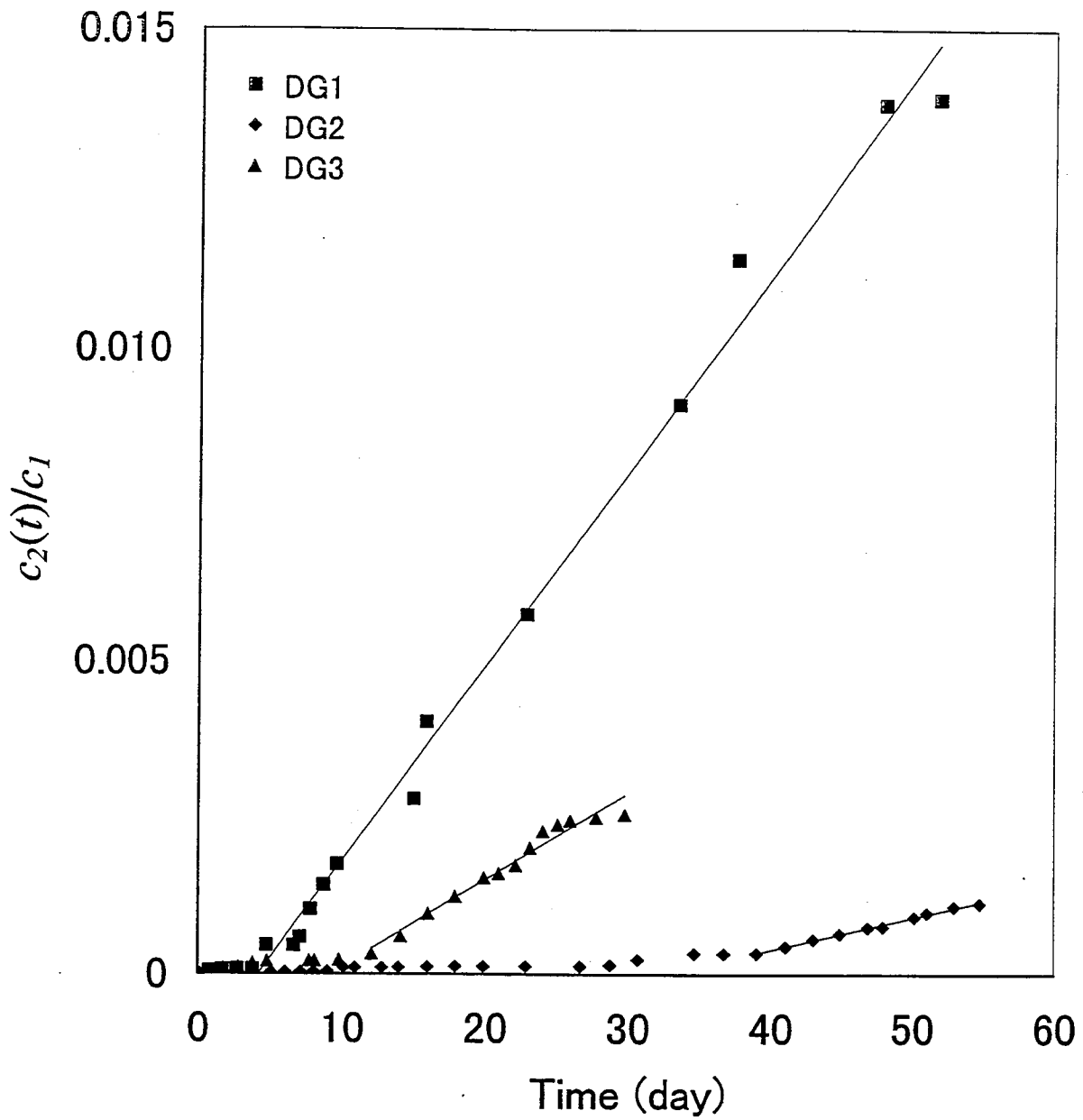
Fig. 3-3   Diffusion curves of strontium through 5×10^{-3}-m thick Inada granite disks, DG1, DG2 and DG3 in the 2nd series of experiments.
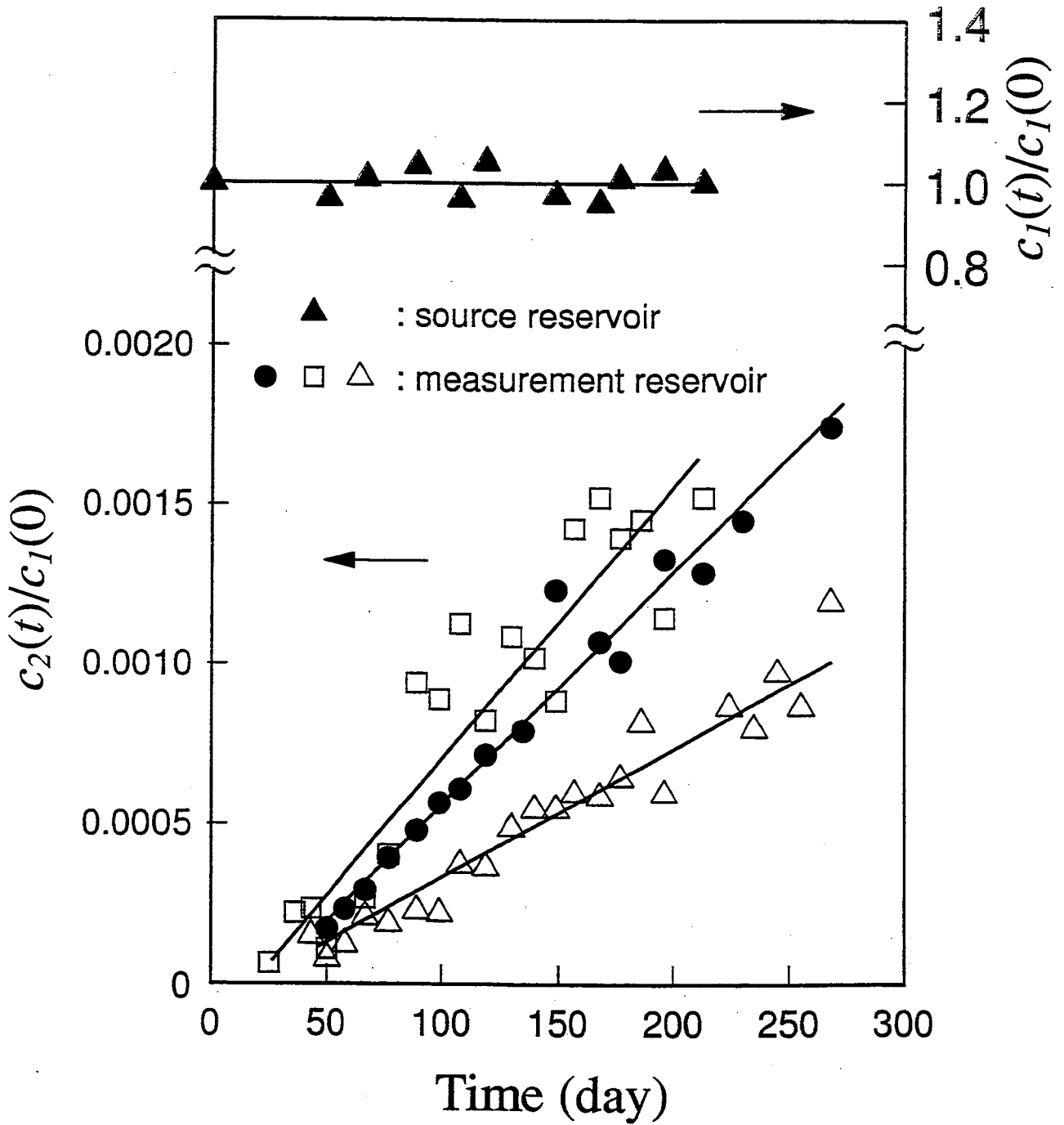
Fig. 3-4. Diffusion curves of uranium through 5×10^{-3}-m thick Inada granite disks, B11 ($\bullet$), B14 ($\triangle$) and B16 ($\square$) in the 3rd series of experiments. Uranium concentration in a source reservoir is presented by closed triangles.
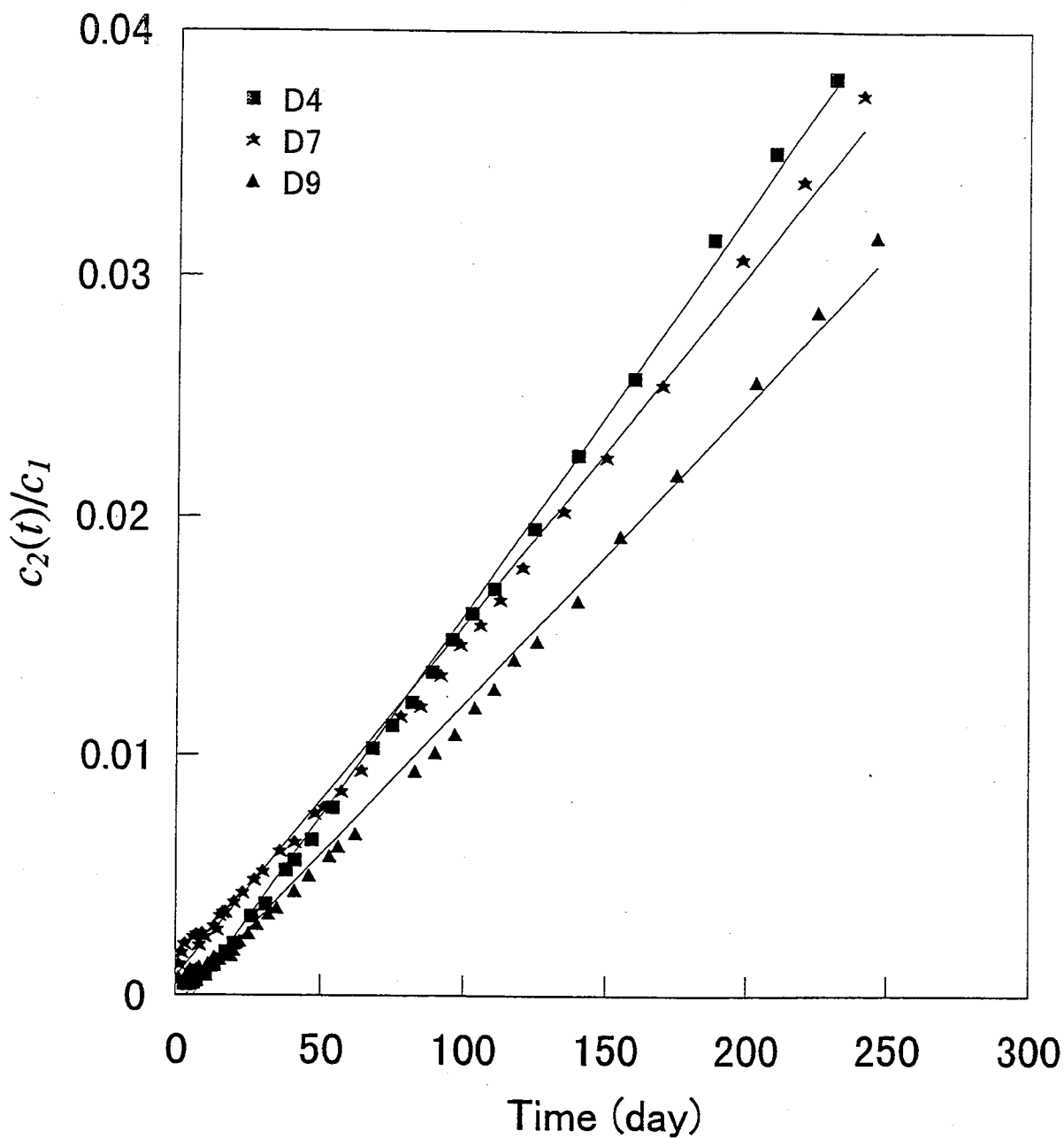
Fig. 3-5 Diffusion curves of tritiated water through 5×10^{-3}-m thick Inada granite disks, D4, D7 and D9 in the 4th series of experiments.
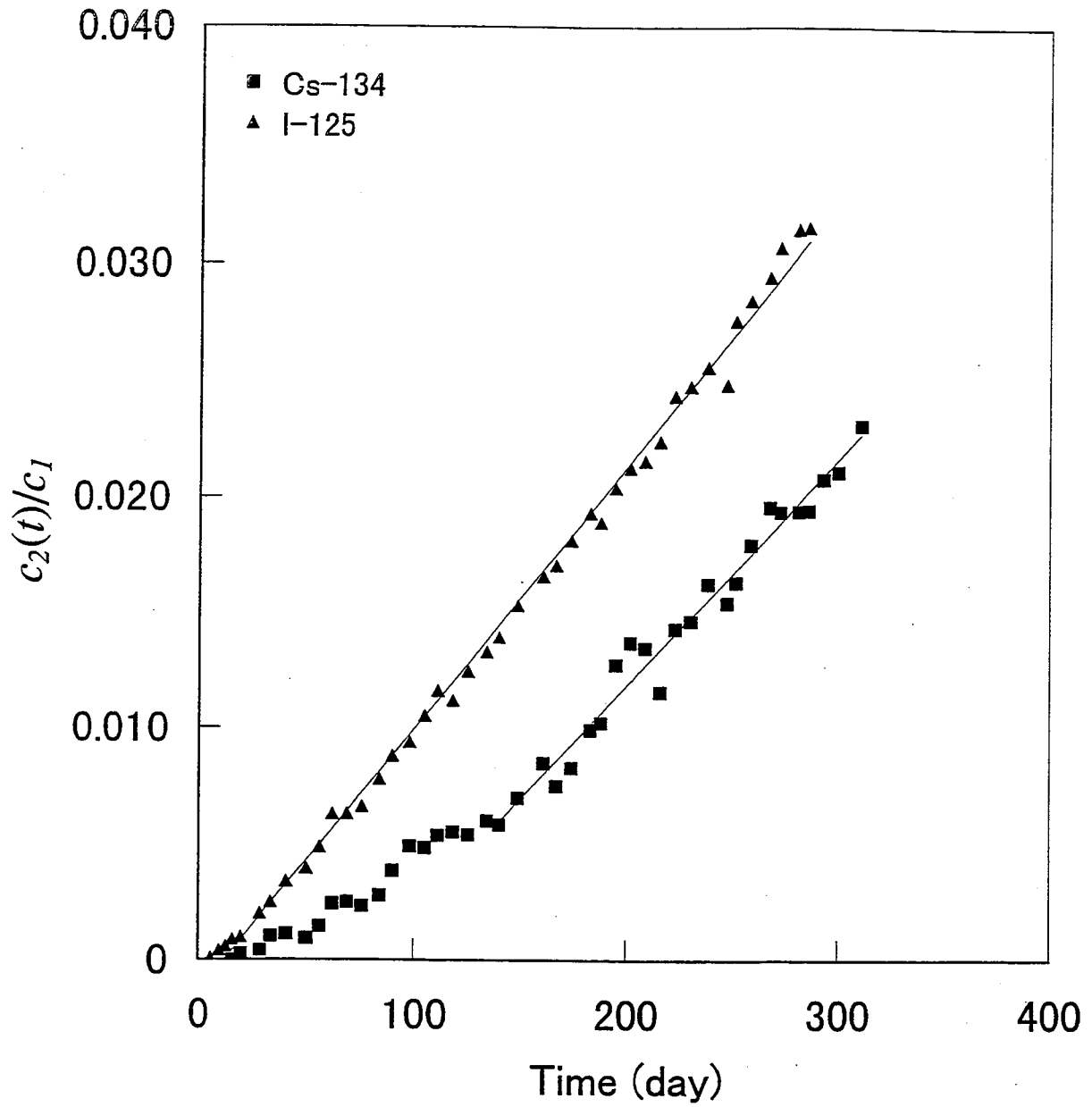
Fig. 3-6   Diffusion curves of cesium and iodine through a 5×10^{-3}-m thick Inada granite disk in the 5th series of experiments.
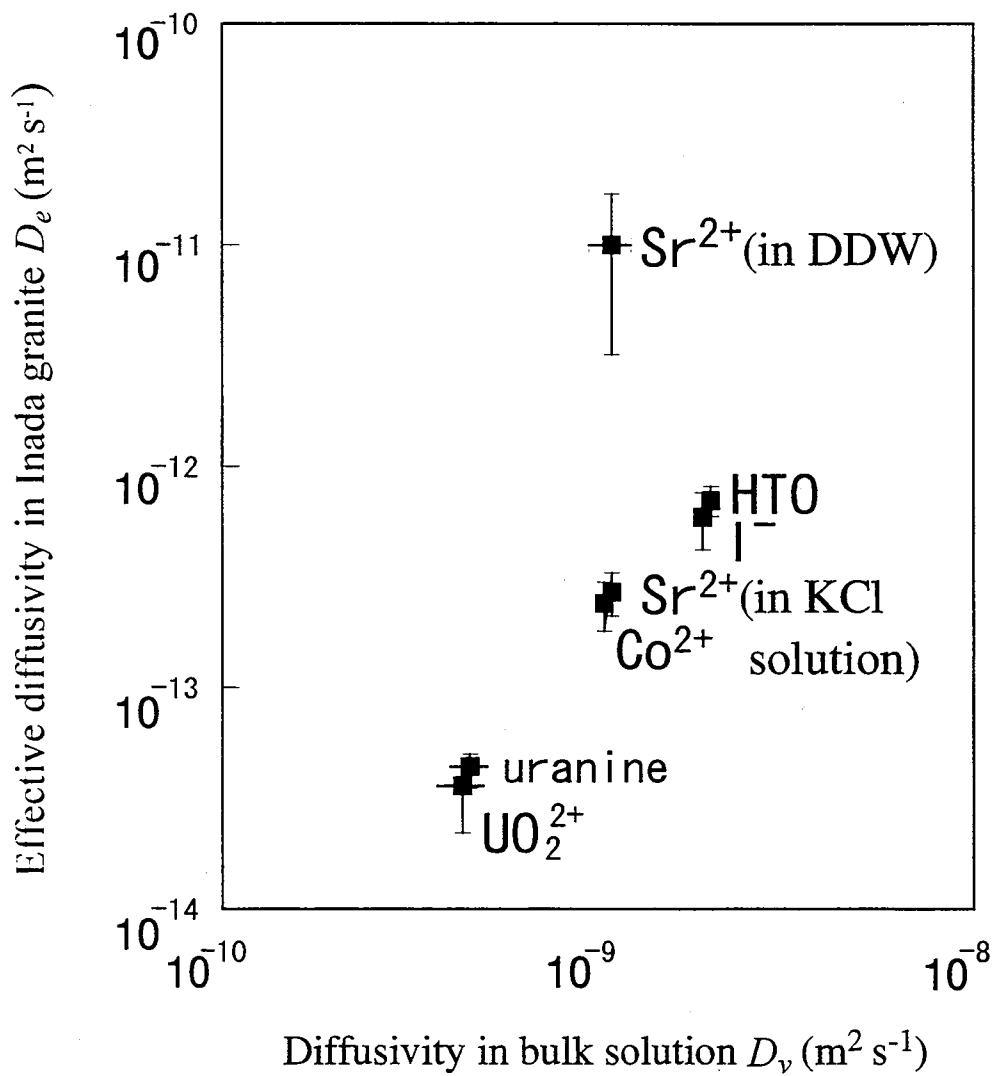
Fig. 3-7 Correlation between effective diffusivities of species in Inada granite and their diffusivities in bulk of the solution.
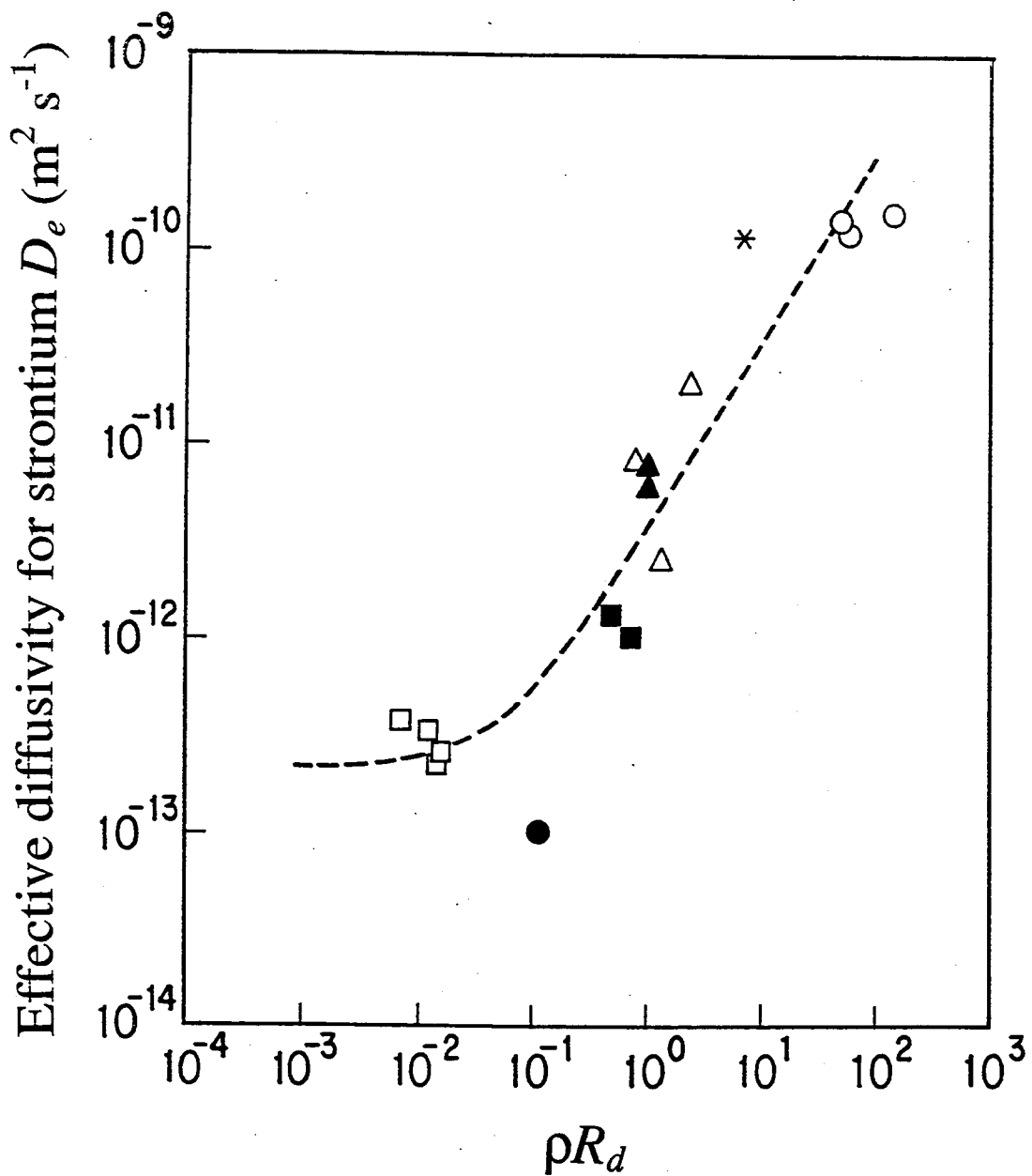
Fig. 3-8 Correlation between effective diffusivity for strontium and ρR_d for several rocks.
□: Inada granite in 10^2 mol m^{-3} KCl solution. △: Inada granite in distilled-
deionized water. ○: Darey Dale sandstone (Bradbury & Stephen, 1986; Smith,
1989). ✳: Cenomanian sample (Lang et al., 1986). ▲: Upper magnesian
limestone (Bradbury et al., 1986). ■: Anhydryte (Bradbury, 1986). ●: Biotite
gneiss (Skagius & Neretnieks, 1988). The broken line presents least squares fitting
to Eq. (3-13).
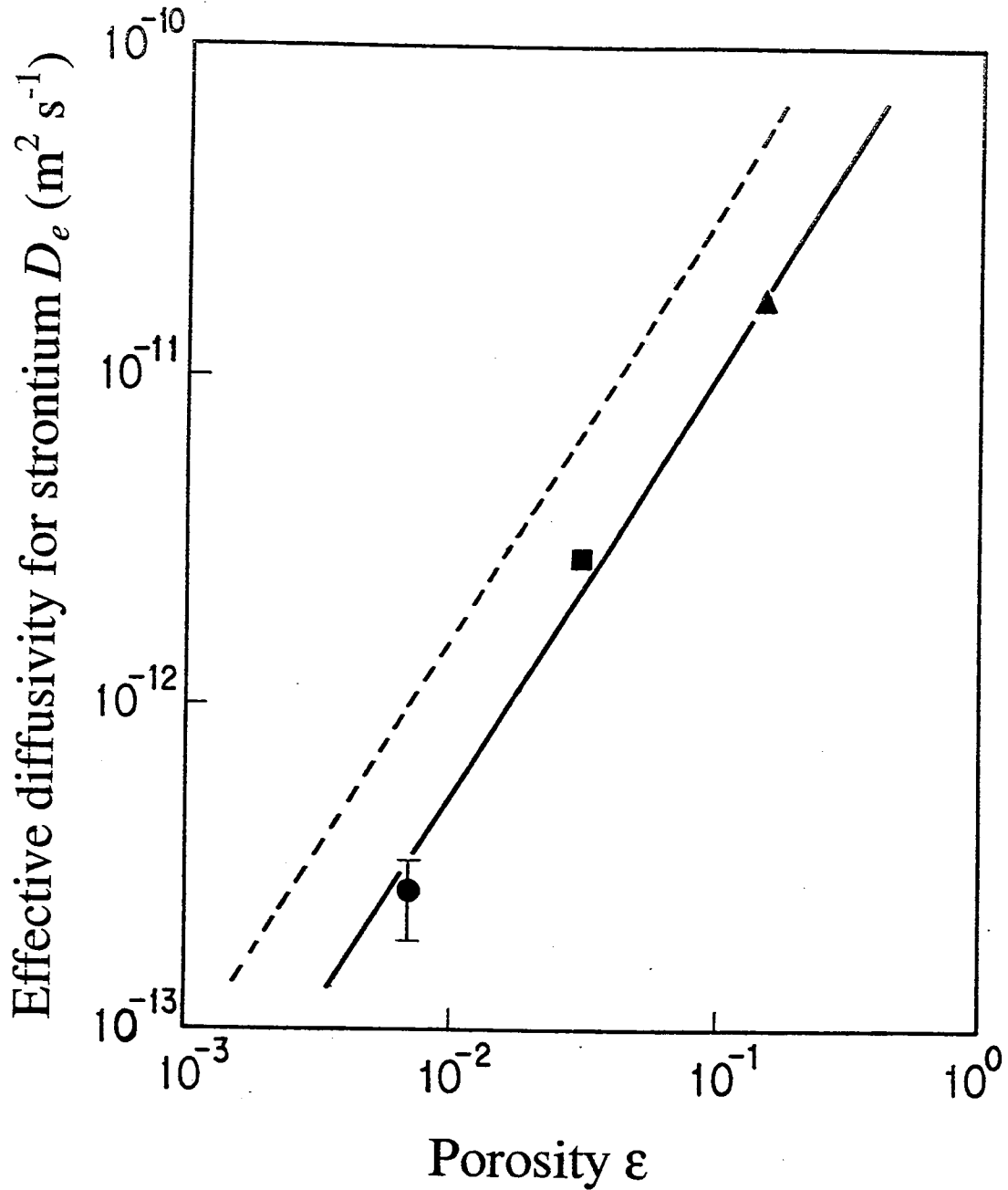
Fig. 3-9 Correlation between effective diffusivity for strontium in rocks and their porosities in case of low distribution ratio. $\blacktriangle$: Coraloolith (Lang et al., 1986), $\blacksquare$: Kimmeridge (Lang et al., 1986), $\bullet$: Inada granite in 10^2 mol m^{-3} KCl solution. The solid line presents the Eq. (3-16). The broken line presents $D_e = 6.4 \times 10^{-10} \varepsilon^{1.3}$, which is the correlation between effective diffusivity for iodine in rocks and their porosities (Nishiyama et al., 1990).

4. Effect of adsorption on apparent diffusivity in granite

4.1. Introduction

Pore-diffusion model assumes that the apparent diffusivity D_a of a species in a porous material is correlated with the diffusivity in bulk of the solution (D_v), geometric parameters of the pores in the rock: ε (porosity), δ (constrictivity) and τ^{-2} (τ: tortuosity), and distribution ratio (R_d) as

$$D_a = D_v \delta \tau^{-2}/(1 + \rho R_d \varepsilon^{-1}). \tag{4-1}$$

Equation (4-1) can be rewritten as

$$D_a = D_v \varepsilon \delta \tau^{-2}/(\varepsilon + \rho R_d) = D_e/(\varepsilon + \rho R_d). \tag{4-2}$$

The values of D_e and ($\varepsilon + \rho R_d$) obtained for UO_2^{2+} from the through-diffusion experiment in chapter 3 supports the Eq. (4-2); the values yield a D_a value of $(1.7 - 3.7) \times 10^{-12}$ m^2 s^{-1}, which is close to the value reported by Idemitsu et al. (1991, 1992 and 1993). Bradbury et al. (1986), however, reported that the apparent diffusivity of cesium and strontium for 3 types of rocks was higher by orders of magnitude than that predicted from Eq. (4-1). The value for D_e can be higher than $D_v \varepsilon \delta \tau^{-2}$ for sorbed species as shown in chapter 3, which can be a reason for the high D_a value reported by Bradbury et al. (1986). Equation (4-1) assumes the retardation of apparent diffusive transport by adsorption as $(1 + \rho R_d \varepsilon^{-1})^{-1}$. If some of the diffusing species can diffuse as adsorbed state, the retardation can be smaller than that expected form R_d value obtained from batch sorption tests, which can be another reason for the high D_a value. Clear understanding of the effect of the adsorption onto minerals on diffusive transport of radionuclides is required because it is one of the most important phenomena for performance assessment of radioactive waste disposal.

The objectives of this chapter are to obtain values for D_a, D_e and R_d for strontium from a through-diffusion experiment using a granite and groundwater from deep underground and to discuss the effect of the adsorption of Sr^{2+} onto minerals on its apparent diffusive transport through the granite.

4.2. Experimental

A granite core with a diameter of 6.1×10^{-2} m was obtained from an exploratory borehole JE 2 that was drilled into the rockmass surrounding the vertical fracture JZ 2 in Underground Research Laboratory (URL), Manitoba, Canada. Four liters of groundwater from JZ 2 was also

obtained from this borehole. The porosity and the modal diameter of the pores of and the granite had been determined to be (0.40±0.10)% and 340 nm, respectively in chapter 2. Chemical composition of the groundwater is given in Table 4-1. Precaution was paid to exclude atmospheric oxygen as much as possible to avoid air oxidation of the granite in this experiment. The rock sawing equipment was modified by enclosing the diamond rotary blade and motor with an acrylic/polyethylene housing. Compressed N_2 gas was used to displace as much of the atmospheric oxygen as possible. To hold the rock core as firmly as possible to prevent chipping during cutting, a new holder was designed and constructed. Eleven 4.8×10^{-3}-m thick disks of granite were cut from the core, using groundwater from Fracture Zone 2 in the URL to cool the blade during cutting. The 11 disks were placed in an acrylic vessel filled with groundwater from Fracture Zone 2. A small polyethylene bag filled with iron powder was added to this vessel to scavenge atmospheric and dissolved oxygen and to maintain reducing conditions.

Three granite disks, F2, F5 and F8, were attached to acrylic frames of diffusion cell with silicone gaskets. Diffusion cells were assembled as shown in Fig. 4-1. These operations were done in a glove box under N_2 with an oxygen concentration of less than 1 ppm. The capacity of the reservoir was 1.18×10^{-4} m^3.

After evacuating all air entrapped in the interconnected pore space in the granite disks as described in chapter 3, the diffusion cells were filled with fresh groundwater because it was felt that loss of CO_2 might have occurred as a result of the evacuation.

The starting solution was prepared by combining 4.0×10^{-4} m^3 of the groundwater, 2.5×10^{-6} m^3 of ^{125}I stock solution, 5×10^{-8} m^3 of ^{85}Sr stock solution and 1.5×10^{-6} m^3 portion of the 9.3×10^{1} mol m^{-3} SrI_2 solution. The initial concentrations of stable SrI_2, ^{125}I and ^{85}Sr in the solution were planned to be 3.4×10^{-1} mol m^{-3}, 1.62×10^{9} Bq m^{-3} and 1.17×10^{8} Bq m^{-3}, respectively. To make sure the concentrations of ^{125}I and ^{85}Sr in the source solution, 1×10^{-6} m^3 aliquot was withdrawn and its activity determined by γ-spectrometry. The half-lives of Sr-85 ($T_{1/2} = 65.2$ days) and I-125 ($T_{1/2} = 59.7$ days) are short in relation to the duration of the diffusion experiments. Stable SrI_2 was added to the source solution to maintain adsorption of these species onto granite in appropriate level through the experimental period. A concentration of SrI_2 of 3.4×10^{-1} mol m^{-3} was selected for the following two reasons: (1) There should be a substantial difference in strontium concentration between the source solution and the groundwater that contained about 3×10^{-3} mol m^{-3} strontium. (2) Changes of ionic strength due to adding SrI_2 should be minimized. The diffusion experiments were started by placing the starting solution in one reservoir (source reservoir) and the groundwater in the other, or measurement, reservoir. The experiment was performed in triplicate at room temperature. At 14 days intervals, 1×10^{-6} m^3 aliquot was taken from both reservoirs to determine the concentrations of ^{125}I and ^{85}Sr. The 1×10^{-6} m^3 aliquot removed from the

measurement reservoir was replaced by an equal volume of the groundwater to maintain the water levels in the two reservoirs. Concentrations of strontium and iodine were measured by γ−spectrometry.

When the diffusion run was terminated after 300 days from the start of the diffusion run, both compartments of the diffusion cell were drained and 6×10^{-6} m^3 aliquots analyzed by γ−spectrometry. Both compartments were then flushed with 1×10^{-5} m^3 distilled and deionized water and 6×10^{-6} m^3 aliquots analyzed by γ−spectrometry. The sides of the disks F5 and F8 facing the source reservoirs were ground with 60-grit waterproof carborundum paper. The disks were weighed prior to grinding to obtain the weights of the material that was removed by grinding. The disks were ground by hand by rubbing them over the carborundum paper. Care was taken to ensure that grinding was as even as possible by rotating the disks periodically. After an initial grinding of the face, the disk was weighed. The surface was then ground again to remove some additional material and the granite disk weighed again. The material removed from the disk by grinding and any carborundum powder that was removed in the process were transferred to a tared polyethylene weighing dish by tapping the carborundum paper gently. This weighing dish was weighed to obtain the amount of material transferred. The material removed from the disk by grinding was analyzed by γ−spectrometry.

4.3. Results and Discussion

Concentrations of ^{85}Sr for 3 diffusion runs (F2, F5 and F8) are shown in Fig. 4-2. The concentration of strontium increased linearly with time for F2 and F5 after 50 days from the start of diffusion. Achievement of a steady state diffusion was confirmed by the fact that the decrease of Sr concentration in the source reservoirs became comparable to the increase in the measurement reservoirs after 50 days. The linear portion of the diffusion curve was analyzed based on the definition of the effective diffusivity:

$$D_e = -J/(\partial c/\partial x) = u \text{VA}^{-1}/\{(\bar{c}_1 - \bar{c}_2)\text{L}^{-1}\} \tag{4-3}$$

where u : slope of the linear portion of through-diffusion curve (Bq m^{-3} s^{-1})

        $\bar{c}_1$: average concentration of ^{85}Sr in the source reservoir in the period of 50-300 days (Bq m^{-3}),

        $\bar{c}_2$: average concentration of ^{85}Sr in the measurement reservoir in the period of 50-300 days (Bq m^{-3}).

An effective diffusivity (D_e) of $(1.9\pm0.3) \times 10^{-12}$ m^2 s^{-1} was obtained for F2 and $(2.2\pm0.5) \times 10^{-12}$ m^2 s^{-1} for F5 by the least squares fitting, and these are averaged to be $(2.1\pm0.6) \times 10^{-12}$ m^2 s^{-1}.

The following equation was proposed in chapter 3 to correlate the effective diffusivity of strontium in rocks with the porosity of the rock and distribution ratio for Sr on granite

$$D_e = 2.1 \times 10^{-10} \varepsilon^{1.3} + D_s \rho R_d \tag{4-4}$$

where D_s : surface diffusivity (m^2 s^{-1}).

The first term, the contribution of pore diffusion, was calculated to be 1.6×10^{-13} m^2 s^{-1} using the value of 0.004 for the porosity. The experimentally obtained D_e value is one order of magnitude higher than this value. Contribution of the second term that stands for the contribution of the surface diffusion seems to be dominant. On the other hand, for non-sorbed iodine, the effective diffusivity can be explained taking only pore diffusion into account. Concentrations of ^{125}I for 3 diffusion runs (F2, F5 and F8) are shown in Fig. 4-3. The effective diffusivity of $(4.4 \pm 0.7) \times 10^{-13}$ m^2 s^{-1} was obtained. Based on the pore diffusion model, the effective diffusivity was calculated to be 4.9×10^{-13} m^2 s^{-1} using the following correlation (Nishiyama et al., 1990):

$$D_e = 6.4 \times 10^{-10} \varepsilon^{1.3} \tag{4-5}$$

The calculated value is close to the value obtained empirically for iodine.

Significant losses of Sr were observed from the source solutions with time: Over the first 50-day period, the Sr concentration in the source reservoirs decreased by one order of magnitude. The decrease in the Sr concentration in the source reservoir over the first 50 days is attributed to sorption and diffusion into the interconnected pore space in the granite disks. The amount of strontium in unit volume of granite in time t at a point whose distance from the granite surface facing to the source reservoir, $C(x, t)$, is described by the following equation.

$$\partial C/\partial t = D_a \partial^2 C/\partial x^2 \tag{4-6}$$

$$C = 0 \qquad (t=0, 0<x\leq L) \tag{4-7}$$

$$C = (\varepsilon + \rho R_d)c_1 \qquad (t>0, x=0) \tag{4-8}$$

$$C = (\varepsilon + \rho R_d)c_2 \qquad (t>0, x=L) \tag{4-9}$$

$$c_1 = c_1(0) - D_a A V^{-1} \int_0^t (-\partial C/\partial x)_{x=0} dt \tag{4-10}$$

$$c_2 = D_a A V^{-1} \int_0^t (-\partial C/\partial x)_{x=L} dt \tag{4-11}$$

The solution of these equations had been given by Spacek & Kubin (1967)

$$(c_1-c_2)/c_1(0) = \sum_{i=1}^{\infty} 4\alpha [z_i^2 + \alpha(2+\alpha)]^{-1} \exp(-z_i^2 D_a t L^{-2}) \tag{4-12}$$

where $\alpha = (\varepsilon + \rho R_d) A L V^{-1}$ and z_i are positive roots of the characteristic equation

$$\tan z = 2\alpha z/(z^2 - \alpha^2) \tag{4-13}$$

The infinite series of Eq. (4-12) converges rapidly, so that for sufficiently large t only the first term with z_1 can be considered. After plotting $\ln[(c_1-c_2)/c_1(0)]$ on t as shown in Fig. 4-4, $-z_1^2 D_a L^{-2}$ and $\ln\{4\alpha[z_1^2 + \alpha(2+\alpha)]^{-1}\}$ were obtained from the slope and the intercept of the linear portion of the plot and tabulated in Table 4-2. An apparent diffusivity of $(2.0\pm1.4)\times10^{-13}$ $m^2\ s^{-1}$ and a value for R_d of $0.156\pm0.023\ m^3\ kg^{-1}$ were obtained on an average of the results from 3 runs. The D_a value is lower than the D_e value by one order of magnitude, which yields an R_d value of $0.004\pm0.003\ m^3\ kg^{-1}$ by using the relation

$$\varepsilon+\rho R_d = D_e / D_a. \tag{4-14}$$

This R_d value is one fortieth of the value of $0.156\pm0.023\ m^3\ kg^{-1}$ obtained by analyzing the change of the concentration of Sr in both reservoirs.

The results obtained in the grinding procedures were shown in Table 4-3. The average weight of granite removed from the four sides of the two disks was 6.65×10^{-5} kg. Using the diameter of the granite disks as 6.1×10^{-2} m and a density of the granite of $2.64\times10^3\ kg\ m^{-3}$, this corresponds to the removal of an average of 8.6×10^{-6} m from the surface of the disks. The specific surface area of the URL granite was earlier given as $20\ m^2\ kg^{-1}$. If the material removed from the granite disks is representative of the rock fabric, the contribution to the surface area by that of the interconnected pore space is 6.71×10^{-5} kg x $20\ m^2\ kg^{-1}$ or 1.34×10^{-3} m^2 for F-5. By adding the outer surface area of the granite disk of $2.92\times10^{-3}\ m^2$, the total surface area of the removed granite material is $4.26\times10^{-3}\ m^2$. The adsorbed activity is then 216 Bq/$4.26\times10^{-3}\ m^2 = 5.1\times10^4\ Bq\ m^{-2}$. The concentration of ^{85}Sr in the source reservoir at the termination of the experiment was $5.95\times10^6\ Bq\ m^{-3}$. This gives R_a value of $5.1\times10^4/5.95\times10^6$ $= 8.5\times10^{-3}$ m or R_d value of $0.171\ m^3\ kg^{-1}$. This value is close to the R_d value obtained by analyzing the change of the concentration of Sr in both reservoirs.

Distribution ratio can also be calculated from the mass balance of strontium, which is described by the following equation:

$$c_{1,\,ini}V_1 = c_{1,\,fin}V_1 + c_{1,\,fn}R_aA + \int_0^L c_{fin}(x)(\varepsilon + \rho R_a\rho_a)Adx + c_{2,\,fin}R_aA + c_{2,\,fin}V_2$$

$$\tag{4-15}$$

where $c_{1,\,ini}$: initial concentration of strontium in the source reservoir ($1.17\times10^8\ Bq\ m^{-3}$)

           $c_{1,\,fin}$: final concentration of strontium in the source reservoir (Bq m^{-3})

           $c_{2,\,fin}$: fianl concentration of strontium in the measurement reservoir (Bq m^{-3})

           $c_{fin}(x)$: final concentration of strontium in the pore water in granite (Bq m^{-3})

           R_a : surface-based distribution ratio ($= R_d/\rho_a$, m)

           ρ_a : specific surface area of the granite ($20\ m^2\ kg^{-1}$)

A   : cross section of the granite sample (2.921×10^{-3} m^2)

Assuming that strontium concentration in the pore water in the granite as

$$c_{fin}(x) = \{c_{1, fin}(L-x) + c_{2, fin}x\}/L, \tag{4-16}$$

R_a value of $(4.5 \pm 0.6) \times 10^{-3}$ m or R_d value of 0.091 ± 0.013 m^3 kg^{-1} was determined. This value is close to the R_d value obtained from the diffusion curve analysis again.

These results show that the strontium was removed from the solution and was adsorbed on the granite, which corresponds to the sorption R_d value of $0.091 - 0.180$ m^3 kg^{-1}. Nevertheless, R_d value assessed from the apparent diffusivity and the effective diffusivity was 0.0041 m^3 kg^{-1}. The contribution of the surface diffusion discussed in chapter 3 can explain this discrepancy; the retardation of the apparent diffusive transport is smaller than that predicted from the sorption R_d value because part of the adsorbed strontium is mobile in adsorbed state.

4.4. Conclusion

A through-diffusion experiment was performed for ^{85}Sr^{2+} to examine the effect of adsorption on minerals on the diffusivity in granite. The ratio, D_e/D_a, was much lower than the value estimated from distribution ratios. Although the reason for the discrepancy has not been identified, the discrepancy should exist if some of the adsorbed species diffuse as adsorbed state.

Table 4-1   Chemical composition of groundwater used in SrI_2 diffusion experiment through granite obtained from Underground Research Laboratory. (All values in 10^{-3} kg m^{-3})

Ion	Concentration (±2s)	Method
Na	102 ± 10	FAA
K	1.13 ± 0.01	FAA
Ca	15.4 ± 0.5	ICP-ES
Mg	6.5 ± 0.2	ICP-ES
Si	4.8 ± 0.1	ICP-ES
Sr	0.178 ± 0.005	ICP-ES
B	0.578 ± 0.017	ICP-ES
Cl	60.7 ± 3.1	IC
Br	0.3 ± 0.1	IC
F	5.42 ± 0.27	IC
SO$_4$	49.4 ± 2.5	IC
Alkalinity*	188 ± 10	titrimetry

*as HCO_3

Table 4-2   The results of the analysis of the Sr concentration change with time in both reservoirs and R_d values obtained from several methods.

Run No.	$z_l^2 D_a L^{-2}$ [a] (10^{-8} s^{-1})	$\ln\{4\alpha[z_l^2+\alpha(2+\alpha)]^{-1}\}$ [a] (-)	D_a [a] (10^{-13} m^2 s^{-1})	$R_{d,C}$ [a] (m^3 kg^{-1})	D_e [b] (10^{-12} m^2 s^{-1})	$R_{d,D}$ [c] (m^3 kg^{-1})	$R_{d,G}$ [d] (m^3 kg^{-1})	$R_{d,M}$ [e] (m^3 kg^{-1})
F2	2.91±0.43	−2.41±0.06	2.94±0.43	0.134	1.9±0.3	0.0024	–	0.098
F5	1.43±0.41	−2.64±0.05	1.45±0.42	0.178	2.2±0.5	0.0057	0.171	0.096
F8	1.71±0.67	−2.55±0.07	1.73±0.68	0.155	–	–	0.184	0.078
avg.			2.0±1.4	0.156±0.023	2.1±0.6	0.004±0.003	0.180±0.010	0.091±0.013

(a)   obtained from the analysis of the concentration of ^{85}Sr in both reservoirs as shown in Fig 4.4.

(b)   obtained from diffusive in steady state shown in Fig 4.2 using Eq(4-3).

(c)   obtained from values for D_a and D_e by $R_{d,D} = (D_a/D_e - \varepsilon)/\rho$.

(d)   obtained by grinding the surface of the granite sample facing to the source reservoir.

(e)   obtained from mass balance between initial inventory of ^{85}Sr in the source reservoir and the final distribution of ^{85}Sr.

Table 4-3 Results of grinding of the surfaces of granite disks used in SrI_2 diffusion experiments.

	F5		F8	
	cold side	hot side	cold side	hot side
initial weight (10^{-3} kg)	37.0254	36.9483	36.2890	36.2262
weight after the 2nd grinding [weight after the 1st grinding] (10^{-3} kg)	36.9602 [36.9712]	36.8812 [36.8882]	36.2177 [36.2354]	36.1639 [36.1760]
total weight loss (10^{-3} kg)	0.0652	0.0671	0.0713	0.0623
Sr-85 in Bq	<86	216	<89	307
Sr-85 in MBq kg^{-1}	<1.3	3.2	<1.2	4.9
weight collected (10^{-3} kg)	0.1042	0.0963	0.1572	0.0745
weight of carborundum (10^{-3} kg)	0.0390	0.0292	0.0859	0.0122

silicone packing

source
reservoir
c_1

measurement
reservoir
c_2

silicone
gasket

silicone packing

URL granite
diameter: 6.1×10^{-2} m
thickness: 5×10^{-3} m
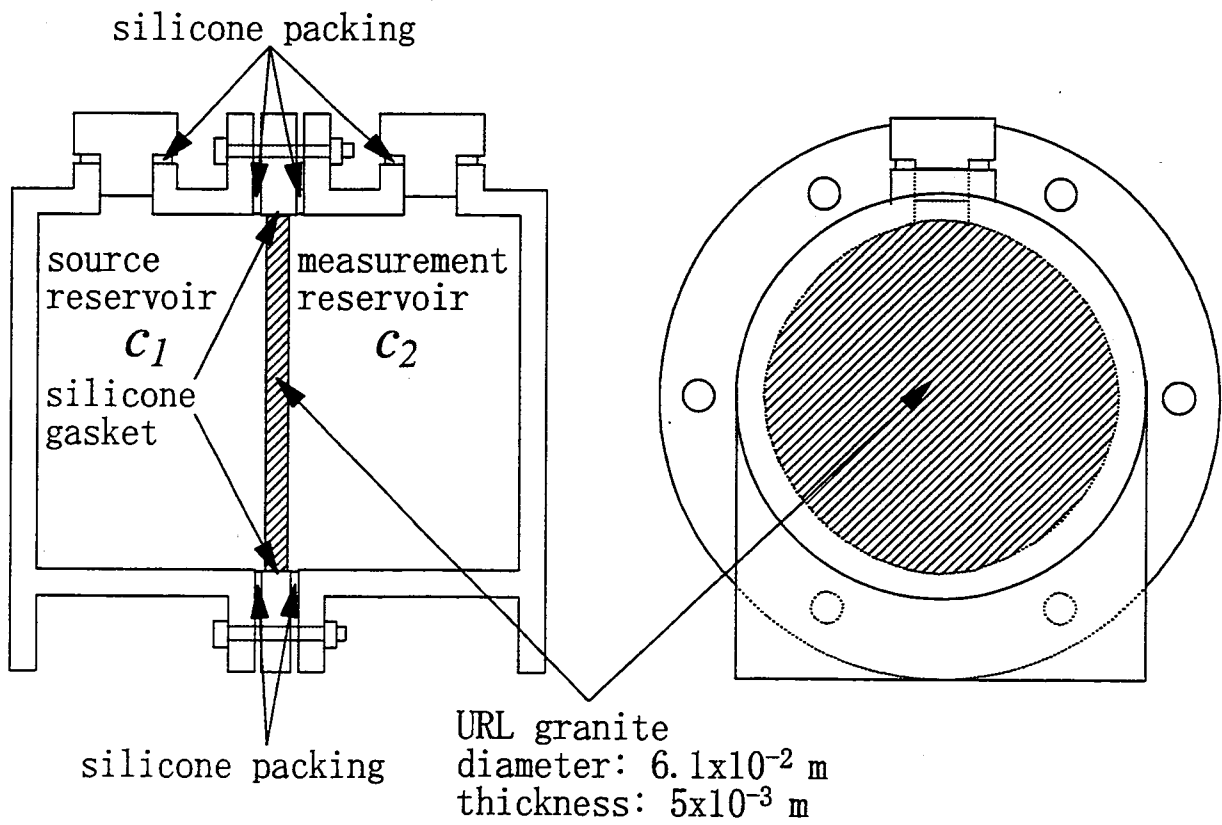
Fig. 4-1   Diffusion cell used in experiment for URL granite.

54
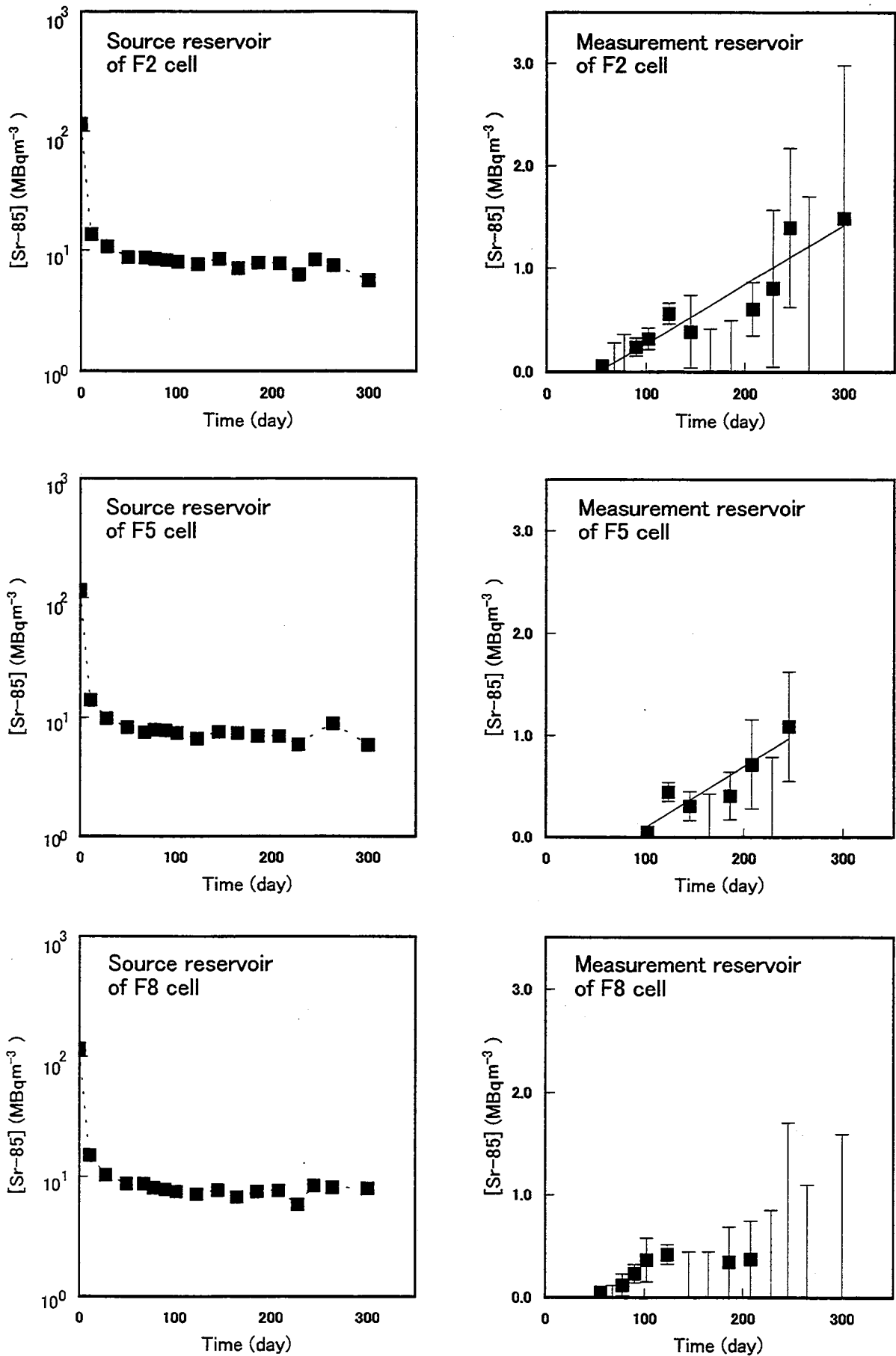
Fig. 4-2   Concentrations of [85]Sr in source and measurement reservoirs as a function of time obtained in the diffusion experiment for SrI$_2$ in URL granite.
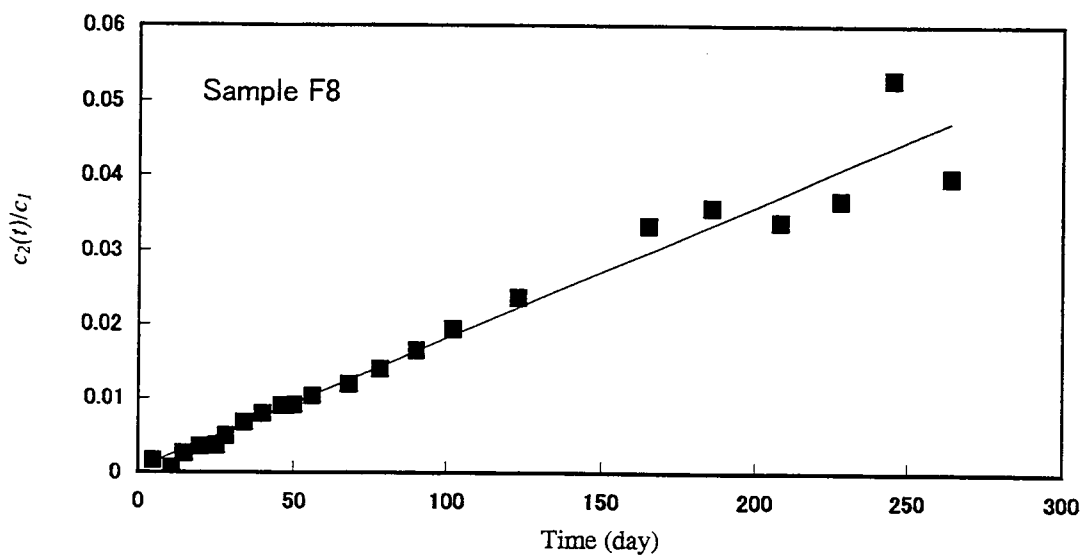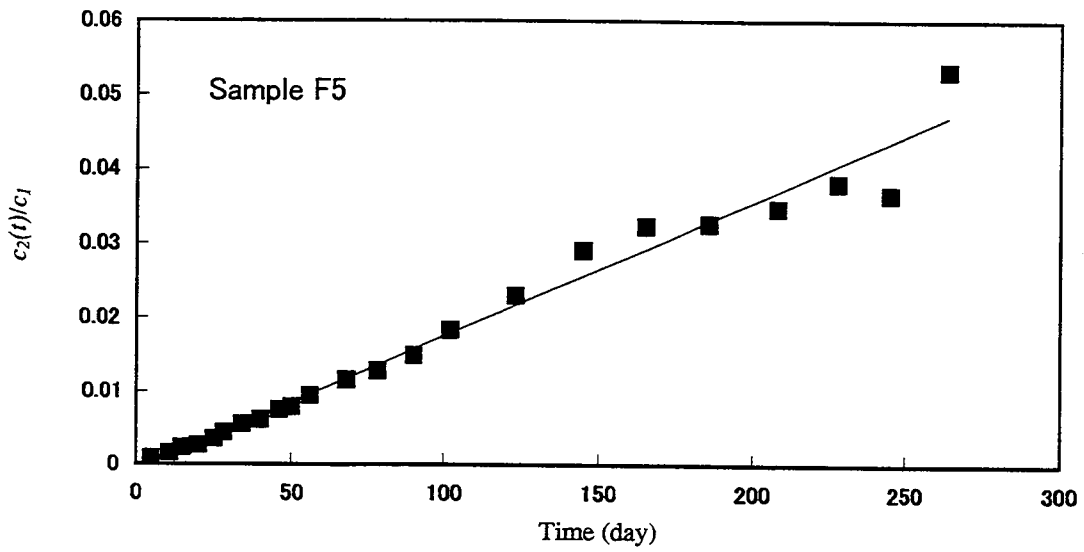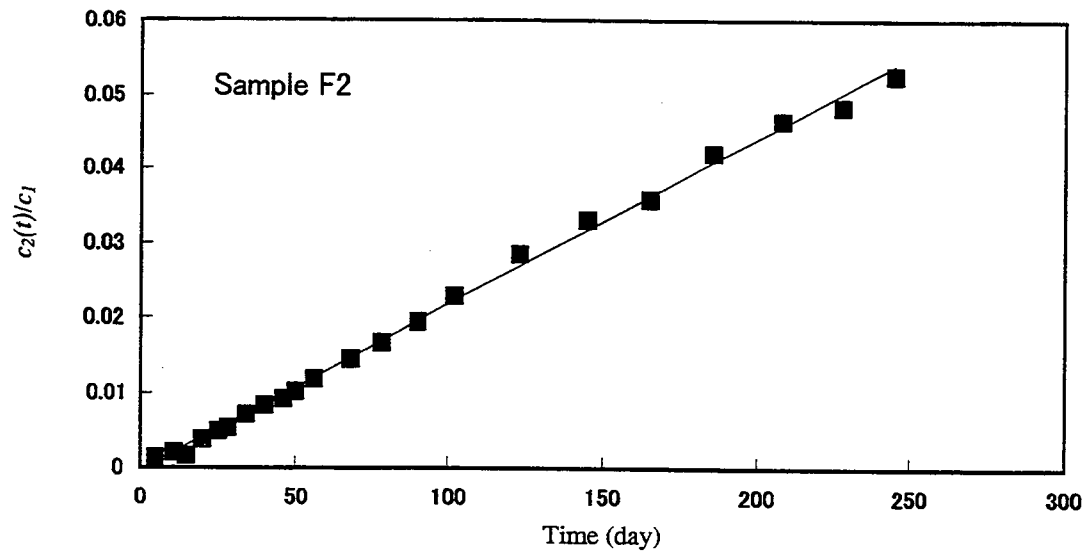
Fig. 4-3　Diffusion curves for ^{125}I through URL granite samples.
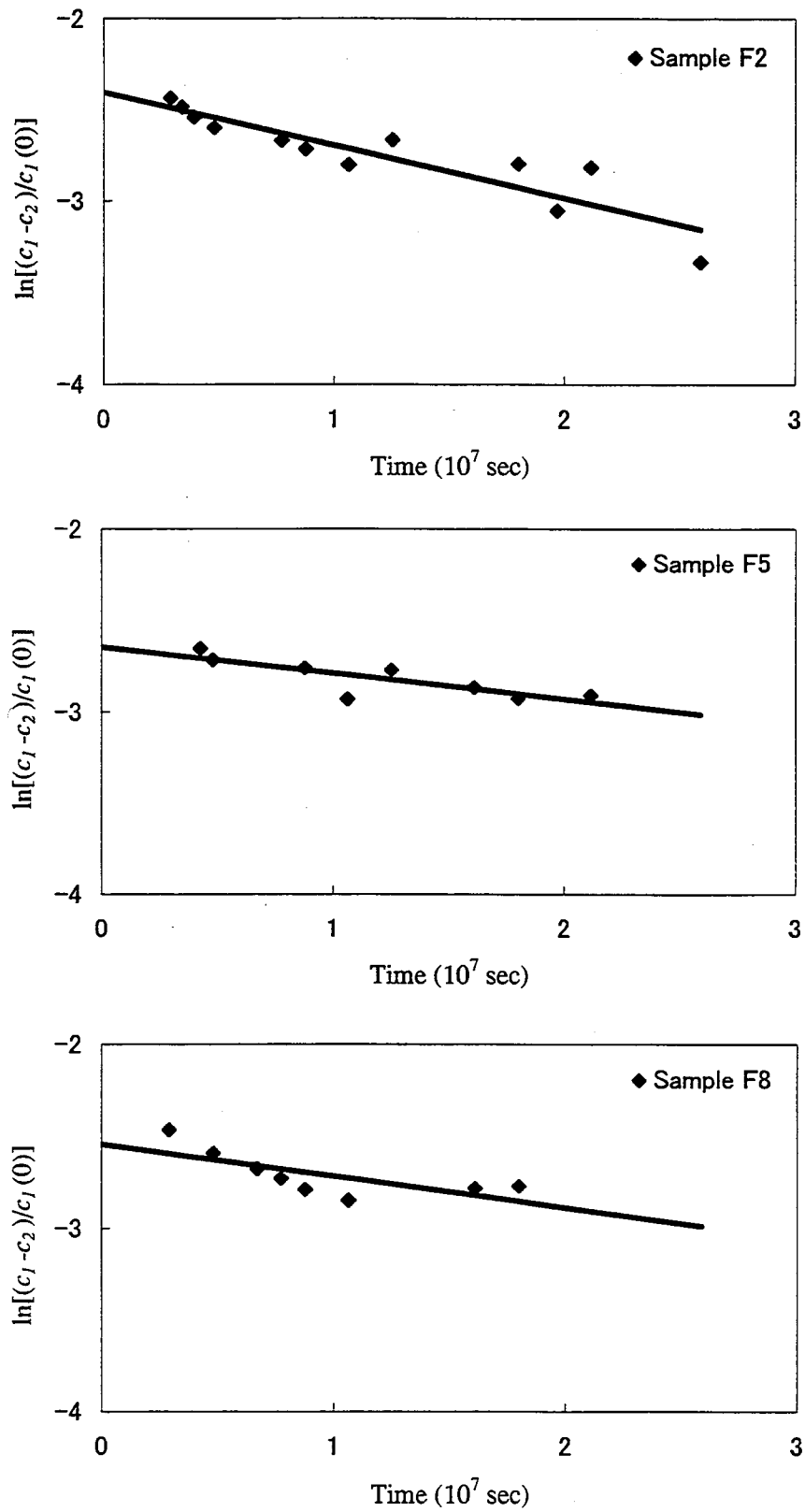
Fig. 4-4   Plots of $\ln[(c_1-c_2)/c_1(0)]$ vs. t for ^{85}Sr diffusion experiment through URL granite disks, F2, F5 and F8.

5. Diffusive behavior of cationic species

5.1. Introduction

Several researchers (Bradbury et al., 1986; Skagius & Neretnieks, 1988; Tsukamoto & Ohe, 1991) suggested contribution of diffusion of adsorbed ion or surface diffusion, based on the fact that effective diffusivity of cationic species was much larger than the calculated value based on Eq. (3-4). The evidence of the surface diffusion, however, has not been provided. In chapter 3, the effective diffusivity of Sr^{2+} in various rocks was found to roughly agree with

$$D_e = D_v \varepsilon \delta \tau^{-2} + D_s \rho R_d \qquad (5\text{-}1)$$

The second term of Eq. (5-1), $D_s \rho R_d$, represents the contribution of diffusion in the adsorbed state. The equation states that the effective diffusivity of an ion increases linearly with its distribution ratios onto rock materials.

The objective of this chapter is to confirm this increase of D_e with R_d. The through-diffusion experiment was performed for Ba^{2+} in a granite as a function of Ba concentration because the through-diffusion method provides the distribution ratio as well as the effective diffusivity.

5.2. Experimental

The preparation of the Inada granite disks and the diffusion cell used in the experiments were the same as those described in chapter 3. After assembling a diffusion cell, the diffusion cell was soaked in deionized water under vacuum for 3 days to evacuate all air from the interconnected pores. The diffusion cell was filled with a 10^2 mol m^{-3} BaCl$_2$ solution to pre-equilibrate the granite disks with the solution for 30 days.

The starting solution was prepared by combining 1.2×10^{-4} m^3 of 10^2 mol m^{-3} BaCl$_2$ solution, 3×10^{-7} m^3 of ^{133}Ba (10.5 y half life) stock solution (10^3 mol m^{-3} HCl) and 3×10^{-7} m^3 of ^{125}I (59.9 days half life) stock solution in a polypropylene bottle. Stock solution of ^{125}I was NaI/Na$_2$S$_2$O$_3$ solution in which the concentrations of I$^-$ and S$_2$O$_3^{2-}$ were 3.3×10^{-1} and 3.2×10^{-1} mol m^{-3}, respectively. Solutions were prepared from reagent grade chemicals (Wako Pure Chemical Industries, Ltd., Tokyo) and deionized water (Milli-Q Labo System, Millipore). To measure the concentrations of ^{133}Ba and ^{125}I in the solution, 1×10^{-6} m^3 aliquot was withdrawn and its activity determined by γ-spectrometry. The diffusion experiments were started by placing the starting solution in the source reservoir and the 10^2 mol m^{-3} BaCl$_2$ solution in the other, or measurement, reservoir. The diffusion experiments were performed at (25.0 ± 0.5)°C

in a water bath.

At 14 days intervals, 1×10^{-6} m^3 aliquot was taken from the measurement reservoirs to determine the concentrations of ^{133}Ba and ^{125}I. The 1×10^{-6} m^3 aliquot removed from the measurement reservoir was replaced by an equal volume of the 10^2 mol m^{-3} $BaCl_2$ solution to maintain the water levels in the two reservoirs. Diffusion experiment for the 10^2 mol m^{-3} $BaCl_2$ solution was performed in triplicate using diffusion cells N3, N12 and O3. The diffusion run was performed in triplicate also for 10, 1 and 10^{-1} mol m^{-3} $BaCl_2$ solution. Diffusion cells L14, N9 and O3 were used in the experiment performed at 10 mol m^{-3} $BaCl_2$ concentration, N6, O6 and O8 at a 1 mol m^{-3}, and L12, O16 and O22 at 10^{-1} mol m^{-3}.

The concentration of ^{133}Ba and ^{125}I in the source reservoir was also determined periodically. At the termination of each experiment, the inner wall of the measurement reservoir was rinsed with 10^3 mol m^{-3} HCl to determine the amount of ^{133}Ba adsorbed on the cell walls. The amount of ^{133}Ba was found to be less than 1 % of the final ^{133}Ba inventory in the measurement reservoir and can be ignored.

Zeta potential of the granite in $BaCl_2$ solutions were measured by a microscope electrophoresis zeta potential analyzer, RANK Brothers MARK II. The granite was crushed into around 2×10^{-3}-m grains and was milled by a mixer mill. The milled material was suspended in the $BaCl_2$ solutions overnight and the supernatant was used for the zeta potential analysis.

5.3. Results

Method of data analysis is the same as that described in chapter 3. Figure 5-1(a) shows the time dependence of the concentration of ^{133}Ba in the measurement reservoirs from the diffusion experiments using the 10^2 mol m^{-3} $BaCl_2$ solution. The statistical error of the determination of the tracer concentration was 1 - 5 % in radioactivity measurement. The concentrations increase linearly with time after 100 days from the start of the diffusion. The effective diffusivity (D_e) of $(2.7 - 10.1) \times 10^{-13}$ m^2 s^{-1} and the rock capacity factor ($\varepsilon + \rho R_d$) of $0.031 - 0.909$ were obtained by the least squares fitting and tabulated in Table 5-1. An average ^{133}Ba concentration in the period of $100 - 400$ days was used as c_1 in this calculation to make a correction for the decrease in ^{133}Ba concentration in the source reservoir during the experimental period. Figure 5-2 shows the time dependence of the concentration of ^{133}Ba in the measurement reservoirs from the diffusion experiments using the 10 mol m^{-3} $BaCl_2$ solution. The concentrations increase linearly with time after 100 days from the start of the diffusion. The effective diffusivity (D_e) of $(1.66 - 2.12) \times 10^{-13}$ m^2 s^{-1} and the rock capacity factor ($\varepsilon + \rho R_d$) of $0.194 - 0.235$ were obtained by the least squares fitting and tabulated in Table 5-1.

Figure 5-2 also shows the time dependence of the concentration of ^{133}Ba in the measurement reservoirs from the diffusion experiments using the 1 mol m^{-3} BaCl$_2$ solution. Linear portion of the curve appeared after 200 days from the start of the diffusion. The effective diffusivity (D_e) of $(1.99 - 2.90) \times 10^{-13}$ m^2 s^{-1} and the rock capacity factor ($\varepsilon + \rho R_d$) of $0.456 - 0.624$ were obtained by the least squares fitting and tabulated in Table 5-1. Figure 5-2 also shows the time dependence of the concentration of ^{133}Ba in the measurement reservoirs from the diffusion experiments using the 10^{-1} mol m^{-3} BaCl$_2$ solution. The concentrations increase linearly with time after 300 days. The effective diffusivity (D_e) of $(5.71 - 7.43) \times 10^{-13}$ m^2 s^{-1} and the rock capacity factor ($\varepsilon + \rho R_d$) of $1.198 - 1.379$ were obtained by the least squares fitting and tabulated in Table 5-1.

Figure 5-1(b) shows the time dependence of the concentration of ^{125}I in the measurement reservoirs from the diffusion experiments using the 10^2 mol m^{-3} BaCl$_2$ solution. The statistical error of the determination of the tracer concentration was 2 - 10 % in radioactivity measurement. The concentrations increase linearly with time after 100 days from the start of the diffusion. The effective diffusivity of $(6.28 - 15.6) \times 10^{-13}$ m^2 s^{-1} and the rock capacity factor ranged between -0.067 and 1.27 were obtained by the least squares fitting and tabulated in Table 5-2. An average ^{125}I concentration in the period of 100 – 250 days was used as c_1 in this calculation to make a correction for the decrease in ^{125}I concentration in the source reservoir during the experimental period. Figure 5-3 shows the time dependence of the concentration of ^{125}I in the measurement reservoirs from the diffusion experiments using the 10 mol m^{-3} BaCl$_2$ solution. The concentrations increase linearly with time for the first 70 days period. The increase of the ^{125}I concentration with time become less steep in the period of 70 – 120 days and another linear increase was observed in the period of 120 – 250 days. The second linear portion was analyzed using Eq. (3-3) to obtain another D_e:

$$D_e = -J/(\partial c/\partial x) = [c_2(250)-c_2(120)]VA^{-1}/[(\bar{c}_1 - \bar{c}_2)L^{-1}] \tag{5-2}$$

where $\bar{c}_1$: average concentration of ^{125}I in the source reservoir in the period of 120-250 days (Bq m^{-3}),

$\bar{c}_2$: average concentration of ^{125}I in the measurement reservoir in the period of 120-250 days (Bq m^{-3}).

An effective diffusivity (D_e) of $(3.07 - 3.91) \times 10^{-13}$ m^2 s^{-1} were obtained by the least squares fitting and tabulated in Table 5-2. Average ^{125}I concentrations in the period of 120 – 250 days was used as c_1 and c_2 in this calculation to make a correction for the change in ^{125}I concentration in the reservoirs during the period. Figure 5-3 also shows the time dependence of the concentration of ^{125}I in the measurement reservoirs from the diffusion experiments using the 1 mol m^{-3} BaCl$_2$ solution. From the first linear portion of the curve, the effective diffusivity of $(6.62 - 10.1) \times 10^{-13}$ m^2 s^{-1} and the rock capacity factor ranged between –0.065 and +0.090

were obtained. From the second linear portion of the curve, the effective diffusivity of $(1.41 - 4.74)\times10^{-13}$ m^2 s^{-1} was obtained. Figure 5-3 also shows the time dependence of the concentration of ^{125}I in the measurement reservoirs from the diffusion experiments using the 10^{-1} mol m^{-3} BaCl$_2$ solution. From the first linear portion of the curve, the D_e value of $(3.90 - 10.0)\times10^{-13}$ m^2 s^{-1} and the rock capacity factor ranged between -0.135 and $+0.152$ were obtained. From the second linear portion of the curve, the effective diffusivity of $(3.06 - 3.89)\times10^{-13}$ m^2 s^{-1} were obtained.

The zeta potential of the milled granite suspension was $+5.1$ mV in 10^2 mol m^{-3} BaCl$_2$ solution, -7.4 mV in 10 mol m^{-3} BaCl$_2$ solution, -13.6 mV in 1 mol m^{-3} BaCl$_2$ solution and -30.7 mV in 10^{-1} mol m^{-3}.

5.4. Discussion

The physical parameters of the granite, $\varepsilon\delta\tau^{-2}$, was estimated to be $(2.5\pm0.6)\times10^{-4}$ based on the D_e and D_v data for strontium described in chapter 3. Since the diffusion of ^{133}Ba in the present experiment was self-diffusion, D_v value of 8.48×10^{-10} m^2 s^{-1} (Li & Gregory, 1974) can be used. Equation (3-4) gave the effective diffusivity of barium of $(2.1\pm0.5)\times10^{-13}$ m^2 s^{-1} under the present experimental conditions. The D_e values obtained at the BaCl$_2$ concentration of 10 mol m^{-3} agreed with the estimated value. The D_e values obtained for the most concentrated solution of BaCl$_2$, 10^2 mol m^{-3}, were largely scattered in the triplicate runs, and further discussion was not made in this paper. The D_e value obtained for the 1 mol m^{-3} BaCl$_2$ solution was slightly higher than the estimated value and the value obtained for the 10^{-1} mol m^{-3} BaCl$_2$ solution was higher by 3 times.

The zeta potential gradually approached zero as the BaCl$_2$ concentration increased, which suggested that the sorption sites were almost saturated by Ba^{2+} ion at the higher BaCl$_2$ concentration. For this reason, the R_d value shown in Table 5-1 has a negative correlation to the BaCl$_2$ concentration. In case of low R_d value due to high BaCl$_2$ concentration, D_e value was low, while in case of higher R_d value due to low BaCl$_2$ concentration, D_e value was high. This positive correlation between D_e and R_d suggests the contribution of the second term of the Eq. (5-1).

The variation in D_e value was not due to the speciation of barium in the solution because complexations of Ba^{2+} by Cl$^-$ and S$_2$O$_3^{2-}$ are negligible and carbonate precipitation is not favorable under the working pH range (5.8 - 6.7) (Dean, 1978). The effective diffusivity of iodine, non-sorbed species, was not affected by BaCl$_2$ concentrations; $(6.1\pm0.8)\times10^{-13}$, $(8.4\pm1.4)\times10^{-13}$ and $(6.7\pm2.5)\times10^{-13}$ m^2 s^{-1} for 10, 1 and 10^{-1} mol m^{-3} BaCl$_2$ solution, respectively. These values are close to an estimated value, 6.4×10^{-13} m^2 s^{-1}, obtained from an equation for the effective diffusivity of iodine in rocks (Nishiyama et al., 1990)

$$D_e = 6.4 \times 10^{-10} \varepsilon^{1.3} \qquad (5\text{-}3)$$

where ε was 0.0049. The results for iodine show that the physical property of the pore structure was almost the same in the experiments, and accordingly the variation in D_e of Ba^{2+} was not physically caused. Both D_v and $\varepsilon\delta\tau^{-2}$ values were independent on the $BaCl_2$ concentration; nevertheless, D_e depended from $BaCl_2$ concentration. One has to deal with the second term of Eq. (5-1) or the contribution of the diffusion in adsorbed state.

The effective diffusivity was plotted versus ρR_d in Fig. 5-4. Because the data lie on a straight line, the data were fitted to Eq. (5-1) using the least squares method to determine the D_s value of $(2.4\pm0.1) \times 10^{-13}$ m^2 s^{-1}. The present D_s value is smaller than the value for Sr^{2+}, 3.5×10^{-12} m^2 s^{-1}, obtained in chapter 3. As presented by Lever (1986),

$$D_a = D_s \qquad (5\text{-}4)$$

if there is strong sorption and there is significant surface diffusion. The present D_s value is close to the D_a value obtained for Sr, $(2.0\pm1.4) \times 10^{-13}$ m^2 s^{-1}, described in chapter 4.

The effective diffusivity of iodine was reduced by half about after 100 days from the start of the diffusion as shown in Fig. 5-3. This reduction may be due to oxidation of I^-. In aerated conditions, iodide anion can be oxidized by dissolved oxygen;

$$I^- + 1.5 O_2(g) = IO_3^- \qquad \log K = 13.38 \text{ (Yamaguchi \& Takeda, 1999)} \qquad (5\text{-}5)$$
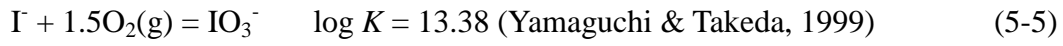
Diffusivity of IO_3^- in water at infinite dilution is 1.06×10^{-9} m^2 s^{-1} while that of I^- is 2.00×10^{-9} m^2 s^{-1} at 25°C (Li & Gregory, 1974).

Figure 5-5 shows schematics of the diffusion of $^{133}Ba^{2+}$ through the granite in the present experiment. Gradient of $^{133}Ba^{2+}$ concentration exists both in aqueous phase and in adsorbed phase between the source reservoir and the measurement reservoir. Diffusion of $^{133}Ba^{2+}$ is driven by both of these gradients. Diffusive flux in adsorbed phase, $-D_s\rho\partial q/\partial x$, prevails over that in aqueous phase, $-D_p\varepsilon\partial c/\partial x$, when distribution ratio is high.

5.5. Conclusion

The effective diffusivity (D_e) and ρR_d of $^{133}Ba^{2+}$ in Inada granite have been determined by the through-diffusion method. Experiments were performed in triplicate for 10^{-1}, 1, 10 and 10^2 mol m^{-3} $BaCl_2$ solution at 25°C. The D_e value obtained at the $BaCl_2$ concentration of 10 mol m^{-3}, agreed to the estimated value based on the pore diffusion model. The lower $BaCl_2$ concentration yielded the higher D_e value and higher ρR_d value. The variation in D_e was neither due to the speciation of barium in the solution nor variation in physical properties of the pores structure in the rock. Contribution of diffusion in adsorbed state should be

responsible for the variation in D_e. The result is strongly indicative of the diffusion in adsorbed state. When we apply pore diffusion model to sorbed ions ignoring the contribution of surface diffusion, diffusive flux may be underestimated.

Table 5-1 Effective diffusivity and rock capacity factor for barium in Inada granite.

[BaCl$_2$] (mol m^{-3})	Run No.	D_e (10^{-13} m^2 s^{-1})	ρR_d (-)
10^{-1}	L12	6.57	2.14
	O16	7.43	2.53
	O22	5.71	2.01
	Avg.	6.6±0.7	2.23±0.22
1	N6	1.99	0.52
	O6	2.25	0.56
	O8	2.90	0.72
	Avg.	2.38±0.38	0.60±0.09
10	L14	1.66	0.20
	N9	2.12	0.24
	O3	2.08	0.21
	Avg.	1.95±0.21	0.216±0.019
10^2	N3	8.40	0.36
	N12	10.1	1.01
	O10	2.70	0.03

Table 5-2 Effective diffusivity and rock capacity factor for iodine in Inada granite.

[BaCl$_2$] (mol m^{-3})	Run No.	0 – 70 days		120 - 250 days
		D_e (10^{-13} m^2 s^{-1})	ρR_d (-)	D_e (10^{-13} m^2 s^{-1})
10^{-1}	L12	10.0	0.15	3.06
	O16	3.90	-0.14	3.54
	O22	6.29	-0.10	3.89
	Avg.	6.7±2.5	-0.03±0.13	3.50±0.34
1	N6	6.62	0.03	2.20
	O6	8.55	-0.07	1.41
	O8	10.1	0.09	4.74
	Avg.	8.4±1.4	0.02±0.06	2.8±1.5
10	L14	5.15	-0.03	3.18
	N9	7.22	0.00	3.07
	O3	6.07	-0.03	3.91
	Avg.	6.2±0.8	-0.019±0.012	3.39±0.38
10^2	N3	15.6	1.27	(*)
	N12	15.0	1.16	(*)
	O10	6.28	-0.07	(*)

(*) No difference was observed between two period.

$\frac{c_2(t)}{c_1}$　　(a): ^{133}Ba　$\frac{c_1(t)}{c_1(0)}$　$\frac{c_2(t)}{c_1}$　　(b): ^{125}I　$\frac{c_1(t)}{c_1(0)}$

1.0

0.8

0.6

0.08　0.4

■ N3
▼ N12
▲ O10
● source

0.06

0.04

0.02

0

0　250　500
Time (day)

1.0

0.8

0.6

0.08　0.4

■ N3
▼ N12
▼ O10
● source

0.06

0.04

0.02

0

0　100　200　300
Time (day)
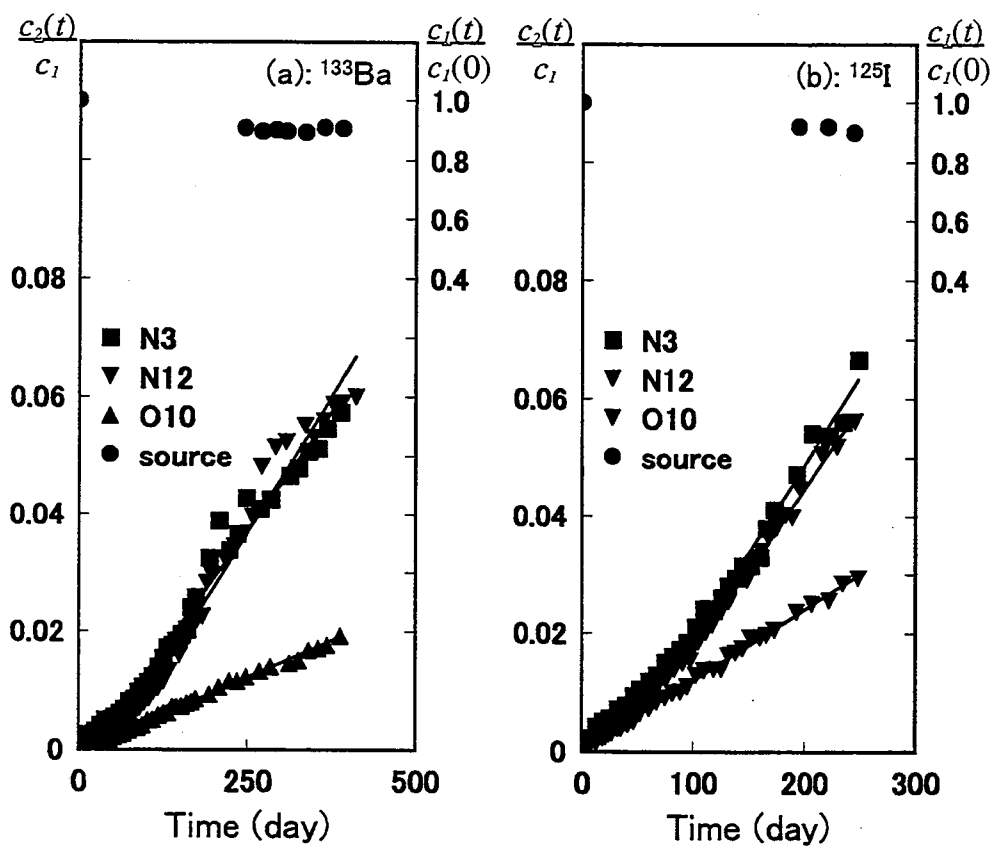
Fig. 5-1　Diffusion curves obtained in 10^2 mol m^{-3} BaCl$_2$ solution. Normalized concentrations of ^{133}Ba in the measurement reservoir and in the source reservoir (a) and normalized concentrations of ^{125}I in the measurement reservoir and in the source reservoir (b).
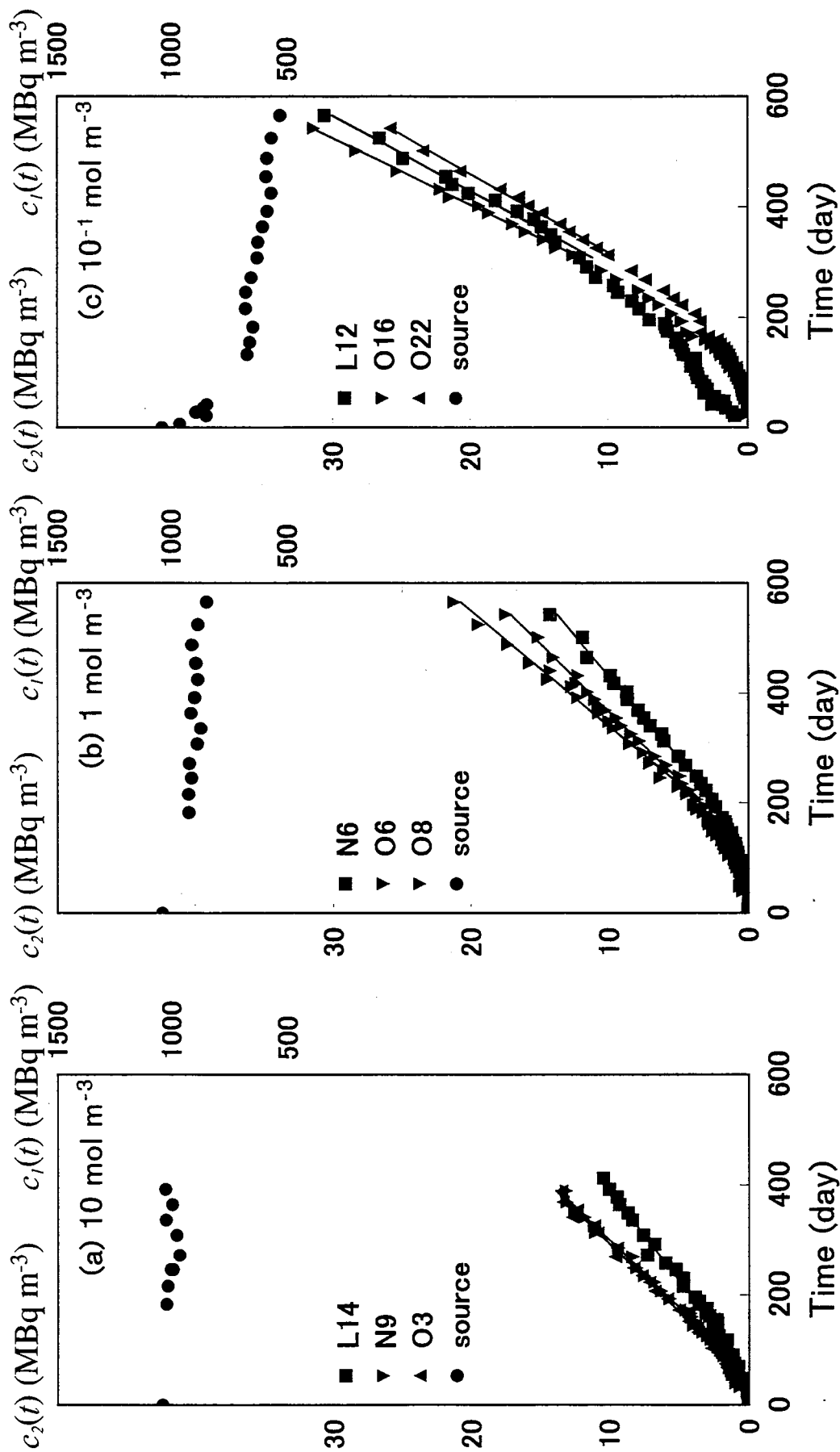
Fig. 5-2 Diffusion curves for ^{133}Ba through Inada granite samples obtained in 10 mol m^{-3} BaCl$_2$ solution (a), in 1 mol m^{-3} BaCl$_2$ solution (b) and in 10^{-1} mol m^{-3} BaCl$_2$ solution (c).
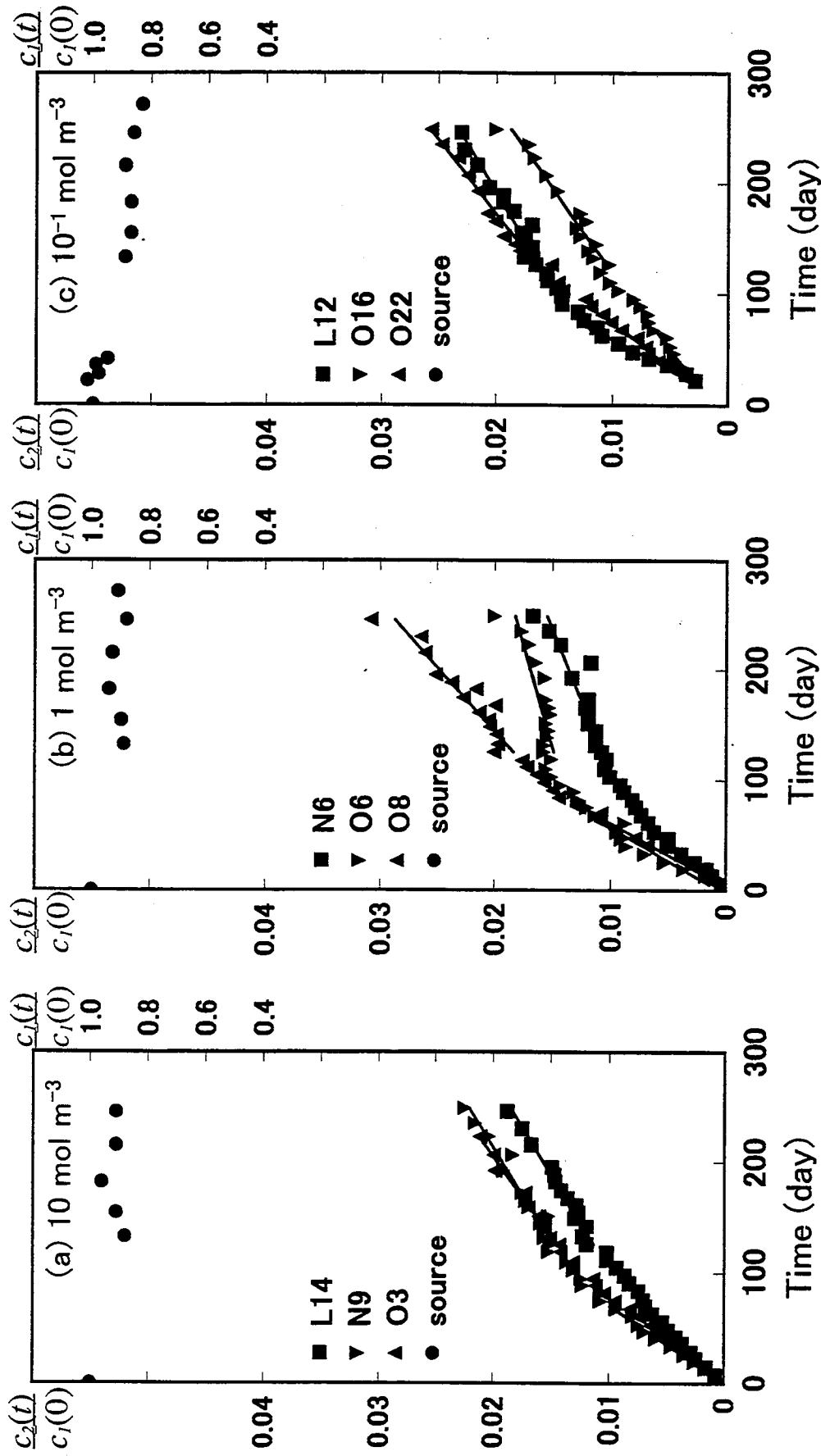
Fig. 5-3 Diffusion curves for ^{125}I obtained through Inada granite samples in 10 mol m^{-3} BaCl$_2$ solution (a), in 1 mol m^{-3} BaCl$_2$ solution (b) and in 10^{-1} mol m^{-3} BaCl$_2$ solution (c).
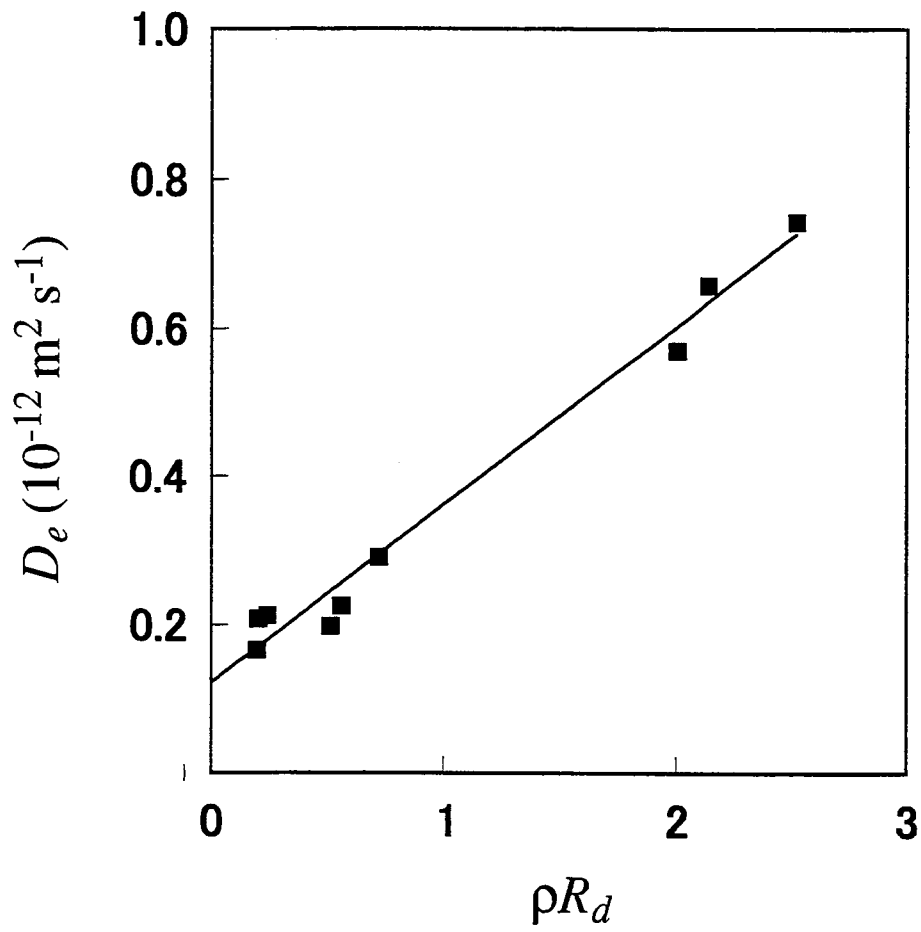
Fig. 5-4   Correlation between effective diffusivity and ρR_d for ^{133}Ba in Inada granite.
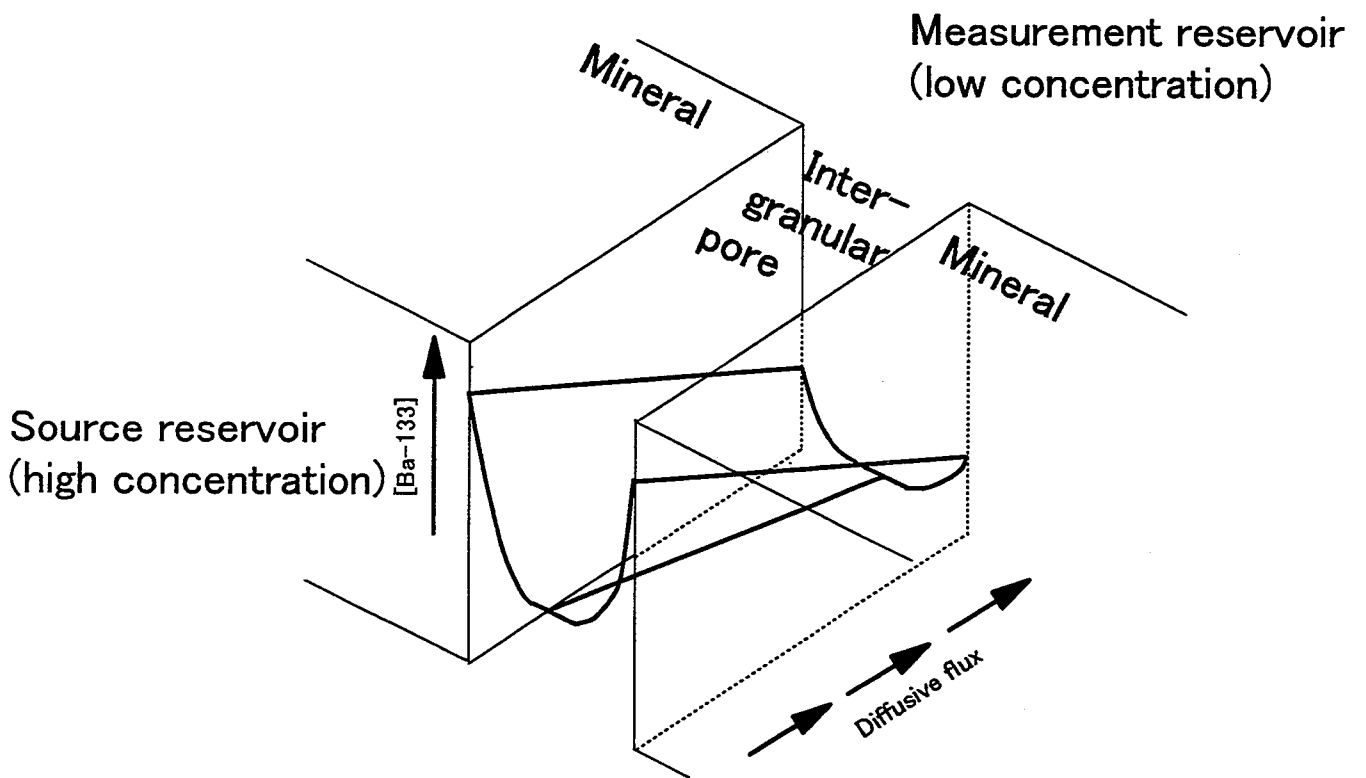
Fig. 5-5　Schematics of the aqueous and sorbed phase diffusion of Ba^{2+} in the diffusion experiments through Inada granite disk.

6. Diffusive behavior of anionic species

6.1. Introduction

For anionic species, diffusion into rock matrix is an important retarding mechanism because retardation by sorption is not promising. Many researchers observed that the effective diffusivity of anionic species in compacted bentonite is smaller than the value estimated by Eq. (1-4). The accessible pore space in the compacted bentonite is considered to be limited for anionic species because of electrostatic repulsion between anionic species and negatively charged surface of the wall of the pores. Nishiyama et al. (1990) reported that the effective diffusivity of I^- in an andesite is smaller than the value estimated by Eq. (1-4).

The objective of this chapter is to examine if the effective diffusivity of anionic species in the granite is reduced or not by electrostatic repulsion between the species and negatively charged surface of the granite.

6.2. Experimental

Two granite disks, D5 and J11, were used. The preparation of the granite disks and the diffusion cell used in the experiments were the same as those described in chapter 3. The starting solution for D5 was prepared by combining 1.2×10^{-4} m^3 of 10^2 mol m^{-3} SrI$_2$ solution and 10^{-8} m^3 of ^{125}I stock solution in a polypropylene bottle. The concentration of ^{125}I in the solution in the source reservoir was planed to be 2.7×10^9 Bq m^{-3}. To make sure the concentrations of ^{125}I in the solution, a 1×10^{-7} m^3 aliquot was withdrawn and its activity determined by γ–spectrometry by a pure Ge detector. After the granite disks were soaked in deionized water under vacuum for a few days to evacuate all air from the interconnected pores, the diffusion experiment was started by placing the starting solution in the source reservoir and the deionized water in the measurement reservoir. The starting solution for J11 was prepared by combining 1.2×10^{-4} m^3 of a 10^2 mol m^{-3} CsI solution, a 1×10^{-8}-m^3 portion of ^{125}I stock solution and a 1×10^{-8}-m^3 portion of ^{134}Cs stock solution in a polypropylene bottle. The concentrations of ^{125}I and ^{134}Cs in the starting solution were planned to be 2.7×10^9 Bq m^{-3} and 3.33×10^8 Bq m^{-3}, respectively. To make sure the concentrations of ^{125}I and ^{134}Cs in the starting solution, a 1×10^{-6} m^3 aliquot was withdrawn and its activity determined by γ-spectrometry. The diffusion experiments were started by placing the starting solution in the source reservoir and the deionized water in the measurement reservoir. At 7 days intervals, 1×10^{-6} m^3 aliquot was taken from the measurement reservoirs to determine the concentrations of ^{125}I and ^{134}Cs. The 1×10^{-6} m^3 aliquot removed from the measurement reservoir was

replaced by an equal volume of the distilled and deionized water to maintain the water levels in the two reservoirs. The diffusion experiments were performed at (25.0±0.5) °C in a water bath.

For comparison, effective diffusivity of HTO and I^- in compacted bentonite were measured. The bentonite clay used in this study was a Na type bentonite, Kunigel V1, from Kunimine Industries Co., Ltd. The acrylic diffusion cell used in this study was shown in Fig. 6-1. The central member of the diffusion cell has a hole that is 2×10^{-2} m in diameter and 1.7×10^{-2} m in depth. A 7.33-g weight of the bentonite powder was placed in the hole and held by a stainless steel sintered filter that is 1.2×10^{-3}-m thick. The density of the bentonite was 1.6×10^{-3} kg m^{-3}. The central member containing the bentonite was sandwiched between the two reservoirs, each with a capacity of 1.15×10^{-4} m^3. The assembled diffusion cell was soaked in 4.5 mol m^{-3} Na$_2$SO$_4$ solution under vacuum to evacuate all air from the interconnected pores in the bentonite. The starting solution was prepared by combining 1.2×10^{-4} m^3 of 4.5 mol m^{-3} Na$_2$SO$_4$ solution and 1.25×10^{-7} m^3 of ^{3}H stock solution in a polypropylene bottle. The concentration of ^{3}H in the solution in the source reservoir was planed to be 8.0×10^8 Bq m^{-3}. To make sure the concentrations of ^{3}H in the solution, five 1×10^{-7} m^3 aliquots were withdrawn and its activity determined by liquid scintillation counter. The diffusion experiment was started by placing the starting solution in the source reservoir and the 4.5 mol m^{-3} Na$_2$SO$_4$ solution in the measurement reservoir. At 7 days intervals, 1×10^{-6} m^3 aliquot was taken from the measurement reservoirs to determine the concentrations of ^{3}H. The 1×10^{-6}-m^3 aliquot removed from the measurement reservoir was replaced by an equal volume of the blank solution to maintain the water levels in the two reservoirs. The diffusion experiments were performed at (25.0±0.5) °C in a water bath. After the ^{3}H diffusion run, another diffusion run was performed using the diffusion cell. The ^{125}I source solution was prepared by combining 1.2×10^{-4} m^3 of 4.5 mol m^{-3} Na$_2$SO$_4$ solution and 1.34×10^{-6} m^3 of ^{125}I stock solution in a polypropylene bottle. The concentration of ^{125}I in the solution in the source reservoir was planed to be 1×10^8 Bq m^{-3}. To make sure the concentrations of ^{125}I in the solution, three 10^{-7} m^3 aliquots were withdrawn and its activity determined by γ-spectrometry. The diffusion experiment was started by replacing the ^{3}H source solution with the ^{125}I source solution. At 7 days intervals, 1×10^{-6} m^3 aliquot was taken from the measurement reservoirs to determine the concentrations of ^{125}I. The 1×10^{-6}-m^3 aliquot removed from the measurement reservoir was replaced by an equal volume of the blank solution to maintain the water levels in the two reservoirs. The diffusion experiments were performed at room temperature (30°C) under Ar in an atmosphere-controlled chamber to minimize the oxidation of iodine.

Solutions were prepared from reagent grade chemicals (Wako Pure Chemical Ind., Ltd., Tokyo), standard radioisotope solutions (SCETI Company Ltd., Tokyo) and deionized water (Milli-Q Labo System, Millipore).

6.3. Results and discussion

The through-diffusion curves obtained from the ^{3}H and ^{125}I diffusion experiments in bentonite were shown in Fig. 6-2. The method described by Crank (1975) was used to analyze these data. Values for D_e were obtained from the slope, and the rock capacity factor, $(\varepsilon + \rho R_d)$, from the intercept on the concentration axis of the extrapolated linear portion,

$$c_2(t)/c_1 = AV^{-1}L^{-1}D_e t - ALV^{-1}(\varepsilon + \rho R_d)/6 \qquad (6\text{-}1)$$

Values for c_1 in this data analysis were determined by correcting the initial iodine concentration in source reservoirs for the decrease in the concentration during the experimental period. The effective diffusivity and the rock capacity factor are presented in Table 6-1. The difference in diffusivity was very clear between ^{3}H and ^{125}I; the effective diffusivity of iodine is much smaller than that of ^{3}H. The result is consistent with literature.

The through-diffusion curves obtained from the iodine diffusion experiments in the granite are shown in figures 6-3. The effective diffusivity and the rock capacity factor obtained by above-mentioned way are presented in Table 6-1. The effective diffusivities of I^- in granite are not so much different from that of HTO. D_e values of anionic species in bentonite is much smaller than that of neutral species because the effective porosity is much smaller for anionic species than for neutral species due to electrostatic repulsion between the mineral surfaces and the diffusing species. This is not the case for the granite because the size of the pore is much larger than the range of the electrostatic force as shown in chapter 2.

The diffusivity of ions in water is affected by the ionic strength of the solution (Ushiki et al., 1993) and by the mode of diffusion (Li & Gregory 1974). The diffusivity of I^- in water under the experimental conditions are tabulated in Table 6-1. The small variation between the experimentally obtained D_e values for I^- is consistent with the variation in D_v as shown in Fig. 6-4. If the D_e value of HTO in a rock, D_e(HTO), is known, the D_e value of I^-, $D_e(I^-)$, can be estimated using their diffusivity in water by

$$D_e(I^-) = D_e(\text{HTO}) \times D_v(I^-) / D_v(\text{HTO}) \qquad (6\text{-}2)$$

as shown with the broken line in Fig. 6-4.

6.4. Conclusion

For non-sorbed anionic species, the effective diffusivity in compacted bentonite is smaller than the value estimated by Eq. (1-4). Such a reduction of the D_e value was not observed for

the diffusion of anionic species in the granite. The electrostatic repulsion between anionic species and negatively charged surface of the wall of the pores does not reduce the effective diffusivity so much because the pores in granite is larger than the range of electrostatic force. The effective diffusivity of anionic species in granite is affected by the ionic strength of the solution and by the mode of diffusion.

Table 6-1 Effective diffusivity (D_e) and rock capacity factor ($\varepsilon+\rho R_d$) of species in granite and in bentonite[a].

Media	Species	D_e (m² s⁻¹)	$\varepsilon+\rho R_d$	Solution	Temp.	Reference	D_v (m² s⁻¹)
Granite	I⁻	$(5.06\pm0.09)\times10^{-13}$	$-0.04\ \pm0.12$	10^2 mol m⁻³ SrI₂ → DDW	25°C	This chapter	1.14×10^{-9}
	I⁻	$(7.98\pm0.07)\times10^{-13}$	$-0.43\ \pm0.17$	10^2 mol m⁻³ CsI → DDW	25°C	This chapter	1.87×10^{-9}
	Cs⁺	$(6.32\pm0.09)\times10^{-13}$	$-0.27\ \pm0.21$				
	HTO	$(7.7\pm1.4)\times10^{-13}$	$+0.01\ \pm0.20$	DDW	25°C	Chapter 3	2.14×10^{-9}
	I⁻	$(5.80\pm0.05)\times10^{-13}$	$+0.36\ \pm0.15$	10^2 mol m⁻³ KI	25°C	Chapter 3	1.86×10^{-9}
	I⁻	$(7.1\pm2.1)\times10^{-13}$	$-0.01\ \pm0.09$	10^{-1}–10^{1} mol m⁻³ BaCl₂	25°C	Chapter 5	2.04×10^{-9}
Bentonite	HTO	$(2.12\pm0.36)\times10^{-10}$	$+0.64\ \pm0.18$	4.5 mol m⁻³ Na₂SO₄	25°C	This chapter	2.14×10^{-9}
	I⁻	$(8.00\pm0.15)\times10^{-12}$	$+0.023\pm0.012$		room(30°C)		2.04×10^{-9}

(a) Kunigel V1 (density: 1.6×10^3 kg m⁻³, calculated porosity: 0.41%).

silicone packing

tracer
c_1

filter
holder

c_2

bentonite
diameter 20 mm
thickness 14.6 mm

sintered SUS filter
thickness 1.2 mm

silicone packing
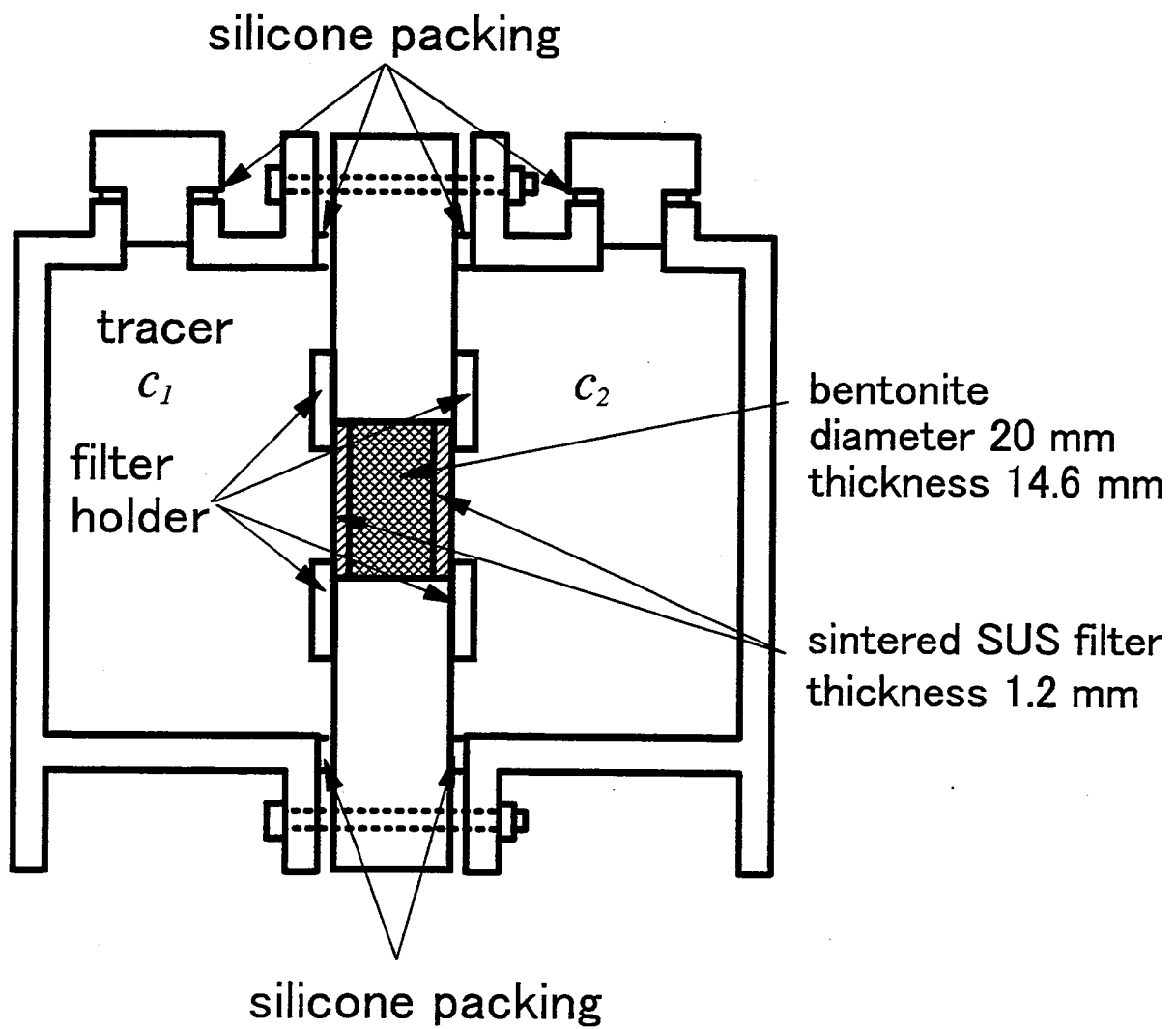
Fig. 6-1 Diffusion cell used in diffusion experiments for HTO and ^{125}I through bentonite.
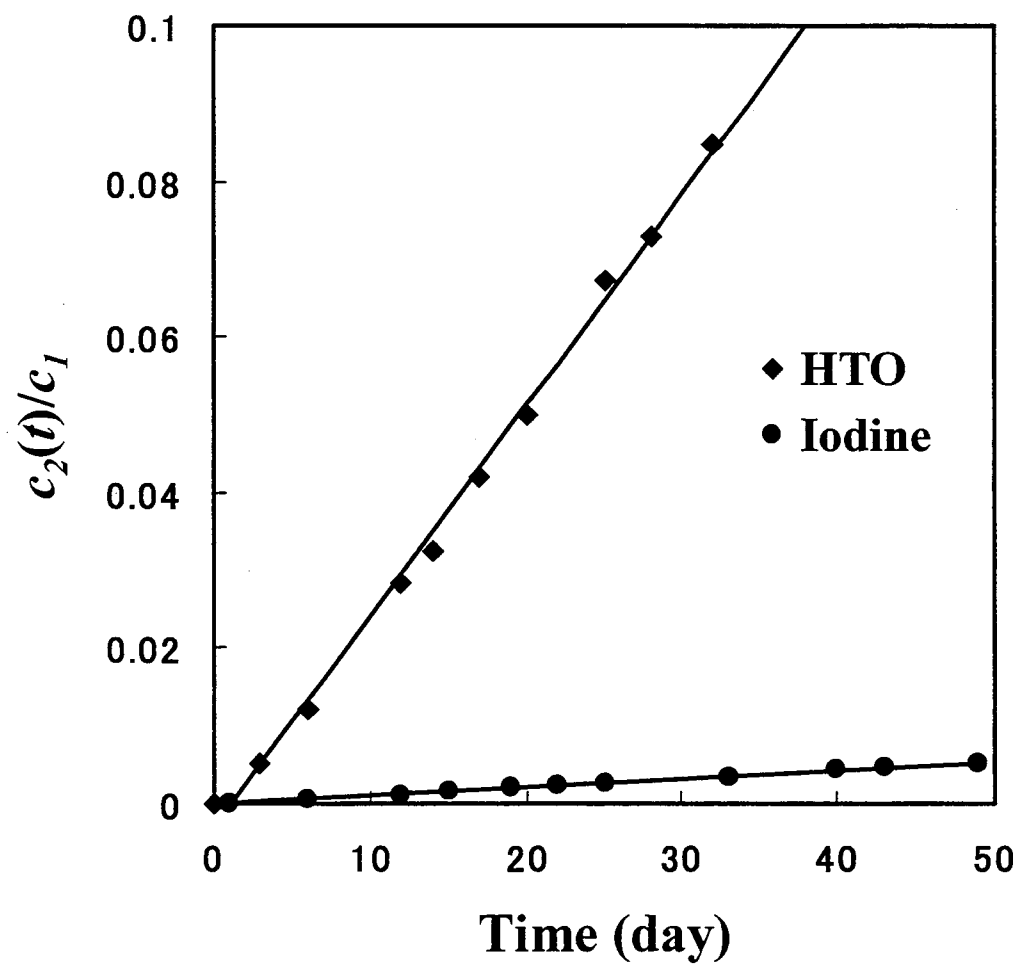
Fig. 6-2   Diffusion curves for HTO and $^{125}I^-$ through bentonite.
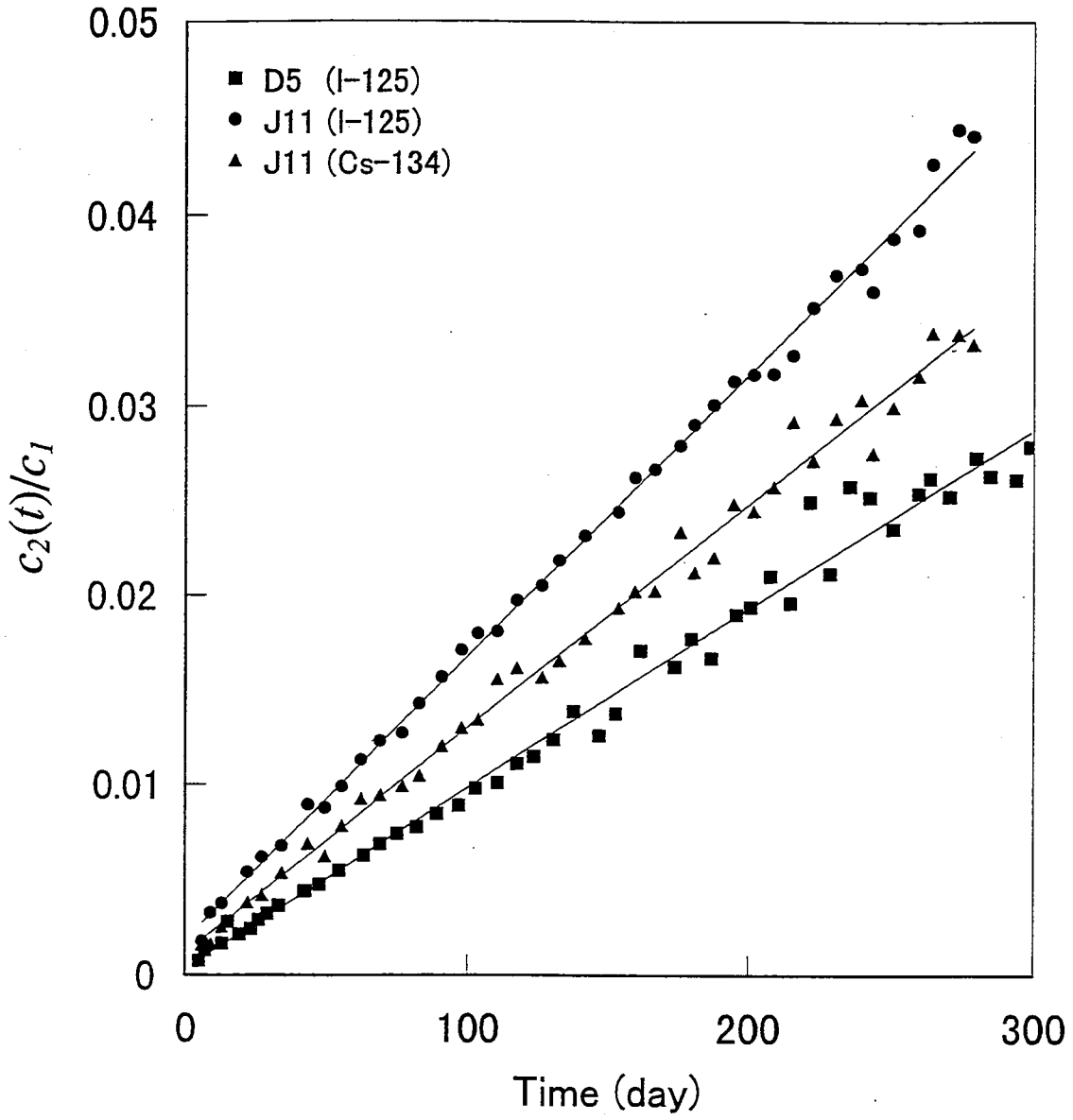
Fig. 6-3 Diffusion curves for ^{125}I through Inada granite samples.
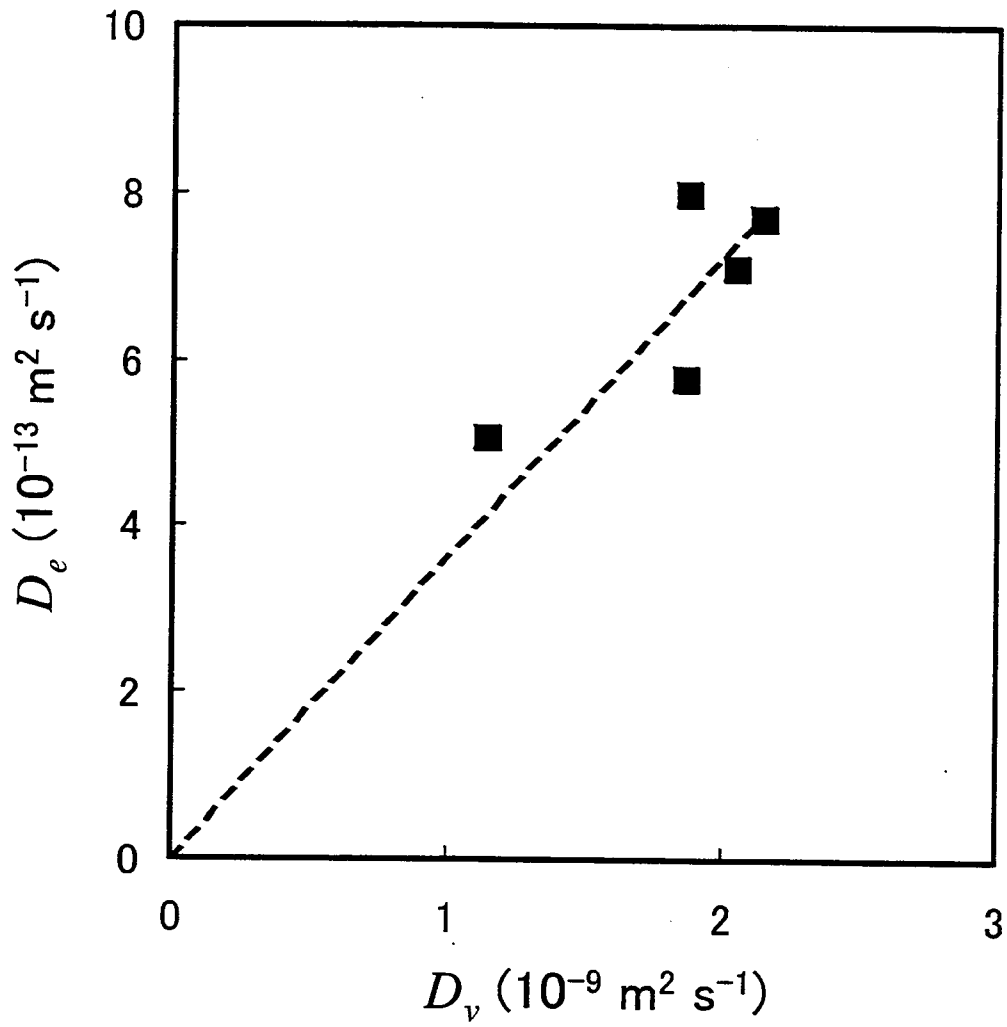
Fig. 6-4 Correlation between effective diffusivity for Γ in granite and its diffusivity in bulk of the solution.

7. Diffusive behavior of actinide carbonate complexes

7.1. Introduction

It may be possible to apply Eq. (1-4) to estimate the D_e value for actinide species such as UO_2^{2+}, Th^{4+}, and several trivalent actinides whose bulk diffusivities in solution are known (Li & Gregory, 1974; Fourest et al., 1995). This is not the case, however, for actinide complex species because data on their bulk diffusivity are not available. It is necessary to experimentally determine the diffusivity in rock matrices for carbonate complex species that are potential dominant aqueous species of actinides in groundwater under geologic disposal conditions.

The objectives of this chapter are to perform series of through-diffusion experiments for actinide carbonate complexes in granite and to see if the surface diffusion is significant or not.

7.2. Experimental

Preparation

The preparation of the Inada granite disk and the acrylic diffusion cell used in this study were the same as those described in chapter 3. After evacuating all air from the interconnected pores in the granite disk, the diffusion cell was transferred into an atmosphere-controlled chamber and was filled with a working solution under atmospheric pressure to pre-condition the disks for the solution for 30 days. The oxygen concentration in the chamber was kept lower than a few ppm. Solutions were prepared from reagent grade chemicals (Wako Pure Chemical Ind., Ltd. or Aldrich Chemical Company, Inc.) and distilled and deionized water (Milli-Q Labo System, Millipore). The diffusion experiments were performed in triplicate at room temperature.

Series 1

The first series of experiments was performed for Pu using the granite and the groundwater from URL described in chapter 4. The diffusion experiment was performed in triplicate using three granite disks, F3, F6 and F9 under N_2 atmosphere. Plutonium-238 was prepared as a 2.6×10^{-2} mol m^{-3} (4×10^{12} Bq m^{-3}) Pu(IV) solution in aqua regia. The starting source solution was prepared by combining a 1.5×10^{-5} m^3 volume of 10^2 mol m^{-3} NaHCO$_3$ solution, a 1×10^{-8} m^3 volume of 1.5×10^4 mol m^{-3} NaOH, a 1×10^{-8} m^3 volume of a Pu stock solution, 3×10^{-6} m^3 volume of 1.2×10^2 mol m^{-3} NaNO$_2$ solution, a 3×10^{-4} m^3 volume of the groundwater and a 42×10^{-6} m^3 volume of deionized water in a polypropylene bottle. The groundwater was filtered through 0.2 μm filter before use. The initial concentrations of Pu, total carbonate and

NO_2^- were planed as 7.2×10^{-7} mol m^{-3}, 2.5 mol m^{-3} and 1 mol m^{-3}, respectively. The pH and Eh were measured. Lowering of the pH of the solution during preparation may cause loss of bicarbonate ion from the solution and precipitation of $PuO_2 \cdot nH_2O$. To minimize pH changes of the groundwater through the preparation, Pu was prepared as $NaHCO_3$ solution and then mixed with groundwater. A couple of 2×10^{-7} m^3 aliquots was taken from the source solution to determine the Pu concentration in the source solution. A Pu diffusion experiment was started by placing the solution into one reservoir of the diffusion cell. A 2×10^{-7}-m^3 aliquot was taken after 4, 24 and 120 hours to measure the Pu concentration by liquid scintillation counting (LSC). A 1×10^{-6}-m^3 aliquot was sampled from the measurement reservoir and 1×10^{-7}-m^3 aliquot from the source reservoir at approximately 10 days intervals to follow the Pu concentration with time. The balance between the water levels in the 2 reservoirs was maintained by adding the groundwater into the measurement reservoir.

The oxidation state of Pu in the source solution was analyzed by using TTA extraction technique (Foti & Freiling, 1964; Nitsche et al., 1988) under N_2. A 2×10^{-7} m^3 volume of the source solution was acidified with 1.8×10^{-6} m^3 of 1.1×10^3 mol m^{-3} HCl in a vial. A 2×10^{-6}-m^3 volume of a 4×10^2 mol m^{-3} TTA xylene solution was added and the mixture was shaken for 10 min. The extraction procedure was triplicated. The mixture was settled for another 10 min for phase separation. A 2×10^{-7} m^3 aliquot was taken from aqueous and organic phase and the Pu concentration was measured. The oxidation state of Pu in the stock solution was also analyzed by the same procedure for comparison.

After terminating the 1st series of experiments, 1×10^{-6}-m^3 aliquots were withdrawn from the reservoirs and analyzed by LSC. The remainder of the solutions was removed from both reservoirs of the three diffusion cells, F3, F6 and F9. Both reservoirs of these three cells were filled with 1×10^{-4}-m^3 volume of distilled and deionized water and left to soak for a 1-hour period. 1×10^{-6}-m^3 aliquots of these rinse solutions were taken from the reservoirs and prepared for radiometric analysis by LSC to determine the amount of Pu readily removed from inner walls of the reservoirs. The remaining rinse solution was removed from the cells and discarded. The three diffusion cells were then removed from the N_2 glove box and disassembled. Both acrylic compartments of the three diffusion cells were washed with 1.1×10^{-4} m^3 of 10^3 mol m^{-3} HCl for a 24-hr period. 1×10^{-6}-m^3 aliquots of the acid washings were taken for radiometric analysis by LSC.

The granite disks were each sandwiched between two photographic plates for a period of 7 days and for a period of 20 days. Four small granite coupons were cut from one of the granite disks using a diamond cut off saw. The dimensions of these coupons is 4×10^{-3} m x 8×10^{-3} m. The surface of the coupon exposed to the source reservoir were ion milled at the rate of 1.2×10^{-10} m min^{-1} or 7×10^{-9} m hr^{-1}. The samples were ion milled for 4, 8, 16, and 32 hours to remove 2.9×10^{-8}, 5.7×10^{-8}, 1.15×10^{-7} and 2.3×10^{-7} m of granite from the surfaces. The

coupons were autoradiographed afterwards. A piece of granite disk used in the Pu diffusion experiment was sliced laterally at an angle using a diamond wheel saw as shown in Fig 7-1. The smallest thickness of the "hot" side of the granite wedge was $\sim 1 \times 10^{-3}$ m. The "cold" side of this wedge was contacted with a piece of LR 115 film.

Series 2

The 2nd series of experiments was performed for Pu through the Inada granite using a 10^2 mol m^{-3} NaHCO$_3$ solution at room temperature (24.5±3.2 °C). The diffusion experiment was performed in triplicate using three granite disks, D4, J4 and J5. A working solution was prepared in an atmosphere-controlled chamber under Ar by adding NaHCO$_3$ powder and Na$_2$S$_2$O$_4$ powder into distilled and deionized water. The total carbonate concentration and the concentration of S$_2$O$_4{}^{2-}$ in the working solution was 10^2 and 10 mol m^{-3}, respectively. Plutonium (0.0031% ^{238}Pu, 97.41% ^{239}Pu, 2.56% ^{240}Pu and 0.026% ^{241}Pu) as chemically purified by TTA extraction and was prepared as 3.2 mol m^{-3} (1.77×10^{12} Bq m^{-1}) Pu(IV) stock solutions in 10^4 mol m^{-3} HNO$_3$. The starting solution was prepared by combining a 6×10^{-4} m^3 of volume of the working solution and a 1×10^{-6}-m^3 volume of 2×10^3 mol m^{-3} NaOH solution and a 2×10^{-7}-m^3 volume of the Pu stock solution in a polypropylene bottle. The pH and the Eh were measured. Three 1×10^{-7}-m^3 aliquots were withdrawn to determine the Pu concentration.

The diffusion experiments were started by placing the starting solution in the source reservoir and an equal volume of the working solution in the other, measurement, reservoir. At 7 days intervals, 1×10^{-6} m^3 aliquot was taken from the measurement reservoir and analyzed by LSC. The 1×10^{-6}-m^3 aliquot removed from the measurement reservoir was replaced by an equal volume of the working solution to maintain the balance between thee water levels in the 2 reservoirs. At 28 days intervals, the pH and Eh of the source solution were measured and two 1×10^{-7}-m^3 aliquots were taken from the source reservoir for radiometric analysis by LSC and for carbonate concentration analysis by carbonate electrode, CE-331 (TOA Electronics Ltd.).

After the 2nd series of experiments, the oxidation state of Pu was analyzed for each reservoir by using TTA extraction technique that was described above. Since the extraction period of 10 min could be long enough to oxidize Pu(III) to Pu(IV), another series of extraction was performed by shaking the mixture for 1 min for comparison. The remainder of the solutions was removed from both reservoirs of the three diffusion cells. The reservoirs were rinsed with a 1×10^{-5}-m^3 volume of distilled and deionized water 3 times and then washed with a 1×10^{-5}-m^3 volume of 10^4 mol m^{-3} HNO$_3$. The washings were sampled for radiometric analysis by α-spectrometry to determine the amount of Pu adsorbed on the inner walls of the diffusion cell.

Series 3

The 3rd series of experiments was performed for Np through the Inada granite at room temperature (26±1 °C). The diffusion experiment was performed in triplicate using three granite disks, D7, J7 and J8. A working solution was prepared in an atmosphere-controlled chamber under Ar by adding $NaHCO_3$ powder and $Na_2S_2O_4$ powder into distilled and deionized water. The total carbonate concentration and the concentration of $S_2O_4^{2-}$ in the working solution was 10^3 and 50 mol m^{-3}, respectively. Neptunium-237 was prepared as 22 mol m^{-3} (1.36×10^{11} Bq m^{-3}) Np(IV) stock solution in 10^3 mol m^{-3} HCl. The starting solution was prepared by combining a 6×10^{-4}-m^3 volume of the working solution and a 1.8×10^{-6}-m^3 volume of the Np stock solution in a polypropylene bottle. The pH and the Eh were measured. Three 1×10^{-7}-m^3 aliquots were withdrawn to determine the Np concentration. The diffusion experiments were started by placing the starting solution in the source reservoir and an equal volume of the working solution in the other, measurement, reservoir. At 10 days intervals, 1×10^{-6}-m^3 aliquot was taken from the measurement reservoir and analyzed by LSC. The 1×10^{-6}-m^3 aliquot removed from the measurement reservoir was replaced by an equal volume of the working solution to maintain the balance between thee water levels in the 2 reservoirs.

After the 3rd series of experiments, three 1×10^{-7}-m^3 aliquots were taken from the source reservoir for radiometric analysis by LSC. The oxidation state of Np in the source solutions was analyzed by using TTA extraction technique that was described above. The pH, Eh and total carbonate concentration were measured for both reservoirs of the three diffusion cells. The amount of Np adsorbed on acrylic walls was determined by the procedures described for the 2nd series of experiments.

Series 4

The 4th series of experiments was performed for U, Pu and Am through Inada granite under aerobic condition for comparison. The diffusion experiment was performed in triplicate using three granite disks, C15, C17 and C19 at (25±1)°C. Uranium-233 and americium-241 were prepared as 8.6×10^{-1} mol m^{-3} (7.1×10^{10} Bq m^{-3}) and 1.8×10^{-3} mol m^{-3} (5.6×10^{10} Bq m^{-3}) stock solutions, respectively, in 10^2 mol m^{-3} HCl. Plutonium-239 was prepared as 4.2×10^{-1} mol m^{-3} (2.3×10^{11} Bq m^{-3}) Pu(IV) stock solution in 10^4 mol m^{-3} HNO$_3$. The starting solution was prepared by combining 1×10^{-4} m^3 of 10^2 mol m^{-3} Na_2CO_3, 2.75×10^{-4} m^3, 10^2 mol m^{-3} $NaHCO_3$, 3×10^{-6} m^3 of the ^{233}U stock solution, 9.5×10^{-7} m^3 of the ^{239}Pu stock solution and 1×10^{-6} m^3 of ^{241}Am stock solution in a polypropylene bottle. To maintain the Pu in the tetravalent state, 0.26 g $NaNO_2$ was added to this mixture. The pH was adjusted to 9.3 by adding dilute NaOH and HCl. The initial concentrations of total carbonate and NO_2^- in the source solution were 10^2 and 10 mol m^{-3}, respectively. The Eh and concentration of ^{233}U, ^{239}Pu and ^{241}Am were determined and the oxidation state of Pu was determined by TTA extraction. To measure the

concentrations of actinides in the source solution, a 5×10^{-8} m^3 aliquot was withdrawn and diluted to 2×10^{-6} m^3 to prevent the salt from interfering with α-spectrometry of the samples. A 5×10^{-8} m^3 aliquot of this diluted solution was evaporated on a stainless steel planchet and its activity determined by α-spectrometry. The solution was stored for 40 days in atmosphere at room temperature to ensure that the concentrations of the actinides remained constant. The pH, Eh, total carbonate concentration and concentrations of the actinides were determined again, and the TTA extraction was performed. A blank solution was prepared by adding NaHCO$_3$ powder and NaNO$_2$ powder into distilled and deionized water. The pH was adjusted to 9.3.

The diffusion experiments were started by placing the actinide-containing solution in the source reservoir and the blank solution in the other, or measurement reservoir. At 10 days intervals, a 5×10^{-8} m^3 aliquot was taken from the measurement reservoir to determine the concentrations of the actinide elements. The 5×10^{-8} m^3 aliquot removed from the measurement reservoir was replaced by an equal volume of the blank solution to maintain the balance between the water levels in the two reservoirs and to avoid actinide transport through the granite by advective flow. The concentrations of U, Pu and Am, pH, Eh and total carbonate concentration of the solution in one of the source reservoirs were determined at the 55th and the 366th day. At the termination of each experiment, the inner wall of the measurement reservoir was washed with 10^4 mol m^{-3} HNO$_3$ to determine the amount of diffusing species adsorbed on the cell walls.

7.3. Results

The result of TTA extraction for the Pu starting solution for the 1st series of experiments was shown in Table 7-1. There is no significant difference between the extraction for the stock solution and that for the source solution. The result suggests the Pu(IV) groundwater solution was successfully prepared. No plutonium was observed in the measurement reservoirs throughout the experiments. That is consistent with the fact that the photographic plates in contact with the "cold" side of the granite disks for 20 days showed no image. Concentrations of ^{238}Pu in the source reservoirs decreased quickly after the start of the diffusion as shown in Table 7-2. Sorption onto granite is responsible for the decrease. The autoradiographic images for the "hot" side of the granite disks exposed for 7 days are shown in Fig. 7-2 with the corresponding optical images. The images show the sorption of Pu on the granite samples. The results of the radiometric analysis for the final contact solution, the DDW rinsings and the acid washings are shown in Table 7-3. The amount of Pu associated with the acrylic compartments was 37 – 68 % of the initial inventory. Adsorption onto the acrylic compartment was also responsible for the decrease of Pu concentration in the source reservoirs. No difference was

observed between the autoradiographs obtained on the disks before ion milling and those obtained on the coupons afterwards. The penetration of Pu into the granite was extended beyond 230 nm. Diffusion into the granite sample is also responsible for the decrease in the concentration of plutonium in the source reservoir. No evidence of alpha activity was observed on "cold" side of the wedge sliced from the granite disk. The penetration depth of Pu into the granite was less than 1×10^{-3} m.

Figure 7-3 shows the time dependence of the concentration of Pu in the measurement reservoirs of the 2nd series of experiments. The concentration of Pu increased linearly with time after 400 days from the start of the diffusion. Figure 7-4 shows the concentration of Pu in the source reservoirs. Although concentration of Pu decreased for 300 days after the start of diffusion, the concentrations of Pu in the source reservoir remained constant after 300 days from the start of the diffusion. These results suggest that the diffusive transport of Pu through the granite disk was in a steady state in the period between 400 and 588 days. The effective diffusivity is defined as:

$$D_e = -J / (\partial c / \partial x). \qquad (7\text{-}1)$$

Diffusive flux, J (Bq m^{-2} s^{-1}), is obtained from

$$J = (\Delta c_2 / \Delta t) k_c \text{VA}^{-1} \qquad (7\text{-}2)$$

where $\Delta c_2 / \Delta t$: rate of the Pu concentration increase in the period between 400 and 588 days (Bq m^{-3} s^{-1}),

k_c : correction factor for the adsorption of Pu onto acrylic wall in the measurement reservoir.

$\Delta c_2 / \Delta t$ was obtained from the slope of the linear portion of the through-diffusion curves shown in Fig. 7-3. The amount of plutonium adsorbed on the acrylic wall of the reservoirs was 86% of the final inventory in the measurement reservoir; the correction factor of k_c=1.86 was used. The concentration gradient, $\partial c / \partial x$, is obtained from the difference of the Pu concentration in both reservoirs;

$$\partial c / \partial x = (\bar{c}_1 - \bar{c}_2) \text{L}^{-1} \qquad (7\text{-}3)$$

where $\bar{c}_1$: average concentration of Pu in the source reservoir in the period of 400-588 days (Bq m^{-3}),

$\bar{c}_2$: average concentration of Pu in the measurement reservoir in the period of 400-588 days (Bq m^{-3}),

Effective diffusivity (D_e) of $(1.28 - 2.76) \times 10^{-13}$ m^2 s^{-1} were obtained by combining Eq. (7-2) and (7-3) into Eq. (7-1) and tabulated in Table 7-4. The D_e value was $(2.0 \pm 1.4) \times 10^{-13}$ m^2 s^{-1} on an average of three runs.

Equation (3-9) cannot be applied to determine $(\varepsilon+\rho R_d)$ because concentration of Pu in the source reservoir changed as shown in Fig. 7-4. Spacek & Kubin (1967) proposed a method to determine apparent diffusivity in the case that the concentration of diffusing species in source reservoir decreases with time due to diffusion into membranes. This method used in chapter 4 can neither be used in this study because the concentration of Pu in the source reservoir decreased due to precipitation of $PuO_2 \cdot xH_2O$ as well as diffusion into granite and subsequent sorption onto mineral surfaces. An intercept on x axis of the linear portion of the Pu through-diffusion curve is 362±14 days. The intercept of 1.21±0.36 days was calculated from Eq. (3-9) for a hypothetical species whose effective diffusivity is $(2.0\pm1.4) \times 10^{-13}$ m^2 s^{-1} that is not adsorbed on the granite. Regarding the ratio of the two intercepts, 300±90, as sorption retardation factor, $(1+\rho R_d \varepsilon^{-1})$, value for $(\varepsilon+\rho R_d)$ was calculated and tabulated in Table 7-4.

Figure 7-5 shows the time dependence of the concentration of Np in the measurement reservoirs of the 3rd series of experiments. The amount of Np adsorbed on the wall of the reservoirs was negligibly small. The concentration of Np increased linearly with time after 50 days from the start of the diffusion. The concentrations of Np in the source reservoirs remain constant throughout the diffusion run. The method described by Crank (1975) was used to analyze the data. After plotting the concentration of diffusing species in the measurement reservoir against time, values for D_e are obtained from the slope, and the rock capacity factor, $(\varepsilon+\rho R_d)$, from the intercept on the concentration axis of the extrapolated linear portion, where ρ is the bulk density of the rock and R_d is the distribution ratio. Effective diffusivity (D_e) ranged from 2.85×10^{-13} m^2 s^{-1} to 5.41×10^{-13} m^2 s^{-1} and $(\varepsilon+\rho R_d)$ ranged from –0.01 to +0.33 were obtained by the least squares fitting and tabulated in Table 7-4. The effective diffusivity and the rock capacity factor was $(4.0\pm1.5) \times 10^{-13}$ m^2 s^{-1} and 0.15±0.22, respectively, on an average of three runs. The result of the TTA extraction analysis presented in Table 7-1 shows that the neptunium was in tetravalent state until the end of the diffusion run.

Figure 7-6 shows the time dependence of the concentrations of ^{233}U, ^{239}Pu and ^{241}Am in the measurement reservoirs for the 4th series of experiments. No americium was observed in the measurement reservoirs throughout the experiments. The concentrations of U and Pu increase linearly with time after 150 days. For all three cells, the increase in relative uranium concentration was greater than that of plutonium. The relative uranium concentration in cell C17 was the largest of the 3 runs and that of C19 the smallest. This order is the same for Pu concentration. The amount of uranium, plutonium and americium adsorbed on the acrylic wall of the reservoirs were found to be 3% of the inventory in the solutions in the reservoirs and can be ignored. The concentrations of all three actinides in the source reservoir remained virtually constant, as shown in Table 7-5, suggesting no significant removal occurred by precipitation and/or sorption on reservoir walls or on the surfaces of the granite disks. The method described by Crank (1975) was used to analyze the data as described above. The

effective diffusivity and the rock capacity factor are presented in Table 7-4 with literature data.

7.4. Discussion

The extent of penetration of the Pu into the granite disk for the 1st series of experiments was estimated using a diffusion model. Pu was assumed to be present initially in a very thin layer on the outer surface of the granite disk because almost all of the Pu in the source reservoir had disappeared from solution in a very short time period. The solution to the diffusion equation is

$$C(x,\ t) = \alpha(\pi D_a t)^{-0.5} \exp(-x^2 / 4 D_a t). \tag{7-4}$$

The minimum D_a value of 1×10^{-21} m^2 s^{-1} was roughly estimated as shown in Fig. 7-7 from the fact that no difference was observed between the autoradiographs obtained before ion milling and those obtained afterwards. The maximum D_a value of 1×10^{-15} was roughly estimated as shown in Fig. 7-7 from the fact that the penetration depth of Pu into the granite was less than 1×10^{-3} m. Using a value of 2.0×10^{-13} m^2 s^{-1} for the effective diffusivity of Pu obtained from the second series of experiments and a R_d of 0.28 m^3 kg^{-1} (Vandergraaf and Ticknor 1994), an apparent diffusivity of 2.7×10^{-16} m^2 s^{-1} is estimated using Eq. (4-2). The calculated Pu profile in the granite after 1000 days contact time is also shown in Figure 7-7. The calculated Pu profile is consistent with the experimental observation that the penetration depth of Pu was more than 230 nm and was less than 1×10^{-3} m. Diffusion of sorbed species in granite can be enhanced through the surface diffusion as discussed in chapters 3, 4 and 5. In the 1st series of experiments, enhancement of the diffusivity was not observed for Pu although Pu was adsorbed on the granite. The contribution of the surface diffusion may be significant for species that is electro-statically adsorbed on the mineral surfaces, but not for the actinide carbonate complexes that is adsorbed on the surfaces through chemical reactions or surface complexation.

The result of the TTA extraction analysis presented in Table 7-3 shows that the plutonium was in tetravalent state until the end of the 2nd series of experiments. Since Pu(III) can be oxidized to Pu(IV) during the 10-min extraction period and extracted by TTA, 1-min extraction was performed for Pu. The results were the same as that of 10-min extraction, which suggests that Pu(III) is unlikely to be dominant. Speciation calculation using a thermodynamic database (Yamaguchi 2000) shows that a hydroxy-carbonate complex of Pu(IV), $Pu(CO_3)_2(OH)_2^{2-}$ is dominant under the employed condition. The effective diffusivity of Pu obtained in the granite obtained from the 4th series of experiments was 1/4 as high as the value from the 2nd series of experiments. The 4th series of experiments were performed under aerobic atmosphere under which Pu was partially oxidized to Pu(VI), which might be

responsible for the difference in the D_e value. The diffusion experiments for neptunium were performed under higher $NaHCO_3$ concentration than that for plutonium where carbonate complexes of Np(IV), $Np(CO_3)_4^{4-}$ and $Np(CO_3)_5^{6-}$ were predicted to be dominant.

The D_e value obtained for uranium in the 4th series of experiments was $(1.42\pm0.29)\times10^{-13}$ $m^2\ s^{-1}$ on an average of three experiments. This value is larger by four times than that of the uncomplexed uranyl ion, UO_2^{2+}, $(3.6\pm1.6)\times10^{-14}\ m^2\ s^{-1}$ obtained in chapter 3. The previous experiment had been performed in $10^2\ mol\ m^{-3}$ KCl solution at pH 4, while this experiment was in $10^2\ mol\ m^{-3}$ $NaHCO_3$ at pH 9.3. In aerated solutions, the dominant oxidation state of uranium is hexavalent. Complexation of UO_2^{2+} by nitrite anion is negligible (Brown and Wanner, 1987). Speciation of uranium(VI) under the conditions under which this experiments was performed was calculated using the data compiled by Yamaguchi & Takeda (1999). More than 99.9 % of the uranium was calculated to be present as a monomeric tri-carbonate complex, $UO_2(CO_3)_3^{4-}$ throughout the experiment. The structure of the complex species is shown elsewhere (Weigel, 1985). The bond length between the uranium atom and the nearest oxygen atoms of the carbonate groups is 0.244-0.246 nm (Weigel, 1985). The bond length between the carbon atom and the oxygen atoms in the carbonate group is 0.122-0.134 nm (Weigel, 1985). Based on these bond length, the size of this species was graphically estimated to be 0.42±0.03 nm. The radius of the ions can be correlated with diffusivity (Yamaguchi et al., 1997a) using the relationship

$$D^0 = RT(r/r_s) / (6\pi N \eta^0 r) \tag{7-5}$$

where D^0 : diffusivity of ion at infinite dilution ($m^2\ s^{-1}$)

   R : gas constant (= 8.314 $J\ mol^{-1}\ K^{-1}$)

   T : absolute temperature (K)

   r : hydrated ion radius (m)

   r/r_s : correction factor (-)

   N : Avogadro's number (= $6.02\times10^{23}\ mol^{-1}$)

   η^0 : viscosity of water ($8.902\times10^{-4}\ N\ s\ m^{-2}$ at 25°C)

The diffusivity of $UO_2(CO_3)_3^{4-}$ was estimated to be $(7.2\pm0.5)\times10^{-10}\ m^2\ s^{-1}$ assuming no significant hydration occurs. In this calculation, the correction factor r/r_s is 1.23 (Nightingale, 1959). An empirical correlation between D_e and D_v has been presented in chapter 3. The value for $UO_2(CO_3)_3^{4-}$ obtained in this experiment is consistent with the previously-obtained correlation as shown in Fig. 7-8.

It is noteworthy that the diffusivity of the $UO_2(CO_3)_3^{4-}$ complex is larger than that of the "master" species, UO_2^{2+}, both in bulk of the solution and in the pores of the granite. A similar

effect of complexation on the diffusivity of metal ions has been observed for Fe^{2+} and Fe^{3+} complexes with CN^- (Dean, 1978). The diffusivity of $Fe(CN)_6^{4-}$ at infinite dilution, 7.3×10^{-10} $m^2 s^{-1}$, is larger than that of Fe^{2+}, 7.1×10^{-10} $m^2 s^{-1}$ and the diffusivity of $Fe(CN)_6^{3-}$ at infinite dilution, 8.8×10^{-10} $m^2 s^{-1}$, is larger than that of Fe^{3+}, 5.9×10^{-10} $m^2 s^{-1}$.

In aerated solutions, the dominant oxidation state of americium is trivalent. Based on the data compiled by Yamaguchi & Takeda (1999), a tri-carbonate complex species, $Am(CO_3)_3^{3-}$ is predicted to be dominant under the employed condition. No diffusion of americium through the granite was detected. This suggests that either the effective diffusivity is very small or the distribution ratio very large. Eq. (3-9) shows that the intercept on the time axis of the extrapolated linear portion of a through-diffusion curve is $(\varepsilon + \rho R_d)L^2/6D_e$ or $L^2/6D_a$. An upper limit to the apparent diffusivity, D_a, of americium in the granite was estimated to be 1.3×10^{-13} $m^2 s^{-1}$ from $L^2/6D_a < 366$ days. For comparison, the apparent diffusivities of uranium and plutonium in the 4th series of experiments were $(4.6 \pm 1.0) \times 10^{-13}$ and $(4.4 \pm 0.9) \times 10^{-13}$ $m^2 s^{-1}$, respectively. The apparent diffusivity of americium was smaller than those for uranium and plutonium. A similar low diffusivity for americium in rock has been observed elsewhere (Torstenfelt, 1982; Muuronen et al., 1986; Suksi et al., 1987; Berry et al., 1987; Ittner and Torstenfelt, 1988; Andersson et al., 1992). Similarly to the results from the 1st series of experiments, enhancement of the diffusivity was not observed for Am species although Am was adsorbed on the granite.

The effective diffusivity of Np and Pu carbonate complexes and that of uranyl tri-carbonate complex species obtained previously are close each other, ranging from 1.4×10^{-13} to 4.0×10^{-13} $m^2 s^{-1}$. The effective diffusivity of aqueous species in the granite obtained in chapter 2 is ranged widely between 3.6×10^{-14} $m^2 s^{-1}$ and 1.0×10^{-11} $m^2 s^{-1}$. Equation (3-4) shows that the variation in D_e is caused by variation in D_v. Rai et al. (1999a) reported structure of $Np(CO_3)_5^{6-}$. The distance between central cation and distal oxygen of carbonate group is 0.42 nm, which was close to that of $UO_2(CO_3)_3^{4-}$, 0.40 nm (Weigel, 1985). Although ionic structure is not known for $Pu(CO_3)_2(OH)_2^{2-}$, the effective radii of the hydroxy-carbonate complex species in solution are expected to be similar to $Np(CO_3)_5^{6-}$ and $UO_2(CO_3)_3^{4-}$ because that is roughly defined by the size of a bulky carbonate group. The effective size is similar for $Np(CO_3)_5^{6-}$, $UO_2(CO_3)_3^{4-}$ and $Pu(CO_3)_2(OH)_2^{2-}$, and their diffusivity in water are expected to be similar based on Eq. (7-5). This may be the reason that the effective diffusivity of the carbonate complexes in granite are close to each other. The contribution of the surface diffusion also induces wide variety in D_e value in the granite for the species that is electrostatically adsorbed on the mineral surfaces. However, this is not the case for the actinide carbonate complexes.

7.5. Conclusion

The diffusivity of uranium, neptunium, plutonium and americium in granite matrices has been studied by the through-diffusion method in the presence of carbonate. Effective diffusivities for $Pu(CO_3)_2(OH)_2^{2-}$, $Np(CO_3)_n^{4-2n}$ (n=4, 5) and $UO_2(CO_3)_3^{4-}$, in Inada granite, of $(2.0\pm1.4)\times10^{-13}$ m^2 s^{-1}, $(4.0\pm1.5)\times10^{-13}$ m^2 s^{-1} and $(1.42\pm0.29)\times10^{-13}$ m^2 s^{-1}, respectively, have been obtained. The effective diffusivity of $UO_2(CO_3)_3^{4-}$ in granite and the estimated bulk diffusivity of this species, $(6.6\pm0.4)\times10^{-10}$ m^2 s^{-1}, are consistent with an empirical correlation between D_e and D_v obtained in chapter 3. In separate series of experiments for plutonium and americium under the conditions that adsorption onto granite is more favorable, enhancement of the diffusivity by surface diffusion was not observed. Upper limits of D_a value were determined to be 1×10^{-15} m^2 s^{-1} and 1.3×10^{-13} m^2 s^{-1} for plutonium and americium, respectively. The contribution of the surface diffusion is not significant for the actinide carbonate complexes that is adsorbed on the surfaces through surface complexation. Actinide complex species that is formed in groundwater under deep geological environments migrate through rock matrix following to the Fick's diffusion law, and the diffusivities are consistent with the pore-diffusion model.

Table 7-1 Total carbonate concentration, pH, Eh and TTA extraction of the solutions used in actinide diffusion experiments under anoxic conditions at the termination of the diffusion.

		Total carbonate concentration (mol m^{-3})	pH	Eh (mV vs NHE)	TTA extraction (%)
Series 1	source reservoir[a]	[2.5][b]	9.0	263	85 [93][c]
Series 2	D4 source reservoir	10^2	9.05	12	98 [97][d]
	D4 measurement reservoir	10^2	9.17	95	>61
	J4 source reservoir	10^2	9.21	70	99 [99][d]
	J4 measurement reservoir	10^2	9.35	124	>64
	J5 source reservoir	10^2	9.11	57	98 [98][d]
	J5 measurement reservoir	10^2	9.35	35	>55 [>57][d]
Series 3	D7 source reservoir	9.9x10^2	8.83	-497	88
	D7 measurement reservoir	9.2x10^2	8.97	-427	66
	J7 source reservoir	9.1x10^2	8.83	-400	78
	J7 measurement reservoir	9.2x10^2	8.87	-493	91
	J8 source reservoir	6.6x10^2	8.83	-489	88
	J8 measurement reservoir	8.5x10^2	8.86	-471	97

a: plutonium containing solution at the start of the diffusion
b: planned concentration
c: result for stock solution
d: result for 1-min extraction

Table 7-2 Concentration of Pu-238 for the 1st series of experiments.

day	F3 MBq m^{-3}	mol m^{-3}	2σ %	F6 MBq m^{-3}	mol m^{-3}	2σ %	F9 MBq m^{-3}	mol m^{-3}	2σ %
0	58.60	3.9E-07	5	69.50	4.6E-07	5	69.50	4.6E-07	5
0.25	47.70	3.2E-07	5	57.00	3.8E-07	5	61.00	4.0E-07	5
1	11.60	7.7E-08	5	49.65	3.3E-07	5	51.50	3.4E-07	5
5	2.82	1.9E-08	12						
11	0.89	5.9E-09	36						
13				5.65	3.7E-08	5	6.33	4.2E-08	5
15	0.68	4.5E-09	46						
20	0.48	3.2E-09	65	2.30	1.5E-08	5	3.76	2.5E-08	5
28	0.59	3.9E-09	12						
30				1.38	9.1E-09	6	2.09	1.4E-08	7
34				1.28	8.5E-09	6	1.78	1.2E-08	6
40	0.49	3.3E-09	14	1.15	7.6E-09	7	1.46	9.7E-09	5
47				0.99	6.6E-09	8	1.25	8.3E-09	5
50	0.50	3.3E-09	13						
56	0.48	3.1E-09	14						
68	0.37	2.4E-09	18	0.80	5.3E-09	9	0.83	5.5E-09	9
78	0.36	2.4E-09	19						
90	0.36	2.4E-09	19						
102	0.32	2.1E-09	21						
123	0.21	1.4E-09	32						
153				0.56	3.7E-09		0.55	3.6E-09	
173				0.51	3.3E-09		0.53	3.5E-09	
190				0.38	2.5E-09		0.43	2.9E-09	
208	0.17	1.2E-09							
209				0.36	2.4E-09		0.47	3.1E-09	
228	0.15	1.0E-09							
245	0.59	3.9E-09		0.30	2.0E-09		0.27	1.8E-09	
264	0.29	1.9E-09							
300	0.19	1.3E-09							
945				2.02	1.3E-08		0.56	3.7E-09	
1000	5.72	3.8E-08							

Table 7-3   Radiometric analysis for the final contact solution, the DDW rinsings and
the acid washings (MBq m^{-3}).

	Sample	F3	F6	F9
Hot side	Final contact solution	5.72	2.02	0.56
	DDW rinsings	1.22	0.38	2.00
	Acid washings	38.1	50.6	27.5
Cold side	Final contact solution	<0.06	<0.06	<0.06
	DDW rinsings	<0.06	<0.06	<0.06
	Acid washings	<2	<2	<2

Table 7-4 Effective diffusivity (D_e) and rock capacity factor ($\varepsilon + \rho R_d$) of species in Inada granite.

Species	D_e (m² s⁻¹)	$\varepsilon + \rho R_d$	Solution	Temp. (°C)	Reference	D_v (m² s⁻¹)
$Pu(CO_3)_2(OH)_2{}^{2-}$	(1.28±0.29)×10⁻¹³ (2.00±0.45)×10⁻¹³ (2.76±0.61)×10⁻¹³ avg.(2.0±1.4)×10⁻¹³	1.5±0.7 [a]	10² mol m⁻³ NaHCO₃ + 10 mol m⁻³ Na₂S₂O₄	room (24.5±3.2)	This chapter	no data available
$Np(CO_3)_4{}^{4-}$, $Np(CO_3)_5{}^{6-}$	(5.41±0.10)×10⁻¹³ (2.85±0.10)×10⁻¹³ (3.84±0.14)×10⁻¹³ avg.(4.0±1.5)×10⁻¹³	+0.33±0.04 +0.13±0.04 -0.01±0.06 avg.(0.15±0.22)	10³ mol m⁻³ NaHCO₃ + 50 mol m⁻³ Na₂S₂O₄	room (26±1)	This chapter	no data available
$UO_2(CO_3)_3{}^{4-}$	(1.56±0.06)×10⁻¹³ (1.43±0.05)×10⁻¹³ (1.28±0.15)×10⁻¹³ avg.(1.42±0.29)×10⁻¹³	0.266±0.047 0.323±0.034 0.37±0.08 avg.(0.32±0.13)	10² mol m⁻³ NaHCO₃	25	This chapter	(7.2±0.5)×10⁻¹⁰ [b]
$Pu(CO_3)_2(OH)_2{}^{2-}$, $PuO_2(CO_3)_3{}^{4-}$	(6.94±0.11)×10⁻¹⁴ (5.34±0.12)×10⁻¹⁴ (2.95±0.18)×10⁻¹⁴ avg.(5.1±2.3)×10⁻¹⁴	0.125±0.006 0.125±0.007 0.085±0.007 avg.(0.112±0.034)				no data available
$Am(CO_3)_3{}^{3-}$		not determined [c]				
Pu(IV)		not determined [d]		room	This chapter	no data available
$UO_2{}^{2+}$	avg.(3.6±1.6)×10⁻¹⁴	avg.(0.011±0.010)	10² mol m⁻³ KCl pH = 4	room	Chapter 3	(4.3±0.6)×10⁻¹⁰ [e]
uranine	avg.(4.4±0.9)×10⁻¹⁴	avg.(0.03±0.04)	1% uranine solution	room	Kumata et al. (1990)	(4.5±0.6)×10⁻¹⁰ [e]
Co^{2+}	avg.(2.4±0.6)×10⁻¹³	avg.(0.014±0.012)	10² mol m⁻³ KCl pH 4	25	Chapter 3	(1.03±0.03)×10⁻⁹ [e]
Sr^{2+}	avg.(2.7±0.6)×10⁻¹³	avg.(0.013±0.008)		25	Chapter 3	(1.11±0.03)×10⁻⁹ [e]
Sr^{2+}	avg.(1.0±0.6)×10⁻¹¹	avg.(1.87±0.39)	10² mol m⁻³ Sr(NO₃)₂ →DDW	room	Chapter 3	(1.08±0.14)×10⁻⁹ [e]
I⁻	(5.80±0.05)×10⁻¹³	+0.36±0.15	10² mol m⁻³ KI	25	Chapter 3	1.99×10⁻⁹ [e]
HTO	avg.(7.7±1.4)×10⁻¹³	avg.(0.01±0.20)	DDW	25	Chapter 3	2.14×10⁻⁹ [e]

(a) estimated from the intercept on time axis of the linear portion of the through-diffusion curve

(b) see text

(c) $D_a < 1.3 \times 10^{-13}$ m² s⁻¹

(d) 1×10^{-21} m² s⁻¹ $< D_a < 1 \times 10^{-15}$ m² s⁻¹

(e) see chapter 3

Table 7-5   pH, Eh, and concentration of total carbonate (C_t), U, Pu and Am in the source
reservoir for the 4th series of experiments.

Time after starting diffusion run (day)	As prepared[a]	0	55	366
pH	9.27	9.27	9.22	9.30
Eh (mV vs NHE)	297.8	306.8	317.8	339.8
C_t (mol m^{-3})	1x10^2	1x10^2	9x10^1	8x10^1
U (mol m^{-3})	6.7x10^{-3}	6.7x10^{-3}	6.5x10^{-3}	6.3x10^{-3}
Pu (mol m^{-3})	1.0x10^{-3} (88%[b])	1.0x10^{-3} (81%[b])	1.0x10^{-3} (79%[b])	9.9x10^{-4} (70%[b])
Am (mol m^{-3})	4.7x10^{-9}	4.9x10^{-9}	5.0x10^{-9}	4.6x10^{-9}

a: The source solution was prepared 40 days prior to the start of the diffusion
   run to ensure that the concentrations of U, Pu and Am had remained constant
   values.

b: percentage of Pu extracted by TTA.

Side in contact with the Pu-containing solution

Saw cut

Side in contact with inactive groundwater
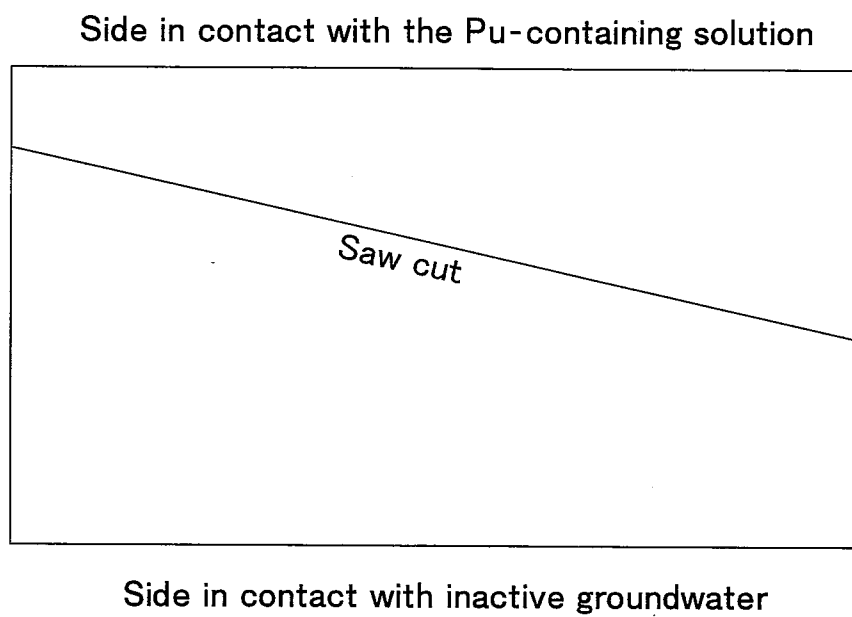
Fig. 7-1　Schematic of slicing a pierce of a granite disk used in the 1st series of actinide diffusion experiment under anoxic conditions to determine the extent of Pu diffusion into URL granite.
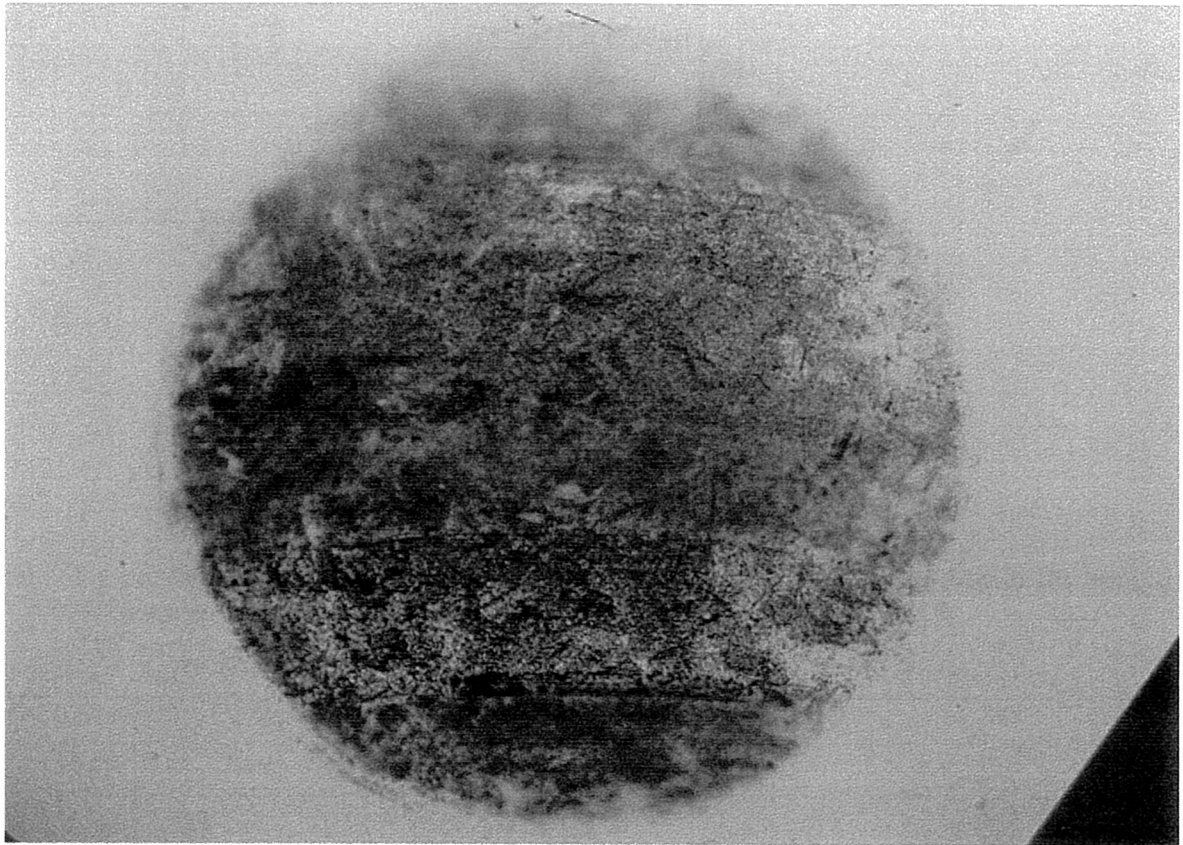
Fig. 7-2a Autoradiographic and optical images for the "hot" side of the granite disk, F3 used in the 1st series of diffusion experiment for actinide carbonate complexes.
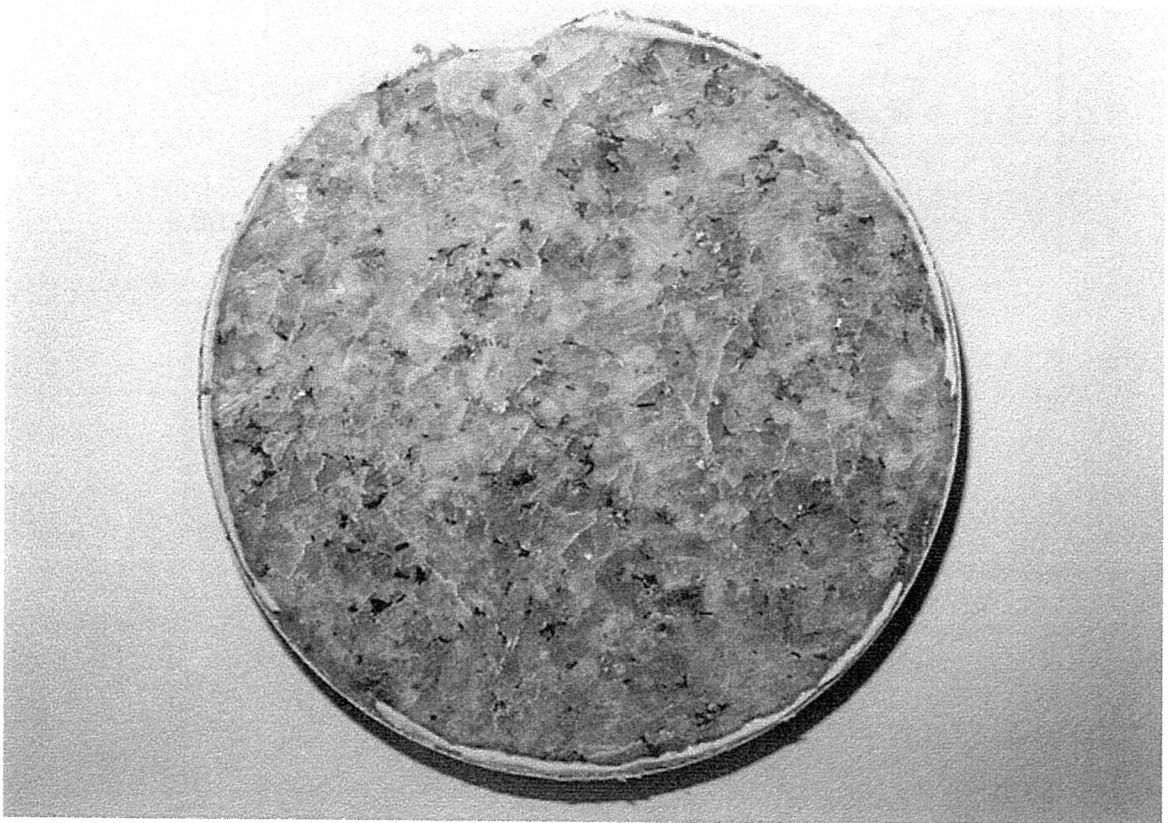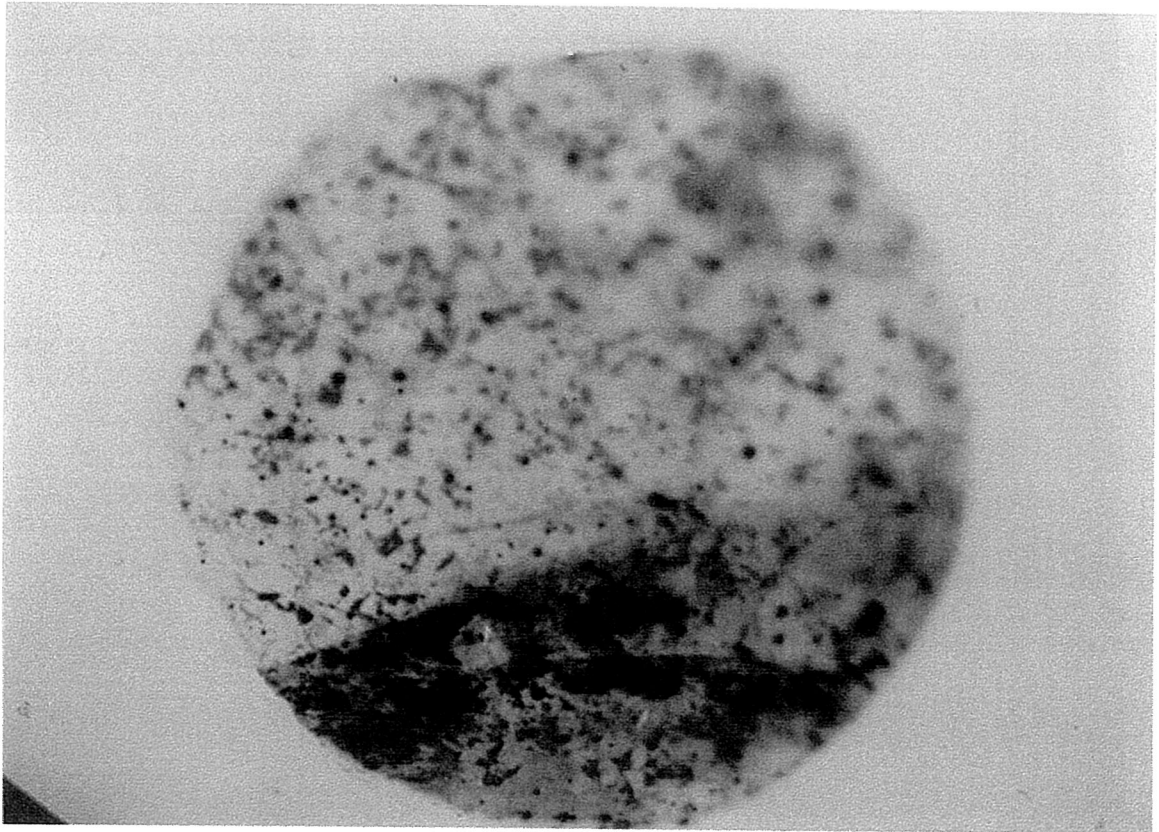
Fig. 7-2b Autoradiographic and optical images for the "hot" side of the granite disk, F6 used in the 1st series of diffusion experiments for actinide carbonate complexes.
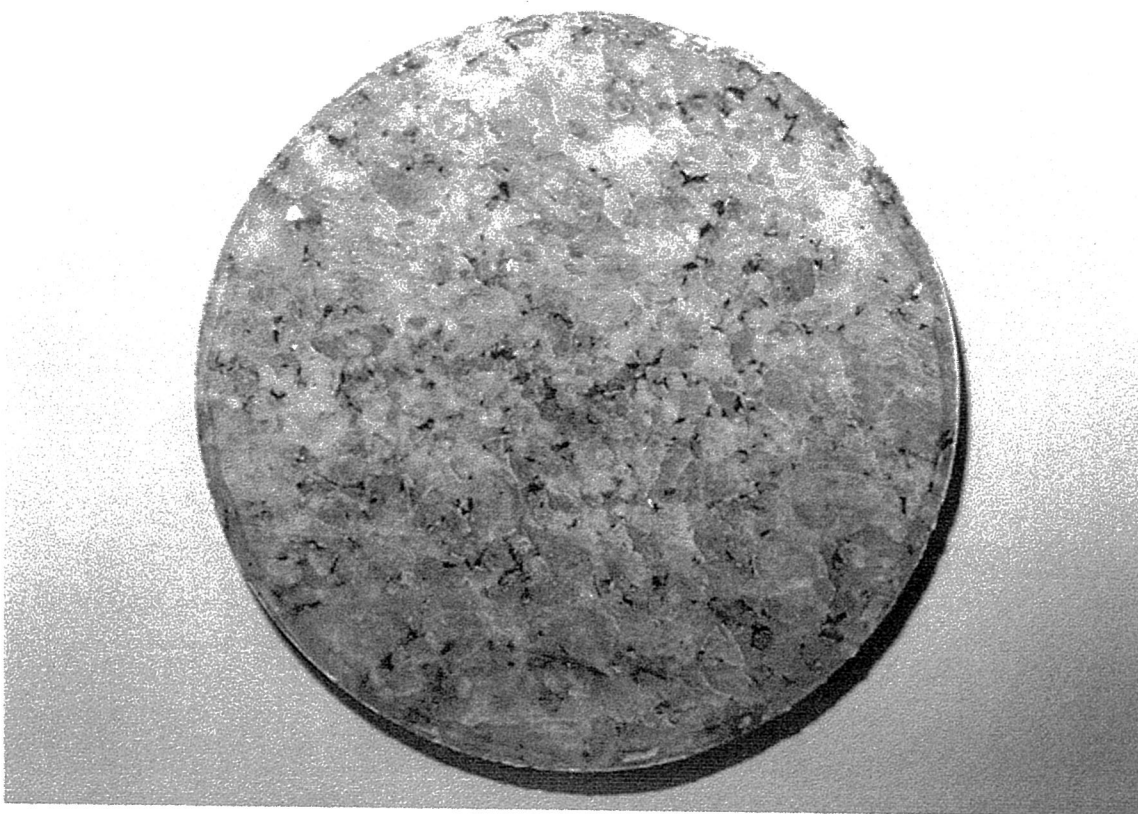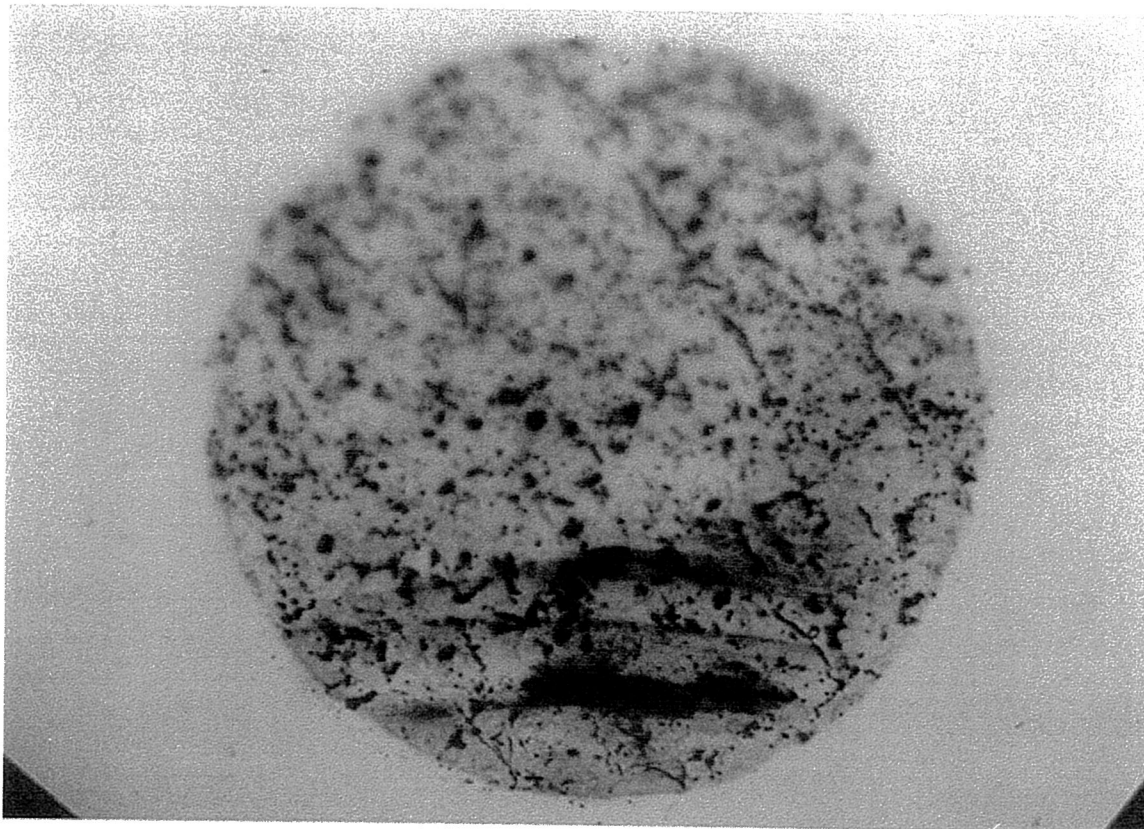
Fig. 7-2c Autoradiographic and optical images for the "hot" side of the granite disk, F9 used in the 1st series of diffusion experiment for actinide carbonate complexes.
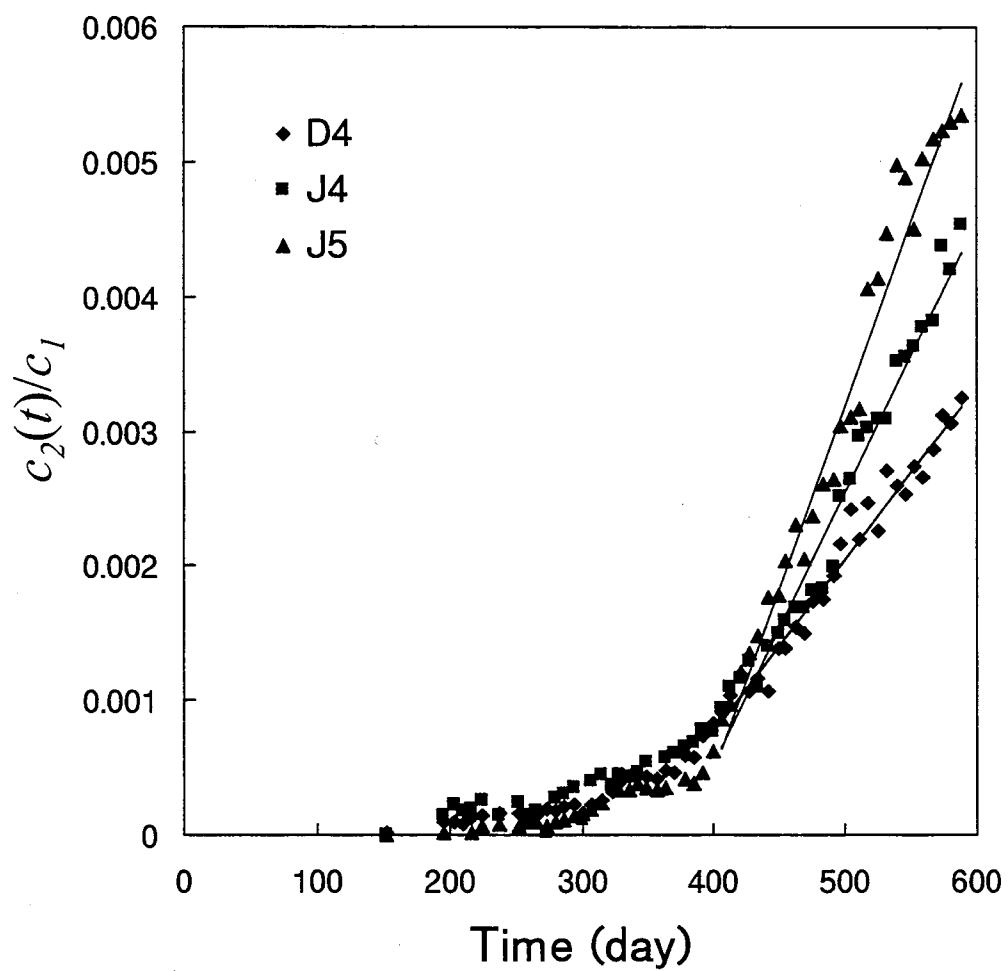
Fig. 7-3 Diffusion curves for plutonium(IV) through Inada granite samples under anoxic conditions in the 2nd series of diffusion experiments for actinide carbonate complexes.
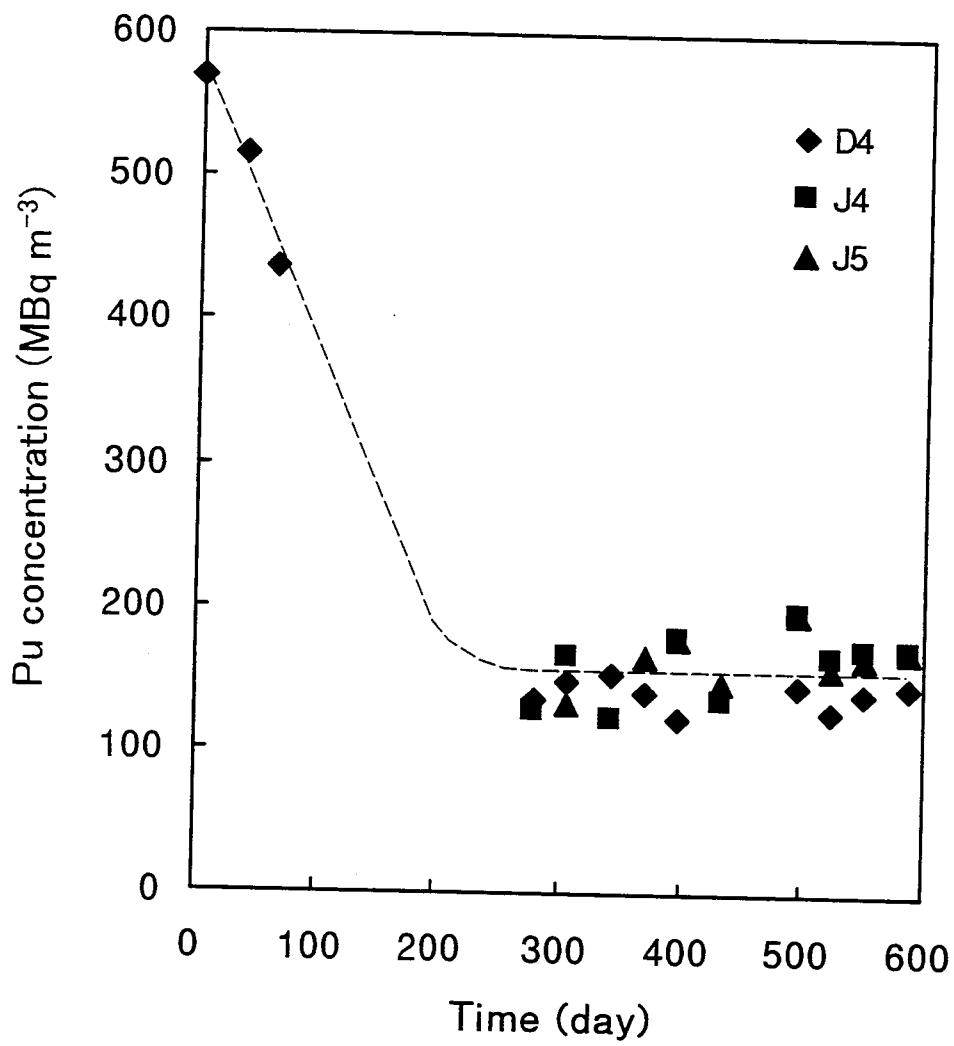
Fig. 7-4 Concentrations of plutonium in source reservoirs in the 2nd series
of diffusion experiments for actinide carbonate complexes. D4, J4
and J5: sample number.
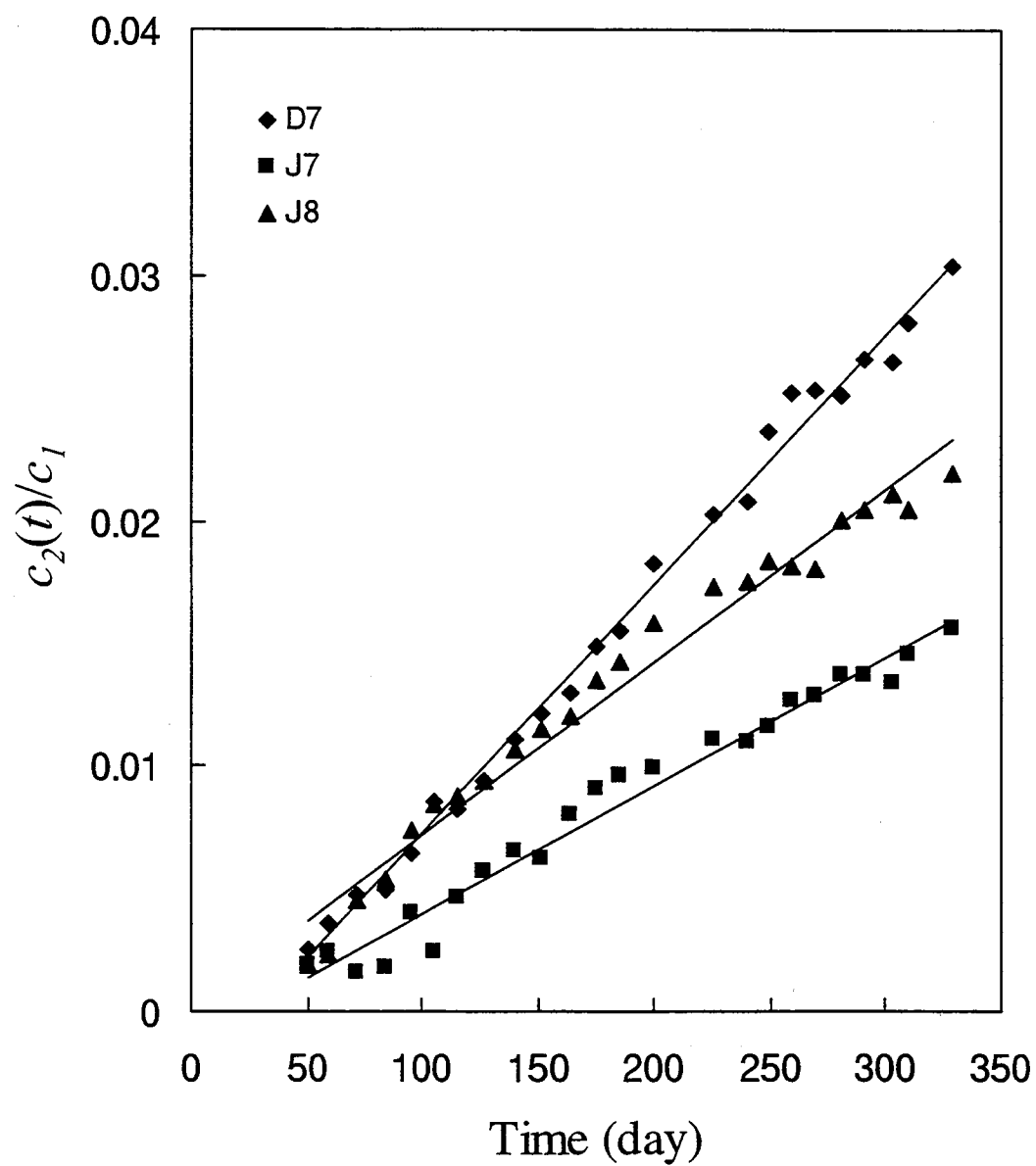
Fig. 7-5 Diffusion curves for neptunium(IV) through Inada granite samples, D7, J7 and J8 under anoxic conditions in the 3rd series of diffusion experiments for actinide carbonate complexes.
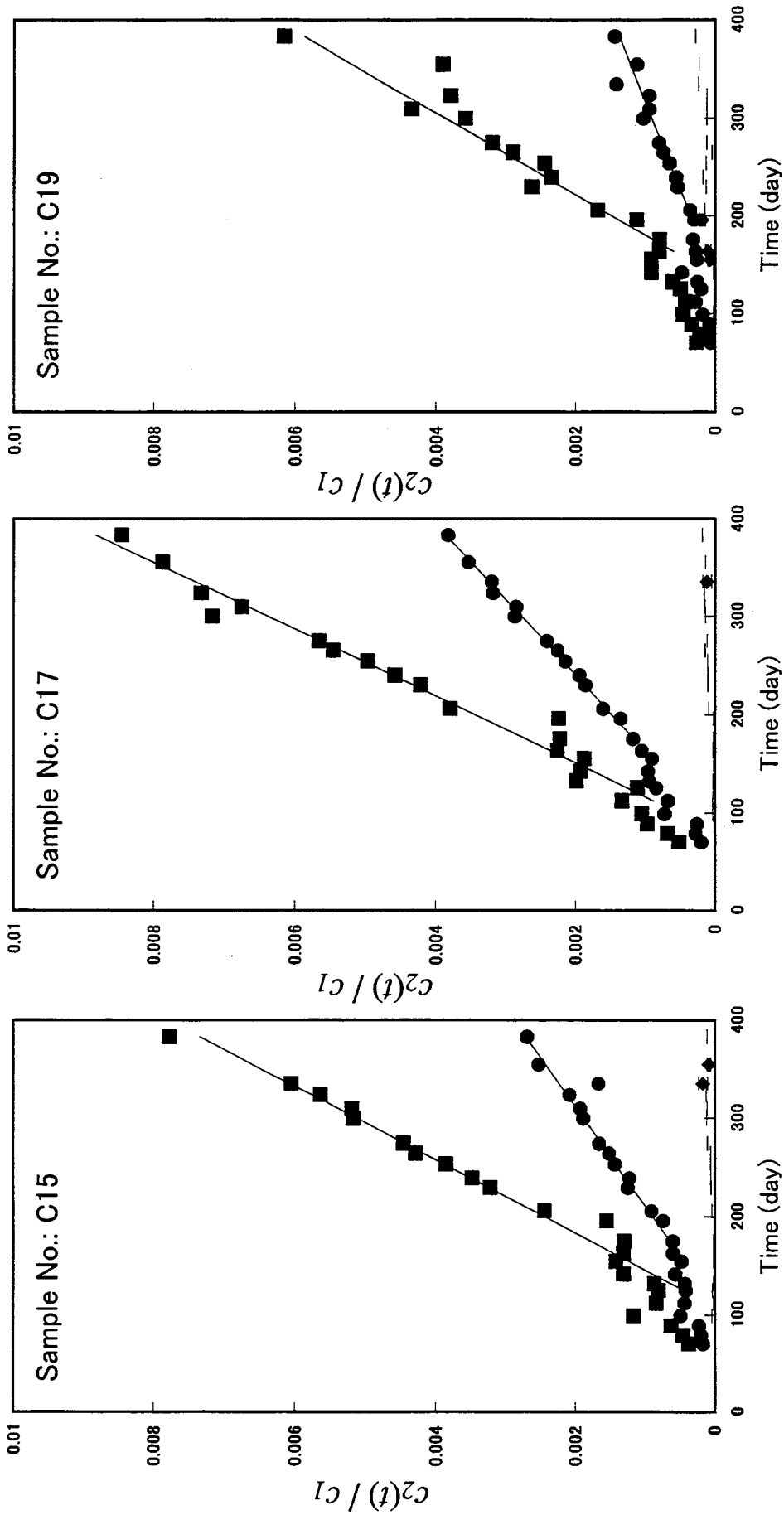
Fig. 7-6 Diffusion curves for uranium (■), plutonium (●) and americium (◆) through Inada granite samples in the 4th series of diffusion experiments for actinide carbonate complexes. When the concentration of americium was under the detection limit, maximum possible concentration was shown by the bars.

102
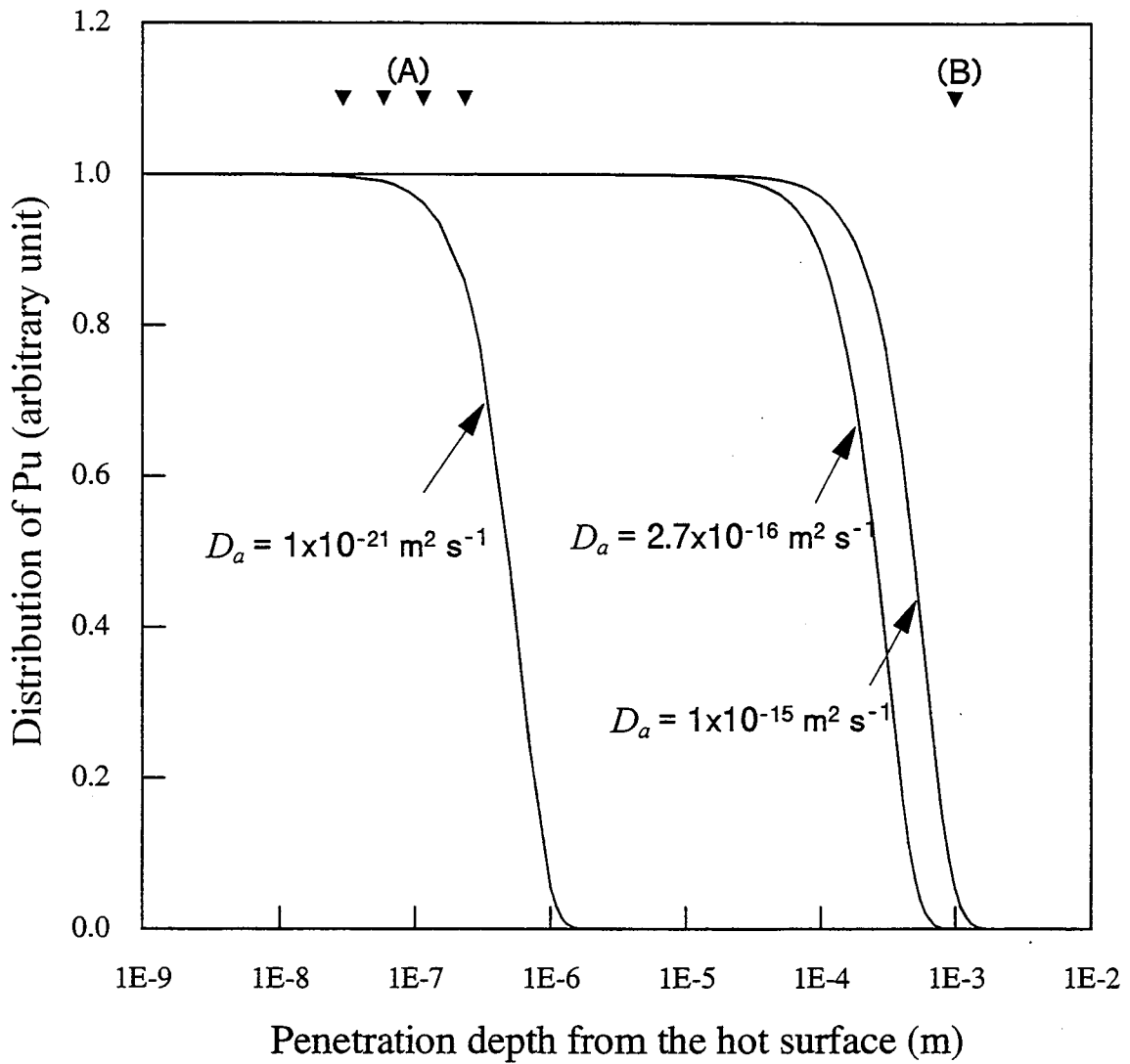
Fig. 7-7 Depth profiles of Pu calculated for D_a values of 1×10^{-21}, 2.7×10^{-16} and 1×10^{-15} m^2 s^{-1} in the 1st series of diffusion experiments for actinide carbonate complexes. (A) and (B) denote the depth ranges investigated by argon milling and saw cutting, respectively.
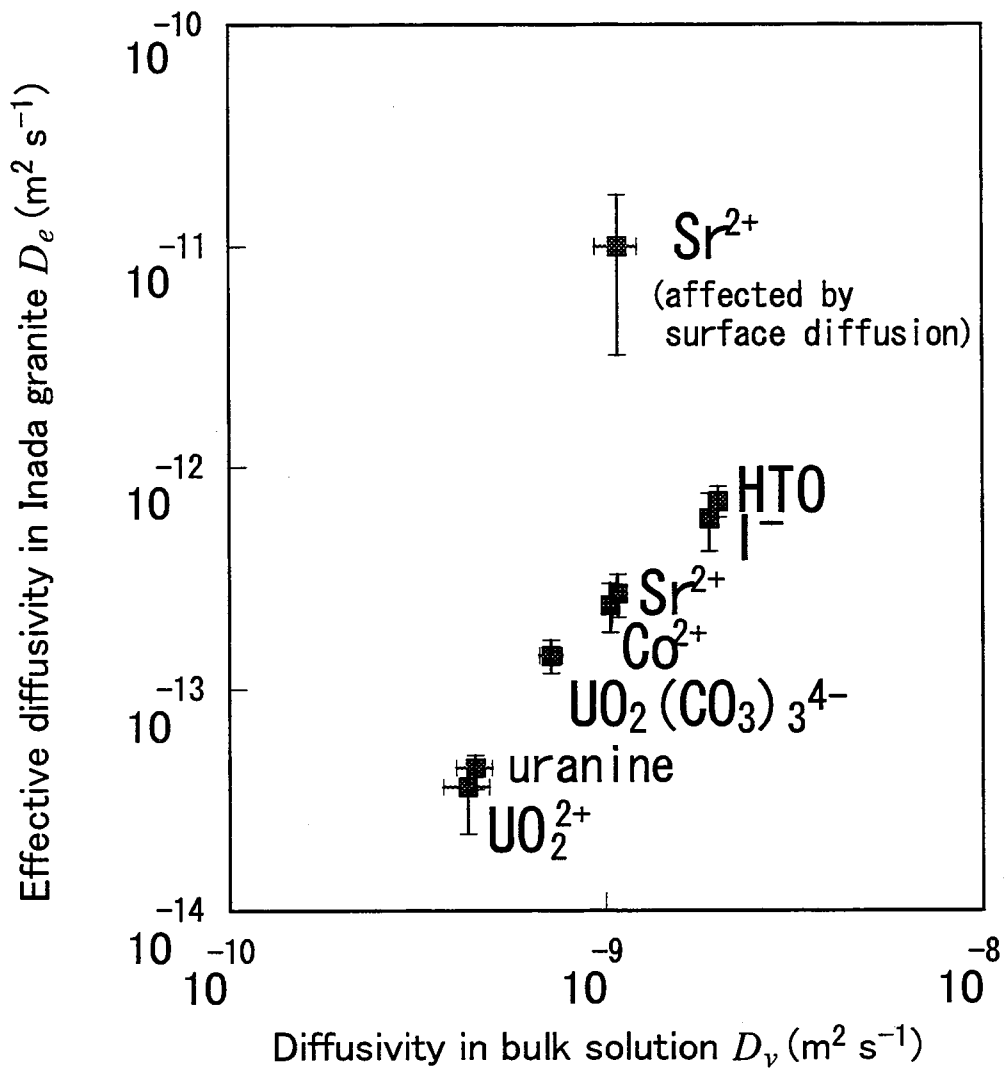
Fig. 7-8   Correlation between effective diffusivities of species in Inada granite and their diffusivities in bulk of the solution.

8. Thermodynamic data acquisition and data compilation

8.1. Introduction

The effective diffusivity of uranium, neptunium and plutonium in Inada granite was determined and the chemical species of the actinides under the experimental conditions were predicted to be $UO_2(CO_3)_3^{4-}$, $Pu(CO_3)_2(OH)_2^{2-}$ and $Np(CO_3)_n^{4-2n}$ (n=4, 5), respectively, in chapter 7. Prediction of the diffusing species that is formed in aqueous solution requires knowledge of all relevant species present in solution. Thermodynamic database is necessary for the prediction. The thermodynamic database is also useful for predicting solubility of radionuclides in groundwater that is one of essential parameters required for performance assessment of geological disposal of radioactive wastes. OECD/NEA released extensive volumes of thermodynamic database for uranium (Grenthe et al., 1992) and for americium (Silva et al., 1995), which enabled reliable speciation for these actinides. Thermodynamic database is necessary for neptunium and plutonium.

Because of their strong tendency of complexation, carbonate or bicarbonate ions are likely to be some of the most significant ligands to be considered (Kim, 1986; Newton & Sullivan, 1985). Therefore, a clearer understanding of the carbonate complexation is needed especially for tetravalent state whish is favorable under geological disposal conditions. Experimental data on the complexation of tetravalent plutonium by carbonate are limited in number and poor in quality. For example, Moskvin & Gel'man (1958) predicted the mono carbonate complex species, $PuCO_3^{2+}$, for 0.36 - 3.6 mol kg^{-1} K_2CO_3 solutions. Their work, however, has been reviewed critically (Lierse, 1985; Puigdomènech & Bruno, 1991), and some misunderstandings have been pointed out. Kim et al. (1983) suggested that $Pu(CO_3)_x^{4-2x}$ (x = 1 - 5) are the dominant aqueous species with $Pu(OH)_2CO_3(s)$ as the solubility-controlling solid in $NaClO_4$ / $NaHCO_3$ / Na_2CO_3 solutions at pH > 8 and I = 1.0. Their interpretation of the solubility data, however, was criticized by Rai & Ryan (1985). Considering the critical role of carbonate complex species in safety assessment of radioactive waste disposal, experiments on the speciation of Pu(IV) in the aqueous carbonate system should be performed.

The objectives of this chapter are to compile thermodynamic database for Np and Pu for predicting dominant diffusing species in granite pore water and to experimentally obtain lacking thermodynamic data for Pu(IV) in aqueous carbonate system.

8.2. Experimental

Sample solutions were prepared from reagent grade chemicals (Wako Pure Chemical Ind., Ltd., Tokyo) and deionized water (Milli-Q System, Millipore). The isotopic composition of the plutonium was 0.0031% ^{238}Pu, 97.41% ^{239}Pu, 2.56% ^{240}Pu and 0.026% ^{241}Pu. Plutonium was chemically purified by anion exchange. The eluted Pu in hydrochloric acid was converted to Pu(IV) as a nitrate and prepared as a 1.8×10^{-1} mol m^{-3} solution in 10^4 mol m^{-3} HNO$_3$.

An aliquot of the Pu(IV) stock solution was added to a 2×10^{-5} m^3 solution containing KCl, K$_2$CO$_3$ and KOH in a polypropylene tube. The initial concentrations of Pu(IV), K$^+$ and total carbonate (C_t) in the sample solution were typically 1.3×10^{-6}, 0.1 and 10^{-4} - 10^{-1} mol kg^{-1}, respectively. The pH was adjusted to values between 9.4 and 13.0 by adding dilute KOH. A 10^{-7} m^3 volume of 10^{-1} mol kg^{-1} NaNO$_2$ solution was added to maintain the Pu in the tetravalent state. The samples were sealed and stored for 2 weeks in air at room temperature (20 - 25°C).

After two weeks, the pH and Eh of the sample solutions were measured with a Ag/AgCl electrode and a Pt/AgCl electrode, respectively. The electrode was calibrated with pH buffer solutions (pH = 6.86 and 9.18) and a ORP standard (95 mV against the reference electrode). The total carbonate concentration was measured with CO$_2$ electrode (TOA Electronics Ltd. Japan, type CE-235, detection limit: 4.0×10^{-5} mol kg^{-1}). The electrode had been calibrated with a KHCO$_3$ solution using the same procedure as for the measurement of the carbonate concentration. The micro-centrifuge system (Millipore) was used to effect the separation processes. A 5×10^{-7} m^3 aliquot of the sample solution was filtered through 0.45 μm durapore (PVDF) and 10,000 NMWL (nominal molecular weight limit) polysulfur filters that had been rinsed with blank solution. The average pore size was estimated to be about 4.5×10^{-7} m and 3×10^{-9} m, respectively. Plutonium remaining on filters was re-dissolved by passing in 10^3 mol m^{-3} HNO$_3$ through these filters. The concentration of Pu was measured with a spectroscopy after evaporating 5×10^{-8} m^3 of the final filtrate on a stainless steel planchet.

The oxidation state of the Pu was determined by TTA extraction (Foti & Freiling, 1964; Nitsche et al., 1988; Pratopo et al., 1990). A 10^{-7} m^3 aliquot of the final filtrate was acidified with 10^{-6} m^3 of 10^3 mol m^{-3} HCl. An equal volume of 4×10^{-4} mol m^{-3} TTA in xylene solution was added and the mixture was shaken for 10 min. This method was validated using K$_2$CO$_3$ solutions spiked with a Pu(IV) stock solution and a Pu(VI) perchloric acid solution and by re-acidifying these solutions (Pu concentration = 10^{-8} mol kg^{-1}) within 10 min for TTA extraction.

Plutonium solid that had formed in a few samples was used for characterization. The initial concentrations of Pu(IV) and C_t in these samples were 1.0×10^{-4} mol kg^{-1} and 10^{-2} – 10^{-1}

mol kg^{-1}, respectively, and the pH was 9.65 - 9.85 and 12. The solid phase was trapped on a 0.45 μm filter, rinsed 3 times with 10^{-6} m^3 of deionized water and re-dissolved in 2×10^{-6} m^3 of 10^3 mol m^{-3} H$_2$SO$_4$. The concentrations of carbonate and plutonium dissolved from the solid were measured with the CO$_2$ electrode and a spectrometer, respectively. To prevent the disturbance on the carbonate measurement by acidic gas, a non-volatile acid (H$_2$SO$_4$) was used to dissolve the solid. The electrode was calibrated with a KHCO$_3$ solution using 10^3 mol m^{-3} H$_2$SO$_4$ as an acidifier. In this case, the detection limit was 6×10^{-5} mol kg^{-1}.

To check the method used to characterize the solid material, a preliminary test was carried out using cobalt (Co^{2+}) in place of plutonium. Cobalt was chosen because both hydroxide and carbonate precipitates can be readily prepared. A cobalt precipitate was prepared from CoCl$_2$ solution with an addition of NaHCO$_3$ at pH = 8.0 and $C_t = 10^{-1}$ mol kg^{-1}. The amount of cobalt was varied from 2.4×10^{-8} to 1.2×10^{-7} kg. Precipitates were also prepared in 10^{-1} mol kg^{-1} Na$_2$CO$_3$ at pH = 11.0 and 10^{-1} mol kg^{-1} NaClO$_4$ at pH = 11.0 for comparison.

8.3. Results and discussion

Cobalt forms Co(OH)$_2$(s) (log K_{sp} = -15.2; Yamaguchi & Takeda, 1999) in alkaline solutions and CoCO$_3$(s) (log K_{sp} = -9.98; Yamaguchi & Takeda, 1999) in carbonate solutions. Cobalt carbonate may be formed in the NaHCO$_3$ solution (pH = 8.0) by the following reaction

$$Co^{2+} + HCO_3^- = CoCO_3(s) + H^+ \tag{8-1}$$

Cobalt hydroxide may be formed in the Na$_2$CO$_3$ (pH = 11.0) and 10^{-1} mol kg^{-1} NaClO$_4$ solutions (pH = 11.0) by the following reaction

$$Co^{2+} + 2OH^- = Co(OH)_2(s) \tag{8-2}$$

The results of the carbonate concentrations for the cobalt precipitates are shown in Table 8-1. The measured carbonate concentration at pH = 8 is almost equal to that of cobalt. At pH = 11, on the other hand, the measured carbonate concentration is much less than that of the cobalt. This indicates that carbonate determination in precipitates can be used to determine whether the plutonium precipitate is carbonate or not. The error of measurement is about 10 % and is possibly the result from incomplete separation and rinsing of the solid. The carbonate concentration for the cobalt precipitates at pH 11 in Na$_2$CO$_3$ are higher than those in NaClO$_4$ and may be due to adsorption of carbonate on the solid and incomplete rinsing of the solid. Hence, detection limit of this determination is considered to be 10^{-4} mol kg^{-1}.

The carbonate concentrations for the Pu(IV) solid phase are shown in Table 8-2. Even in the 10^{-1} mol kg^{-1} KHCO$_3$ solution, the carbonate content was below the detection limit (10^{-4} mol kg^{-1}). The virtual absence of carbonate suggests the formation of hydrated oxide

$PuO_2 \cdot xH_2O$.

Our results do not agree with earlier predictions (Kim et al., 1983; Lierse, 1985) suggesting the transformation of solid species from oxide to hydroxy-carbonate in solutions of $> 10^{-4}$ mol kg^{-1} carbonate. In the present study, the mole fraction of hydrated oxide and hydroxy-carbonate were > 0.9 and < 0.1, respectively. The equilibrium constant of the transformation reaction:

$$PuO_2 \cdot xH_2O + CO_3^{2-} + H_2O = PuOCO_3 \cdot xH_2O + 2OH^- \tag{8-3}$$
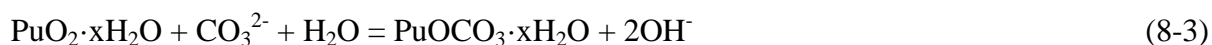
was estimated to be $K < 10^{-6.7}$. This calculation was based on the assumption that the ratio of the mole fraction between the solid phases was equal to their activity ratio. The solubility product of $PuO_2 \cdot xH_2O$ at $I = 0.1$ was estimated to be log $K_{sp} = -54.70$ using the Davies equation (Rai, 1984). A solubility product, K_{sp}, of $> 10^{-48.0}$ was estimated for $PuOCO_3 \cdot xH_2O$.

Carbonate concentrations in the range of $10^{-4} - 5 \times 10^{-1}$ mol kg^{-1} were kept approximately constant for about 100 days under the experimental conditions as shown in Fig. 8-1. A sample of the concentration as low as 10^{-5} mol kg^{-1} was affected by the atmospheric CO_2.

Figure 8-2 shows the redox potential of the sample solutions at different pHs. The following reaction is likely to control the redox condition of the sample solutions:

$$0.5NO_2^- + 0.5H_2O = 0.5NO_3^- + H^+ + e^- \qquad\qquad K = 10^{-14.15} \tag{8-4}$$

Pu(IV) is extracted by TTA while other oxidation states of Pu(V) and Pu(VI) remain in the aqueous phase (Foti & Freiling, 1964; Nitsche et al., 1988) in 10^3 mol m^{-3} HCl. The extraction of Pu(IV) from carbonate solution was (92.9±2.4) %, while that of Pu(VI) was less than 0.3 % was determined from the validation experiment. More than 90 % of the Pu was extracted from the sample solutions under the condition indicating that the Pu was mainly in the tetravalent state, although a 10 % uncertainty exists.

A series of solubility measurements was carried out at pHs 9.4, 10.1, 13 from the direction of over-saturation to determine the time required for equilibrium to be reached. As shown in Fig. 8-3, the Pu concentrations reach equilibrium within the first 14 days from the direction of over-saturation. The total carbonate concentration of a sample of pH 10.1 was increased at the 14th day by adding $KHCO_3$ and K_2CO_3. The solid phase began to dissolve and took 100 days to reach a new equilibrium concentration. This suggests that longer equilibration times are needed from the under-saturation direction than from the over-saturation direction. Although the equilibrium from the under-saturation direction was also investigated at pH = 13, the concentration was still increasing after 200 days. The equilibrium was not confirmed because Eh and total carbonate concentration were significantly affected by atmospheric O_2 and CO_2. An equilibration period of 14 days and the over-saturation direction were chosen for the present study. Considering that the solid phase will proceed to crystallize, the equilibrium

state discussed here may be a pseudo equilibrium state.

The measured solubility of Pu(IV) is shown in Fig. 8-4. In low carbonate solutions, an aqueous neutral species of $Pu(OH)_4^0$ is dominant. Its solubility was reported by Ewart et al. (1985). The solubility measured at $C_t > 10^{-4}$ mol kg^{-1} is far higher than that of $Pu(OH)_4^0$, which is due to complexation. Although the chloride anion is the main anionic species in the sample solutions, the complex formation of Pu(IV) by Cl$^-$ is negligible according to the predicted formation constant ($\log\beta_{PuCl^{3+}} = 1.33$; Brown & Wanner, 1987). Carbonate and bicarbonate concentrations were calculated from C_t and pH using the following equilibrium constants (Smith & Martell, 1976) at I = 0.1.

$$H_2CO_3(aq) = H^+ + HCO_3^- \qquad\qquad K = 10^{-6.16} \qquad\qquad (8\text{-}5)$$

$$HCO_3^- = H^+ + CO_3^{2-} \qquad\qquad K = 10^{-10.00} \qquad\qquad (8\text{-}6)$$

$$H_2O = H^+ + OH^- \qquad\qquad K = 10^{-13.78} \qquad\qquad (8\text{-}7)$$

Because the Pu fraction remaining on the filter was one order of magnitude lower than that in the final filtrate, the size of main Pu species in sample solutions was less than 3×10^{-9} m. The data analysis presented in this paper is based on two assumptions: (a) the thermodynamic activity of the solid is the same for all carbonate and bicarbonate concentrations, and (b) bi-nuclear or polynuclear species are not involved.

Because bicarbonate ion is dominant over the pH range of 9.4 - 10.1, the measured Pu concentrations are plotted versus [HCO$_3^-$]. The Pu solubility depends on the bicarbonate concentration over this pH range; log[Pu(IV)] is proportional to log[HCO$_3^-$] with the slope of 2. Hence we considered the following reaction:

$$PuO_2 \cdot xH_2O + 2HCO_3^- = Pu(CO_3)_2(OH)_n^{-n} + (2\text{-}n)OH^- + xH_2O \qquad\qquad (8\text{-}8)$$
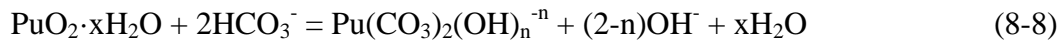
To determine the value for n, the slope of log ($[Pu(CO_3)_2(OH)_n^{-n}/[HCO_3^-]^2$) against log[OH$^-$] was calculated to be 0.23±0.57. The best fit for this data is n = 2 although a certain error (n = 2.23±0.57) is associated with this fit. The Pu concentration in bicarbonate solution is given by the sum of $[Pu(OH)_4^0]$ (= $10^{-10.14}$ mol kg^{-1}; Ewart et al., 1985) and $[Pu(CO_3)_2(OH)_2^{2-}]$. A least-squares method gives the equilibrium constant of $10^{-2.7\pm0.5}$ for Eq. (8-9).

$$PuO_2 \cdot xH_2O + 2HCO_3^- = Pu(CO_3)_2(OH)_2^{2-} + xH_2O \qquad\qquad (8\text{-}9)$$
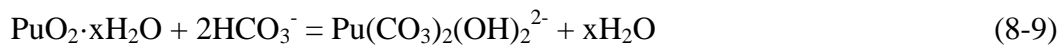
Carbonate ion dominates in the higher pH range, in place of bicarbonate. At pH = 12 and 13, the solubility at [CO$_3^{2-}$] > 10^{-3} mol kg^{-1} is proportional to the square of the carbonate concentrations and can be estimated by Eq. (8-10).

$$PuO_2 \cdot xH_2O + 2CO_3^{2-} = Pu(CO_3)_2(OH)_4^{4-} + (x\text{-}2)H_2O \qquad\qquad (8\text{-}10)$$
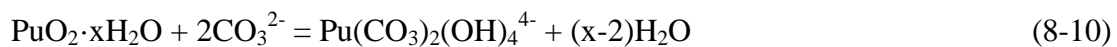
The Pu concentration in the carbonate solution is given by the sum of $[Pu(OH)_4^0]$ and $[Pu(CO_3)_2(OH)_4^{4-}]$. A least-squares method gives an equilibrium constant of $10^{-4.98\pm0.31}$ for

Eq. (8-10). Since the data at pH 12 are nearly identical to those at pH 13, the following pH-dependent reaction was ruled out.

$$PuO_2 \cdot xH_2O + 2CO_3^{2-} = Pu(CO_3)_2(OH)_3^{3-} + OH^- + (x-2)H_2O \qquad (8-11)$$
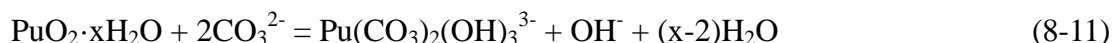
The conditional equilibrium constants of the hydroxy-carbonate complex species are tabulated in Table 8-3.

The present interpretation for Pu(IV) carbonates is similar to that for Np(IV) carbonates (Pratopo et al., 1990). The formation of $Pu(CO_3)_x^{4-2x}$ (x = 1 - 5) and $Pu(OH)_2CO_3(s)$, both of which have been predicted by Kim et al. (1983) and Lierse (1985), were not consistent with our experimental results. Their solubility in the pH range of 9 to 11 can be fitted with Eq. (8-9) as well as their interpretation in which the formation of $Pu(CO_3)_3^{2-}$ was taken into account. Their solubility in higher pH range was proportional to the square of the carbonate concentration and can be fitted with Eq. (8-10) as well as their interpretation in which the formation of $Pu(CO_3)_x^{4-2x}$ x = 4, 5 was taken into account.

8.4. Thermodynamic data compilation

Diffusive behavior of an element in geological media depends on the complex species that may form under the relevant conditions. This information is provided by speciation calculation using chemical thermodynamic data. The thermodynamic data for compounds and complexes of neptunium and plutonium were compiled. Original papers were reviewed to select thermodynamic data for hydrolysis and carbonate complexes that are particularly important under geological conditions. Some of the data for other species were cited from existing databases. In order to pick up reliable data from original papers, they were evaluated from the following viewpoints: (a) the experiments were appropriately performed, and (b) the experimental data were appropriately analyzed to obtain thermodynamic data. If two or more experimental data are available, statistical treatments were applied. Auxiliary data were taken from Silva et al.(1995).

Although Np^{3+} and Pu^{3+} are stable in acidic solutions, their formation constants of complexes are poorly known. The formation constant of Am^{3+} hydroxide, carbonate, sulphate, nitrate and fluorine complexes were used for the complexes of Np^{3+} and Pu^{3+}. The formation constants of NpO_2^+ and UO_2^{2+} complexes were also used for PuO_2^+ and NpO_2^{2+}, respectively, for supplement. In order to assess the potential effect of nitrate, sulfate and ammonia on the speciation of actinide elements in groundwater, theoretical formation constants (Brown & Wanner, 1987) were adopted. The selected data are tabulated in Table 8-4 and Table 8-5.

Table 8-1   Carbonate content analysis for cobalt precipitates.

Co 10^{-9} kg	condition of precipitation	solid	$[Co]^{(a)}$ mmol kg^{-1}	$\Sigma[CO_2]^{(b)}$ mmol kg^{-1}
24	0.1 mol kg^{-1} NaHCO$_3$ (pH=8)	CoCO$_3$	0.2	0.23
48	0.1 mol kg^{-1} NaHCO$_3$ (pH=8)	CoCO$_3$	0.4	0.40
72	0.1 mol kg^{-1} NaHCO$_3$ (pH=8)	CoCO$_3$	0.6	0.66
96	0.1 mol kg^{-1} NaHCO$_3$ (pH=8)	CoCO$_3$	0.8	0.84
120	0.1 mol kg^{-1} NaHCO$_3$ (pH=8)	CoCO$_3$	1.0	0.98
120	0.1 mol kg^{-1} Na$_2$CO$_3$ (pH=11)	Co(OH)$_2$	1.0	0.09$^{(c)}$
120	0.1 mol kg^{-1} Na$_2$CO$_3$ (pH=11)	Co(OH)$_2$	1.0	0.11$^{(c)}$
120	0.1 mol kg^{-1} Na$_2$CO$_3$ (pH=11)	Co(OH)$_2$	1.0	0.11$^{(c)}$
120	0.1 mol kg^{-1} NaClO$_4$ (pH=11)	Co(OH)$_2$	1.0	< 0.06
120	0.1 mol kg^{-1} NaClO$_4$ (pH=11)	Co(OH)$_2$	1.0	< 0.06
120	0.1 mol kg^{-1} NaClO$_4$ (pH=11)	Co(OH)$_2$	1.0	< 0.06

(a) Assuming that all the cobalt was dissolved in 10^3 mol m^{-3} H$_2$SO$_4$

(b) Total carbonate concentration measured in 10^3 mol m^{-3} H$_2$SO$_4$

(c) About 0.1 mmol kg^{-1} carbonate was detected, which is likely due to incomplete rinsing of the solid.

Table 8-2   Carbonate content in Pu solid phase.

Pu 10^{-9} kg	condition of precipitation	[Pu] mmol kg^{-1}	$\Sigma[CO_2]^{(a)}$ mmol kg^{-1}
500	0.01 mol kg^{-1} KHCO$_3$ (pH = 9.65)	1.0	< 0.1
500	0.03 mol kg^{-1} KHCO$_3$ (pH = 9.82)	1.0	< 0.1
500	0.10 mol kg^{-1} KHCO$_3$ (pH = 9.85)	1.0	< 0.1
500	0.05 mol kg^{-1} K$_2$CO$_3$ (pH = 12.0)	1.0	< 0.1

(a) The detection limit of this measurement in carbonate and bicarbonate solution is 0.1 mmol kg^{-1} (see text).

Table 8-3 Equilibrium constants of Pu(IV) hydrolysis and carbonate species.

reaction	I	$\log K$
$PuO_2 \cdot xH_2O + 2HCO_3^- = Pu(CO_3)_2(OH)_2^{2-} + xH_2O$	0.1	-2.7±0.5
$PuO_2 \cdot xH_2O + 2CO_3^{2-} = Pu(CO_3)_2(OH)_4^{4-} + (x-2)H_2O$	0.1	-4.98±0.31
$PuO_2 \cdot xH_2O = Pu(OH)_4^0 + (x-2)H_2O$	0.1	-10.14±0.28[a]
$PuO_2 \cdot xH_2O + H_2O + CO_3^{2-} = PuOCO_3 \cdot xH_2O + 2OH^-$	0.1	<-6.7

(a) taken from Ewart et al.,(1985).

Table 8-4 Neptunium thermodynamic data (1/4).

Species	reaction	$\log K^0$
Np(III)		
Np^{3+}	$Np(\alpha) + 3H^+ = Np^{3+} + 1.5H_2(g)$	90.6 ± 0.6^a
$NpOH^{2+}$	$Np^{3+} + H_2O = NpOH^{2+} + H^+$	-6.4 ± 0.7^b
$Np(OH)_2^+$	$Np^{3+} + 2H_2O = Np(OH)_2^+ + 2H^+$	-14.1 ± 0.6^b
$Np(OH)_3^0$	$Np^{3+} + 3H_2O = Np(OH)_3^0 + 3H^+$	-25.7 ± 0.5^b
$NpCO_3^+$	$Np^{3+} + CO_3^{2-} = NpCO_3^+$	7.8 ± 0.8^b
$Np(CO_3)_2^-$	$Np^{3+} + 2CO_3^{2-} = Np(CO_3)_2^-$	11.9 ± 1.0^c
$Np(CO_3)_3^{3-}$	$Np^{3+} + 3CO_3^{2-} = Np(CO_3)_3^{3-}$	15.2 ± 0.6^b
$Np(CO_3)(OH)^0$	$Np^{3+} + CO_3^{2-} + H_2O = Np(CO_3)(OH)^0 + H^+$	-0.4 ± 0.2^c
$Np(CO_3)(OH)_2^-$	$Np^{3+} + CO_3^{2-} + 2H_2O = Np(CO_3)(OH)_2^- + 2H^+$	-8.9 ± 0.9^c
$Np(CO_3)_2(OH)^{2-}$	$Np^{3+} + 2CO_3^{2-} + H_2O = Np(CO_3)_2(OH)^{2-} + H^+$	3.6 ± 0.2^c
$NpSO_4^+$	$Np^{3+} + SO_4^{2-} = NpSO_4^+$	3.850 ± 0.030^b
$Np(SO_4)_2^-$	$Np^{3+} + 2SO_4^{2-} = Np(SO_4)_2^-$	5.4 ± 0.8^b
$Np(SO_4)_3^{3-}$	$Np^{3+} + 3SO_4^{2-} = Np(SO_4)_3^{3-}$	4.8 ± 1.0^d
$Np(SO_4)_4^{5-}$	$Np^{3+} + 4SO_4^{2-} = Np(SO_4)_4^{5-}$	3.7 ± 1.0^d
$Np(SO_4)_5^{7-}$	$Np^{3+} + 5SO_4^{2-} = Np(SO_4)_5^{7-}$	1.4 ± 1.0^d
$NpNH_3^{3+}$	$Np^{3+} + NH_3^0 = NpNH_3^{3+}$	3.3 ± 1.0^d
$Np(NH_3)_2^{3+}$	$Np^{3+} + 2NH_3^0 = Np(NH_3)_2^{3+}$	5.8 ± 1.0^d
$Np(NH_3)_3^{3+}$	$Np^{3+} + 3NH_3^3 = Np(NH_3)_3^{3+}$	7.6 ± 1.0^d
$Np(NH_3)_4^{3+}$	$Np^{3+} + 4NH_3^0 = Np(NH_3)_4^{3+}$	8.7 ± 1.0^d
$Np(NH_3)_5^{3+}$	$Np^{3+} + 5NH_3^0 = Np(NH_3)_5^{3+}$	9.1 ± 1.0^d
$Np(NH_3)_6^{3+}$	$Np^{3+} + 6NH_3^0 = Np(NH_3)_6^{3+}$	8.9 ± 1.0^d
$NpNO_3^{2+}$	$Np^{3+} + NO_3^- = NpNO_3^{2+}$	1.33 ± 0.20^b
$Np(NO_3)_2^+$	$Np^{3+} + 2NO_3^- = Np(NO_3)_2^+$	0.9 ± 1.0^d
$Np(NO_3)_3^0$	$Np^{3+} + 3NO_3^- = Np(NO_3)_3^0$	0.0 ± 1.0^d
$Np(NO_3)_4^-$	$Np^{3+} + 4NO_3^- = Np(NO_3)_4^-$	-1.7 ± 1.0^d
$Np(NO_3)_5^{2-}$	$Np^{3+} + 5NO_3^- = Np(NO_3)_5^{2-}$	-4.0 ± 1.0^d
NpF^{2+}	$Np^{3+} + F^- = NpF^{2+}$	3.40 ± 0.40^b
NpF_2^+	$Np^{3+} + 2F^- = NpF_2^+$	5.80 ± 0.20^b
$Np(H_2PO_4)^{2+}$	$Np^{3+} + H_2PO_4^- = Np(H_2PO_4)^{2+}$	2.5 ± 0.1^e
$Np(OH)_3(am)$	$Np^{3+} + 3H_2O = Np(OH)_3(am) + 3H^+$	-17.0 ± 0.6^b
$Np(OH)_3(cr)$	$Np^{3+} + 3H_2O = Np(OH)_3(cr) + 3H^+$	-15.2 ± 0.6^b
$NpCO_3OH(cr)$	$Np^{3+} + H_2O + CO_3^{2-} = NpCO_3OH(cr) + H^+$	7.2 ± 1.4^b
$Np_2(CO_3)_3(cr)$	$Np^{3+} + 1.5CO_3^{2-} = Np(CO_3)_{1.5}(cr)$	16.7 ± 1.1^b
$NpF_3(cr)$	$Np^{3+} + 3F^- = NpF_3(cr)$	17.3 ± 1.2^f
$NpCl_3(cr)$	$Np^{3+} + 3Cl^- = NpCl_3(cr)$	-13.9 ± 0.9^f
$NpBr_3(cr)$	$Np^{3+} + 3Br^- = NpBr_3(cr)$	-21.5 ± 1.2^f
$NpI_3(cr)$	$Np^{3+} + 3I^- = NpI_3(cr)$	-27.9 ± 1.1^f
Np(IV)		
Np^{4+}	$Np(\alpha) + 4H^+ = Np^{4+} + 2H_2(g)$	88.1 ± 1.3^a
$NpOH^{3+}$	$Np^{4+} + H_2O = NpOH^{3+} + H^+$	-0.51 ± 0.03^g
$Np(OH)_4^0$	$NpO_2(am) + 2H_2O = Np(OH)_4^0$	-7.7 ± 1.0^h
$Np(OH)_5^-$	$NpO_2(am) + 3H_2O = Np(OH)_5^- + H^+$	-22.2 ± 1.0^i
$Np(CO_3)_4^{4-}$	$Np(CO_3)_5^{6-} = Np(CO_3)_4^{4-} + CO_3^{2-}$	0.98 ± 0.15^j
$Np(CO_3)_5^{6-}$	$NpO_2(am) + 5CO_3^{2-} + 4H^+ = Np(CO_3)_5^{6-} + 2H_2O$	34.9 ± 1.1^k

Table 8-4   continued (2/4)

Species	reaction	$\log K^0$
$Np(CO_3)_2(OH)_2^{2-}$	$NpO_2(am) + 2HCO_3^- = Np(CO_3)_2(OH)_2^{2-}$	-4.44 ± 0.42^k
$NpSO_4^{2+}$	$Np^{4+} + SO_4^{2-} = NpSO_4^{2+}$	9.0 ± 0.2^l
$Np(SO_4)_2^0$	$Np^{4+} + 2SO_4^{2-} = Np(SO_4)_2^0$	11.7 ± 0.2^l
$Np(SO_4)_3^{2-}$	$Np^{4+} + 3SO_4^{2-} = Np(SO_4)_3^{2-}$	11.0 ± 1.0^d
$Np(SO_4)_4^{4-}$	$Np^{4+} + 4SO_4^{2-} = Np(SO_4)_4^{4-}$	12.4 ± 1.0^d
$Np(SO_4)_5^{6-}$	$Np^{4+} + 5SO_4^{2-} = Np(SO_4)_5^{6-}$	12.7 ± 1.0^d
$Np(SO_4)_6^{8-}$	$Np^{4+} + 6SO_4^{2-} = Np(SO_4)_6^{8-}$	12.0 ± 1.0^d
$NpNH_3^{4+}$	$Np^{4+} + NH_3^0 = NpNH_3^{4+}$	7.6 ± 1.0^d
$Np(NH_3)_2^{4+}$	$Np^{4+} + 2NH_3^0 = Np(NH_3)_2^{4+}$	14.7 ± 1.0^d
$Np(NH_3)_3^{4+}$	$Np^{4+} + 3NH_3^0 = Np(NH_3)_3^{4+}$	21.5 ± 1.0^d
$Np(NH_3)_4^{4+}$	$Np^{4+} + 4NH_3^0 = Np(NH_3)_4^{4+}$	27.9 ± 1.0^d
$Np(NH_3)_5^{4+}$	$Np^{4+} + 5NH_3^0 = Np(NH_3)_5^{4+}$	34.1 ± 1.0^d
$Np(NH_3)_6^{4+}$	$Np^{4+} + 6NH_3^0 = Np(NH_3)_6^{4+}$	40.0 ± 1.0^d
$NpNO_3^{3+}$	$Np^{4+} + NO_3^- = NpNO_3^{3+}$	2.2 ± 0.5^e
$Np(NO_3)_2^{2+}$	$Np^{4+} + 2NO_3^- = Np(NO_3)_2^{2+}$	3.0 ± 1.0^d
$Np(NO_3)_3^-$	$Np^{4+} + 3NO_3^- = Np(NO_3)_3^+$	3.6 ± 1.0^d
$Np(NO_3)_4^0$	$Np^{4+} + 4NO_3^- = Np(NO_3)_4^0$	3.8 ± 1.0^d
$Np(NO_3)_5^-$	$Np^{4+} + 5NO_3^- = Np(NO_3)_5^-$	3.6 ± 1.0^d
$Np(NO_3)_6^{2-}$	$Np^{4+} + 6NO_3^- = Np(NO_3)_6^{2-}$	3.2 ± 1.0^d
NpF^{3+}	$Np^{4+} + HF^0 = NpF^{3+} + H^+$	5.8 ± 0.1^e
$NpCl^{3+}$	$Np^{4+} + Cl^- = NpCl^{3+}$	1.8 ± 0.5^e
$NpCrO_4^{2+}$	$Np^{4+} + HCr_4^- = NpCrO_4^{2+} + H^+$	2.5 ± 0.2^e
$Np(ISA)(OH)_3^0$	$NpO_2(am) + H^+ + ISA^- + H_2O = Np(ISA)(OH)_3^0$	2.7 ± 0.1^m
$Np(ISA)_2(OH)_2^0$	$NpO_2(am) + 2H^+ + 2ISA^- = Np(ISA)_2(OH)_2^0$	10.4 ± 0.1^m
$NpO_2(am)$	$Np^{4+} + 2H_2O = NpO_2(am) + 4H^+$	-1.5 ± 1.0^n
$Np(C_2O_4)_2(cr)$	$Np^{4+} + 2C_2O_4^{2-} = Np(C_2O_4)_2(cr)$	21.8 ± 1.5^o
$NpF_4(cr)$	$Np^{4+} + 4F^- = NpF_4(cr)$	27.2 ± 2.6^f
$NpCl_4(cr)$	$Np^{4+} + 4Cl^- = NpCl_4(cr)$	-23.1 ± 3.9^f
$NpOCl_2(cr)$	$Np^{4+} + 2Cl^- + H_2O = NpOCl_2(cr) + 2H^+$	-6.0 ± 2.6^f
$NpBr_4(cr)$	$Np^{4+} + 4Br^- = NpBr_4(cr)$	-31.7 ± 1.5^f
$NpOBr_2(cr)$	$Np^{4+} + 2Br^- + H_2O = NpOBr_2(cr) + 2H^+$	-8.0 ± 2.6^f
$Np(V)$		
NpO_2^+	$Np(\alpha) + H^+ + 2H_2O = NpO_2^+ + 2.5H_2(g)$	77.2 ± 0.9^a
NpO_2OH^0	$NpO_2^+ + H_2O = NpO_2OH^0 + H^+$	-10.70 ± 0.35^p
$NpO_2(OH)_2^-$	$NpO_2^+ + 2H_2O = NpO_2(OH)_2^- + 2H^+$	-22.42 ± 0.31^p
$NpO_2CO_3^-$	$NpO_2^+ + CO_3^{2-} = NpO_2CO_3^-$	5.39 ± 0.49^q
$NpO_2(CO_3)_2^{3-}$	$NpO_2^+ + 2CO_3^{2-} = NpO_2(CO_3)_2^{3-}$	5.8 ± 1.3^q
$NpO_2(CO_3)_3^{5-}$	$NpO_2^+ + 3CO_3^{2-} = NpO_2(CO_3)_3^{5-}$	5.15 ± 0.36^q
$NpO_2SO_3^-$	$NpO_2^+ + SO_3^{2-} = NpO_2SO_3^-$	3.2 ± 0.2^e
$NpO_2(SO_3)_2^{3-}$	$NpO_2^+ + 2SO_3^{2-} = NpO_2(SO_3)_2^{3-}$	3.0 ± 0.1^e
$NpO_2SO_4^-$	$NpO_2^+ + SO_4^{2-} = NpO_2SO_4^-$	0.6 ± 0.2^e
$NpO_2(SO_4)_2^{3-}$	$NpO_2^+ + 2SO_4^{2-} = NpO_2(SO_4)_2^{3-}$	1.3 ± 1.0^d
$NpO_2(SO_4)_3^{5-}$	$NpO_2^+ + 3SO_4^{2-} = NpO_2(SO_4)_3^{5-}$	-0.2 ± 1.0^d
$NpO_2(SO_4)_4^{7-}$	$NpO_2^+ + 4SO_4^{2-} = NpO_2(SO_4)_4^{7-}$	-2.9 ± 1.0^d

Table 8-4 continued (3/4)

Species	reaction	log K^0
$NpO_2NH_3^+$	$NpO_2^+ + NH_3^0 = NpO_2NH_3^+$	0.5 ± 1.0^d
$NpO_2(NH_3)_2^+$	$NpO_2^+ + 2NH_3^0 = NpO_2(NH_3)_2^+$	0.3 ± 1.0^d
$NpO_2(NH_3)_3^+$	$NpO_2^+ + 3NH_3^0 = NpO_2(NH_3)_3^+$	-0.3 ± 1.0^d
$NpO_2(NH_3)_4^+$	$NpO_2^+ + 4NH_3^0 = NpO_2(NH_3)_4^+$	-1.5 ± 1.0^d
$NpO_2(NH_3)_5^+$	$NpO_2^+ + 5NH_3^0 = NpO_2(NH_3)_5^+$	-3.0 ± 1.0^d
$NpO_2NO_3^0$	$NpO_2^+ + NO_3^- = NpO_2NO_3^0$	0.2 ± 1.0^d
$NpO_2(NO_3)_2^-$	$NpO_2^+ + 2NO_3^- = NpO_2(NO_3)_2^-$	-0.5 ± 1.0^d
$NpO_2(NO_3)_3^{2-}$	$NpO_2^+ + 3NO_3^- = NpO_2(NO_3)_3^{2-}$	-1.8 ± 1.0^d
$NpO_2(NO_3)_4^{3-}$	$NpO_2^+ + 4NO_3^- = NpO_2(NO_3)_4^{3-}$	-3.7 ± 1.0^d
$NpO_2(NO_3)_5^{4-}$	$NpO_2^+ + 5NO_3^- = NpO_2(NO_3)_5^{4-}$	-6.1 ± 1.0^d
NpO_2Cl^0	$NpO_2^+ + Cl^- = NpO_2Cl^0$	-0.29 ± 0.05^r
NpO_2F^0	$NpO_2^+ + F^- = NpO_2F^0$	1.9 ± 0.2^e
$NpO_2HPO_4^-$	$NpO_2^+ + HPO_4^{2-} = NpO_2HPO_4^-$	3.4 ± 0.4^e
$NpO_2PO_4^{2-}$	$NpO_2^+ + PO_4^{3-} = NpO_2PO_4^{2-}$	7.20 ± 0.08^s
$NpO_2OH(s)$	$NpO_2^+ + H_2O = NpO_2OH(s) + H^+$	-5.32 ± 0.26^p
$NaNpO_2CO_3(s)$	$NpO_2^+ + Na^+ + CO_3^{2-} = NaNpO_2CO_3(s)$	11.12 ± 0.36^g
$NaNpO_2CO_3 \cdot 3.5H_2O$	$NpO_2^+ + Na^+ + 3.5H_2O + CO_3^{2-} = NaNpO_2CO_3 \cdot 3.5H_2O$	11.09 ± 0.11^t
$Na_3NpO_2(CO_3)_2(cr)$	$NpO_2^+ + 3Na^+ + 2CO_3^{2-} = Na_3NpO_2(CO_3)_2(cr)$	14.18 ± 0.13^t

Np(VI)

Species	reaction	log K^0
NpO_2^{2+}	$NpO_2^+ + H^+ = NpO_2^{2+} + 0.5H_2(g)$	-20.89 ± 0.17^a
NpO_2OH^+	$NpO_2^{2+} + H_2O = NpO_2OH+ + H^+$	-5.20 ± 0.30^u
$NpO_2(OH)_2^0$	$NpO_2^{2+} + 2H_2O = NpO_2(OH)_2^0 + 2H^+$	-12.21 ± 0.09^v
$NpO_2(OH)_3^-$	$NpO_3 \cdot H_2O(s) + H_2O = NpO_2(OH)_3^- + H^+$	-17.09 ± 0.11^w
$NpO_2(OH)_4^{2-}$	$NpO_2^{2+} + 4H_2O = NpO_2(OH)_4^{2-} + 4H^+$	-32.4 ± 0.7^x
$(NpO_2)_2OH^{3+}$	$2NpO_2^{2+} + H_2O = (NpO_2)_2OH^{3+} + H^+$	-2.7 ± 1.0^u
$(NpO_2)_2(OH)_2^{2+}$	$2NpO_2^{2+} + 2H_2O = (NpO_2)_2(OH)_2^{2+} + 2H^+$	-5.62 ± 0.04^u
$(NpO_2)_3(OH)_4^{2+}$	$3NpO_2^{2+} + 4H_2O = (NpO_2)_3(OH)_4^{2+} + 4H^+$	-11.9 ± 0.30^u
$(NpO_2)_3(OH)_5^+$	$3NpO_2^{2+} + 5H_2O = (NpO_2)_3(OH)_5^+ + 5H^+$	-15.55 ± 0.12^u
$(NpO_2)_4(OH)_7^+$	$4NpO_2^{2+} + 7H_2O = (NpO_2)_4(OH)_7^+ + 7H^+$	-21.9 ± 1.0^u
$(NpO_2)_3(OH)_7^-$	$3NpO_2^{2+} + 7H_2O = (NpO_2)_3(OH)_7^- + 7H^+$	-31.0 ± 2.0^u
$NpO_2CO_3^0$	$NpO_2^{2+} + CO_3^{2-} = NpO_2CO_3^0$	9.85 ± 0.10^y
$NpO_2(CO_3)_2^{2-}$	$NpO_2^{2+} + 2CO_3^{2-} = NpO_2(CO_3)_2^{2-}$	15.0 ± 1.0^y
$NpO_2(CO_3)_3^{4-}$	$NpO_2^{2+} + 3CO_3^{2-} = NpO_2(CO_3)_3^{4-}$	17.0 ± 1.0^w
$(NpO_2)_3(CO_3)_6^{6-}$	$3NpO_2(CO_3)_3^{4-} = (NpO_2)_3(CO_3)_6^{6-} + 3CO_3^{2-}$	-9.5 ± 0.1^z
$NpO_2CO_3(OH)_2^{2-}$	$NpO_3 \cdot H_2O + CO_3^{2-} = NpO_2CO_3(OH)_2^{2-}$	-2.59 ± 0.23^w
$(NpO_2)_3CO_3(OH)_3^+$	$3NpO_2^{2+} + CO_2(g) + 4H_2O = (NpO_2)_3CO_3(OH)_3^+ + 5H^+$	-17.50 ± 0.50^u
$(NpO_2)_2CO_3(OH)_3^-$	$2NpO_2^{2+} + CO_2(g) + 4H_2O = (NpO_2)_2CO_3(OH)_3^- + 5H^+$	-19.01 ± 0.50^u
$(NpO_2)_{11}(CO_3)_6(OH)_{12}^{2-}$	$11NpO_2^{2+} + 6CO_2(g) + 18H_2O = (NpO_2)_{11}(CO_3)_6(OH)_{12}^{2-} + 24H^+$	-72.5 ± 2.0^u
$NpO_2SO_4^0$	$NpO_2^{2+} + SO_4^{2-} = NpO_2SO_4^0$	3.4 ± 0.3^e
$NpO_2(SO_4)_2^{2-}$	$NpO_2^{2+} + 2SO_4^{2-} = NpO_2(SO_4)_2^{2-}$	4.14 ± 0.07^u
$NpO_2(SO_4)_3^{4-}$	$NpO_2^{2+} + 3SO_4^{2-} = NpO_2(SO_4)_3^{4-}$	4.1 ± 1.0^d
$NpO_2(SO_4)_4^{6-}$	$NpO_2^{2+} + 4SO_4^{2-} = NpO_2(SO_4)_4^{6-}$	3.4 ± 1.0^d
$NpO_2(SO_4)_5^{8-}$	$NpO_2^{2+} + 5SO_4^{2-} = NpO_2(SO_4)_5^{8-}$	1.8 ± 1.0^d

Table 8-4   concluded (4/4)

Species	reaction	log K^0
$NpO_2NH_3^{2+}$	$NpO_2^{2+} + NH_3^0 = NpO_2NH_3^{2+}$	3.9 ± 1.0^d
$NpO_2(NH_3)_2^{2+}$	$NpO_2^{2+} + 2NH_3^0 = NpO_2(NH_3)_2^{2+}$	7.4 ± 1.0^d
$NpO_2(NH_3)_3^{2+}$	$NpO_2^{2+} + 3NH_3^0 = NpO_2(NH_3)_3^{2+}$	10.6 ± 1.0^d
$NpO_2(NH_3)_4^{2+}$	$NpO_2^{2+} + 4NH_3^0 = NpO_2(NH_3)_4^{2+}$	13.6 ± 1.0^d
$NpO_2(NH_3)_5^{2+}$	$NpO_2^{2+} + 5NH_3^0 = NpO_2(NH_3)_5^{2+}$	16.3 ± 1.0^d
$NpO_2NO_3^+$	$NpO_2^{2+} + NO_3^- = NpO_2NO_3^+$	0.30 ± 0.15^u
$NpO_2(NO_3)_2^0$	$NpO_2^{2+} + 2NO_3^- = NpO_2(NO_3)_2^0$	0.5 ± 1.0^d
$NpO_2(NO_3)_3^-$	$NpO_2^{2+} + 3NO_3^- = NpO_2(NO_3)_3^-$	0.1 ± 1.0^d
$NpO_2(NO_3)_4^{2-}$	$NpO_2^{2+} + 4NO_3^- = NpO_2(NO_3)_4^{2-}$	-0.8 ± 1.0^d
$NpO_2(NO_3)_5^{3-}$	$NpO_2^{2+} + 5NO_3^- = NpO_2(NO_3)_5^{3-}$	-2.0 ± 1.0^d
NpO_2F^+	$NpO_2^{2+} + F^- = NpO_2F_2^+$	4.66 ± 0.15^e
$NpO_2F_2^0$	$NpO_2^{2+} + 2F^- = NpO_2F_2^0$	7.8 ± 0.1^e
$NpO_2F_3^-$	$NpO_2^{2+} + 3F^- = NpO_2F_3^-$	10.4 ± 0.1^e
NpO_2Cl^+	$NpO_2^{2+} + Cl^- = NpO_2Cl^+$	0.4 ± 0.1^e
$(UO_2)_2NpO_2(CO_3)_6^{6-}$	$NpO_2(CO_3)_3^{4-} + 2UO_2(CO_3)_3^{4-} = (UO_2)_2NpO_2(CO_3)_6^{6-} + 3CO_3^{2-}$	-9.4 ± 1.3^b
$NpO_3 \cdot H_2O(s)$	$NpO_2^{2+} + 2H_2O = NpO_3 \cdot H_2O(s) + 2H^+$	-5.67 ± 0.17^{2a}
$NpO_2CO_3(s)$	$NpO_2^{2+} + CO_3^{2-} = NpO_2CO_3(s)$	14.87 ± 0.58^y
$NpO_2(NO_3)_2 \cdot 6H_2O(cr)$	$NpO_2^{2+} + 2NO_3^- + 6H_2O = NpO_2(NO_3)_2 \cdot 6H_2O(cr)$	-2.16 ± 0.19^o

neptunium hydride

$NpH_2(cr)$	$Np(\alpha) + H_2(g) = NpH_2(cr)$	16.0 ± 3.4^{2b}

[a] Fuger & Oetting(1976)
[b] Silva et al.(1995)
[c] Yamaguchi & Nakayama(1996)
[d] Brown & Wanner(1987)
[e] Fuger et al.(1992)
[f] Fuger et al.(1983)
[g] Yamaguchi et al.(2000)
[h] Nakayama et al.(1996)
[i] Rai & Ryan(1985)
[j] Delmau et al.(1996)
[k] Rai et al.(1999a)
[l] Xia et al.(1999)
[m] Rai et al.(1998)
[n] Rai et al.(1987)
[o] Cordfunke & O'Hare(1978)
[p] Itagaki et al.(1992)
[q] Novak & Roberts(1995)
[r] Neck et al.(1995b)
[s] Morgenstern & Kim(1996)
[t] Neck et al.(1995a)
[u] Grenthe et al.(1992)
[v] Choppin & Mathur(1991)
[w] Moriyama et al.(1995)
[x] Yamamura et al.(1998)
[y] Kato et al.(1998)
[z] Grenthe et al.(1986)
[2a] Kato et al.(1996)
[2b] Flotow et al.(1984)

Table 8-5 Plutonium thermodynamic data (1/4)

Species	reaction	log K^0
Pu(III)		
Pu^{3+}	$Pu(\alpha) + 3H^+ = Pu^{3+} + 1.5H^+(g)$	101.4 ± 0.6^a
$PuOH^{2+}$	$Pu^{3+} + H_2O = PuOH^{2+} + H^+$	-6.4 ± 0.7^b
$Pu(OH)_2^+$	$Pu^{3+} + 2H_2O = Pu(OH)_2^+ + 2H^+$	-14.1 ± 0.6^b
$Pu(OH)_3^0$	$Pu^{3+} + 3H_2O = Pu(OH)_3^0 + 3H^+$	-25.7 ± 0.5^b
$PuCO_3^+$	$Pu^{3+} + CO_3^{2-} = PuCO_3^+$	7.8 ± 0.8^b
$Pu(CO_3)_2^-$	$Pu^{3+} + 2CO_3^{2-} = Pu(CO_3)_2^-$	11.9 ± 1.0^c
$Pu(CO_3)_3^{3-}$	$Pu^{3+} + 3CO_3^{2-} = Pu(CO_3)_3^{3-}$	15.2 ± 0.6^b
$Pu(CO_3)(OH)^0$	$Pu^{3+} + CO_3^{2-} + H_2O = Pu(CO_3)(OH)^0 + H^+$	-0.4 ± 0.2^c
$Pu(CO_3)(OH)_2^-$	$Pu^{3+} + CO_3^{2-} + 2H_2O = Pu(CO_3)(OH)_2^- + 2H^+$	-8.9 ± 0.9^c
$Pu(CO_3)_2(OH)^{2-}$	$Pu^{3+} + 2CO_3^{2-} + H_2O = Pu(CO_3)_2(OH)^{2-} + H^+$	3.6 ± 0.2^c
$PuSO_4^+$	$Pu^{3+} + SO_4^{2-} = PuSO_4^+$	4.5 ± 0.5^d
$Pu(SO_4)_2^-$	$Pu^{3+} + 2SO_4^{2-} = Pu(SO_4)_2^-$	6.7 ± 0.6^d
$Pu(SO_4)_3^{3-}$	$Pu^{3+} + 3SO_4^{2-} = Pu(SO_4)_3^{3-}$	5.0 ± 1.0^e
$Pu(SO_4)_4^{5-}$	$Pu^{3+} + 4SO_4^{2-} = Pu(SO_4)_4^{5-}$	4.0 ± 1.0^e
$Pu(SO_4)_5^{7-}$	$Pu^{3+} + 5SO_4^{2-} = Pu(SO_4)_5^{7-}$	1.8 ± 1.0^e
$PuNH_3^{3+}$	$Pu^{3+} + NH_3^0 = PuNH_3^{3+}$	3.5 ± 1.0^e
$Pu(NH_3)_2^{3+}$	$Pu^{3+} + 2NH_3^0 = Pu(NH_3)_2^{3+}$	6.2 ± 1.0^e
$Pu(NH_3)_3^{3+}$	$Pu^{3+} + 3NH_3^3 = Pu(NH_3)_3^{3+}$	8.1 ± 1.0^e
$Pu(NH_3)_4^{3+}$	$Pu^{3+} + 4NH_3^0 = Pu(NH_3)_4^{3+}$	9.4 ± 1.0^e
$Pu(NH_3)_5^{3+}$	$Pu^{3+} + 5NH_3^0 = Pu(NH_3)_5^{3+}$	10.1 ± 1.0^e
$Pu(NH_3)_6^{3+}$	$Pu^{3+} + 6NH_3^0 = Pu(NH_3)_6^{3+}$	10.1 ± 1.0^e
$PuNO_3^{2+}$	$Pu^{3+} + NO_3^- = PuNO_3^{2+}$	1.0 ± 1.0^e
$Pu(NO_3)_2^+$	$Pu^{3+} + 2NO_3^- = Pu(NO_3)_2^+$	1.0 ± 1.0^e
$Pu(NO_3)_3^0$	$Pu^{3+} + 3NO_3^- = Pu(NO_3)_3^0$	0.1 ± 1.0^e
$Pu(NO_3)_4^-$	$Pu^{3+} + 4NO_3^- = Pu(NO_3)_4^-$	-1.5 ± 1.0^e
$Pu(NO_3)_5^{2-}$	$Pu^{3+} + 5NO_3^- = Pu(NO_3)_5^{2-}$	-3.8 ± 1.0^e
$Pu(NO_3)_6^{3-}$	$Pu^{3+} + 6NO_3^- = Pu(NO_3)_6^{3-}$	-6.7 ± 1.0^e
PuF^{2+}	$Pu^{3+} + F^- = PuF^{2+}$	3.40 ± 0.40^b
PuF_2^+	$Pu^{3+} + 2F^- = PuF_2^+$	5.80 ± 0.20^b
$PuCl^{2+}$	$Pu^{3+} + Cl^- = PuCl^{2+}$	1.3 ± 0.1^d
$PuH_2PO_4^{2+}$	$Pu^{3+} + H_2PO_4^- = PuH_2PO_4^{2+}$	2.5 ± 0.1^d
$Pu(OH)_3(s)$	$Pu^{3+} + 3H_2O = Pu(OH)_3(s) + 3H^+$	-15.8 ± 0.8^f
$PuCO_3OH(cr)$	$Pu^{3+} + H_2O + CO_3^{2-} = PuCO_3OH(cr) + H^+$	7.2 ± 1.4^b
$Pu_2(CO_3)_3(cr)$	$Pu^{3+} + 1.5CO_3^{2-} = Pu(CO_3)_{1.5}(cr)$	16.7 ± 1.1^b
$PuF_3(cr)$	$Pu^{3+} + 3F^- = PuF_3(cr)$	16.3 ± 0.9^g
$PuCl_3(cr)$	$Pu^{3+} + 3Cl^- = PuCl_3(cr)$	-14.1 ± 0.7^g
$PuCl_3\cdot6H_2O(s)$	$Pu^{3+} + 3Cl^- + 6H_2O = PuCl_3\cdot6H_2O(s)$	-5.2 ± 0.8^g
$PuOCl(cr)$	$Pu^{3+} + Cl^- + H_2O = PuOCl_3(cr) + 2H^+$	-11.5 ± 0.7^g
$PuBr_3(cr)$	$Pu^{3+} + 3Br^- = PuBr_3(cr)$	-21.4 ± 1.1^g
$PuOBr(cr)$	$Pu^{3+} + Br^- + H_2O = PuOBr_3(cr) + 2H^-$	-14.7 ± 1.4^g
$PuI_3(cr)$	$Pu^{3+} + 3I^- = PuI_3(cr)$	-27.0 ± 1.1^g

Table 8-5 continued (2/4)

Species	reaction	log K^0
Pu (IV)		
Pu^{4+}	$Pu^{3+} + H^+ = Pu^{4+} + 0.5H_2(g)$	17.65 ± 0.17^h
$PuOH^{3+}$	$Pu^{4+} + H_2O = PuOH^{3+} + H^+$	-0.51 ± 0.03^i
$Pu(OH)_4^0$	$PuO_2(am) + 2H_2O = Pu(OH)_4^0$	-10.14 ± 0.28^j
$Pu(OH)_5^-$	$Pu(OH)_4^0 + H_2O = Pu(OH)_5^- + H^+$	-13.0 ± 1.0^j
$PuCO_3^{2+}$	$Pu^{4+} + CO_3^{2-} = PuCO_3^{2+}$	12.3 ± 1.0^k
$Pu(CO_3)_2^0$	$Pu^{4+} + 2CO_3^{2-} = Pu(CO_3)_2^0$	23.4 ± 1.0^k
$Pu(CO_3)_3^{2-}$	$Pu^{4+} + 3CO_3^{2-} = Pu(CO_3)_3^{2-}$	30.0 ± 1.0^k
$Pu(CO_3)_4^{4-}$	$Pu(CO_3)_5^{6-} = Pu(CO_3)_4^{4-} + CO_3^{2-}$	1.36 ± 0.09^l
$Pu(CO_3)_5^{6-}$	$PuO_2(am) + 5CO_3^{2-} + 4H^+ = Pu(CO_3)_5^{6-} + 2H_2O$	33.3 ± 0.6^m
$Pu(OH)_2(CO_3)_2^{2-}$	$PuO_2(am) + 2HCO_3^- = Pu(OH)_2(CO_3)_2^{2-}$	-3.8 ± 1.4^i
$Pu(OH)_4(CO_3)_2^{4-}$	$PuO_2(am) + 2CO_3^{2-} + 2H_2O = Pu(OH)_4(CO_3)_2^{4-}$	-5.85 ± 0.31^n
$PuSO_4^{2+}$	$Pu^{4+} + HSO_4^- = PuSO_4^{2+} + H^+$	5.5 ± 0.5^d
$Pu(SO_4)_2^0$	$Pu^{4+} + 2HSO_4^{2-} = Pu(SO_4)_2^0 + 2H^+$	7.7 ± 0.7^d
$Pu(SO_4)_3^{2-}$	$Pu^{4+} + 3SO_4^{2-} = Pu(SO_4)_3^{2-}$	11.0 ± 1.0^e
$Pu(SO_4)_4^{4-}$	$Pu^{4+} + 4SO_4^{2-} = Pu(SO_4)_4^{4-}$	12.4 ± 1.0^e
$Pu(SO_4)_5^{6-}$	$Pu^{4+} + 5SO_4^{2-} = Pu(SO_4)_5^{6-}$	12.5 ± 1.0^e
$Pu(SO_4)_6^{8-}$	$Pu^{4+} + 6SO_4^{2-} = Pu(SO_4)_6^{8-}$	11.6 ± 1.0^e
$PuNH_3^{4+}$	$Pu^{4+} + NH_3^0 = PuNH_3^{4+}$	7.8 ± 1.0^e
$Pu(NH_3)_2^{4+}$	$Pu^{4+} + 2NH_3^0 = Pu(NH_3)_2^{4+}$	15.1 ± 1.0^e
$Pu(NH_3)_3^{4+}$	$Pu^{4+} + 3NH_3^0 = Pu(NH_3)_3^{4+}$	22.0 ± 1.0^e
$Pu(NH_3)_4^{4+}$	$Pu^{4+} + 4NH_3^0 = Pu(NH_3)_4^{4+}$	28.5 ± 1.0^e
$Pu(NH_3)_5^{4+}$	$Pu^{4+} + 5NH_3^0 = Pu(NH_3)_5^{4+}$	34.7 ± 1.0^e
$Pu(NH_3)_6^{4+}$	$Pu^{4+} + 6NH_3^0 = Pu(NH_3)_6^{4+}$	40.6 ± 1.0^e
$PuNO_3^{3+}$	$Pu^{4+} + NO_3^- = PuNO_3^{3+}$	2.6 ± 0.5^d
$Pu(NO_3)_2^{2+}$	$Pu^{4+} + 2NO_3^- = Pu(NO_3)_2^{2+}$	3.0 ± 1.0^e
$Pu(NO_3)_3^+$	$Pu^{4+} + 3NO_3^- = Pu(NO_3)_3^+$	3.6 ± 1.0^e
$Pu(NO_3)_4^0$	$Pu^{4+} + 4NO_3^- = Pu(NO_3)_4^0$	3.7 ± 1.0^e
$Pu(NO_3)_5^-$	$Pu^{4+} + 5NO_3^- = Pu(NO_3)_5^-$	3.4 ± 1.0^e
$Pu(NO_3)_6^{2-}$	$Pu^{4+} + 6NO_3^- = Pu(NO_3)_6^{2-}$	2.7 ± 1.0^e
PuF^{3+}	$Pu^{4+} + HF^0 = PuF^{3+} + H^+$	5.24 ± 0.11^d
$PuCl^{3+}$	$Pu^{4+} + Cl^- = PuCl^{3+}$	2.0 ± 0.5^d
$PuO_2(am)$	$Pu^{4+} + 2H_2O = PuO_2(am) + 4H^+$	1.7 ± 0.9^i
$PuOCO_3(s)$	$PuO_2(am) + CO_3^{2-} + 2H^+ = PuOCO_3(s) + 2H_2O$	21.5 ± 1.0^n
$Pu(SO_4)_2(cr)$	$Pu^{4+} + 2SO_4^{2-} = Pu(SO_4)_2(cr)$	8 ± 7°
$PuF_4(cr)$	$Pu^{4+} + 4F^- = PuF_4(cr)$	25.4 ± 3.7^g

118

Table 8-5   continued (3/4)

Species	reaction	log K^0
Pu(V)		
PuO_2^+	$PuO_2^{2+} + 0.5H_2(g) = PuO_2^+ + H^+$	15.86 ± 0.17^h
PuO_2OH^0	$PuO_2^+ + H_2O = PuO_2OH^0 + H^+$	-9.73 ± 0.10^p
$PuO_2(OH)_2^-$	$PuO_2^+ + 2H_2O = PuO_2(OH)_2^- + 2H^+$	-22.42 ± 0.31^q
$PuO_2CO_3^-$	$PuO_2^+ + CO_3^{2-} = PuO_2CO_3^-$	5.12 ± 0.07^p
$PuO_2(CO_3)_2^{3-}$	$PuO_2^+ + 2CO_3^{2-} = PuO_2(CO_3)_2^{3-}$	5.8 ± 1.3^r
$PuO_2(CO_3)_3^{5-}$	$PuO_2^+ + 3CO_3^{2-} = PuO_2(CO_3)_3^{5-}$	5.15 ± 0.36^r
$PuO_2SO_4^-$	$PuO_2^+ + SO_4^{2-} = PuO_2SO_4^-$	0.6 ± 0.2^d
$PuO_2(SO_4)_2^{3-}$	$PuO_2^+ + 2SO_4^{2-} = PuO_2(SO_4)_2^{3-}$	1.2 ± 1.0^e
$PuO_2(SO_4)_3^{5-}$	$PuO_2^+ + 3SO_4^{2-} = PuO_2(SO_4)_3^{5-}$	-0.3 ± 1.0^e
$PuO_2(SO_4)_4^{7-}$	$PuO_2^+ + 4SO_4^{2-} = PuO_2(SO_4)_4^{7-}$	-3.1 ± 1.0^e
$PuO_2NH_3^+$	$PuO_2^+ + NH_3^0 = PuO_2NH_3^+$	0.5 ± 1.0^e
$PuO_2(NH_3)_2^+$	$PuO_2^+ + 2NH_3^0 = PuO_2(NH_3)_2^+$	0.2 ± 1.0^e
$PuO_2(NH_3)_3^+$	$PuO_2^+ + 3NH_3^0 = PuO_2(NH_3)_3^+$	-0.7 ± 1.0^e
$PuO_2(NH_3)_4^+$	$PuO_2^+ + 4NH_3^0 = PuO_2(NH_3)_4^+$	-2.0 ± 1.0^e
$PuO_2(NH_3)_5^+$	$PuO_2^+ + 5NH_3^0 = PuO_2(NH_3)_5^+$	-3.9 ± 1.0^e
$PuO_2NO_3^0$	$PuO_2^+ + NO_3^- = PuO_2NO_3^0$	0.2 ± 1.0^e
$PuO_2(NO_3)_2^-$	$PuO_2^+ + 2NO_3^- = PuO_2(NO_3)_2^-$	-0.6 ± 1.0^e
$PuO_2(NO_3)_3^{2-}$	$PuO_2^+ + 3NO_3^- = PuO_2(NO_3)_3^{2-}$	-2.1 ± 1.0^e
$PuO_2(NO_3)_4^{3-}$	$PuO_2^+ + 4NO_3^- = PuO_2(NO_3)_4^{3-}$	-4.2 ± 1.0^e
$PuO_2(NO_3)_5^{4-}$	$PuO_2^+ + 5NO_3^- = PuO_2(NO_3)_5^{4-}$	-6.8 ± 1.0^e
PuO_2F^0	$PuO_2^+ + F^- = PuO_2F^0$	1.9 ± 0.2^d
$PuO_2OH(s)$	$PuO_2^+ + H_2O = PuO_2OH(s) + H^+$	-5.32 ± 0.26^q
$NaPuO_2CO_3(s)$	$PuO_2^+ + Na^+ + CO_3^{2-} = NaPuO_2CO_3(s)$	11.12 ± 0.36^r
$NaPuO_2CO_3 \cdot 3.5H_2O$	$PuO_2^+ + Na^+ + 3.5H_2O + CO_3^{2-} = NaPuO_2CO_3 \cdot 3.5H_2O$	11.09 ± 0.11^s
$Na_3PuO_2(CO_3)_2(cr)$	$PuO_2^+ + 3Na^+ + 2CO_3^{2-} = Na_3PuO_2(CO_3)_2(cr)$	14.18 ± 0.13^s
Pu(VI)		
PuO_2^{2+}	$Pu^{3+} + 2H_2O = PuO_2^{2+} + H^+ + 1.5H_2(g)$	-51.8 ± 1.1^a
PuO_2OH^-	$PuO_2^{2+} + H_2O = PuO_2OH^+ + H^+$	-5.48 ± 0.15^t
$(PuO_2)_2(OH)_2^{2+}$	$2PuO_2^{2+} + 2H_2O = (PuO_2)_2(OH)_2^{2+} + 2H^+$	-7.1 ± 0.2^u
$(PuO_2)_4(OH)_7^-$	$4PuO_2^{2+} + 7H_2O = (PuO_2)_4(OH)_7^+ + 7H^+$	-21.9 ± 1.0^v
$PuO_2(OH)_2^0$	$PuO_2^{2+} + 2H_2O = PuO_2(OH)_2^0 + 2H^+$	-13.36 ± 0.18^t
$PuO_2(OH)_3^-$	$PuO_2^{2+} + 3H_2O = PuO_2(OH)_3^- + 3H^+$	-22.9 ± 2.0^w
$PuO_2CO_3^0$	$PuO_2^{2+} + CO_3^{2-} = PuO_2CO_3^0$	9.56 ± 0.36^x
$PuO_2(CO_3)_2^{2-}$	$PuO_2^{2+} + 2CO_3^{2-} = PuO_2(CO_3)_2^{2-}$	15.0 ± 0.5^x
$PuO_2(CO_3)_3^{4-}$	$PuO_2^{2+} + 3CO_3^{2-} = PuO_2(CO_3)_3^{4-}$	17.53 ± 0.20^x
$(PuO_2)_3(CO_3)_6^{6-}$	$3PuO_2(CO_3)_3^{4-} = (PuO_2)_3(CO_3)_6^{6-} + 3CO_3^{2-}$	-6.8 ± 0.2^y
$PuO_2SO_4^0$	$PuO_2^{2+} + SO_4^{2-} = PuO_2SO_4^0$	3.150 ± 0.020^v
$PuO_2(SO_4)_2^{2-}$	$PuO_2^{2+} + 2SO_4^{2-} = PuO_2(SO_4)_2^{2-}$	4.14 ± 0.07^v
$PuO_2(SO_4)_3^{4-}$	$PuO_2^{2+} + 3SO_4^{2-} = PuO_2(SO_4)_3^{4-}$	3.7 ± 1.0^e
$PuO_2(SO_4)_4^{6-}$	$PuO_2^{2+} + 4SO_4^{2-} = PuO_2(SO_4)_4^{6-}$	2.6 ± 1.0^e
$PuO_2(SO_4)_5^{8-}$	$PuO_2^{2+} + 5SO_4^{2-} = PuO_2(SO_4)_5^{8-}$	0.5 ± 1.0^e

119

Table 8-5　concluded (4/4)

Species	reaction	log K^0
$PuO_2NH_3^{2+}$	$PuO_2^{2+} + NH_3^0 = PuO_2NH_3^{2+}$	3.8 ± 1.0^e
$PuO_2(NH_3)_2^{2+}$	$PuO_2^{2+} + 2NH_3^0 = PuO_2(NH_3)_2^{2+}$	7.2 ± 1.0^e
$PuO_2(NH_3)_3^{2+}$	$PuO_2^{2+} + 3NH_3^0 = PuO_2(NH_3)_3^{2+}$	10.2 ± 1.0^e
$PuO_2(NH_3)_4^{2+}$	$PuO_2^{2+} + 4NH_3^0 = PuO_2(NH_3)_4^{2+}$	12.9 ± 1.0^e
$PuO_2(NH_3)_5^{2+}$	$PuO_2^{2+} + 5NH_3^0 = PuO_2(NH_3)_5^{2+}$	15.4 ± 1.0^e
$PuO_2NO_3^+$	$PuO_2^{2+} + NO_3^- = PuO_2NO_3^+$	0.6 ± 1.0^e
$PuO_2(NO_3)_2^0$	$PuO_2^{2+} + 2NO_3^- = PuO_2(NO_3)_2^0$	0.5 ± 1.0^e
$PuO_2(NO_3)_3^-$	$PuO_2^{2+} + 3NO_3^- = PuO_2(NO_3)_3^-$	-0.1 ± 1.0^e
$PuO_2(NO_3)_4^{2-}$	$PuO_2^{2+} + 4NO_3^- = PuO_2(NO_3)_4^{2-}$	-1.1 ± 1.0^e
$PuO_2(NO_3)_5^{3-}$	$PuO_2^{2+} + 5NO_3^- = PuO_2(NO_3)_5^{3-}$	-2.5 ± 1.0^e
PuO_2F^+	$PuO_2^{2+} + F^- = PuO_2F_3^+$	4.57 ± 0.10^d
$PuO_2F_2^0$	$PuO_2^{2+} + 2F^- = PuO_2F_2^0$	8.24 ± 0.10^d
$PuO_2F_3^-$	$PuO_2^{2+} + 3F^- = PuO_2F_3^-$	9.80 ± 0.10^d
PuO_2Cl^+	$PuO_2^{2+} + Cl^- = PuO_2Cl^+$	0.09 ± 0.05^d
$PuO_2Cl_2^0$	$PuO_2^{2+} + 2Cl^- = PuO_2Cl_2^0$	-0.45 ± 0.10^d
$(UO_2)_2PuO_2(CO_3)_6^{6-}$	$PuO_2(CO_3)_3^{4-} + 2UO_2(CO_3)_3^{4-} = (UO_2)_2PuO_2(CO_3)_6^{6-} + 3CO_3^{2-}$	-8.2 ± 1.3^v
$PuO_2(OH)_2(s)$	$PuO_2^{2+} + 2H_2O = PuO_2(OH)_2(s) + 2H^+$	-4.4 ± 0.2^z
$PuO_2CO_3(s)$	$PuO_2^{2+} + CO_3^{2-} = PuO_2CO_3(s)$	14.84 ± 0.64^{2a}
$PuF_6(cr)$	$PuO_2^{2+} + 6F^- + 4H^+ = PuF_6(cr) + 2H_2O$	-43 ± 5^g

plutonium hydride

$PuH_2(cr)$	$Pu(\alpha) + H_2(g) = PuH_2(cr)$	22.9 ± 2.2^{2b}

[a] Fuger & Oetting (1976)
[b] Silva et al. (1995)
[c] Yamaguchi & Nakayama (1996)
[d] Fuger et al. (1992)
[e] Brown & Wanner (1987)
[f] Felmy et al. (1989)
[g] Fuger et al. (1983)
[h] Capdevila & Vitorge (1995)
[i] Yamaguchi et al. (2000)
[j] Ewart et al. (1985)
[k] Nitsche & Silva (1996)
[l] Capdevila et al. (1996)
[m] Rai et al. (1999b)
[n] Yamaguchi et al. (1994)
[o] Cordfunke & O'Hare (1978)
[p] Bennett et al. (1992)
[q] Itagaki et al. (1992)
[r] Novak & Roberts (1995)
[s] Neck et al. (1995a)
[t] Pashalidis et al. (1995)
[u] Okajima & Reed (1993)
[v] Grenthe et al. (1992)
[w] Puigdomènech & Bruno (1991)
[x] Pashalidis et al. (1997)
[y] Grenthe et al. (1986)
[z] Kim et al. (1984)
[2a] Pashalidis et al. (1993)
[2b] Flotow et al. (1984)
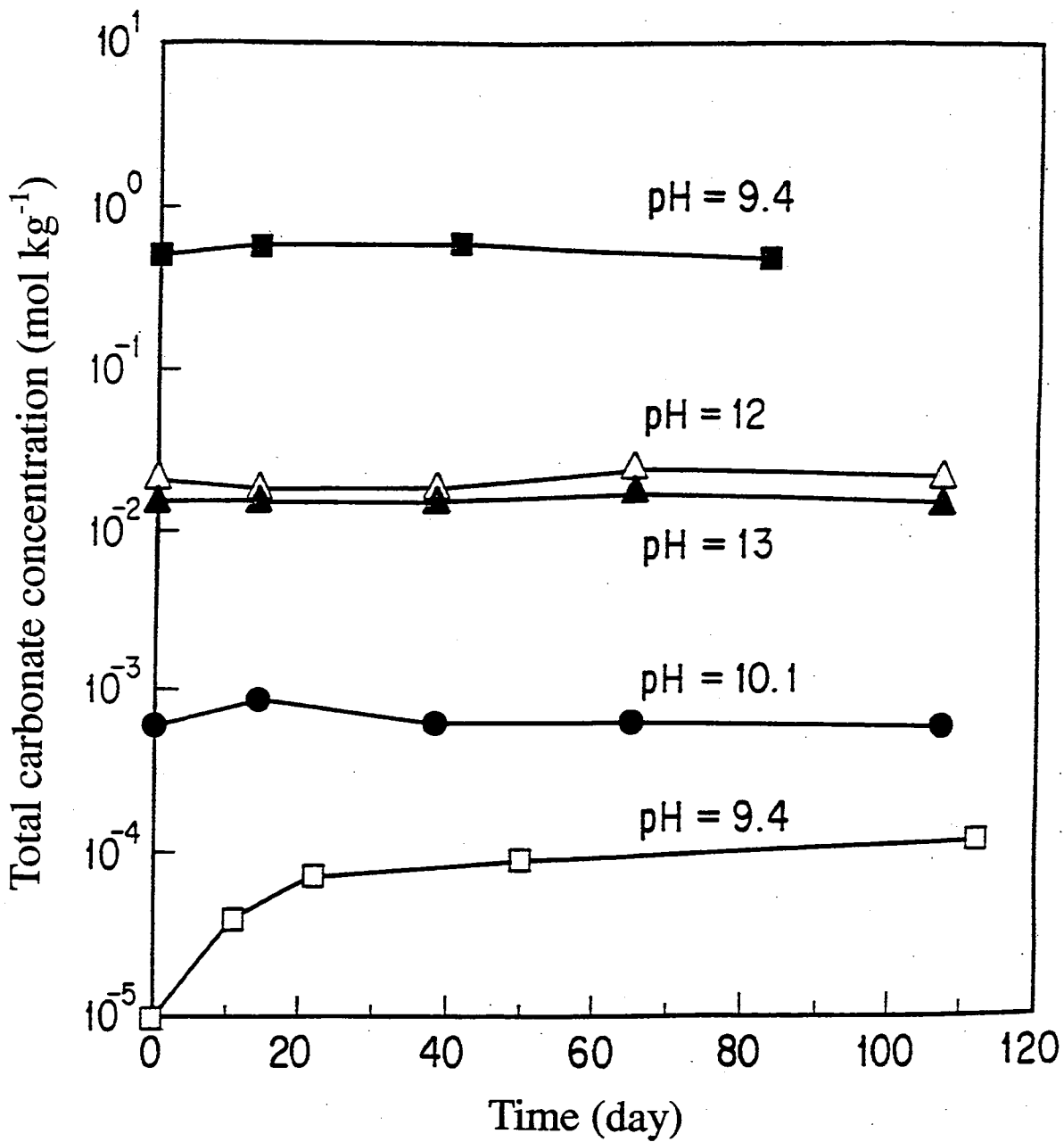
Fig. 8-1 Time dependence of total carbonate concentrations for 10^{-5} - 0.5 mol kg^{-1} KHCO$_3$ / K$_2$CO$_3$ solutions in the pH range of 9.4 - 13.
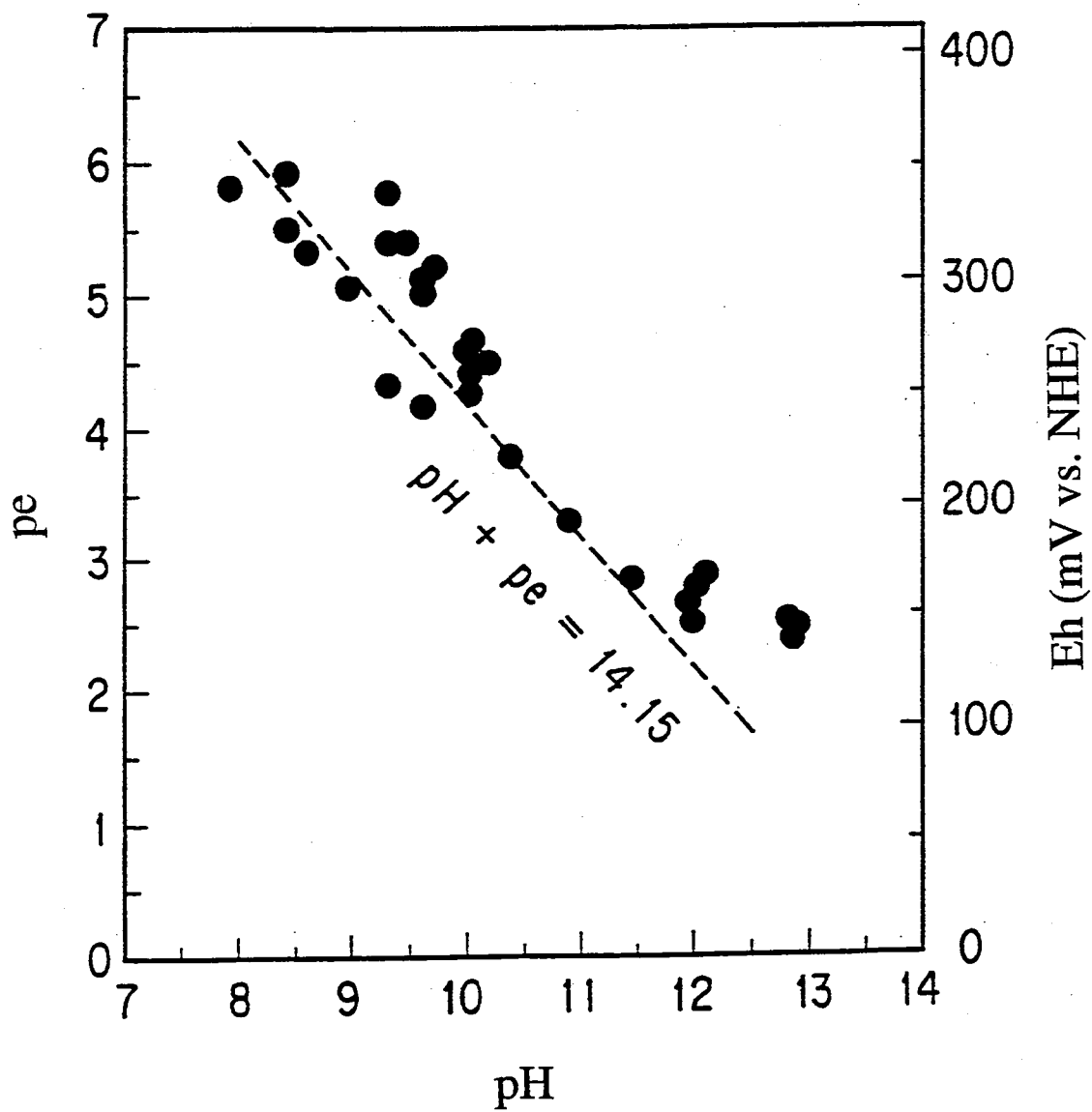
Fig. 8-2 Measured redox potential versus pH for the Pu(IV) carbonate-bicarbonate solutions
with NaNO₂. The line corresponds to Eq. (8-4).
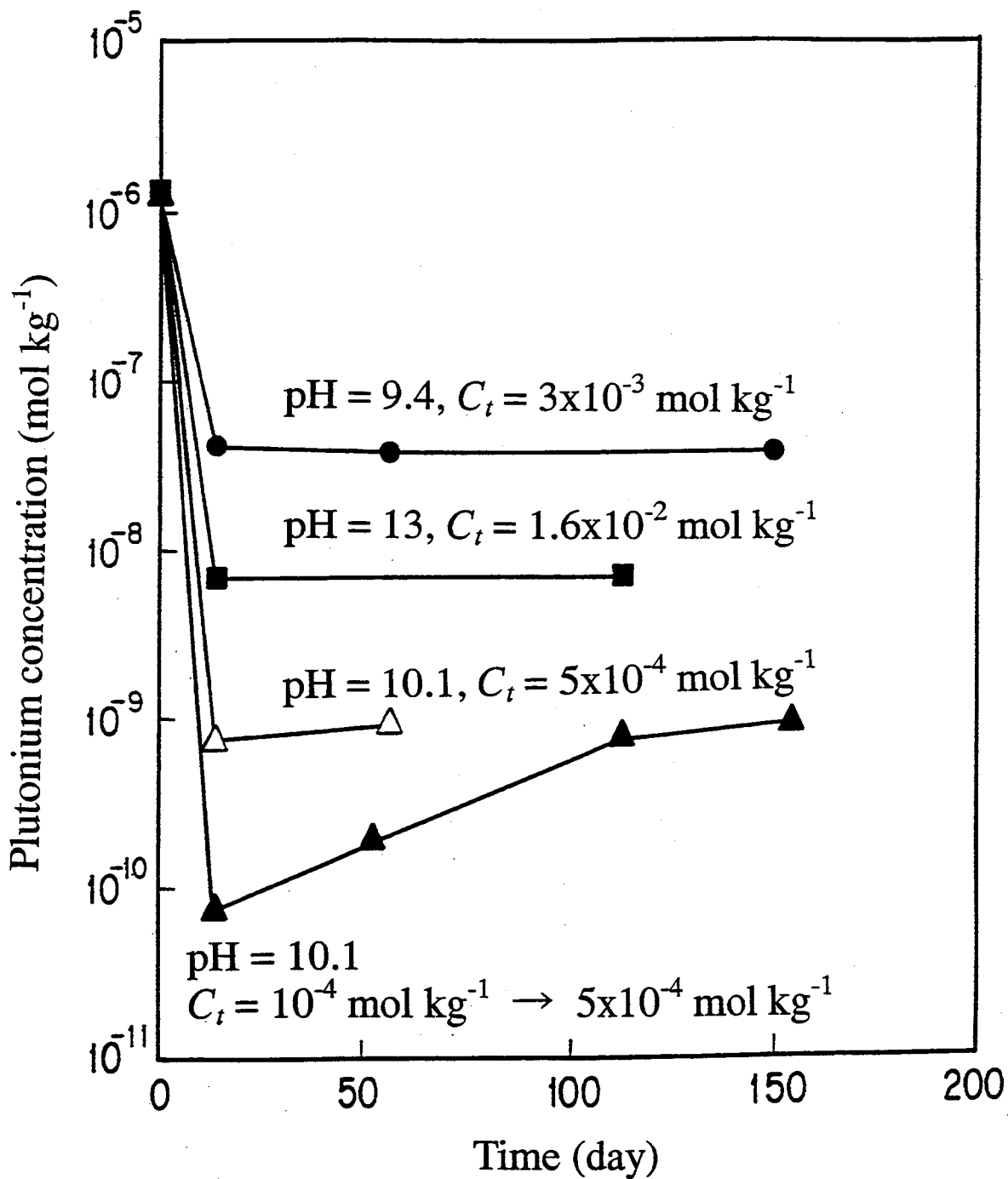
Fig. 8-3   Equilibration of plutonium(IV) concentrations for 10^{-4} - 1.6×10^{-2} mol kg^{-1} KHCO$_3$ / K$_2$CO$_3$ solutions in the pH range of 9.4 - 13; ●, ■, △: oversaturation, ▲: undersaturation.
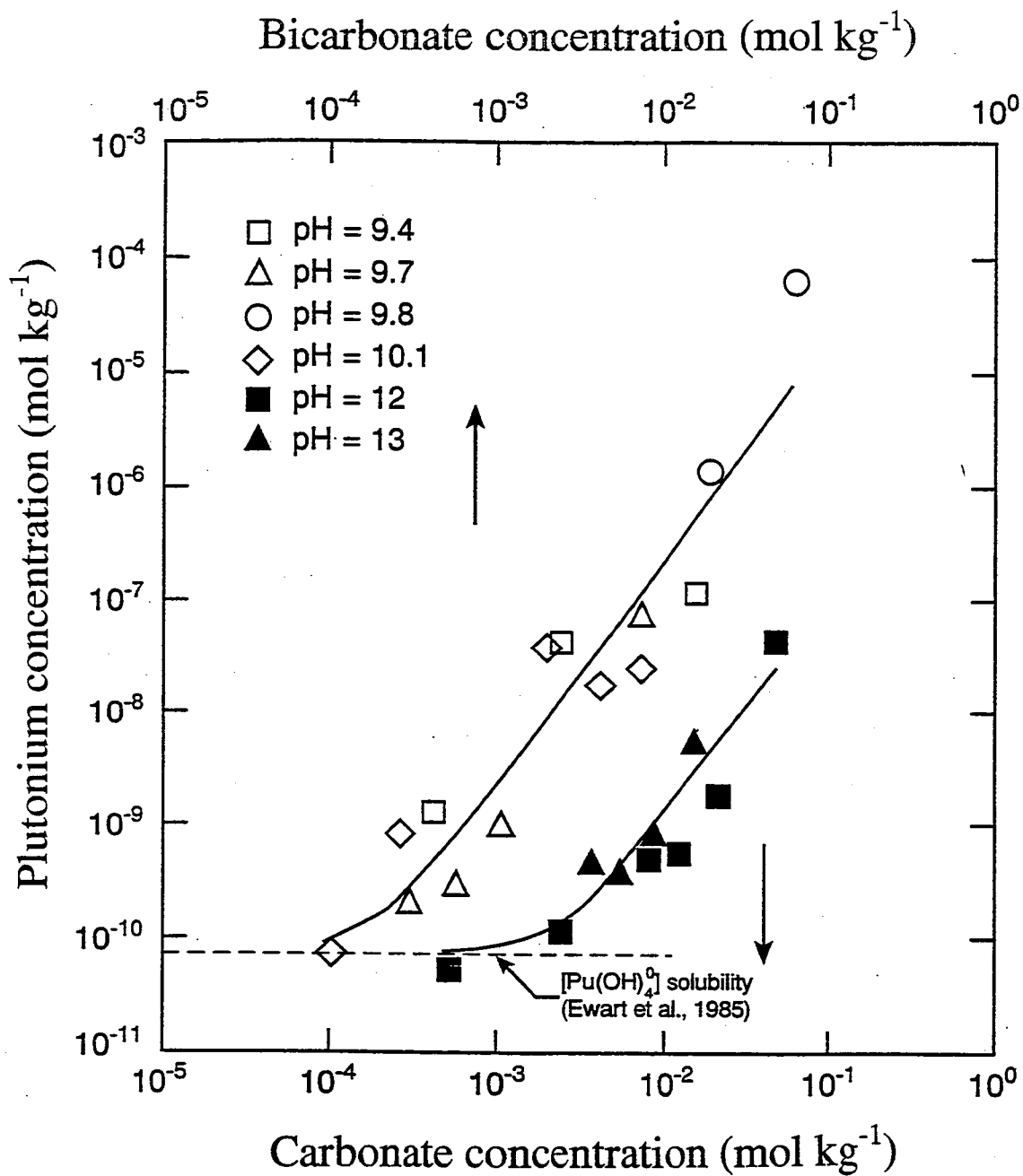
Fig. 8-4. Effect of bicarbonate concentration on solubility of Pu(IV) at pH = 9.4, 9.7, 9.8 and 10.1, and effect of carbonate concentration at pH 12 and 13. The solid curves show the results of the least-squares fitting. The dashed line shows the contribution of $Pu(OH)_4^0$.

9. Concluding remarks

The structure of interconnected pores that act as diffusion paths of aqueous species was analyzed for a granite from Inada, Ibaraki, Japan by improved techniques. The pore structure was uniform and the pore size was much larger than aqueous diffusing species; these conditions allow the application of the Fick's diffusion law and pore-diffusion model to interpret the mass transfer of the species in the granite. A positive correlation was observed between the effective diffusivity for Ba^{2+}, Sr^{2+}, Mg^{2+}, Co^{2+}, Ni^{2+}, UO_2^{2+}, HTO, Cs^+ and I^- determined under low sorption conditions and their diffusivity in bulk of the solution. Reduction of the effective diffus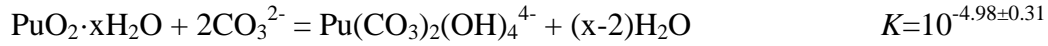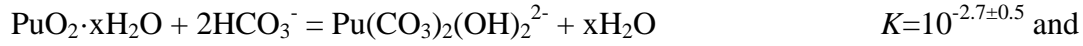ivity of I^- in granite by electrostatic repulsion between the anion and negatively charged surface of the pores was not observed. When strontium was allowed to be adsorbed on the granite, the diffusive flux of strontium through the granite was higher than that estimated from the pore-diffusion model by 42 times. Based on this result, a model which takes into account contribution of both the surface and the pore diffusion was proposed for the diffusion of sorbed species in the granite. The surface diffusivity of strontium in Inada granite of 3.5×10^{-12} m^2 s^{-1} was obtained.

A through-diffusion experiment was performed under anoxic conditions for $^{85}Sr^{2+}$ for the granite and the groundwater obtained from 240-m level of Underground Research Laboratory (URL) of Atomic Energy of Canada Limited (AECL) in Manitoba, Canada. The effective diffusivity of Sr^{2+} was higher than predicted from the pore-diffusion model by 13 times. Apparent existence of surface diffusion was confirmed for the diffusion of Sr^{2+} in the granite under geological conditions. In the experiment, a fair amount of strontium was removed from the solution and was adsorbed on the granite, which corresponded to the distribution ratio, R_d, of 0.091 - 0.180 m^3 kg^{-1}. Nevertheless, R_d value assessed from the apparent diffusivity and the effective diffusivity was 0.0041 m^3 kg^{-1}. The contribution of the surface diffusion can explain this discrepancy; the retardation of the apparent diffusive transport is smaller than that predicted from the sorption R_d value because part of the adsorbed strontium is mobile in adsorbed state.

The effective diffusivity and distribution ratio of $^{133}Ba^{2+}$ in Inada granite have been determined by the through-diffusion method. Experiments were performed in triplicate for 10^{-1}, 1, 10 and 10^2 mol m^{-3} $BaCl_2$ solution. The D_e value obtained for the $BaCl_2$ concentration of 10 mol m^{-3} agreed to the estimated value based on the pore diffusion model. The lower $BaCl_2$ concentration yielded the higher D_e value and higher R_d value than those for 10 mol m^{-3}. The variation in D_e was neither due to the speciation of barium in the solution nor variation in physical properties of the pore structure in the rock. Contribution of diffusion in adsorbed state should be responsible for the variation in D_e. The result is strongly indicative

of the diffusion in adsorbed state. The surface diffusivity of 2.4×10^{-13} m^2 s^{-1} was obtained for Ba^{2+} in Inada granite.

Solubility of Pu(IV) was measured over a total carbonate concentration range of 10^{-4} to 10^{-1} mol kg^{-1} at $I = 0.1$. The equilibrium constants of

$$PuO_2 \cdot xH_2O + 2HCO_3^- = Pu(CO_3)_2(OH)_2^{2-} + xH_2O \qquad K=10^{-2.7\pm0.5} \text{ and}$$

$$PuO_2 \cdot xH_2O + 2CO_3^{2-} = Pu(CO_3)_2(OH)_4^{4-} + (x-2)H_2O \qquad K=10^{-4.98\pm0.31}$$

were obtained. Thermodynamic database was compiled for Np and Pu by adopting these data and other equilibrium constants of formation of aqueous species and compounds from literature. The database allowed prediction of dominant actinide species in granite pore water and discussion on mechanism of their diffusion in granite.

The diffusivity of uranium, neptunium, plutonium and americium in granite matrices has been studied by the through-diffusion method in the presence of carbonate. Effective diffusivities obtained for $Pu(CO_3)_2(OH)_2^{2-}$, $Np(CO_3)_n^{4-2n}$ (n=4, 5) and $UO_2(CO_3)_3^{4-}$ were ranged between 1.4×10^{-13} m^2 s^{-1} and 4.0×10^{-13} m^2 s^{-1}, which were consistent with the pore diffusion model. Enhancement of the diffusivity by surface diffusion was not observed in the case that Pu and Am were adsorbed on mineral surfaces. The contribution of the surface diffusion is insignificant for actinide carbonate complexes which are adsorbed on the mineral surfaces through chemical reactions or surface complexation. Actinide complex species formed in groundwater under deep geological environments migrate through rock matrix following to the Fick's diffusion law, and the diffusivities are consistent with the pore-diffusion model.

As shown in this study, aqueous species including actinide complex species can diffuse into micro-pores in intact granites. The diffusivity can be higher than the value expected from the pore-diffusion model. Evidences of the contribution of the surface diffusion were obtained for divalent cations. The results of this study enable one to estimate an appropriate effective diffusivity of aqueous species in the granite taking the surface diffusion into account. The contribution of the surface diffusion directly enhances the radionuclide migration in geosphere in the case that the diffusion is the main transport mechanism under extremely low groundwater flow rate. Investigations are necessary for the contribution of the surface diffusion on diffusive transport of radionuclides in bentonite buffer and in cementitious materials that compose engineered barrier system of radioactive waste disposal. In these materials, extremely narrow pore spacing does not allow water to be free from mineral surfaces. The pore-diffusion model dealing with the concentration of the species in free pore water may not predict their diffusive behavior in bentonite buffer and in cementitious materials.

Acknowledgement

References

Agterberg, F. P., Katsube, T. J. and Lew, S. N., 1984. Statistical analysis of granite pore size distribution data, Lac du Bonnet batholith, eastern Manitoba. In Current Research, Part A, Geological Survey of Canada, Paper, 84-1A, pp. 29-38.

Andersson, K., Torstenfelt, B. and Allard, B., 1983. Sorption of radionuclides in geologic systems. SKBF/KBS TR-83-63.

Andersson, K., Evans, S. and Albinsson, Y., 1992. Diffusion of radionuclides in sediments. Radiochim. Acta, 58/59, 321.

Bennett, D. A., Hoffman, D., Nitsche, H., Russo, R. E., Torres, R. A., Baisden, P. A., Andrews, J. E., Palmer, C. E. A. and Silva, R. J., 1992. Hydrolysis and carbonate complexation of dioxoplutonium(V). Radiochim. Acta, 56, 15.

Berry, J. A., Bourke, P. J., Green, A. and Littleboy, A. K., 1987. Sorption of radionuclides on hard rocks. AERE-R-12844.

Berry, J. A. and Bond, K. A., 1992. Studies of the extent of surface diffusion in the migration of radionuclides through geological materials. Radiochim. Acta 58/59, 329.

Berry, J. A., Bond, K. A., Cowper, M. M., Green, A. and Linklater, C. M., 1994. Factors influencing the diffusion of uranium, plutonium and radium through Sherwood Sandstone from Shellafield, Cumbria. Radiochim. Acta 66/67, 447-452.

Brace, W. F., Orange, A. S. and Madden, T. R., 1965. The effect of pressure on the electrical resistivity of water-saturated crystalline rocks. J. Geophys. Res. 70, 5669-5678.

Bradbury, M. H., Green, A. Lever, D. and Stephen, I. G., 1986. Diffusion and permeability based sorption measurements in sandstone, anhydrite and upper magnesian limestone samples. AERE-R 11995.

Bradbury, M. H., Stephen, I. G., 1986. Diffusion and permeability based sorption measurements in intact rock samples. In: Sci. Basis for Nucl. Waste Manag. IX (Mat. Res. Soc. Symp. Proc. Vol. 50) (L. O. Werme, ed.). Stockholm, Sep. 9-12, 1985, p. 81-90.

Brakel, J. V., Heertjes, P. M., 1974. Analysis of Diffusion in Macroporous Media in Terms of a Porosity, a Tortuosity and a Constrictivity Factor, Int. J. Heat Mass Transfer 17, 1093.

Brink, M. B., Phinney, D. L. and Smith, D. K., 1991a. Actinide transport in topopah spring tuff: pore size, particle size and diffusion. UCRL-JC-104530, Lawrence Livermore National Lab.

Brink, M. B., Phinney, D. L. and Smith, D. K., 1991b. Effect of heterogeneity on actinide diffusion rates in tuffaceous rock. UCRL-JC-104754, Lawrence Livermore National Lab.

Brown, P.L. and Wanner, H., 1987. Predicted formation constants using the unified theory of metal ion complexation (OECD/NEA, Paris)..

Capdevila, H. and Vitorge, P., 1995. Redox potentials of PuO_2^{2+}/PuO_2^+ and Pu^{4+}/Pu^{3+} at different ionic strengths and temperatures. Entropy and heat capacity. Radiochim. Acta, 68, 51.

Capdevila, H., Vitorge, P., Giffaut, E. and Delmau, L., 1996. Spectrophotometric study of the dissociation of the Pu(IV) carbonate limiting complex. Radiochim. Acta, 74, 93.

Choppin, G. R. and Mathur, J. N., 1991. Hydrolysis of actinyl(VI) cations. Radiochim. Acta, 52/53, 25.

Cordfunke, E. H. P. and O'Hare, P. A. G., 1978. The chemical thermodynamics of actinide elements and compounds, Part 3: Miscellaneous actinide compounds. IAEA, Vienna.

Crank, J., 1975. The mathematics of diffusion. (2nd ed.) Oxford Univ. Press, London.

Dean, A., 1978. Lange's Handbook of Chemistry (McGraw-Hill, New York).

Delmau, L. H., Vitorge, P. and Capdevila, H., 1996. Np(V)/Np)IV in concentrated carbonate/bicarbonate solutions. CEA-N-2807, CEA, France.

Ewart. F. T., Howse, R. M., Thomason, H. P., Williams, S. J. and Cross, J. E., 1985. The solubility of actinides in the near-field. In: Sci. Basis for Nucl. Waste Manag. IX (Mat. Res. Soc. Symp. Proc. Vol. 50) (L. O. Werme, ed.). Stockholm, Sep. 9-12, 1985, p. 701.

Felmy, A. R., Rai. D., Schramke, J. A. and Ryan, J. L., 1989. The solubility of plutonium hydroxide in dilute solution and in high-ionic-strength chloride brines. Radiochim. Acta, 48, 29.

Flotow, H. E. and Haschke, J. M. Yamauchi S., 1984. The chemical thermodynamics of actinide elements and compounds, Part 9: The actinide hydrides. IAEA, Vienna.

Foti, S. C. and Freiling, E. C., 1964. The determination of the oxidation states of tracer uranium, neptunium and plutonium in aqueous media, Talanta 11, 385.

Fourest, B., Morss, L. R., Blain, G., David, F. and M'Halla, J., 1995. Determination of limiting ionic conductivity of Am^{3+} (aq) and Cf^{3+}(aq). Radiochim. Acta, 69, 215.

Fuger, J. and Oetting, F. L., 1976. The chemical thermodynamics of actinide elements and compounds, Part 2: The actinide aqueous ions. IAEA, Vienna.

Fuger, J., Parker, V. B., Hubbard, W. N. and Oetting, F. L., 1983. The chemical

thermodynamics of actinide elements and compounds, Part 8: The actinide halides. IAEA, Vienna.

Fuger, J., Medvedev, V. A., Khodakovsky, I. L., Navratil, J. D. and Sergeyeva, E. I., 1992. The chemical thermodynamics of actinide elements and compounds, Part 12: The actinide aqueous inorganic complexes. IAEA, Vienna.

Garrels, R. M., Dreyer, R. M. and Howland, A. L., 1949. Diffusion of ions through intergranular spaces in water-saturated rocks. Bull. Geol. Soc. Am., 60, 1809-1828.

Good, R. J. and R. S. Mikhail, 1981. The contact angle in mercury intrusion porosimetry. Powder Technol., 29, pp. 53-62.

Grenthe, I., Riglet, C. and Vitorge, P., 1986. Studies of metal-carbonate complexes. 14. Composition and equilibria of trinuclear neptunium(VI)- and plutonium(VI)-carbonate complexes. Inorg. Chem. 25, 1679.

Grenthe, I., Fuger, J., Konings, R. J. M., Lemire, R. J. Muller, A. B., Nguyen-Trung, C. and Wanner, H., 1992. Chemical Thermodynamics of Uranium. (North-Holland, Amsterdam).

Idemitsu, K., Furuya, H., Inagaki, Y., Sato, S., 1991. Migration of uranium(VI) in laboratory scale granite. Proc. of the Third Int. Symp. on Advanced Nucl. Energy Res., Mito, Japan, Mar. 13-15, 1991, p.207.

Idemitsu, K., Furuya, H., Murayama, K. and Inagaki, Y., 1992. Diffusivity of uranium(VI) in water-saturated Inada granite. In: Sci. Basis for Nucl. Waste Manag. XV (Mat. Res. Soc. Symp. Proc. Vol. 257) (C. G. Sombret, ed.), Strasbourg, Nov. 4, 1991, p. 625-632.

Idemitsu, K., Furuya, H., Murayama, K., Asao, T., Inagaki, Y., 1993. Primary diffusion path of uranium(VI) in laboratory scale water saturated Inada granite. Proc. of the 1993 Int. Conf. on Nucl. Waste Manag. and Environ. Remed. (D. Alexandre, R. Baker, R. Kohout, and J. Marek, eds.), Vol. 1, Prague, Czech Republic. Sep. 5-11, 1993, p. 207-212.

Itagaki, H. Nakayama, S., Tanaka, S. and Yamawaki, M., 1992. Effect of ionic strength on the solubility of neptunium(V) hydroxide. Radiochim. Acta, 58/59, 61.

Ittner, T. and Torstenfelt, B., 1988. Diffusion of neptunium, plutonium and americium in granitic rock. Radiochim. Acta, 44/45, 171.

Kato, Y., Kimura, T., Yoshida, Z. and Nitani, N., 1996. Solid-liquid phase equilibria of Np(VI) and of U(VI) under controlled CO_2 partial pressures. Radiochim. Acta, 74, 21.

Kato, Y., Kimura, T., Yoshida, Z. and Nitani, N., 1998. Carbonate complexation of neptunyl(VI). Radiochim. Acta, 82, 63.

Katsube, T. J. and Hume, J. P., 1987. Pore structure characteristics of granitic rock samples from Whiteshell Research Area. In Geotechnical studies at Whiteshell research area (RA-3), CANMET, Report MRL 87-52. pp. 111-158.

Kim, J. I., Lierse, Ch. and Baumgärtner, F., 1983. Complexation of the plutonium(IV) ion in carbonate-bicarbonate solutions, Chapter 21, in: Plutonium Chemistry (Carnall, W. T., Choppin, G. R. eds.) ACS Symp. Ser. 216, Amer. Chem. Soc., Washington, D.C., p.317.

Kim, J. I., Bernkopf, M., Lierse, Ch. and Koppold, F., 1984. Hydrolysis reactions of Am(III) and Pu(VI) ions in near-neutral solutions. In: Barney, S., Navratil, J. D. and Schultz, W. W. (eds.), Geochemical behavior of disposed radioactive waste. ACS Symp. Ser. 246, Am. Chem. Soc., Washington D. C.

Kim, J. I., 1986. Chemical behaviour of transuranic elements in natural aquatic systems. In: Handbook on the Physics and Chemistry of the Actinides (Freeman, A. J. and Keller, C., eds.) Vol. 4, p. 413, North Holland, Amsterdam.

Kumata, M., Iwai, T., Sagawa, T., Suzuki, T. and Nishiyama, K., 1990. Diffusion experiment of a radionuclide in granitic rock cores, JAERI-M 90-179 (in Japanese), JAERI, Tokai, Japan, 21 pp.

Lang, H., Klotz, D. and Moser, H., 1986. Nuclide migration in porous fractured rock., EUR-10121, pp. 232-242.

Lever, D. A, 1986. Some notes on experiments measuring diffusion of sorbed nuclides through porous media, AERE-R-12321.

Li, Y. H., Gregory, S., 1974. Diffusion of ions in sea water and in deep-sea sediments. Geochim. Cosmochim. Acta, 38, 703.

Lierse, Ch. 1985. Chemical behaviour of plutonium in natural aquatic system: hydrolysis, carbonate complexation and redox reaction., Ph. D. Thesis (in German), Technische Universität München, München.

Mahoney, J. J. and Langmuir, D., 1991. Adsorption of Sr on kaolinite, illite and montmorillonite at high ionic strengths. Radiochim. Acta, 54, 139.

McKeegan, K. D., Phinney, D., Oversby, V. M., Brink, M. B. and Smith, D. K., 1989. Uranium transport in Topopah spring tuff: an ion-microscope investigation. In: Sci. Basis for Nucl. Waste Manag. XII (Mat. Res. Soc. Symp. Proc. Vol. 127) (W. Lutz and R. C. Ewing, eds.). Berlin, Oct. 10-13, 1988, p. 813-821.

Meier, H. Zimmerhackl, E., Hecker, W., Zeitler, G. and Menge, P., 1988. Measurement of diffusion of radionuclides in sediment rocks. Radiochim. Acta 44/45, 239-244.

Melnyk, T. W. and Skeet, A. M. M., 1986. An improved technique for the determination of rock

porosity. Canadian Journal of Earth Science, 23, 1068-1074.

Mills, R., 1961. Trace-ion diffusion in electrolyte solutions, Rev. Pure Appl. Chem. 11, 78.

Morgenstern, A. and Kim, J. I., 1996. The phosphate complexation of neptunium(V). Radiochim. Acta, 72, 73.

Moriyama H., Pratopo, M. I. and Higashi, K., 1995. Hydrolysis and carbonate complexation of Np(VI) in high pH solutions. Radiochim. Acta, 69, 49.

Moskvin, A. I., Gel'man, A. D., 1958. Determination of the composition and instability constants of oxalate and carbonate complexes of plutonium(IV), Russ. Jour. Inorg. Chem. (Engl. Transl.) 3, 198.

Muuronen, S., Kämäräinen, E-L., Jaakkola, T., Pinnioja, S. and Lindberg, A., 1986. Sorption and diffusion of radionuclides in rock matrix and natural fracture surfaces studied by autoradiography. In: Sci. Basis for Nucl. Waste Manag. IX (Mat. Res. Soc. Symp. Proc. Vol. 50) (L. O. Werme, ed.). Stockholm, Sep. 9-12, 1985, p. 747-754.

Nakayama, S., Yamaguchi, T. and Sekine, K., 1996. Solubility of neptunium(IV) hydrous oxide in aqueous solutions. Radiochim. Acta, 74, 15.

Neck, V., Runde, W. and Kim, J. I., 1995a. Solid-liquid equilibria of neptunium(V) in carbonate solutions of different ionic strengths: II. Stability of the solid phases. J. Alloys and Compounds, 225, 295.

Neck, V., Fanghänel, Th., Rudolph, G. and Kim, J. I., 1995b. Thermodynamics of neptunium(V) in concentrated salt solutions: chloride complexation and ion interaction (Pitzer) parameters for the NpO_2^+ ion. Radiochim. Acta, 69, 39.

Neretnieks, I., 1980. Diffusion in the rock matix: an important factor in radionuclide retardation? J. Geophys. Res. 85, 4379-4397.

Newton, T. W. and Sullivan, J. C., 1985. Actinide carbonate complexes in aqueous solution. In: Handbook on the Physics and Chemistry of the Actinides (Freeman, A. J. and Keller, C., eds.) Vol. 3, p. 387, North Holland, Amsterdam.

Nightingale, E. R., 1959. Phenomenological theory of ion solvation. Effective radii of hydrated ions, J. Phys. Chem. 63, 1381.

Nishiyama, K., Nakashima, S. Tada, R. and Uchida, T., 1990. Diffusion of an ion in rock pore water and its relation to pore characteristics, Mining Geol. (in Japanese) 40, 323-326.

Nitsche, H., Lee, S. C. and Gatti, R. C., 1988. Determination of plutonium oxidation states at trace levels pertinent to nuclear waste disposal, J. Radioanal. Chem. 124, 171.

Nitsche, H. and Silva, R., 1996. Investigation of the carbonate complexation of Pu(IV) in

aqueous solution. Radiochim. Acta, 72, 65.

Novak, C. F. and Roberts, K. E., 1995. Thermodynamics modeling of neptunium(V) solubility in concentrated Na-CO$_3$-HCO$_3$-Cl-ClO$_4$-H-OH-H$_2$O systems. In: Sci. Basis for Nucl. Waste Manag. XVIII (Mat. Res. Soc. Symp. Proc. Vol. 353) (T. Murakami and R. C. Ewing, eds.). Kyoto. Japan, Oct. 23-27, 1994, p. 1119-1128.

Ohe, T., 1984. Ion exchange adsorption of radioactive cesium, cobalt, manganese, and strontium to granitoid rocks in the presence of competing cations. Nucl. Technol., 67, 92-101.

Ohlsson, Y. and Neretnieks, I., 1998. Some evidence for surface ion mobility in rock. J. Contamin. Hydrol. 35, 91-100.

Okajima, S. and Reed, D. T., 1993. Initial hydrolysis of plutonium(VI). Radiochim. Acta, 60, 173.

Pashalidis, I., Runde, W. and Kim, J. I., 1993. A study of solid-liquid phase equilibria of Pu(VI) and U(VI) in aqueous carbonate systems. Radiochim. Acta, 61, 141.

Pashalidis, I., Kim, J. I., Ashida, T. and Grenthe, I., 1995. Spectroscopic study of the hydrolysis of PuO$_2$$^{2+}$ in aqueous solution. Radiochim. Acta, 68, 99.

Pashalidis, I., Czerwinski, K. R., Fanghänel, Th. and Kim, J. I., 1997. Solid-liquid phase equilibria of Pu(VI) and U(VI) in aqueous carbonate systems. Determination of stability constants. Radiochim. Acta, 76, 55.

Pratopo, M. I., Moriyama, H. and Higashi, K., 1990. Carbonate complexation of neptunium(IV) and analogous complexation of ground-water uranium, Radiochim. Acta 51, 27.

Puigdomènech, I. and Bruno, J., 1991. Plutonium solubilities. SKB-TR-91-04, Swedish Nuclear Fuel and Waste Management Co., Stockholm.

Puukko, E., Heikkinen, T., Hakanen, M. and Lindberg, A., 1993. Diffusion of water, cesium and neptunium in pores of rocks. YJT-93-23, Nuclear Waste Commission of Finnish Power Companies, Helsinki.

Rai, D., 1984. Solubility product of Pu(IV) hydrous oxide and equilibrium constants of Pu(IV)/Pu(V), Pu(IV)/Pu(VI), and Pu(V)/Pu(VI) couples, Radiochim. Acta 35, 97.

Rai, D. and Ryan, J. L., 1985. Neptunium(IV) hydrous oxide solubility under reducing and carbonate conditions. Inorg. Chem., 24, 247.

Rai, D., Swanson, J. L. and Ryan, L., 1987. Solubility of NpO$_2$·xH$_2$O in the presence of Cu(I)/Cu(II) redox buffer. Radiochim. Acta, 42, 35.

Rai, D., Rao, L. and Moore, D. A., 1998. The influence of isosaccharinic acid on the solubility of Np(IV) hydrous oxide. Radiochim. Acta, 83, 9.

Rai, D., Hess, N. J., Felmy, A. R., Moore, D. A. and Yui, M., 1999a. A thermodynamic model for the solubility of $NpO_2(am)$ in the aqueous K^+-HCO_3^--CO_3^{2-}-OH^--H_2O system. Radiochim. Acta, 84, 159.

Rai, D., Hess, N. J., Felmy, A. R., Moore, D. A., Moore, D. A., Yui, M. and Vitorge, P., 1999b. A thermodynamic model for the solubility of $PuO_2(am)$ in the aqueous K^+-HCO_3^--CO_3^{2-}-OH^--H_2O system. Radiochim. Acta, 86, 89.

Robinson, R. A. and Stokes, R. H., 1955. Electrolyte Solutions. Butterworths, London.

Sato, S. Furuya, H., Araya, S. and Matsuo, K., 1986. Migration behavior of U(VI) in tuff. In: Sci. Basis for Nucl. Waste Manag. IX (Mat. Res. Soc. Symp. Proc. Vol. 50) (L. O. Werme, ed.). Stockholm, Sep. 9-12, 1985, p. 763-770.

Silva, R. J., Bidoglio, G., Rand, M. H., Robouch, P. B., Wanner, H. and Puigdomènech, I., 1995. Chemical Thermodynamics of Americium. (Elsevier, Amsterdam).

Skagius, K. and Neretnieks, I., 1982. Diffusion in crystalline rocks of some sorbing and nonsorbing species. KBS-TR-82-12, SKBF/KBS, Stockholm.

Skagius, K., Svedberg, G. and Neretnieks, I., 1982. A study of strontium and cesium sorption on granite. Nucl. Technol., 59, 302.

Skagius, K. and Neretnieks, I., 1986. Porosities and diffusivities of some nonsorbing species in crystalline rocks, Water Resour. Res. 22, 389.

Skagius, K. and Neretnieks, I., 1988. Measurement of cesium and strontium diffusion in biotite gneiss, Water Resour. Res. 24, 75.

Smith, P. A., 1989. Modeling of a diffusion-sorption experiment on sandstone. PSI-Bericht, Nr.53.

Smith, R. M. and Martell, A. E., 1976. Critical stability constants Vol. 4, Plenum press, New York.

Spacek, P. and Kubin, M., 1967. Diffusion in gels. J. Polym. Sci: Part C, 16, 705.

Suksi, S., Kämäräinen, E-L., Siitari-Kauppi, M. and Lindberg, A., 1987. Sorption and diffusion of cobalt, nickel, strontium, iodine, cesium and americium in natural fissure surfaces and drill core cups studied by autoradiography, III. YJT-87-17.

Suksi, S., Siitari-Kauppi, M., Kämäräinen, E-L. and Lindberg, A., 1989. The effect of ground water-rock interactions on the migration of redox sensitive radionuclides. In: Sci. Basis for Nucl. Waste Manag. XII (Mat. Res. Soc. Symp. Proc. Vol. 127) (W. Lutz and R. C.

Ewing, eds.). Berlin, Oct. 10-13, 1988, p. 965-972.

Torstenfelt, B., 1982. Mobilities of radionuclides in fresh and fractured crystalline rock. SKBF-KBS-TR 82-26.

Triay, I. R., Birdsell, K. H., Mitchell, A. J. and Ott, M. A., 1993. Diffusion of sorbing and non-sorbing radionuclides. LA-UR-93-437, Los Alamos National Lab.

Tsukamoto, M. and Ohe, T., 1991. Intraparticle diffusion of cesium and strontium cations into rock materials. Chem. Geol. 90, 31.

Uematsu, K., 1988. Japanese approaches to the assessment of radionuclide migration in the geosphere. Radioactive Waste Management and the Nuclear Fuel Cycle, Vol. 10, 145-158.

Ushiki, H., Okada, I., Takahashi Y., Tanaka, K. and Hashiya, T., 1993. Transport phenomena. In: Handbook of Chemistry, 4th edition, basic volume, p. II-61 (in Japanese), The Chemical Society of Japan, Tokyo.

Vandergraaf, T. T. and Ticknor, K. V., 1994. A compilation and evaluation of sorption coefficients used in the geosphere model of SYVAC for the 1990 assessment of the Whiteshell Research Area. Atomic Energy of Canada Limited Report AECL-10546, COG-92-59.001.

Wakao, N. and Smith, J. M., 1962. Diffusion in catalyst pellets. Chemical Engineering Science 17, 825-834.

Weigel, F., 1985. The carbonates, phosphates and arsenates of the hexavalent and pentavalent actinides. In: Handbook on the Physics and Chemistry of the Actinides (Freeman, A. J. and Keller, C., eds.) Vol. 3, North Holland, Amsterdam, pp. 243-288.

Xia, Y., Rao, L., Rai, D. and Felmy, A. R., 1999. Solvent extraction study of Np(IV) sulphate complexation in Na^+-Np^{4+}-OH^--SO_4^{2-}-HSO_4^--ClO_4^- and Na^+-Np^{4+}-OH^--SO_4^{2-}-HSO_4^--Cl^- systems. Radiochim. Acta, 86, 33.

Yamaguchi, T., Pratopo, M. I., Moriyama, H. and Higashi, K., 1991. Adsorption of cesium and neptunium(V) on bentonite, Proceedings of the Third International Conference on Nuclear Fuel Reprocessing and Waste Management (RECOD'91), Sendai, Japan, Vol.2, p.999.

Yamaguchi, T., Sakamoto, Y. and Senoo, M., 1993. Consideration on effective diffusivity of strontium in granite. J. Nucl. Sci. Technol. 30, 796-803.

Yamaguchi, T., Sakamoto, Y. and Ohnuki, T., 1994. Effect of complexation on solubility of Pu(IV) in aqueous carbonate system, Radiochim. Acta, 66/67, 9.

Yamaguchi, T. and Nakayama, S., 1996. Consideration on thermodynamic data for

americium(III) aqueous carbonate system. Radioactive Waste Research (in Japanese), 3 (1), 49.

Yamaguchi, T., Sakamoto, Y., Nakayama, S. and Vandergraaf, T. T., 1997a. Effective diffusivity of the uranyl ion in a granite from Inada, Ibaraki, Japan. J. Contaminant Hydrology, 26, 109.

Yamaguchi, T., Isobe, H. and Nakayama, S., 1997b. Analysis of Microporous Structure in Granite. Radioactive Waste Research (in Japanese), 3, 99.

Yamaguchi, T. and Nakayama, S., 1998. Diffusivity of U, Pu and Am carbonate complexes in a granite from Inada, Ibaraki, Japan studied by through diffusion. Journal of Contaminant Hydrology, 35, 55-65.

Yamaguchi, T. and Takeda, S., 1999. Consideration on thermodynamic data for predicting solubility and chemical species of elements in groundwater, Part 1: Tc, U, Am. JAERI-Data/Code 99-001 (in Japanese).

Yamaguchi, T., 2000. Consideration of thermodynamic data for predicting solubility and chemical species of elements in groundwater. Part 2: Np, Pu. JAERI-Data/Code 2000-031 [in Japanese], JAERI, Tokai, Japan.

Yamaura, T., Kitamura, A., Fukui, A., Nishikawa, S., Yamamoto, T. and Moriyama, H., 1998. Solubility of U(VI) in highly basic solutions. Radiochim. Acta, 83, 139.